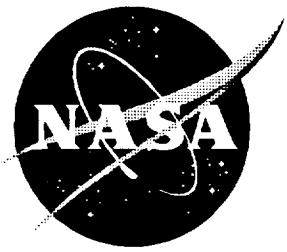

NASA Contractor Report 4664

Analysis of Materials Flown on the Long Duration Exposure Facility: Summary of Results of the Materials Special Investigation Group

H. Gary Pippin

Contracts NAS1-18224 and NAS1-19247
Prepared for Langley Research Center

July 1995

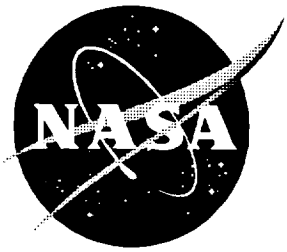

NASA Contractor Report 4664

Analysis of Materials Flown on the Long Duration Exposure Facility: Summary of Results of the Materials Special Investigation Group

H. Gary Pippin
Boeing Defense & Space Group • Seattle, Washington

National Aeronautics and Space Administration
Langley Research Center • Hampton, Virginia 23681-0001

Prepared for Langley Research Center
under Contracts NAS1-18224 and NAS1-19247

July 1995

Printed copies available from the following:

NASA Center for AeroSpace Information
800 Elkridge Landing Road
Linthicum Heights, MD 21090-2934
(301) 621-0390

National Technical Information Service (NTIS)
5285 Port Royal Road
Springfield, VA 22161-2171
(703) 487-4650

FOREWORD

This report describes the results from the testing and analysis of materials flown on the Long Duration Exposure Facility (LDEF). This work was carried out by Boeing Defense & Space Group under two Contracts, NAS1-18224, Task 12 (October 1989 through May 1991), and NAS1-19247, Tasks 1 and 8 (initiated May 1991). Sponsorship for these two programs was provided by the National Aeronautics and Space Administration, Langley Research Center (LaRC), Hampton, Virginia.

Mr. Lou Teichman, NASA LaRC, was the NASA Task Technical Monitor. Mr. Teichman was replaced by Ms. Joan Funk, NASA LaRC, following his retirement. Mr. Bland Stein, NASA LaRC, was the Materials Special Investigation Group Chairman, and was replaced by Ms. Joan Funk and Dr. Ann Whitaker, NASA Marshall Space Flight Center (MSFC), following Mr. Stein's retirement. The Materials & Processes Technology organization of the Boeing Defense & Space Group was responsible for providing the support to both contracts. The following Boeing personnel provided critical support throughout the program.

Sylvester Hill	Program Manager
Dr. Gary Pippin	Technical Leader
Harry Dursch	Materials Analysis
Johnny Golden	Materials Analysis
Roger Bourassa	Materials Analysis
Gail Bohnhoff-Hlavacek	Databases and Information Processing

TABLE OF CONTENTS

TABLE OF CONTENTS (Continued)

List of Figures

1.0 EXECUTIVE SUMMARY

The Long Duration Exposure Facility (LDEF) was a 21,400-lb satellite stabilized in a fixed flight orientation. LDEF carried 57 science and technology experiments from 11 countries in a total of 86 experiment trays. Deployment was on April 7, 1984 at a 257-nmi altitude in a 28.5° inclination and retrieval was on January 12, 1990 at a 171-nmi altitude after 69 months in low Earth orbit (LEO).

Prior to retrieval, NASA formed four Special Investigation Groups (Materials, Systems, Ionizing Radiation, and Meteoroids and Debris) to augment the examination of the LDEF. The objectives of the Materials Special Investigation Group (MSIG) were to: (1) examine materials and support hardware from LDEF not being investigated as part of the actual experiments being flown, (2) suggest additional evaluation on experimenters' materials which may not have been included in the original scope of a particular experiment, and (3) convey all materials findings to interested organizations within the Government, aerospace industry, and supporting academic community. The MSIG also assumed the responsibility of defining the atomic oxygen and solar exposures, and identifying both particulate and molecular contamination levels around the spacecraft.

This document describes work carried out under the direction of the MSIG from 1989 to 1995. This report is a combination summary, detailed technical report, and guide to further materials information from the LDEF. Summary sections are included for selected materials and experiments. Detailed sections are included on both atomic oxygen and solar exposure modeling and molecular contamination because these topics have not been previously reported in stand alone reports. Detailed results are included for work carried out since the 3rd LDEF Post-Retrieval Symposium, particularly surface analyses of the stainless steel bolts used to hold the tray clamps and of the black chrome plated panels at the Earth end of LDEF. Data not previously published and/or made widely available are also included in appropriate sections to ensure that such information is documented.

The LDEF results have become the baseline for understanding long-term exposure to LEO environments for several reasons:

1) The stability of the LDEF orientation during flight allowed a precise definition of environments around the spacecraft and indication of performance of specific materials as a function of exposure level.
2) The spacecraft was exposed to a variety of space environments over an extended period of time.
3) The ability to examine the large quantity and variety of materials upon return.
4) Even though LDEF was launched in 1984, a number of the materials flown are still essential for use on spacecraft and evaluation of their performance is technologically significant.
5) LDEF results confirmed the satisfactory performance of a number of materials, components, and systems. The performance of systems on LDEF will be documented with the publications of the final report from the LDEF Systems Special Investigation Group.
6) The collection of on-orbit and post-flight photographs are extensive and are an extremely valuable archive.
7) LDEF experimental results verified the models used to predict atomic oxygen exposure levels.
8) A collection of particulate debris was observed trailing the LDEF as the Space Shuttle approached for retrieval. Vapor deposited aluminum backing from failed thermal control blankets on the leading edge of the spacecraft is the apparent source of the particles. The particles appeared to be spinning as individual particles periodically reflected sunlight into the camera.

Inorganic thermal control paints, anodized aluminum and silverized Teflon thermal control blankets maintained their optical properties, and thus their thermal control function. Organic materials such as Mylar, Kapton, paint binders, and bare composites showed the expected severe erosion and degradation under atomic oxygen exposure. Coated composite materials survived and generally maintained their mechanical properties.

Due to the extended mission life, some thin film polymeric films and blanket materials were virtually destroyed and created on-orbit debris which was distributed over adjacent surfaces. A low-density particulate debris cloud collected in the LDEF wake. Severe darkening from UV polymerized molecular deposits was observed around vent paths from the interior of the spacecraft.

Extremely thin, patchy films of silicon-based contamination was distributed all around LDEF. It was found that silicone deposited on leading edge surfaces had been oxidized into silicates by the atomic oxygen. However, analysis of LDEF tray clamp bolt heads examined from a variety of exterior locations showed the molecular film contained silicone. This silicone had to have been deposited after the surfaces were shielded from atomic oxygen, such as would have occurred when LDEF was re-berthed in the Shuttle. Outgassed silicones exposed to atomic oxygen during the 69 month flight would have been oxidized to silicates prior to retrieval. In addition, the silicone found on leading edge locations had to originate from non-LDEF surfaces as all LDEF materials were thoroughly outgassed by the time LDEF was retrieved. Post-flight outgassing measurements of silicone-based adhesive materials gave total mass loss values of about 75% of pre-flight values (ref. 1). On-orbit temperature ranges for these materials were rather mild and in-service outgassing rates at the end of the flight were likely extremely low. Any small amounts outgassed toward the end of the mission would have been quickly oxidized by the high flux of atomic oxygen and an additional significant source of silicone would be required to produce the silicone observed.

LDEF results are mostly from post-flight analysis from hardware which underwent exposure to a variety of conditions. The on-orbit effects must be separated from ground, launch, and reentry effects. An on-orbit spacecraft will not experience the turbulence of reentry, with its potential for redistributing or removing particulate contaminants, the post-flight re-adsorption of moisture, deposition of a ground contamination layer, and/or changes in thermal control paints due to reaction with molecular oxygen in air, as did LDEF. Such post-flight processes are all artifacts which may disguise processes which occurred on-orbit and are significant for satellite performance. Pre-flight ground exposures and the launch environment are also important because these environments may effect the in-service operations of a spacecraft. The solutions available for ground based problems could be quite different than for problems induced by the space environment.

Time resolved data available from LDEF include: (1) solar absorptance of selected thermal control coatings obtained on a monthly basis until the S0069 experiment batteries failed after about 19 months, (2) temperatures monitored by thermocouples at selected intervals during the flight, (3) meteoroid and debris impacts on experiment AO201 monitored for over a year, and (4) five environmental exposure control canisters housing passive material specimens opened for about 10 months and then closed for the duration of the mission. Two of these canisters opened in three stages, providing additional time-resolved exposures.

Examination of LDEF greatly extended the knowledge of materials performance in low Earth orbit. Results of the MSIG investigations have been distributed through publication in numerous conference presentations and proceedings (refs. 2-6), NASA contractor reports (refs. 7-16), electronic databases (ref. 17), and literally hundreds of contacts with engineers and scientists seeking specific information about virtually every aspect of materials performance investigated by the MSIG.

2.0 INTRODUCTION

This report summarizes the results of extensive materials' analyses conducted over the last 5 years on hardware and test specimens from the LDEF. The understanding of materials' performance under the exposure conditions found on the LDEF is the result of investigations by many organizations. The work has been extensively documented in NASA-sponsored symposia and contractor reports, technical journal articles, and presentations at conferences put on by a wide variety of technical organizations (ref. 2-18).

Due to the extension of the LDEF flight beyond its planned 10-month duration, NASA organized four groups to conduct examinations of the LDEF support hardware which was not part of the experimenters' test plans. These groups are the Materials, Systems, Induced Radiation, and Meteoroid and Debris Special Investigation Groups. This report draws upon all available sources of information in forming conclusions about materials performance; however, the majority of information provided here was developed under the direction of the Materials Special Investigation Group (MSIG).

The following reports for specific materials disciplines have already been produced by the MSIG and are available.

a. "Space Environmental Effects on the Integrity of Chromic Acid Anodized Aluminum." NASA-CR-191468, May 1993.
b. "Results of Examination of LDEF Polyurethane Thermal Control Coatings." NASA-CR-4617, July 1994.
c. "Analysis of Silverized Teflon Thermal Control Material Flown on the Long Duration Exposure Facility." NASA-CR-4663, May 1995.
d. "Composite Materials Flown on the Long Duration Exposure Facility." NASA-CR-4657, April 1995.
e. "Effects of Space Exposure on Metals Flown on the Long Duration Exposure Facility." NASA-CR-4662, May 1995.
f. "Evaluation of Seals and Lubricants Used on the Long Duration Exposure Facility." NASA-CR-4604, June 1994.
g. "Evaluation of Adhesive Materials Used on the Long Duration Exposure Facility." NASA-CR-4646, March 1995.
h. "Analysis of Selected Materials Flown on Interior Locations of the Long Duration Exposure Facility." NASA-CR-4586, April 1994.

A set of computer models developed at Boeing have been used to define the atomic oxygen and solar ultraviolet radiation environments around LDEF. These computer codes have been transferred to NASA Langley Research Center (LaRC), and creation of users guides providing instruction in the use of these codes has been funded by NASA. Contractor reports detailing the atomic oxygen and solar exposures as functions of time and location have been published (refs. 10,15). The following series of databases, available with a user's manual (ref. 17), have also been funded by both the the Materials and Systems Special Investigation Groups:

a. Anodized Aluminum.
b. Thermal Control Paints.
c. Silverized Teflon.
d. Optical Materials.
e. LDEF Environmental Exposures.

The following sections contain a final engineering assessment of the performance of each material type examined under MSIG direction. Materials measurements acquired after each discipline area report was issued are reported here for completeness. An environments definition, discussion of contamination sources and effects, and results of microenvironments modeling calculations for specific locations on LDEF are included in this report. The LDEF data is also put in context by comparison with results from other flights.

3.0 LDEF MISSION OBJECTIVE

Flying the LDEF provided a recoverable test platform for a selected set of experiments which required exposure to at least some aspect of the space environment. LDEF was deployed in low Earth orbit in April, 1984. The initial flight was planned to last approximately 1 year. Priority of other shuttle payloads pushed the planned recovery into 1986. The Challenger accident then stopped Space Shuttle flights for an extended period of time. The retrieval mission was rescheduled for early 1990, at which time LDEF was returned to Earth. NASA SP-473 (ref. 18) includes a summary description of the LDEF and each experiment selected for the 1984 flight.

LDEF was flown in a similar range of altitudes and in the same fixed orientation as the planned International Space Station. The extended duration of the exposure benefited some experiments, impaired others by altering surfaces or causing failure of some hardware, and essentially completely removed some materials.

4.0 MATERIALS SPECIAL INVESTIGATION GROUP

The Materials Special Investigation Group (MSIG) was one of four groups created by NASA to augment the evaluations being carried out by individual LDEF experimenters. Mr. Bland Stein was the MSIG chairman until his retirement in 1993, at which time Ms. Joan Funk and Dr. Ann Whitaker became co-chairs of the group. The membership of this committee is listed in figure 4.0-1. In 1989, the MSIG selected Boeing Defense & Space Group as the contractor responsible for carrying out the analysis of all materials on the LDEF which were not otherwise the direct responsibility of the individual investigators. The MSIG was responsible for examination of all non-experiment support materials on LDEF, including the primary structure, trays, tray clamps, nuts, bolts, thermal control blankets, coatings and paints, grounding straps, seals, lubricants, adhesives, and wiring materials. This group also assumed responsibility for analysis of contamination on the LDEF and definition of the atomic oxygen and solar UV radiation environments.

Selected experimental specimens were also further examined once the principal investigators had completed their studies. Data from numerous paints, metals, and composite materials specimens were compiled from experimenters' reports and included in the reports together with MSIG-generated results. Results from analysis of the materials are documented in papers from the three LDEF post-retrieval symposia, two materials workshops, and a series of reports covering specific materials subjects (ref. 1-17). Several members of the MSIG were among the primary experimenters on LDEF and have individually reported their findings at the post-retrieval symposia and materials workshops.

Name	Affiliation
Bland Stein	NASA-LaRC
Joan Funk	NASA-LaRC
Ann Whitaker	NASA-MSFC
Lou Teichman	NASA-LaRC
Roger Linton	NASA-MSFC
Wayne Stuckey	The Aerospace Corp.
Lubert Leger	NASA-JSC
Bruce Banks	NASA-LeRC
Wayne Slemp	NASA-LaRC
Jack Berengoltz	JPL
Jack Triolo	NASA-GSFC
Lou McCreight	The Aerospace Corp.
Charles Bersch	IDA/SDIO
Tom Crooker	NASA-HQ
Phil Young	NASA-LaRC
Paul Sagalyn	Army Mat'ls Lab.
Sally Little	NASA-SSFPO
Lon Kauder	NASA-GSFC
David Brinza	JPL
Jim Mason	NASA-GSFC
Bill Kinard	NASA-LaRC
Tom Parnell	NASA-MSFC

Figure 4.0-1 Membership of the LDEF Materials Special Investigation Group.

5.0 LDEF ENVIRONMENTS

5.1 Meteoroids and Orbital Debris

A thorough survey of impacts on all sides of the LDEF was carried out by personnel from the Meteoroid and Debris Special Investigation Group (M&D SIG) upon return of LDEF to Kennedy Space Center. At least two impactors penetrated through 0.060-inch aluminum (ref. 19). Numerous penetrations through the silverized Teflon blankets occurred. Impacts were observed on a number of material test specimens. The distribution of impacts was extremely asymmetric, with several times as many impacts on leading edge surfaces as trailing edge surfaces. Man-made debris tended to impact toward the leading edge because debris particles in similar orbits generally did not have sufficient velocity to catch the LDEF.

Impacts with differing momentum reached different depths in a given material. For materials susceptible to atomic oxygen attack, as the material recessed, information about impact events may have been lost. Unprotected leading edge composites suffered severe recession, losing up to 5 mils of material in the worst case. The atomic oxygen fluence was predominantly at the end of the mission, therefore erosion would have erased most of the shallow impacts. Erosion rates vary with material and possibly with the angle of impingement. Impact counts on anodized aluminum have the most validity. This material did not erode, was present at all exposure angles, and provided the largest cross-sectional areas for collection.

Impacts on leading edge painted surfaces removed relatively large areas of loose paint in comparison with the size of the impact crater. This occurred because the paints' organic binder was lost due to atomic oxygen exposure prior to the time of the impact. Figure 5.1-1 shows an example of this loss of paint from the A276-paint-coated composite panel from AO038 experiment on tray F6. Notice that the entire paint layer was not lost; this may be a way of "dating" the time of impact because previously degraded layers were much more easily removed due to the impact, especially at distances relatively far from the impact site. Precise measurements of the depth of the removed layer relative to nearby unimpacted areas would be required. The example in figure 5.1-1 likely occurred quite early in the mission prior to atomic oxygen removing all the binder.

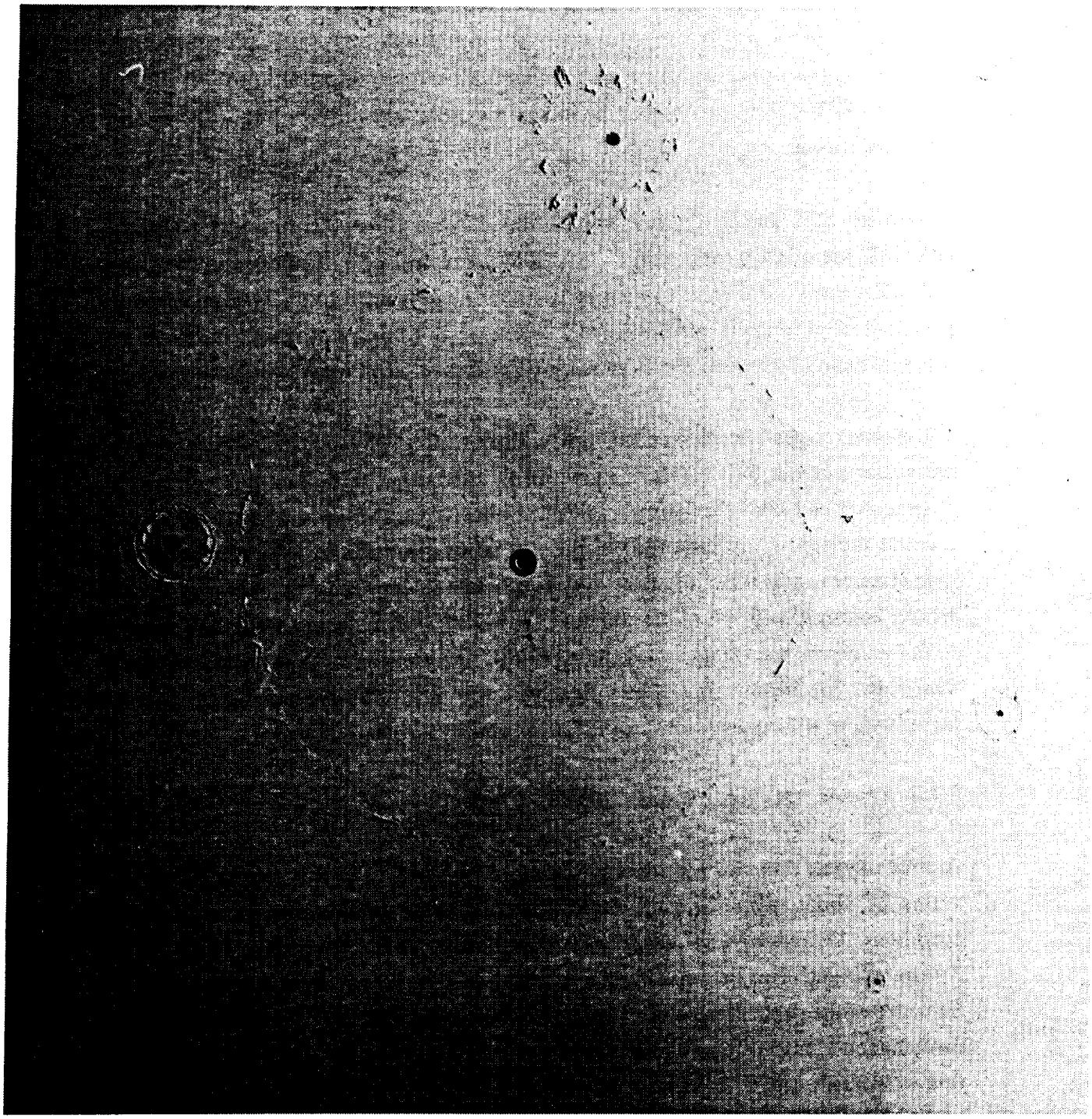

Figure 5.1-1. Painted composite panel from A0038 with impacts visible on one of the white painted areas. (Color figure C-1)

5.2 Atomic Oxygen

5.2.1 Atomic Oxygen Fluence Versus Incidence Angle

Atomic oxygen fluxes and fluences for LDEF have been calculated (ref. 10). A brief summary of the factors effecting the atomic oxygen exposure of LDEF experiments is presented herein.

Molecules in a gas in thermal equilibrium have a Maxwellian speed distribution characteristic of their temperature. At 1000K, a typical LEO temperature, the average molecular speed of atomic oxygen is 1.15 km/sec compared to an average speed of a spacecraft relative to the atmosphere of 7.24 km/sec at 400-km altitude in an easterly orbit. Thermal molecular motion effects atomic-oxygen flux on a surface at high incidence angles.

The atomic oxygen calculation developed by Boeing takes into account the effect of thermal molecular motion. This effect is shown in figure 5.2.1-1. The plot compares atomic oxygen flux corrected for thermal molecular velocity with values calculated by ignoring thermal molecular velocity. When thermal molecular velocity is considered, at the temperatures encountered, the calculations show that surfaces parallel to the ram direction receive approximately 4% of the ram flux. On LDEF, surfaces out to angles of about 105° from ram experienced atomic oxygen fluxes which caused measurable changes on specific materials. For incident angles less than approximately 87.5°, predicted atomic oxygen fluxes with or without the inclusion of thermal velocity are nearly equal.

5.2.2 Atomic Oxygen Fluence Versus Time

Atomic oxygen flux was not constant during the mission. The flux rate to the surfaces varies by about two orders of magnitude from solar minimum to solar maximum conditions. Decreasing solar activity caused atomic oxygen flux to decrease during the first 3 years of flight. This decrease in solar activity was sufficient to overcome the countering influence of the slight altitude decrease on the flux during this time period. Thereafter, the combination of increasing solar activity and decreasing altitude caused the atomic oxygen flux to increase rapidly. Figure 5.2.2-1 shows ram direction atomic oxygen fluence for LDEF expressed as a percent of total fluence for the mission. This plot reflects the combined effect on atomic oxygen fluence caused by varying solar activity and loss of altitude. Because the flight began near solar minimum conditions and ended essentially at

solar maximum, coupled with the decrease in altitude over the mission, the majority of the oxygen exposure occurred rather late in the mission. About 57% of the atomic oxygen exposure accumulated during the last 6 months of the LDEF mission. The last year of the flight accounted for roughly 75% of the total exposure.

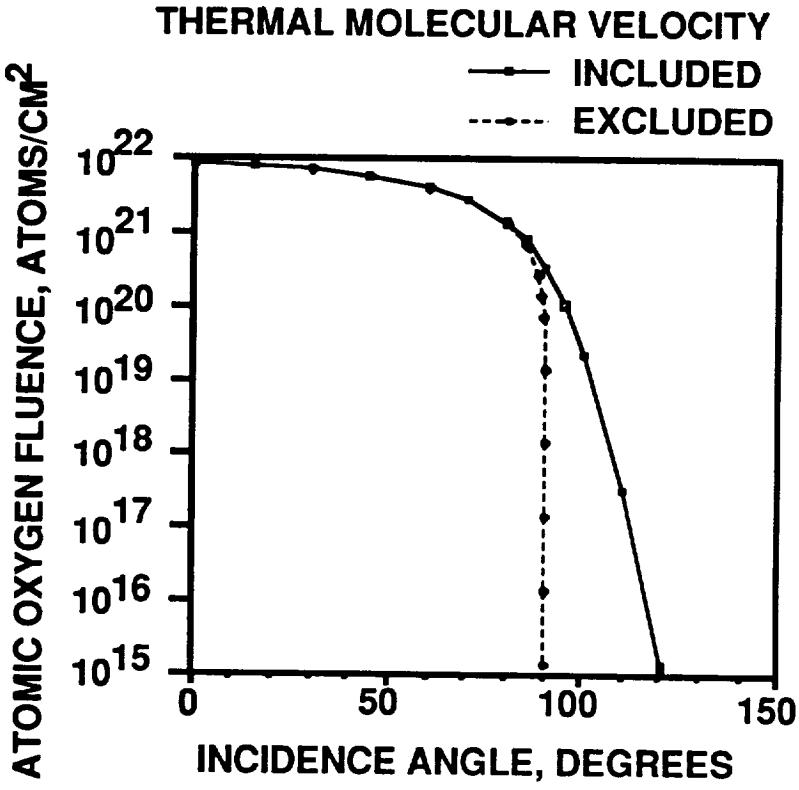

Figure 5.2.1-1. Atomic oxygen flux as a function of incidence angle.

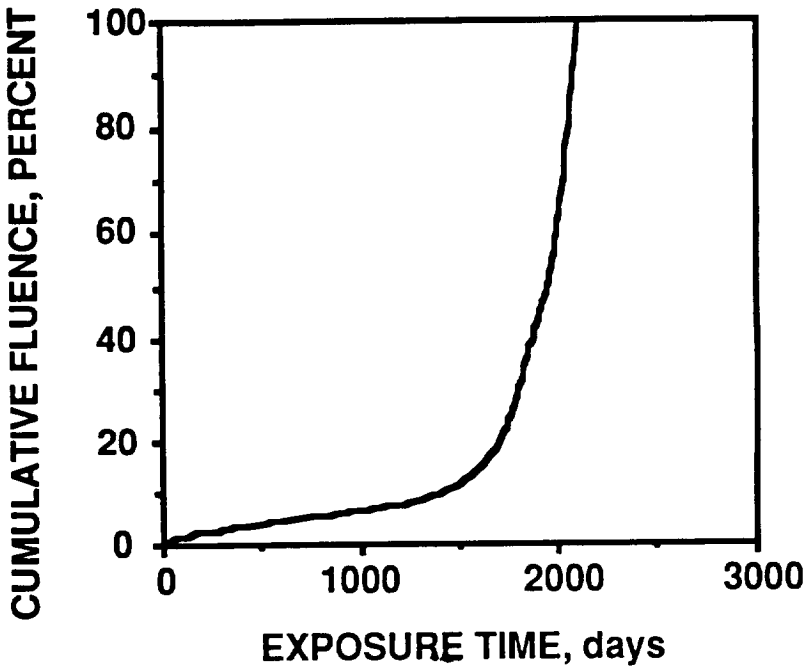

Figure 5.2.2-1 Percent of ram fluence as a function of mission time.

5.2.3 Total Atomic Oxygen Fluence

Figure 5.2.3-1 shows the mission total atomic oxygen exposure accumulated on each row and longeron during the LDEF mission. The view is of the Earth end of the spacecraft. In this view, row numbers increase in the clockwise direction. The ram direction lies between rows 9 and 10. All trays on a row received the same atomic oxygen fluence.

The data given in figure 5.2.3-1 includes an estimate of atomic oxygen exposure received by LDEF during an attitude excursion subsequent to retrieval. This excursion added to the fluence accumulated during orbital flight. The attitude excursion provided most of the atomic oxygen fluence on rows 1 through 3. Row 1 received a fluence of 1.2×10^{17} atoms/cm^2 prior to retrieval. Insignificant amounts of atomic oxygen impinged on the longeron between rows 1 and 2 through row 3 prior to retrieval, as shown in figure 5.2.3-2.

Because the vehicle was pitched so that the space end was forward of vertical (by 0.8°), trays on the space end of the vehicle received more atomic oxygen than did trays on the Earth end of the vehicle.

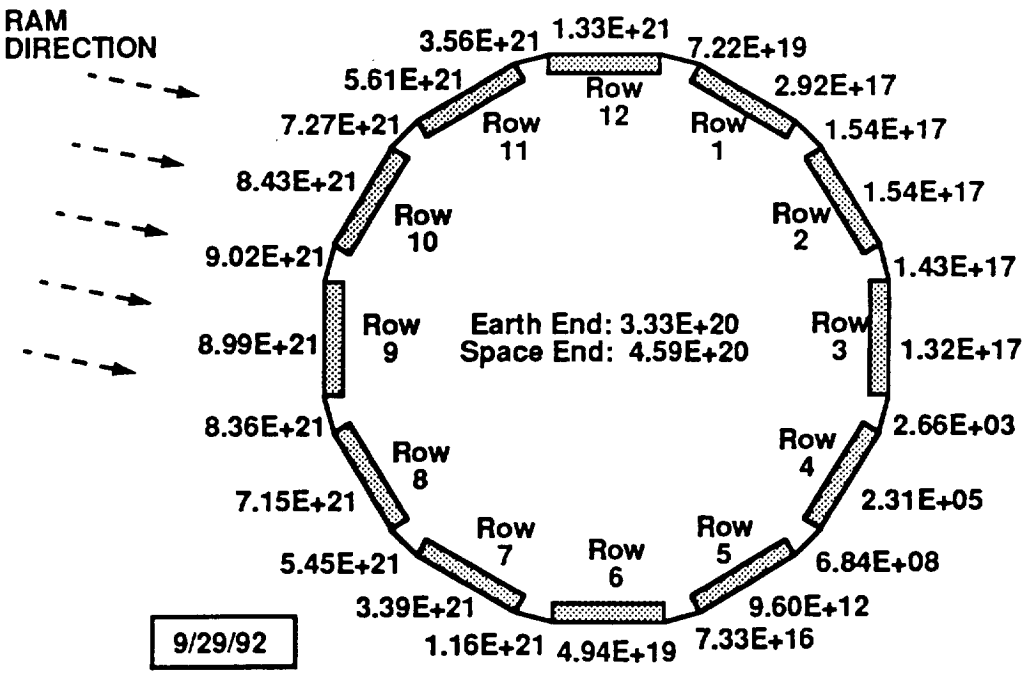

Figure 5.2.3-1 Atomic oxygen fluence as a function of angle from ram.

LOCATION	FLUENCE (atoms/cm^2)
row 1	1.7×10^{17}
longeron between rows 1 & 2	1.5×10^{17}
row 2	1.5×10^{17}
longeron between rows 2 & 3	1.4×10^{17}
row 3	1.3×10^{17}

Figure 5.2.3-2. Atomic oxygen fluence received by locations between rows 1 and 3 during attitude excursion following retrieval.

5.3 Solar Exposure

Figure 5.3-1 shows the fluence of solar ultraviolet radiation to the major surfaces of the LDEF. These calculated exposure levels include both direct solar and reflected Earth albedo. The values reported are Equivalent Sun Hours (ESH) of radiation normal to a given surface. The solar UV exposure rate is relatively stable in comparison with the variation of atomic oxygen flux. However, there are variations in the flux rates for specific vacuum ultraviolet wavelengths of 50 to 100% over the range of solar minimum to solar maximum conditions. Short term activity from solar flares can also temporarily increase the intensity of vacuum ultraviolet energy. This variability is not reflected in the calculation of hours of solar exposure.

Most of the Earth albedo data available were derived from satellite-borne infrared radiometer data. We have assumed, lacking better knowledge, that the spectral dependence is approximately constant from the infrared to the ultraviolet. Based on this assumption, we have used the monthly average albedo data derived from Nimbus 7 short wave radiometer measurements of Smith et al. as updated by Rutan (ref. 20) to calculate an annual average Earth albedo under the LDEF orbit of 0.246. Maps of annual and seasonal Earth albedo are presented in reference 21. Bourassa and Gillis (ref.15) used this albedo value to calculate direct solar and Earth reflected solar exposure to LDEF. Figure 5.3-2 summarizes solar exposure to unshielded LDEF surfaces. Figure 5.3-3 is a plot of solar irradiance at the top of the atmosphere taken from reference 22. The best measurement of the total solar irradiance at the top of the atmosphere is 1368 ± 7 W/m^2 (ref. 22).

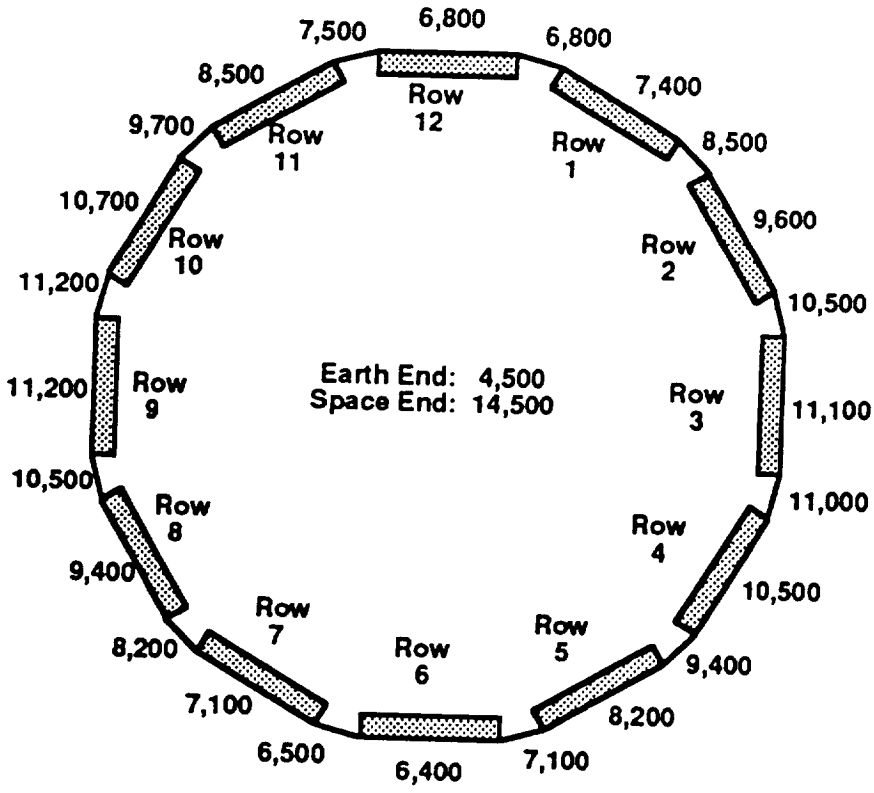

Figure 5.3-1 Solar UV fluence as a function of angle from ram.

Position	Total Solar Exposure in ESH	% of Total Exposure Due to Earth Reflection
Row 1	7400	14
Row 2	9600	10
Row 3	11100	9
Row 4	10500	10
Row 5	8200	12
Row 6	6400	16
Row 7	7100	14
Row 8	9400	11
Row 9	11200	9
Row 10	10700	9
Row 11	8500	12
Row 12	6800	13
Space End	14500	0
Earth End	4500	73

Figure 5.3-2. Solar exposure to LDEF surfaces in Equivalent Sun Hours (ESH).

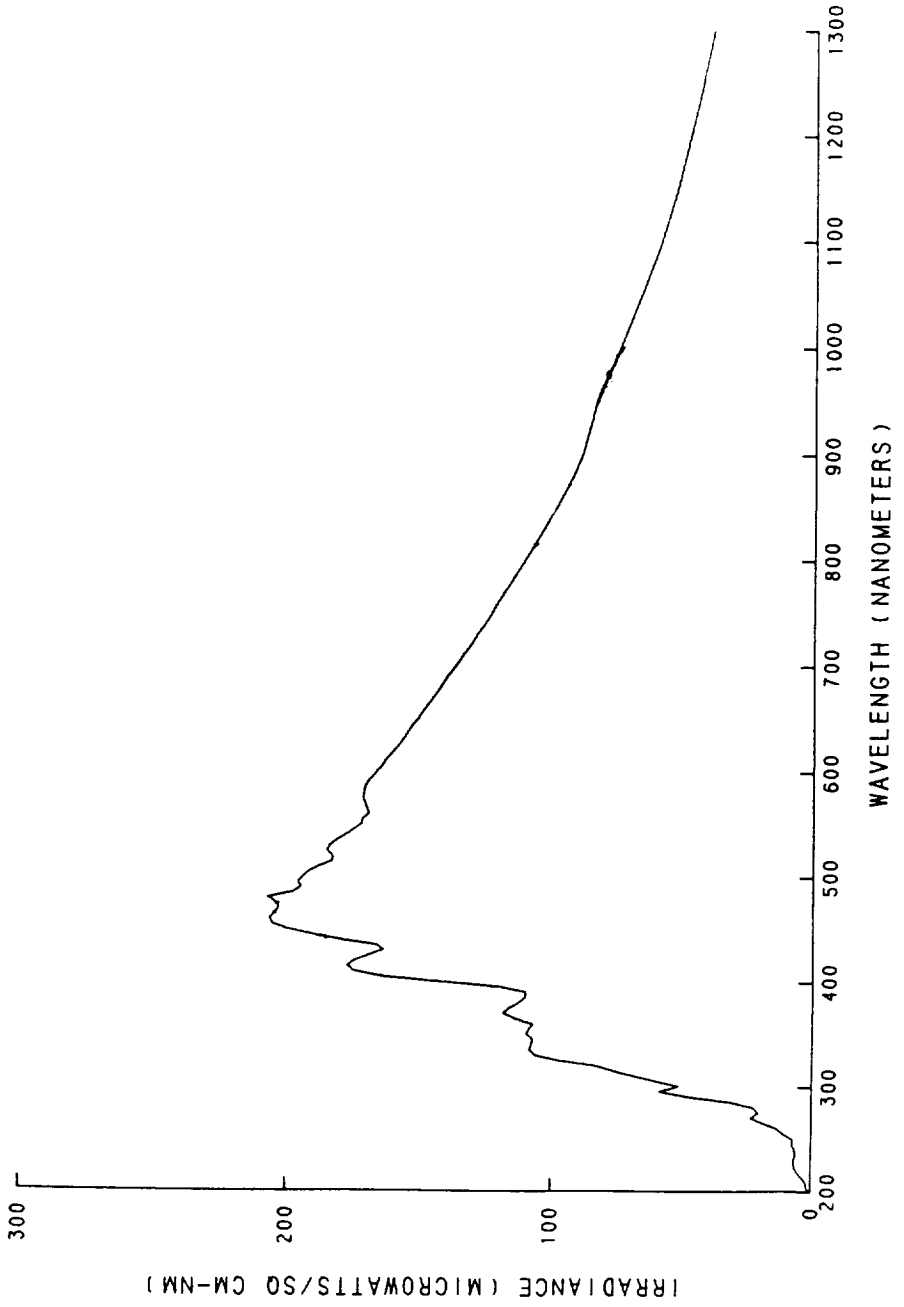

Figure 5.3-3. Solar Irradiance at the top of the atmosphere. This figure is taken from figure 2.3 of the Solar Cell Radiation Handbook, JPL Publication 82-69, November, 1982.

5.4 Particulate Radiation

The LDEF altitude range was significantly below the trapped radiation belts, in a non-polar orbit, and experienced its primary exposure to protons and electrons during its passages through the South Atlantic Anomaly. No deleterious effects on LDEF materials have been identified as being caused by the particulate radiation dose. Armstrong and Colborn (ref. 23) report detailed comparisons between LDEF data obtained by use of Thermoluminescent dosimetry (TLD) measurements and models for trapped proton and trapped electron fluxes and trapped proton directional distributions. Measured dose levels of electrons and protons, in comparison with selected model predictions, is presented in detail in the proceedings of the 2nd Post-Retrieval Symposium (ref. 4).

5.4.1 Solar Wind

Solar electrons and protons were not a major factor due to the low altitude of the spacecraft. The majority of the experiments were passive in nature. Those that were active did not require substantial amounts of electronic hardware, or operated for only the first $1^1/_2$ years, and/or were well shielded. LDEF was a large structure with the necessary electronics mounted on the back of the experiment trays (i.e., on the interior of the spacecraft). These factors minimized the potential for single-event upsets which could scramble information, induce unplanned signals in electronics hardware, and therefore send spurious commands to active systems.

5.4.2 Cosmic Rays

The AO178 and M0001 experiments collected the large majority of the world's data on heavy nuclei cosmic rays impacts on spacecraft. The total dose was extremely low and the LDEF was a largely passive spacecraft. Except for the tracks left in the detectors, no practical changes in any materials properties due to cosmic rays were observed. Lexan detector stacks were used to record cosmic ray events. Areas of the lexan stack on the space end were directly exposed to the Sun after failure of adhesive tape holding the protective thermal blankets. The solar-induced darkening of the lexan concealed any damage due to cosmic rays in these exposed areas.

5.5 Thermal Cycling

LDEF completed one thermal cycle for each orbit around the Earth for a total of 32,422 thermal cycles. On-orbit measurements taken in several locations, for the first 390 days, showed relatively moderate temperature ranges on the interior, typically 52° to 89°F, with a worst case of 35° to 134°F. Exterior surface temperatures varied depending on the optical properties of the specific hardware in each tray. Stainless steel calibration tubes on experiment AO180 cycled between -30° and 140°F during the first 2 years of the mission. Figure 5.5-1 shows a table of LDEF temperature ranges at selected locations around the LDEF. THERM, in figure 5.5-1, refers to the LDEF experiment which monitored on-orbit temperatures at selected locations (ref. 24). Further details of thermal systems performance are found in the Systems Special Investigation Group report of April 1992. (ref. 11)

LDEF Location	Temperature Design Limits (°F)	Measured from THERM Experiment (°F)	Post-Flight Calculated (°F)
Interior average	10 to 120	52 to 89	58 to 89
Structure (rows 6/12)	-10 to 150	35 to 134	39 to 136
Structure (rows 3/9)	-10 to 150	N/A	53 to 100
Structure-Earth end	10 to 135	56 to 103	57 to 104
Structure-space end	10 to 135	60 to 90	64 to 96

Figure 5.5-1. LDEF temperature ranges for selected locations on the spacecraft.

6.0 CONTAMINATION

6.1 Particulates

Particulate contaminants were identified from pre-flight exposure sources, from Space Shuttle sources, from on-orbit material degradation, and from post-flight exposures. These sources are discussed in detail in the Proceedings of the 1st LDEF Post-Retrieval Symposium (refs. 25-26). Except for introduction of sources of stray light scattering on optical materials, small particulates had no effect on materials performance. Where large-scale failure of blanket materials occurred, with subsequent distribution of small particulates, effects on nearby surfaces were often significant. The part of the black radiator panel on F9 which was covered by the failed aluminum backing from an adjacent thermal blanket underwent large color changes. Lexan exposed by failure of the adhesive tape on M0001 and subsequent flexing of the blanket material was severely discolored.

Failed blanket materials from trays D9 and D10 distributed small particles of aluminum over many nearby surfaces. It is hard to quantify the effects for these occurrences because the time of failure is not known, and the particle distribution probably changed with time.

6.2 Molecular Films

The consideration of molecular contaminant films should be separated into what happened to carbon-based (organic) material and what happened to silicon-containing material. Organics exposed to atomic oxygen are removed rather rapidly. Exposure to atomic oxygen caused silicone surfaces to oxidize to silicates. The carbon based functional groups of the silicones were easily oxidized and removed by abstraction processes, leaving the Si-O portion of the polymer chain. Subsequent oxygen atoms added to the Si-O chains, producing a glassy, non-volatile surface. Silicone remaining trapped beneath the surface darkened under UV exposure.

Within the consideration of each material type there are the questions of defining the contamination sources; their sources' quantity, location, and thermal/environmental exposure history. Deposition surfaces must be identified as well as the deposition surfaces' temperature and location relative to the sources. their temperature, and their locations relative to the sources, must be identified. Post-deposition processes must be characterized relative to the exposure of the deposition surface. Investigation of contaminant deposits on LDEF is a continuing activity.

6.2.1 Silicon-Based Molecular Contamination

Collectively, there were many sources of silicon contamination on LDEF. Some areas were contaminated prior to flight, silicone-based materials outgassed during flight, and the Space Shuttle was a potential source during both deployment and retrieval. Post-flight contamination must also be considered. The aforementioned sources are in addition to the processes which occurred during the 69 months in orbit.

In addition to silicone-based coatings and adhesives used on several experiments, a number of other materials used have silicon present as a basic constituent, or left from the manufacturing process. The S13 type and A276 paints contain silicon, the stainless steel bolts have 1 to 2% silicon by weight in the alloy, and the copper grounding straps have a silicone release film. These facts mask the attempt to evaluate silicon contamination on these particular surfaces. The silverized Teflon (Ag/FEP) and chromic acid anodized surfaces, which together covered >78% of the spacecraft exposed surfaces, are materials which contain no silicon. These materials are excellent witness plates when attempting to determine the quantity of silicon deposited.

The gasket seals used on the ground handling tray covers were pre-flight sources of silicones and compromised certain areas of the anodized tray surfaces. This material was not space qualified and outgassed extensively, with a total mass loss (TML) of over 3%. A solvent extraction process removed about 2.5% (by weight) of material from a sample of gasket material, showing the presence of many potentially volatile species. The tray covers were on the experiment trays for an extended period of time prior to flight (months) allowing sufficient time for volatile species in the gasket material to diffuse to the surface, volatilize, and deposit on the (line-of-sight) adjacent external surfaces of the trays.

Post-flight photos of external tray surfaces from leading edge trays (some with tray covers reinstalled so the close proximity is obvious) show contamination patterns, which are just the width of the gasket material, on the external tray lips and sides, and at the tray corners where these surfaces were in direct line-of-sight to the gasket material. These patterns appear both on trays which were known to contain sources of silicone and on trays which were known not to contain silicone sources. The discoloration patterns show distinct orientation effects which correlate to their respective environmental exposures. Examples of this phenomenon are included in section 7.2, which contains post-flight photos. Trailing edge locations do not show the same intense darkening, implying that the mechanism involves both solar exposure and atomic oxygen. Faintly discolored areas also appear along the tops of the tray lips where the gaskets were in contact with the tray surface prior to flight.

Electron Spectroscopy for Chemical Analysis (ESCA) measurements of surface silicon on a variety of materials, which did not originally contain silicon, show silicon present in amounts ranging from 0.1% (lower limit of detection) to over 30%. The amounts present are extremely exposure and location dependent. Interpretation of results are complicated by local conditions, i.e., multiple silicone sources within the same tray, vents, outgassing by adjacent specimens, and changes in exposure conditions over time (such as failed materials moving and covering or partially shielding surfaces). Tray clamp surface studies at Virginia Polytechnic Institute and State University (ref. 27) generally showed larger percentages of silicon on leading edge clamps relative to trailing edge clamps. Clamps from space and Earth end locations also tended to be relatively high in silicon surface content.

Examination of multiple locations on an individual space end clamp (H6-11) and on an Earth end clamp (G6-5), which were each selected for close proximity to a vent, showed very high surface silicon content. Figure 6.2.1-1 shows the results of the surface analysis for these clamps.

Light scattering measurements using the bi-directional reflectance distribution function (BRDF) were used on selected clamps to try to correlate BRDF measurements with silicon content. Light of a chosen wavelength is directed onto a surface at a given angle and the intensity of reflected light is measured at selected scattering angles. Figures 6.2.1-2 and 6.2.1-3 are diagrams showing the location of individual measurements on clamps G6-5 and H6-11, respectively. The locations of the ESCA measurements on clamps G6-5 and H6-11 were chosen to provide a sampling of visually different areas. Surface analysis showed that the range of silicon contents was not sufficient to develop a correlation. Bolt heads on the clamps also influenced the deposition patterns. Auger studies on selected specimens have all demonstrated that any contamination layer is extremely thin, 50 to 200Å.

ESCA measurements on black chrome plated panels from the Earth end of LDEF indicated significant silicon content (ref. 12). Detailed results of a study of surface conditions on this material are covered in section 8.3, thermal control materials.

Reported results from M0003 and AO133 show significant deposition of silicon due to space exposure (refs. 28-29).

X-ray photoelectron spectra of Kapton from AO133, located on the space end, show 8.8% silicon on the surface. Control specimens for this experiment showed no silicon present (ref. 28).

Solar absorptance changes on fused silica mirrors on both the leading and trailing edges are relatively small (< 0.04 in all cases) (ref. 30).

Clamp	Location	%Si	%C	%O	%Al
G6-5	1	29.58	9.68	51.12	9.62
G6-5	2	14.71	8.69	37.98	38.61
G6-5	3	11.96	2.66	37.63	47.75
G6-5	4	9.26	4.34	33.48	52.92
G6-5	5	27.79	8.11	49.58	14.52
G6-5	6	27.54	15.95	47.49	9.02
G6-5	7	25.12	19.28	43.53	12.06
G6-5	8	24.86	6.87	47.45	20.82
G6-5	9	12.56	4.66	36.99	45.79
G6-5	10	10.25	7.47	33.76	48.53
G6-5	11	11.90	9.36	33.51	44.23
H6-11	1	25.59	22.95	40.18	14.29
H6-11	2	19.79	54.36	23.76	2.09
H6-11	3	31.26	12.05	51.81	4.87
H6-11	4	28.72	15.01	49.28	6.99
H6-11	5	29.60	6.75	52.21	11.44
H6-11	6	29.69	10.19	52.00	8.12
H6-11	7	27.93	8.76	48.97	14.34
H6-11	8	28.15	9.18	51.92	10.75
H6-11	9	28.27	9.28	49.19	13.25
H6-11	10	28.52	25.12	42.13	4.23
H6-11	11	29.19	5.83	51.99	12.99
H6-11	12	31.29	10.17	52.91	5.63
H6-11	13	32.96	12.45	50.69	3.90

Figure 6.2.1-1. Elemental percent on aluminum tray clamps G6-5 and H6-11 as determined by ESCA.

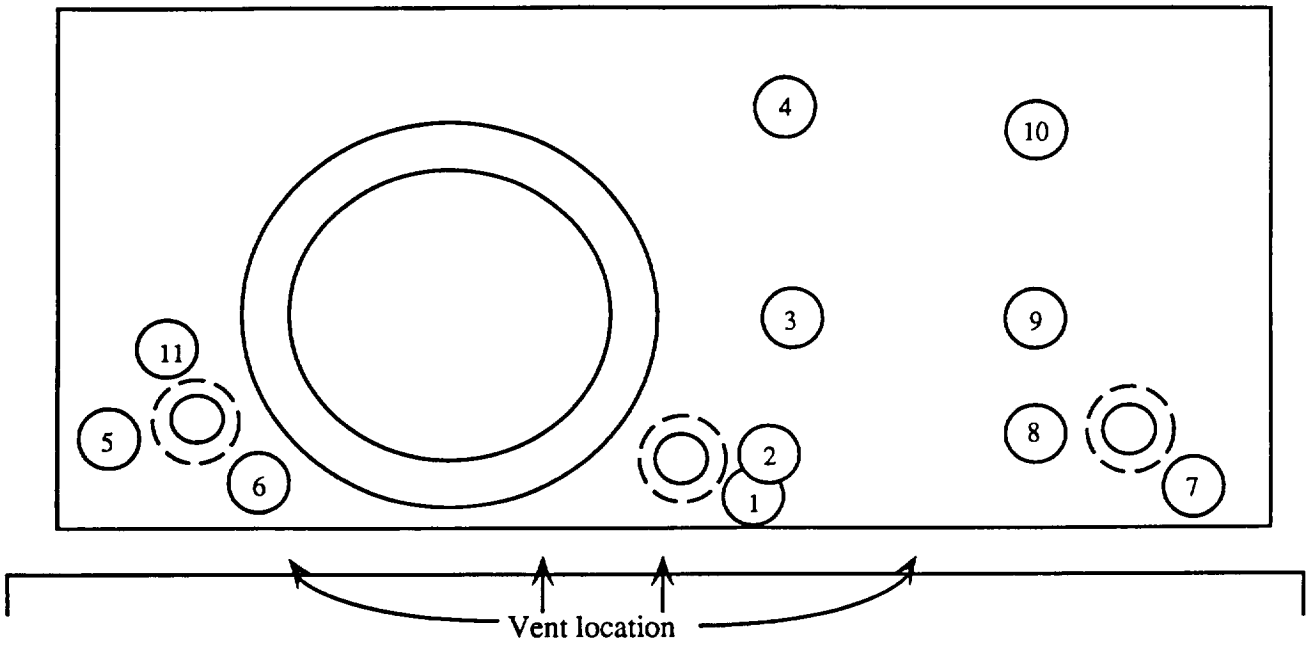

Figure 6.2.1-2. G6-5 tray clamp showing BRDF, reflectance, and surface analysis measurement locations.

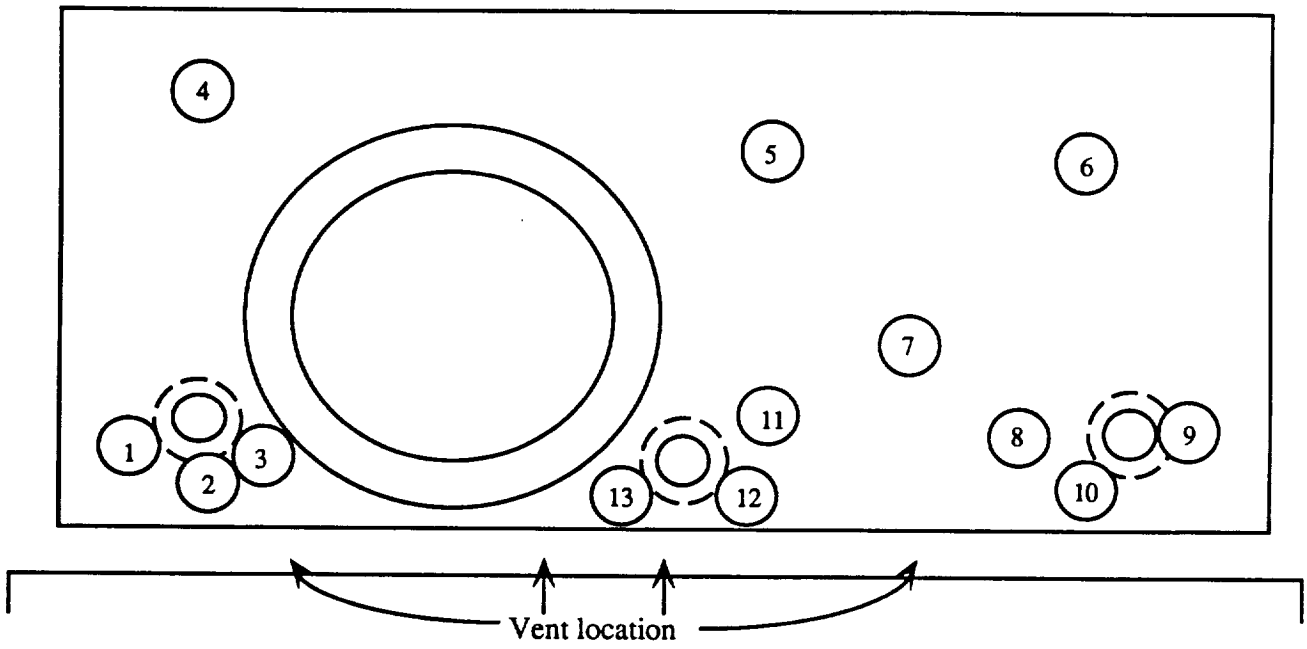

Figure 6.2.1-3. H6-11 tray clamp showing BRDF, reflectance, and surface analysis measurement locations.

Figure 6.2.1-4 shows absorptance data from The Aerospace Corporation for SiO_2/Al second-surface mirrors flown on LDEF (ref. 30). Changes on these mirrors are due to contamination deposits. The SiO_2 is stable in this environment.

SPECIMEN	SOLAR ABSORPTANCE
Lab control	0.103
Leading edge, 300 days	0.107
Leading edge, full mission	0.112
Trailing edge, 300 days	0.113
Trailing edge, full mission	0.136

Figure 6.2.1-4. Solar absorptance (α) from SiO_2/Al second-surface mirrors flown on experiment M0003.

6.2.2 Carbon(organic)-Based Molecular Contamination

Characterization of individual material surfaces by ESCA gave an indication of the extent of carbon based (organic) contamination on LDEF. In virtually every case where auger profiles were made, the thickness of the film was quite thin, a few hundred Å or less. Any material surface exposed to a ground environment, even in a clean room, will show some organic material (carbon) in an ESCA analysis. Those surfaces exposed to atomic oxygen showed relatively less carbon in the ESCA profiles than surfaces not exposed to atomic oxygen during flight. Pre-flight and on-orbit deposited carbon on leading edge surfaces was removed by oxidation. Only the post-flight contributions were left on such surfaces. Examination of tray clamp stainless steel bolt heads shows very clearly the pattern of organic contamination around the LDEF (ref 12). Bolts from locations between the rows 3 and 4 longeron to the longeron between row 5 and 6 show the highest carbon percent in their ESCA spectrums. For all other locations, even those which received the minimal doses of atomic oxygen during the brief post-retrieval attitude excursion, the percent carbon in the ESCA spectra is substantially lower.

Except for deposition thick enough to reduce transmission on optical windows and mirrors, organic-based deposits on ram facing surfaces should generally not be a problem. The possible exception is organics trapped under silicone deposits which could contribute to

darkening by photoreactions with solar radiation. This possibility has not been thoroughly investigated using thin films from LDEF. For wake side surfaces, not exposed to atomic oxygen, all contaminant exposures are accumulated; pre-flight, on-orbit, and post-flight. The brief atomic oxygen exposure during the post-retrieval attitude excursion was sufficient to remove most of the organic-based contamination on surfaces not previously exposed to atomic oxygen.

6.2.3 Bi-directional Reflectance Distribution Function (BRDF), Reflectance, and Surface Analysis Measurements on Selected Hardware

A portable, fixed wavelength BRDF device was used to measure surface characteristics on selected tray clamps and an FEP surface from LDEF. An attempt was made to correlate the BRDF and reflectance measurements results with the amount of Si present on the surface. However, the silicon contamination levels reported in figure 6.2.1-1 did not vary enough to allow a correlation to be made.

Results of the BRDF and reflectance measurements on the aluminum surfaces of tray clamps H6-11, G6-5, F6-8, H7-2, Ag/FEP from C8, and white paint buttons from H3-11 and H1-11 are tabulated in appendix A. The locations of these measurements on clamps G6-5 and H6-11 match the surface analysis measurements locations on the clamps shown in figures 6.2.1-2 and 6.2.1-3.

7.0 VISUAL OBSERVATIONS

The on-orbit photographic survey provides a unique record of the condition of all hardware after a long-term exposure in LEO. The appearance of the failed materials is documented prior to the turbulent conditions of reentry, which removed particulate contaminants from some surfaces, deposited those same contaminants in new locations, altered the positions of thin films and blankets, and completed the destruction of materials severely damaged by the flight exposure conditions. The appearances of numerous coatings are of interest because of the concern of molecular oxygen induced bleaching upon return to the ground, changes due to moisture re-adsorption, and deposition of fresh films of organic-based contaminants.

Section 7.1 highlights some of the observations made from the on-orbit photos. Particular emphasis is placed upon observations which may be of practical interest to engineers who design and build spacecraft intended for long-term use. Following the on-orbit photos is a selection of post-flight photos (sec. 7.2) chosen to emphasis key aspects of the materials investigations carried out by the MSIG.

The on-orbit videos also provide a unique perspective on the performance of selected materials. The collection of particles observed in the LDEF wake is clearly visible because of the reflection of sunlight from individual pieces as the particles (apparently) rotated. The particulate "cloud" is trailing the LDEF. The failed materials, such as the aluminized Kapton and Mylar, were all on the leading edge. This raises the question of what mechanism brought the particulates into the LDEF wake, and is this an expected phenomenon for all spacecraft in long-term LEO? This question is at least of potential interest to the International Space Station, which will be periodically re-boosted, perhaps changing orientation, even if only temporarily, in the process. Effects of rapid temperature changes as the LDEF travels in and out of the Earth's shadow are visible on the video as the areas of the velcro fastened AO178 Ag/FEP blankets not in contact with the velcro appear stretched under solar exposure.

7.1 On-Orbit Photographic Survey

Upon capture of the LDEF with the Space Shuttle remote manipulator system, a $4^1/_2$ hour photographic survey was undertaken to document the condition of each tray. Close-ups of each tray were obtained in addition to overall photos of each row and the Earth and space ends. The subsequent ground photos allowed determination of any changes due to reentry.

The on-orbit photo of C-8 in figure 7.1-1 shows the effects of multiple impacts. Row 9 (leading edge) is to the right in this photograph. At the center of each dark spot is a penetration of the blanket. Each dark spot associated with an impact is both a record of, and result of, the shock created by the impact. The discoloration is not due to atomic oxygen attack because the same ring patterns are seen on trailing-edge blankets. Darkening of silverized Teflon by mechanical deflection was known prior to LDEF. The physical structure of the silver layer is altered, changing its appearance.

The "L" shaped angle bracket in the upper right corner of figure 7.1-1 is one of the few unanodized tray clamps. This clamp is distinctly darker in appearance from the more typical anodized clamps. This darker appearance is due to its as-manufactured condition and was not due to LEO exposure. The poorer optical properties of untreated aluminum was the reason for anodizing the structure.

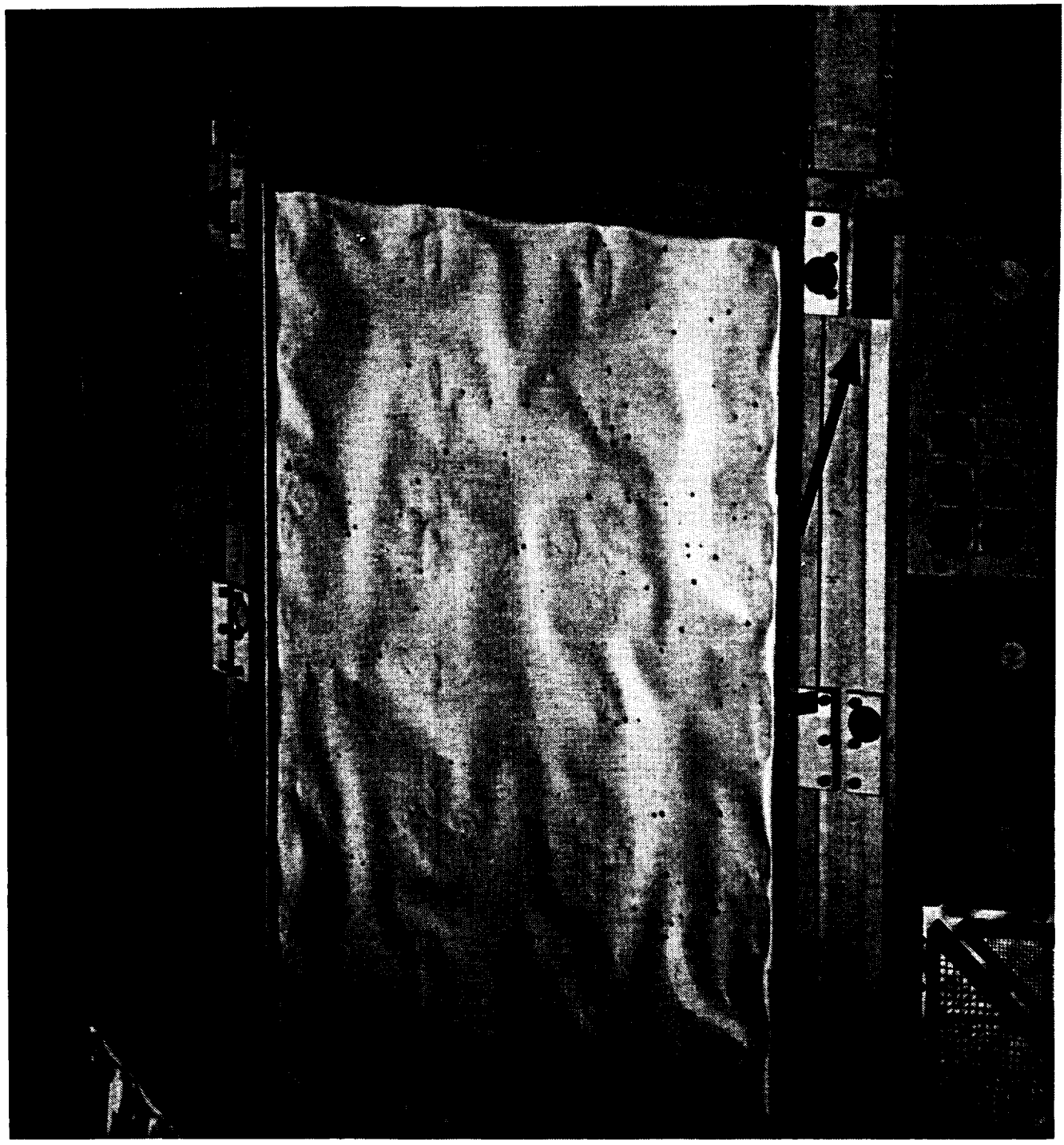

Figure 7.1-1. NASA on-orbit photo of thermal control blanket on tray C8, also showing the unanodized tray clamp on C9. (Color figure C-2)

The NASA on-orbit photo in figure 7.1-2 shows the center tray E10 with a particularly large damage area toward the row 11 side of the tray. A second large damage area, associated with underlying velcro, is visible toward the center of the tray. Impacts at locations on the silvered Teflon blankets with underlying velcro tended to produce much larger damage areas in comparison with impacts at unsupported locations. This is likely due to reflected shock waves from the underlying hardware.

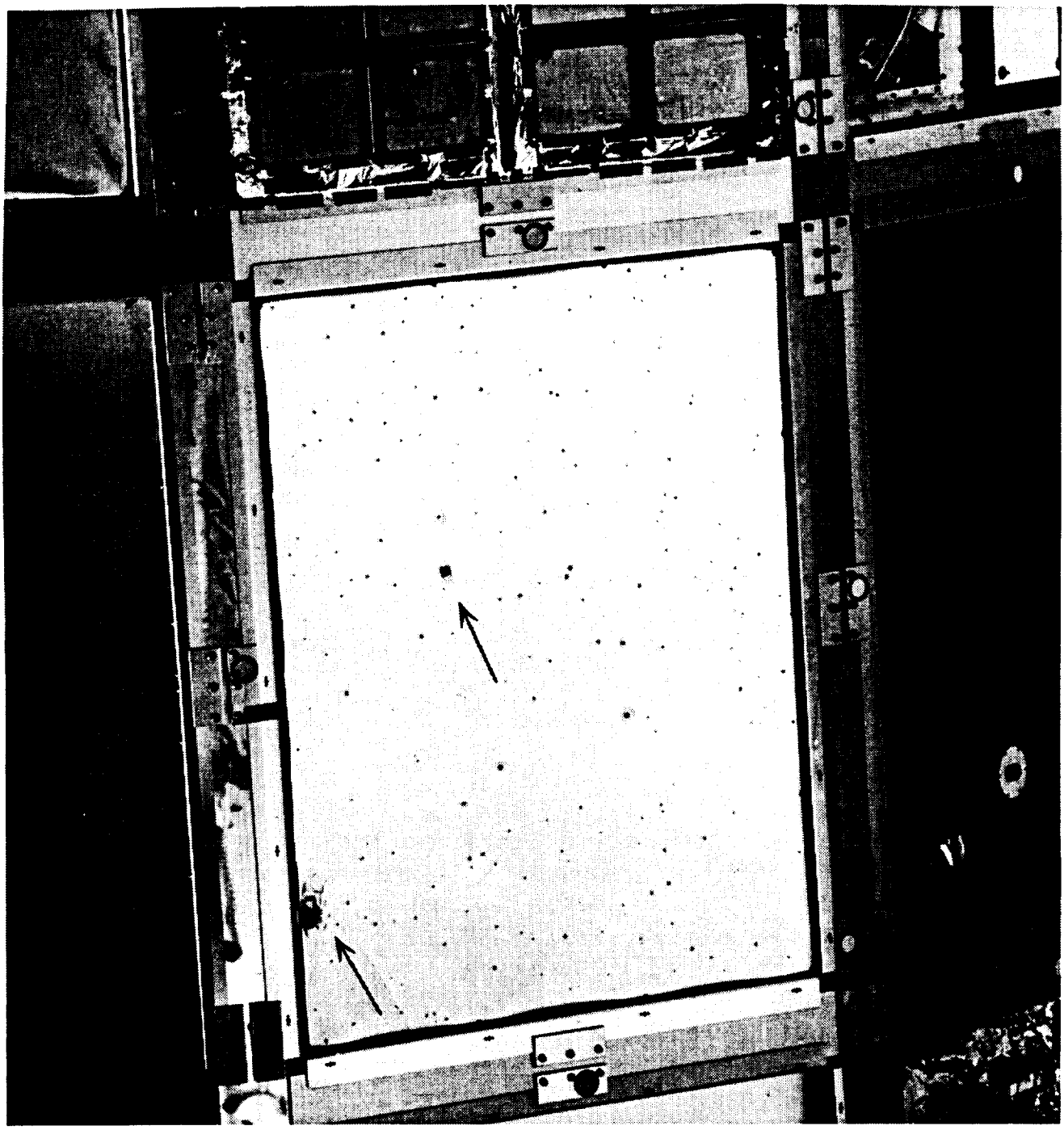

Figure 7.1-2. NASA on-orbit photo of tray E10 showing large impacts on areas supported by velcro. (Color figure C-3)

The NASA on-orbit photo in figure 7.1-3 shows tray A9, containing experiment S0069. The streaking of the thermal control material due to solar-induced darkening of adhesive which had bled through cracks in the silver-Inconel layer is visible. The adhesive is trapped between the FEP and silver layer. The cracks were formed during the application process. The silverized Teflon is also very diffuse due to the roughening of this surface by atomic oxygen. The rough texture gives the material the diffuse, milky appearance. This is also shown by the white, milky appearance of blanket A10 (to the right).

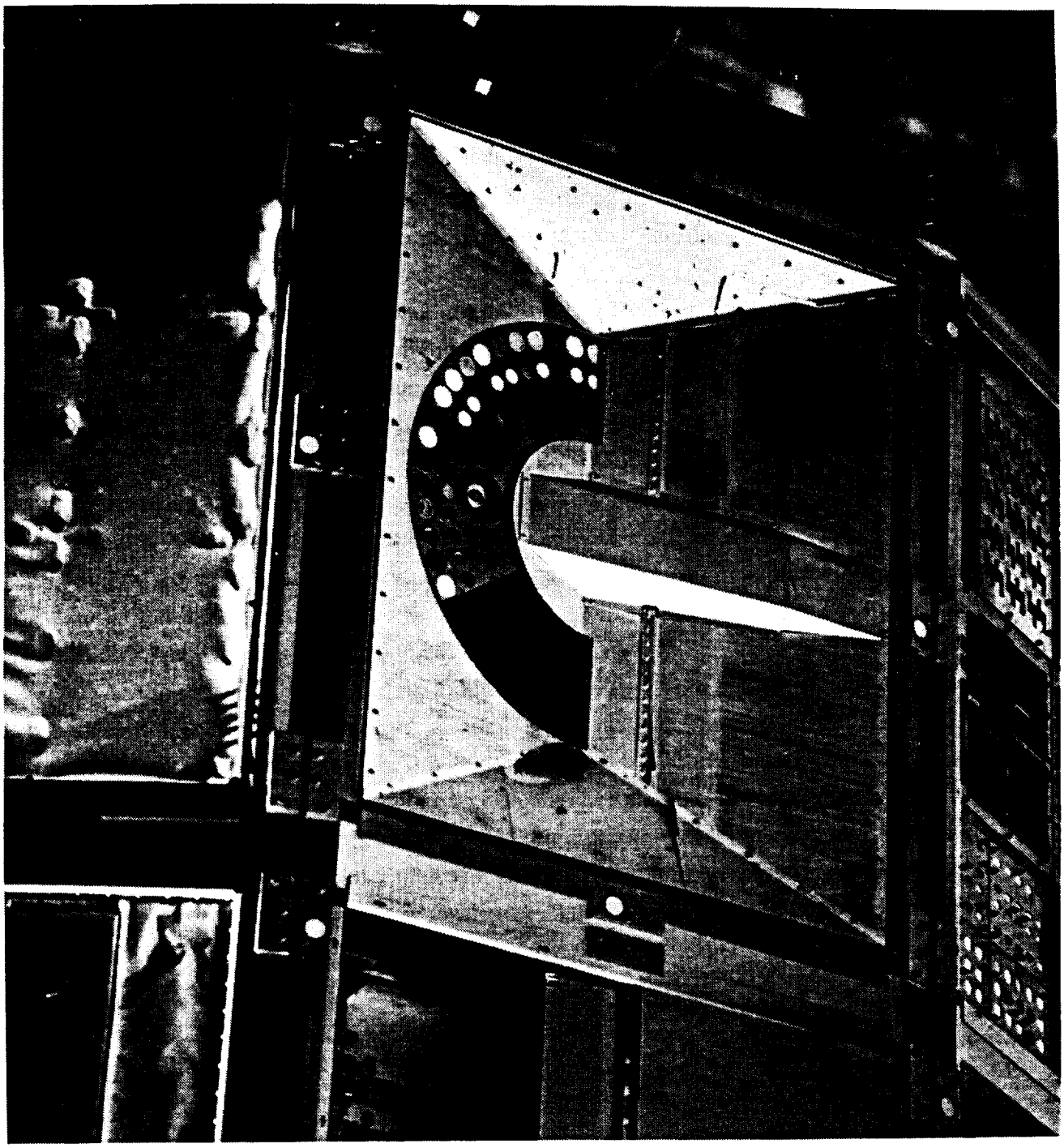

Figure 7.1-3. NASA on-orbit photo of tray A9, containing experiment S0069.

(Color figure C-4)

Figure 7.1-4 shows a NASA on-orbit photo of tray B9. This tray contained a number of composite specimens, an environmental exposure control canister (EECC), shown closed at the top of the photograph, and a selection of polymeric thin films. The photo shows only remnants of the Mylar, Kapton, and FEP thin films.

There were five EECCs on LDEF, each of which opened after 10 days on orbit, remained open for about 10 months, and then were closed for the duration. The EECCs were flown on rows 3, 4, 8, and 9. The French Cooperative Passive Payload (FRECOPA) experiment at location B3 also had 3 canisters which opened and closed on the same schedule.

The two M0003 EECCs opened in three stages, at controlled time intervals, providing a set of distinct exposure levels. The exposure sequences for the five EECCs is shown in figure 7.1-5. The column titled "Exposure" in this figure shows the fraction of the canister sample area directly exposed during each time period.

Because the EECC's were opened for the first 10 months of the mission, the specimens in the leading edge canisters received relatively small doses of atomic oxygen. Similarly the solar exposure levels were also small fractions of the mission totals for these rows. Figure 7.1-5 also shows the exposure levels for each EECC during the time period they were open, from day 10 to day 297 of the mission. The M0003 canisters on rows 4 and 8 were opened in stages, starting at the 10 day mark with a partial opening, further opened 9 weeks later, and finally completely opened at 19 weeks. For the canisters which opened in stages, the visual appearance of the three areas of differing exposure level was quite different, with the area of maximum exposure being the most discolored. This is consistent with rapid outgassing of material in the first several weeks of the mission, followed by UV fixing when the material redeposits on a surface. The lighter color of the other areas is due to decreased outgassing at the time which these surfaces were exposed.

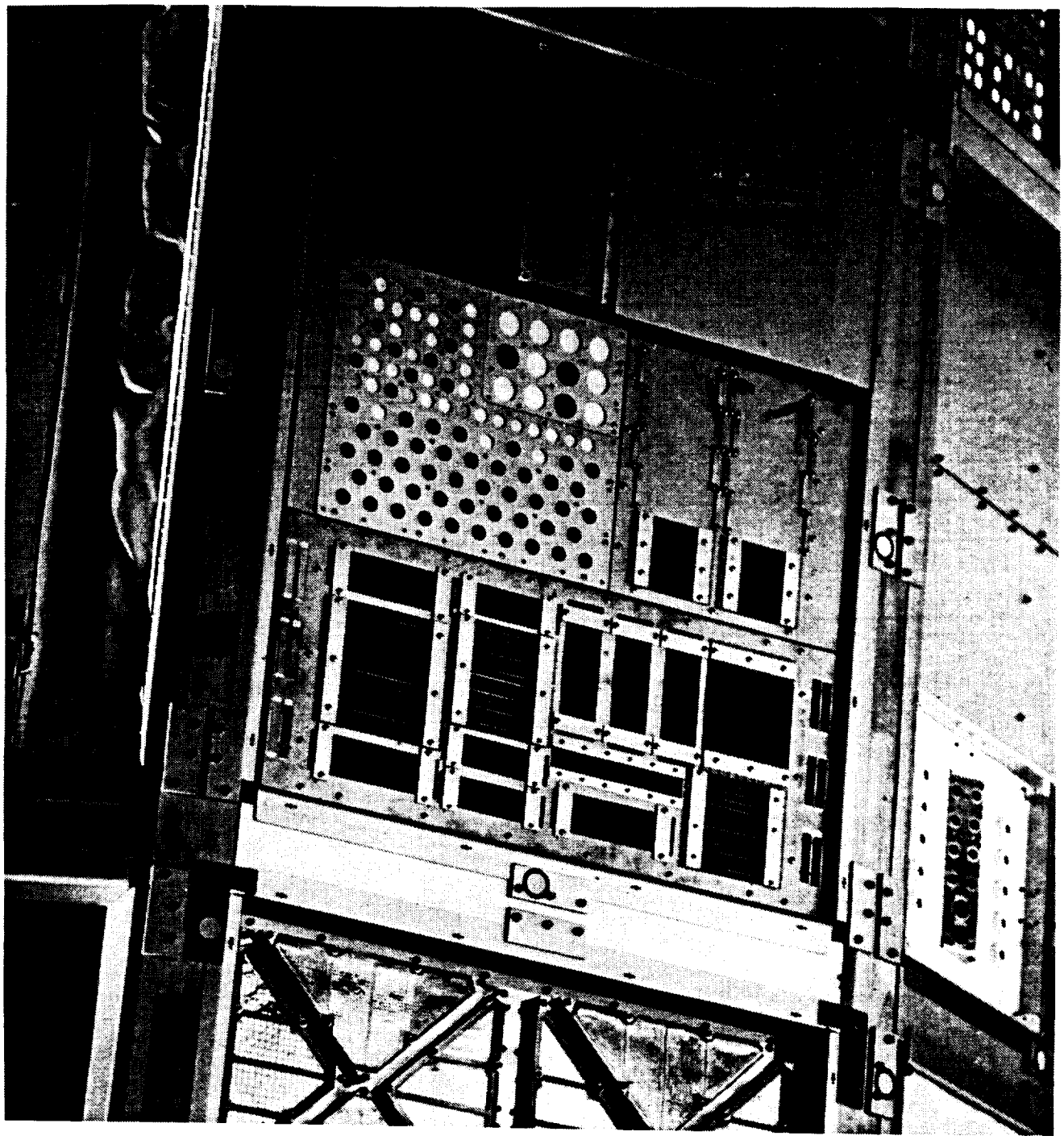

Figure 7.1-4. NASA on-orbit photo of experiments on tray B9, including the closed EECC. (Color figure C-5)

EECC Locations	Fraction of Canister Exposed	Exposure Start Date	Exposure End Date	Solar Exposure (Equivalent sun hours)	Atomic Oxygen Fluence (10^{20} atoms/cm^2)
B-9	100%	April 21, 1984	Jan.26, 1985	1505	2.54
C-2	100%	April 21, 1984	Jan. 26, 1985	1339	-
E-3	100%	April 21, 1984	Jan.26, 1985	1515	-
D-4	75%	April 21, 1984	Sept. 15, 1984	1398	-
D-4	87.5%	Sept. 15, 1984	Nov. 26, 1984	1162	-
D-4	100%	Nov.26, 1984	Jan. 26, 1985	846	-
D-8	75%	April 21, 1984	Sept.15, 1984	1244	2.02
D-8	87.5%	Sept. 15, 1984	Nov. 26, 1984	1078	1.66
D-8	100%	Nov.26, 1984	Jan. 26, 1985	823	1.22
FRECOPA (B-3)	100%	April 21, 1984	Jan. 26, 1985	1516	-

Figure 7.1-5. Exposure sequences, dates, atomic oxygen and solar exposure levels for EECC and FRECOPA canisters flown on LDEF.

A NASA on-orbit photo of tray A7, containing Rockwell experiment AO175 composite panels is shown in figure 7.1-6. The frame holding each panel was alodined. The alodine appeared discolored relative to pre-flight photos, but no quantitative pre-flight data exists for comparison. The yellow identification markings visible on the composite panels were found to be pigment, the binder having been removed by atomic oxygen.

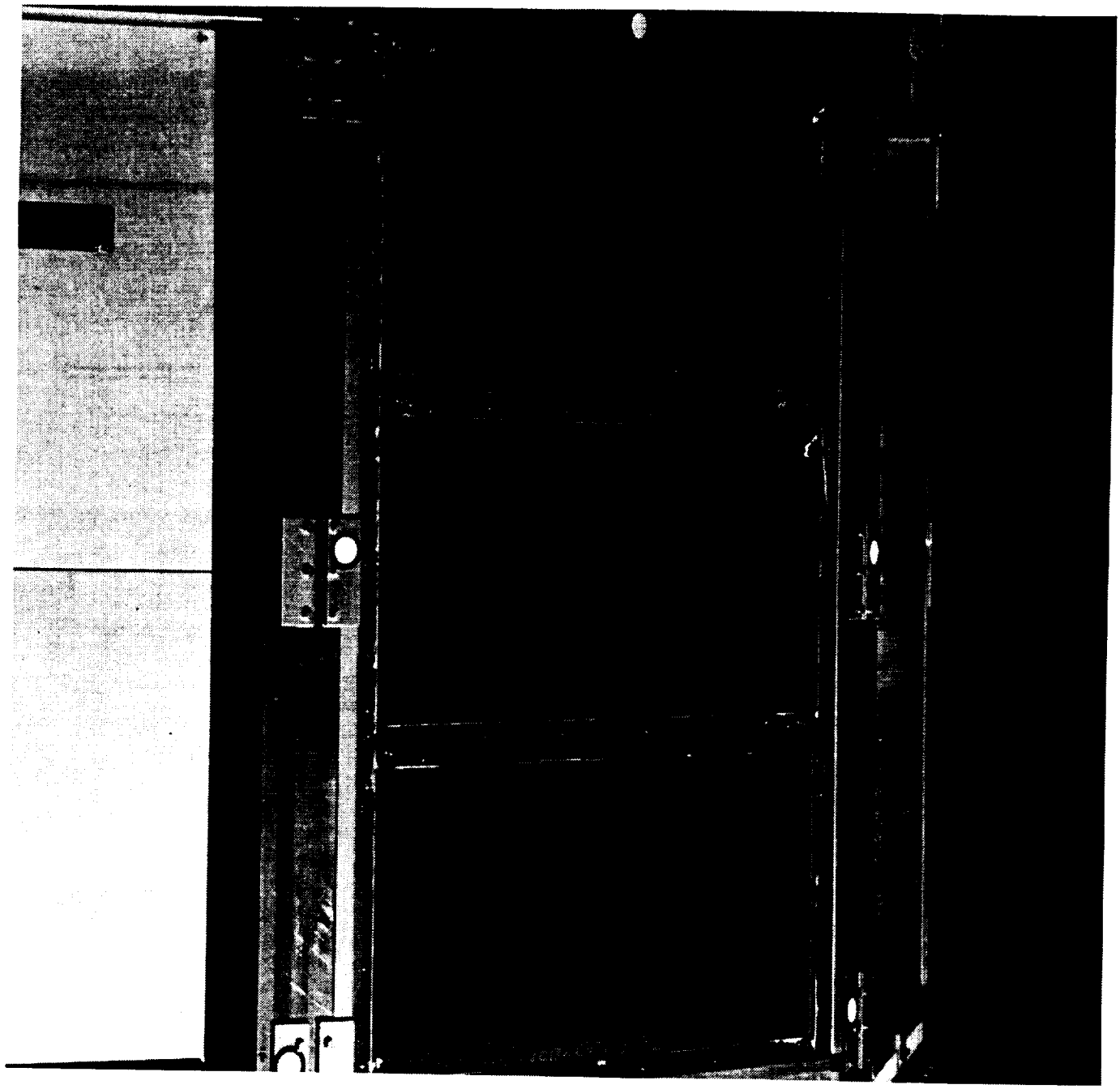

Figure 7.1-6. NASA on-orbit photo of experiment A0175 composite panels on tray A7. (Color figure C-6)

The space end on-orbit photo in figure 7.1-7 shows the failed thermal control blankets on the M0001 modules. These modules are indicated by the arrows in the figure. The darkened, brown areas on these modules are Lexan polycarbonate track detectors which were exposed to solar radiation, leaving those areas useless for the purposes of this experiment. The AO038 Interstellar Gas Experiment (IGE) trays have a number of areas discolored by contamination deposits, particularly around connectors with wire feeds from the interior of the tray. It is also significant that large areas coated with A276 white thermal control paint have not significantly discolored, in spite of the over 14,000 equivalent hours of direct solar exposure. The lighter discoloration patterns are each in the half of the tray toward the trailing edge. Areas which remained visibly white are toward the leading edge. The oxygen exposure for these locations is still quite low, about 5×10^{19} atoms/cm^2, but mostly occurred late in the mission and was apparently enough to remove the very thin UV damaged binder layer.

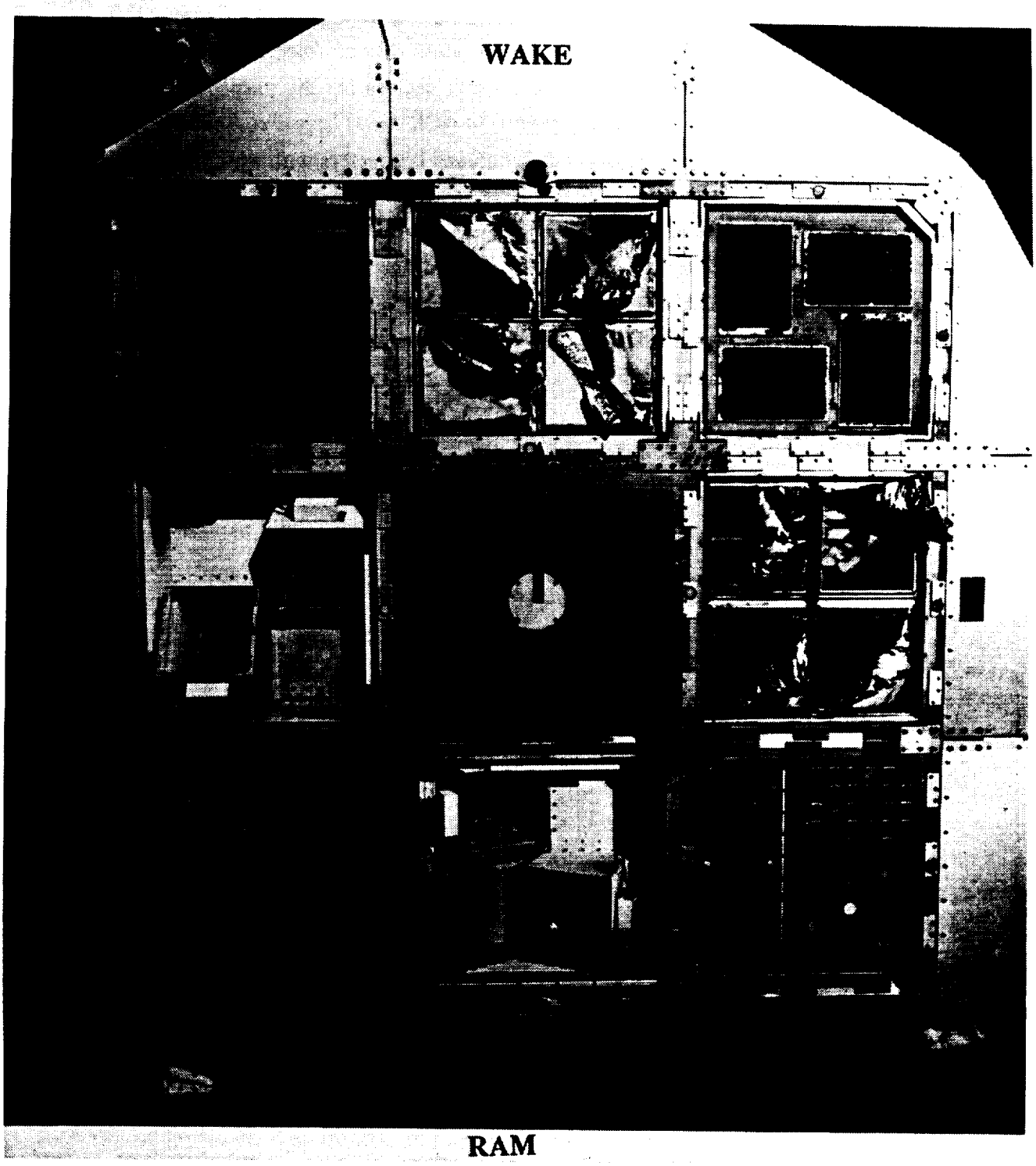

Figure 7.1-7. NASA on-orbit photo of M0001 experiment modules on space end.

(Color figure C-7)

Figure 7.1-8 is a close-up on-orbit photo of the failed thermal control blankets on an NRL M0001 experiment module. At the lower right are the solar arrays which recharged a NiCd battery used to power the NASA Goddard heat pipe experiment. These arrays operated during the entire flight.

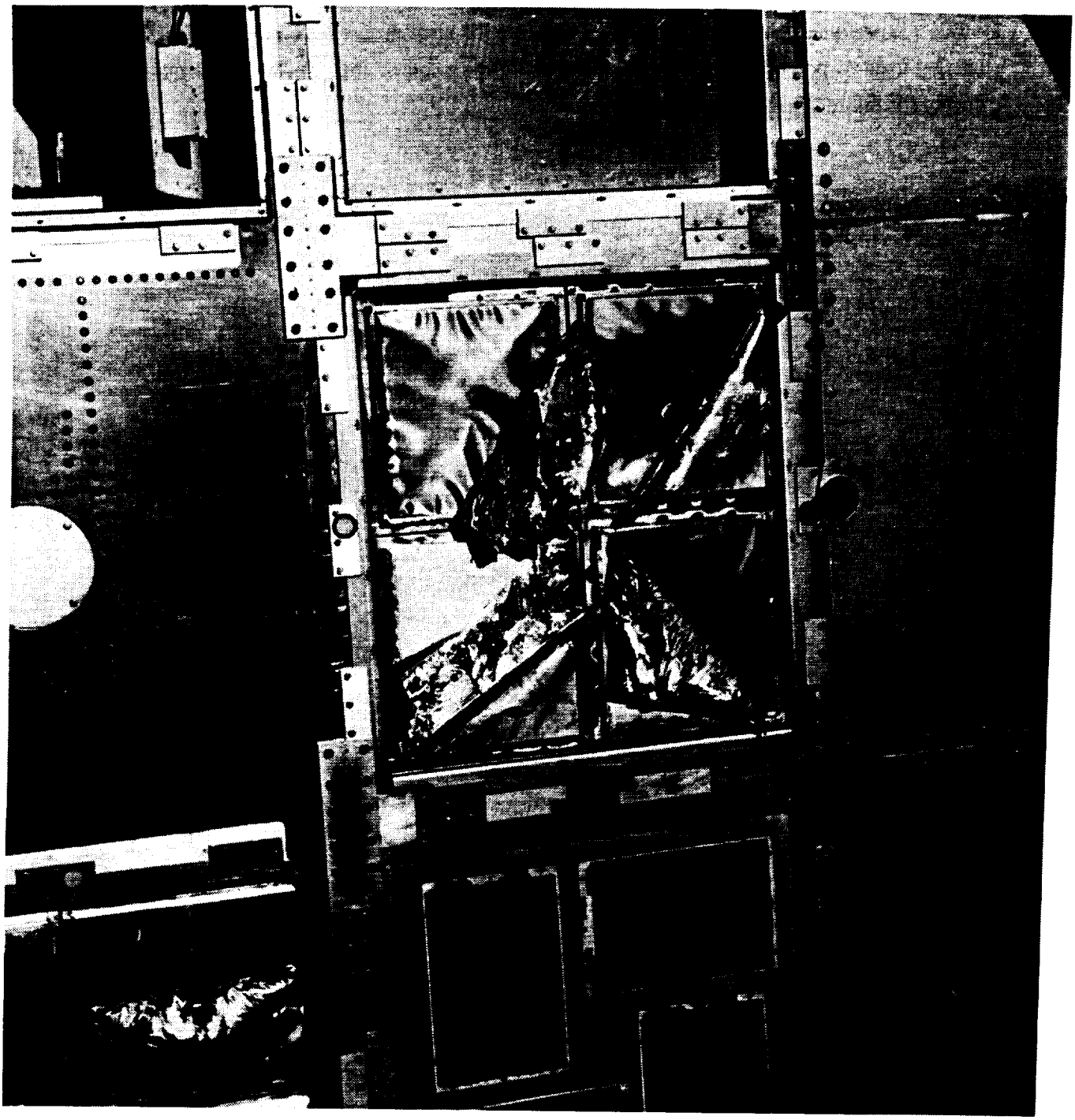

Figure 7.1-8. NASA on-orbit close-up photo of failed thermal control blankets on space end. (Color figure C-8)

The trays for experiment AO038 (E12, H12, H6) were designed to be the coldest location on LDEF. Figure 7.1-9 is an on-orbit photo of tray E12 showing the contamination around the electrical connectors. The lower right corner of the tray also shows discoloration. Cold surfaces facilitate the deposition of volatile species. The contaminated areas are very distinct and localized on these trays, suggesting very specific sources.

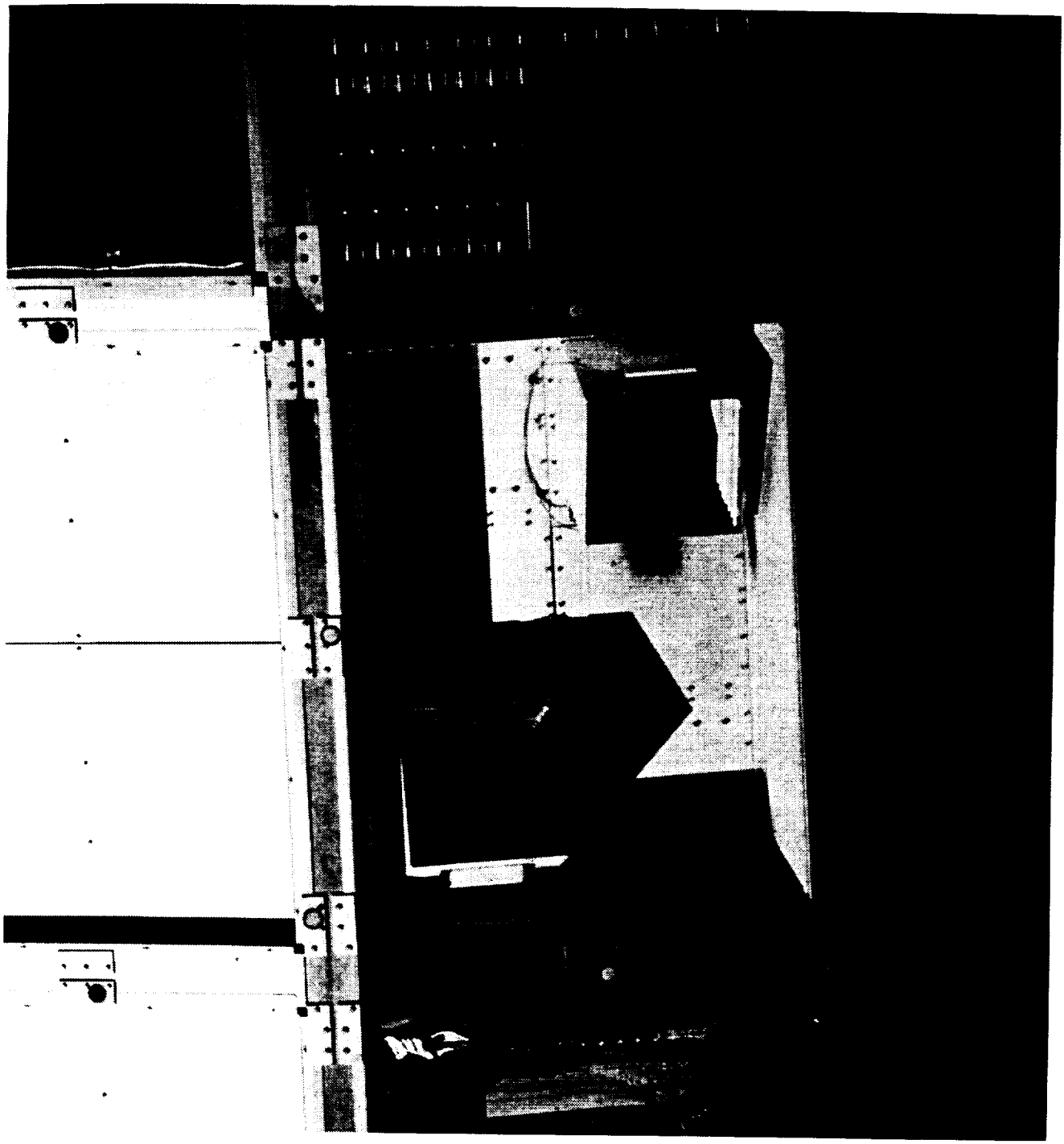

Figure 7.1-9. NASA on-orbit photo of tray E12, showing experiment A0038.

(Color figure C-9)

Figure 7.1-10 is an on-orbit photo showing an anodized aluminum thermal balance panel, E11, and a portion of tray E12 on the right. The IGE "camera" openings (tray E12) have wire grids toward their tops. This grid had collected a number of gold-colored flecks of material, most likely debris from the failed aluminized mylar and/or Kapton blankets on the leading edge. Most of this material was removed during reentry.

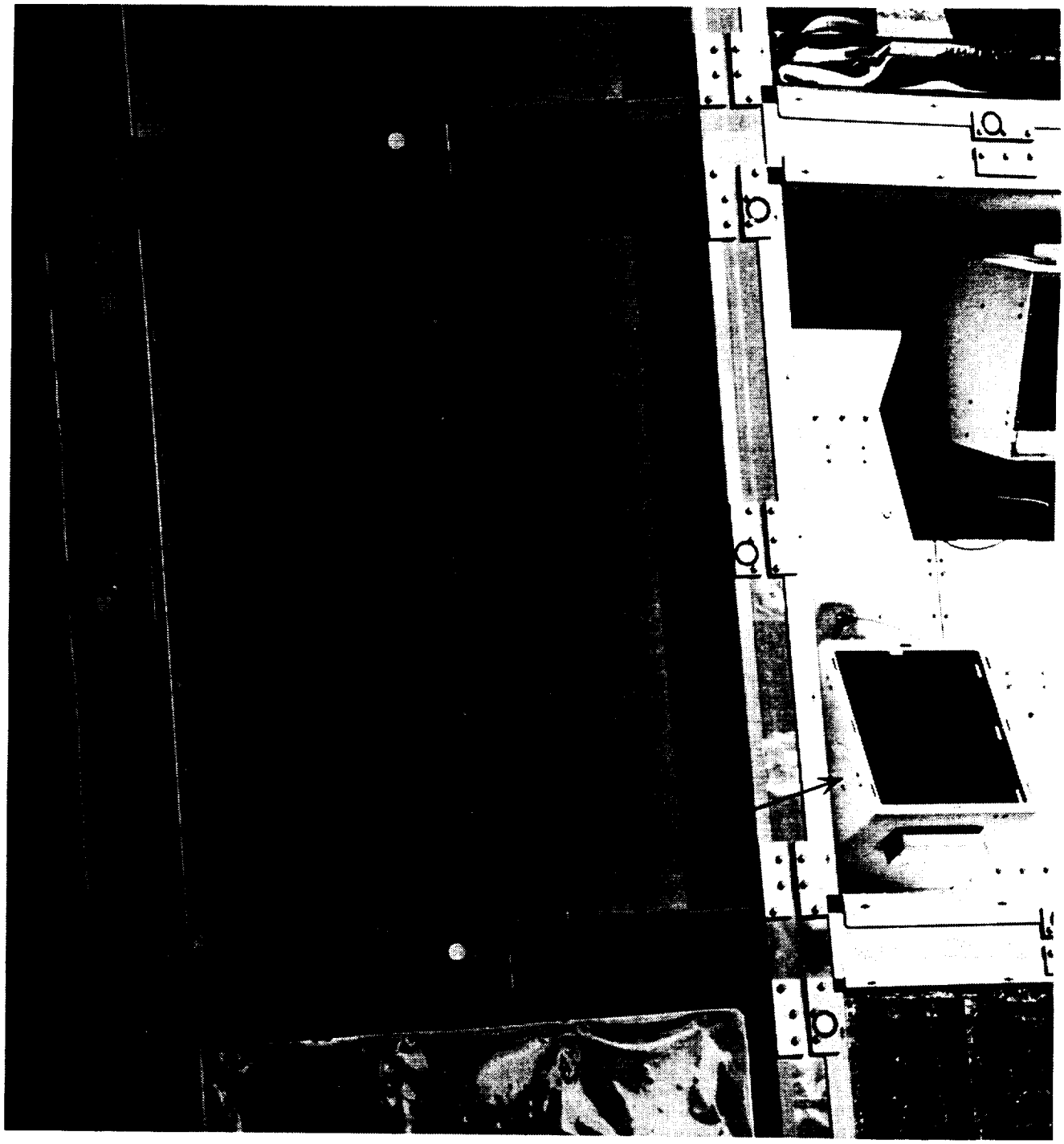

Figure 7.1-10 NASA on-orbit photo showing debris particles on the wire grid of the interstellar gas experiment cameras. (Color figure C-10)

Figure 7.1-11 is a NASA on-orbit photo showing tray D9. Particulate debris from failed blankets on M0002 is distributed across tray D9. This debris was also essentially removed during reentry. The time of failure, when the particulates were distributed over tray D9, which may have been an extended time period, is unknown.

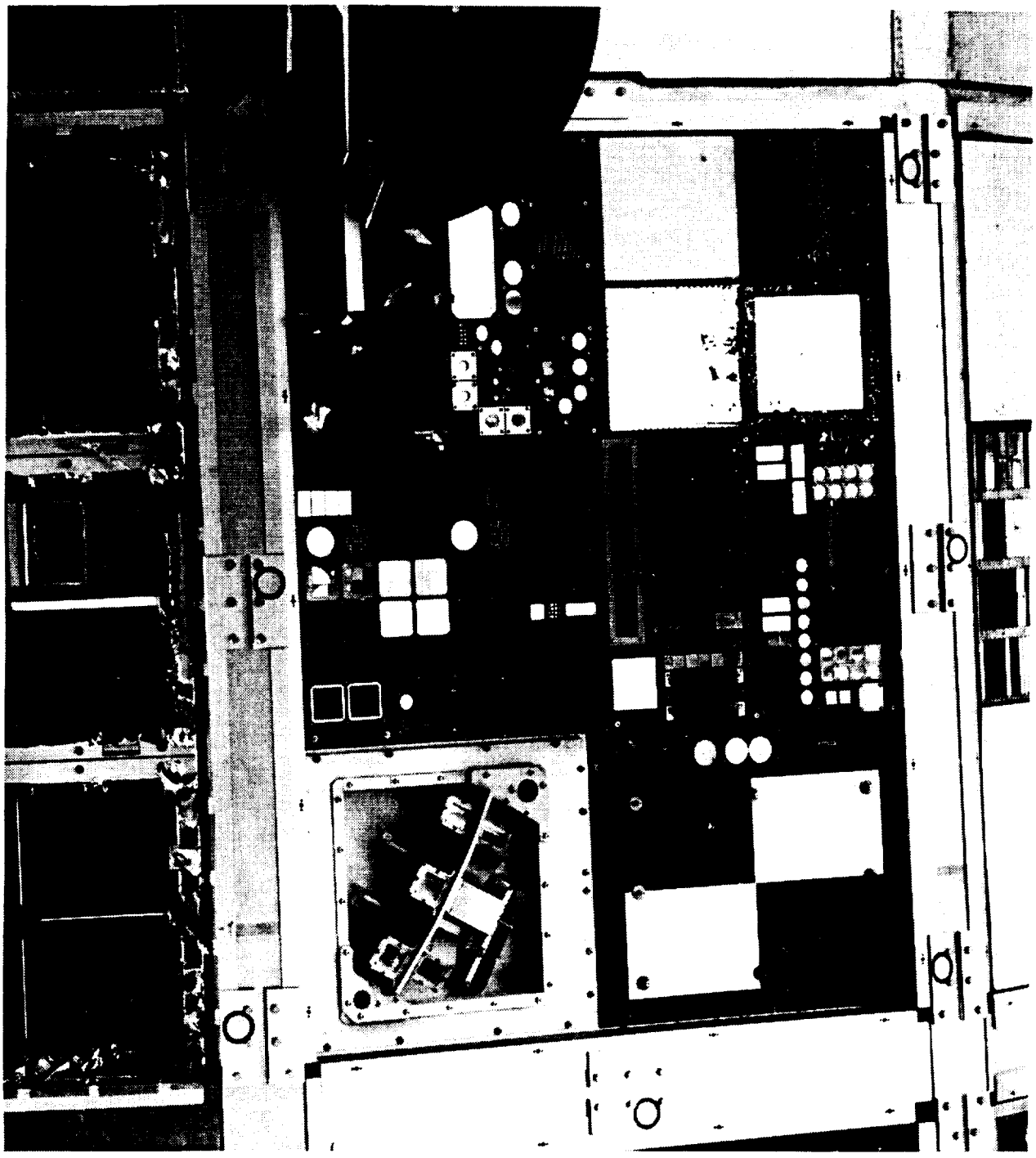

Figure 7.1-11. NASA on-orbit photo showing debris on tray D9. (Color figure C-11)

7.2 Post-Flight Photographs

Figure 7.2-1 is a close-up of the edge of a silverized Teflon blanket and tray wall of tray C11. This photo shows molecular film contaminants vented through the slot in the blanket, condensed on the tray wall, and subsequently darkened by solar exposure. The extent of the discoloration suggests that the significant outgassing deposits are essentially line-of-sight from the interior of the tray. Even the raised rivet at the edge of the vent provides some shielding. It is not known if the deposition occurred quickly, during or soon after initial venting and depressurization, or slowly over a long period of time.

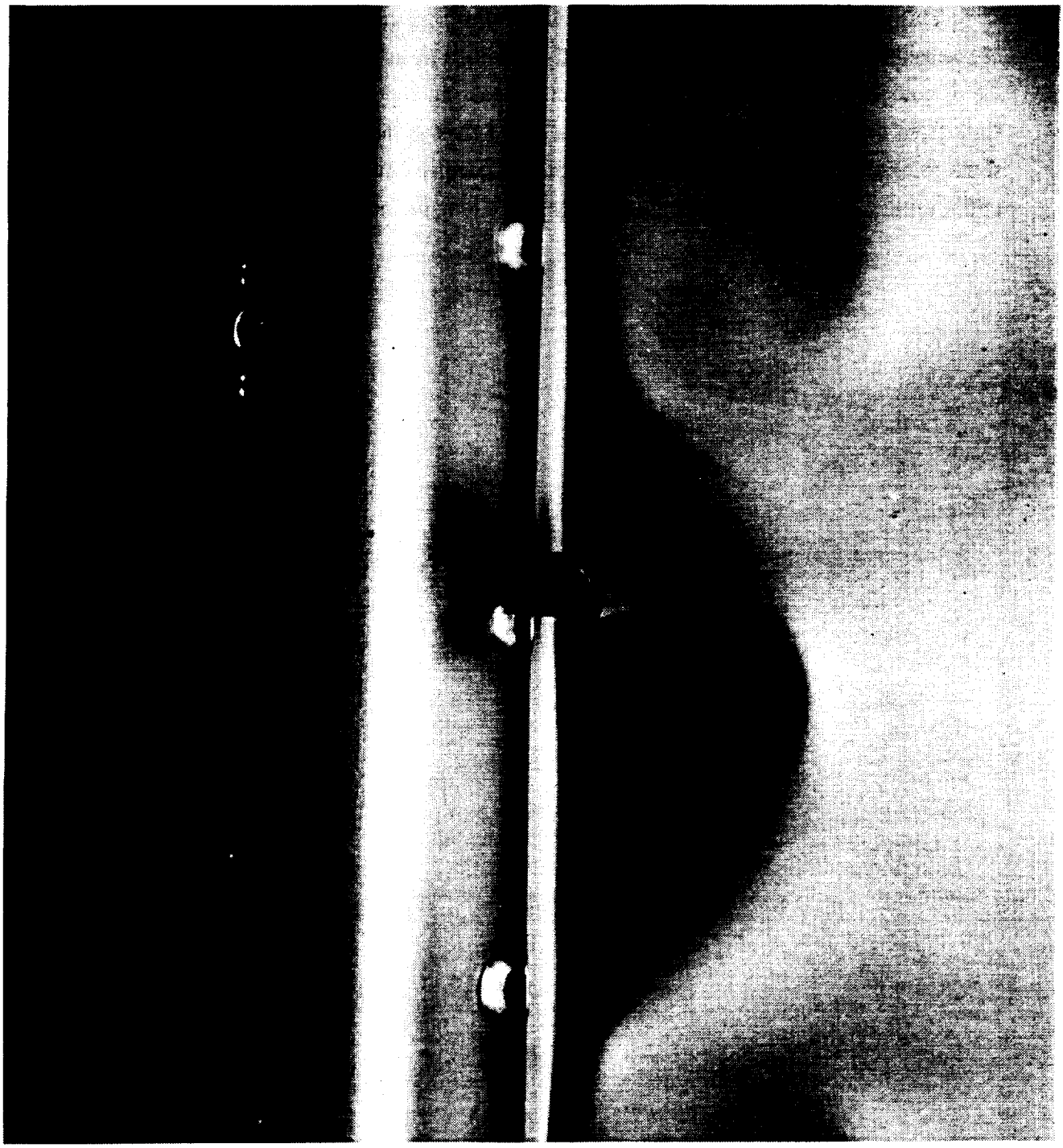

Figure 7.2-1. Photo of the edge of tray C11, showing contamination deposits. (Color figure C-12)

Figure 7.2-2 is a NASA post-flight close-up photo of the longeron between rows 11-12 near the space end of LDEF. This photo shows the interaction between material outgassed and vented from the interior and deposited on exterior surfaces, the environmental exposures, and the three-dimensional structure of the spacecraft. The panels at the space end are raised above the longeron surfaces. The bolts shield parts of the longeron surface from AO but not UV. Several details are apparent from the discoloration patterns. The heaviest deposits are around the bolts toward the edge of the spacecraft where there were no intervening surfaces to block or deflect the flow of vented material.

To explain the specific patterns observed, it must be remembered that parts of the surface were continually exposed to atomic oxygen, periodically to solar radiation, and that the temperatures on the surfaces varied as the LDEF went in and out of the Earth's shadow.

In figure 7.2-2, atomic oxygen exposure was from the left at 67° from normal to the longeron surface. This exposure "cleaned" the area of the longeron surface between the lower set of bolts in the photo. The remainder of the pattern was dependent upon which areas immediately saw sunlight upon coming out of the Earth's shadow, and which areas were in shadow and heated indirectly due to thermal conduction through the aluminum prior to receiving direct solar radiation. "Sunrise" was "above" the photo. Areas where material had deposited and were exposed to sunlight while still cold have significant discoloration where material was photopolymerized. Areas in shadow at "sunrise," such as just below the lower set of bolts, or at the extreme top of the longeron, which was shielded by the raised panel, were warmed indirectly. This allow materials at these locations to volatilize before the Sun moved into a position to radiate directly onto these areas. The net result was that areas still in shadow at "sunrise" did not have any contaminant material left to react and darken.

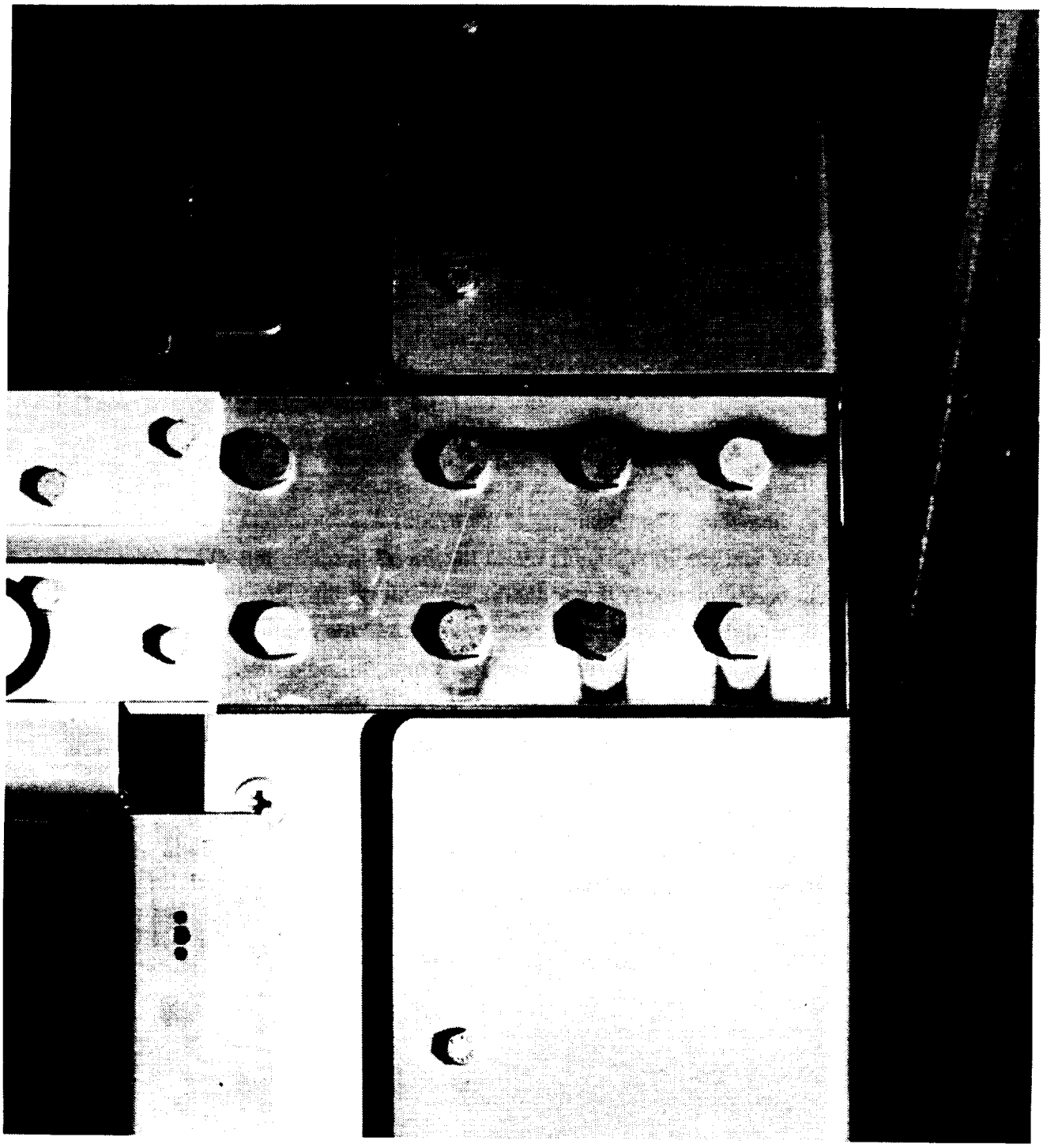

Figure 7.2-2. NASA post-flight photo of contamination deposits on longeron between trays F11 and F12. (Color figure C-13 rotated 90°)

Figure 7.2-3 is a close-up of the longeron between rows 10 and 11 at the space end of LDEF. This photo also shows large outgassing deposits of material outgassed and vented from the interior and deposited along both open sides of each near space end panel. This photo shows the limited distance traveled by significant amounts of outgassed material. The atomic oxygen approached the actual surfaces from the direction of the top of this photograph at about 37° to the longeron.

The amount of material vented at this location appears greater than for the location in figure 7.2-2. Darkened areas are seen along the rows 10 and 11 facing surfaces, as well as both sides of the longeron. The heavier deposit seen at the top half of the longeron in the photo are in an area shielded from atomic oxygen. The darkened area at the bottom half of the longeron has likely been eroded by atomic oxygen. This material has not been analyzed, but it likely contains significant amounts of silicates which have both trapped and protected other species from atomic oxygen.

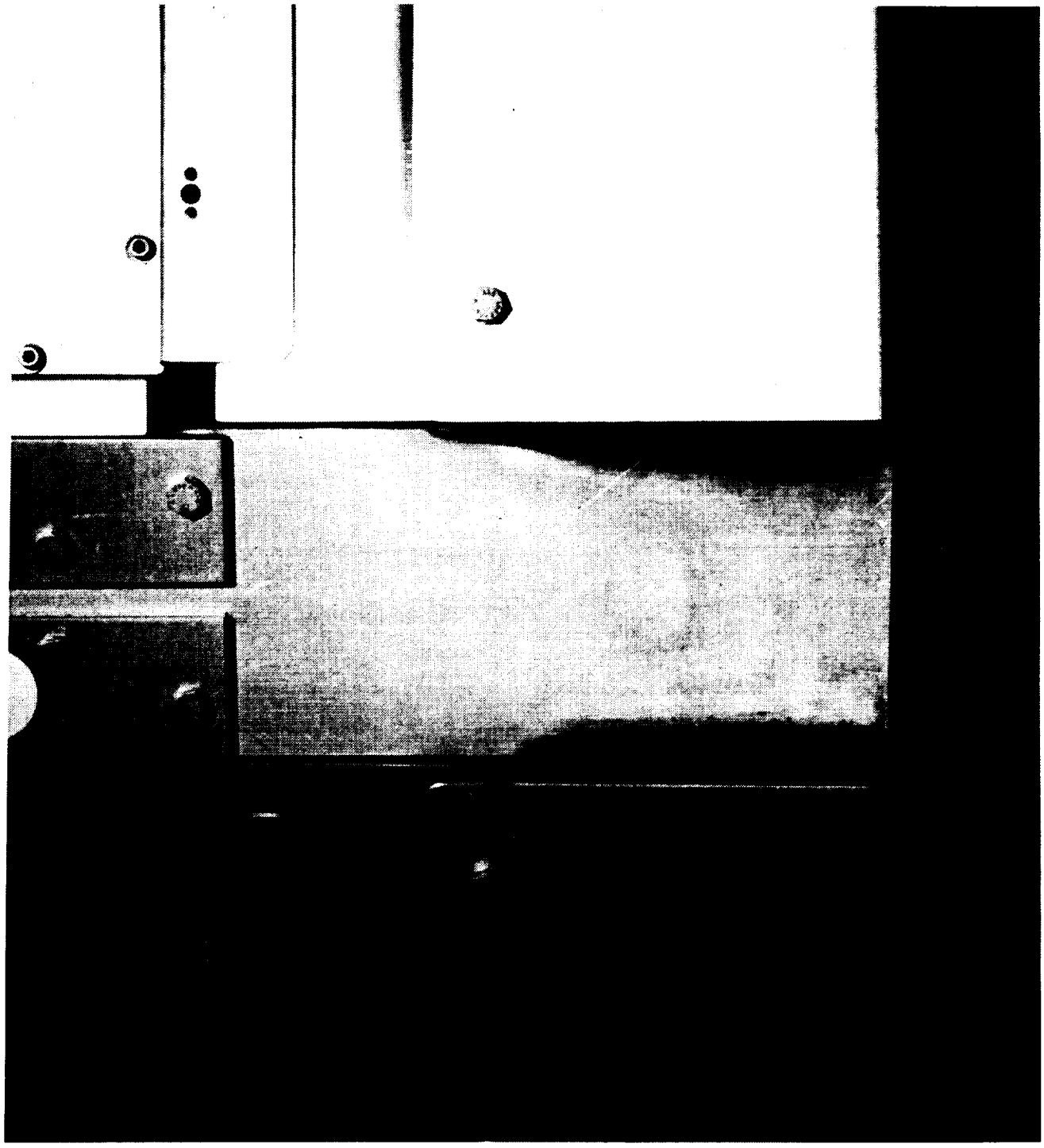

Figure 7.2-3. NASA post-flight photo of contamination deposits on longeron between trays F10 and F11. (Color figure C-14)

Figures 7.2-4 and 7.2-5 are photos showing near Earth-end vent locations between rows 11 and 12, and rows 7 and 8, respectively, The photos in these figures show essentially the same contamination patterns as figures 7.2-2 and 7.2-3, respectively. It is clear that the end-of-flight patterns are the result of multiple, sequential processes, including initial venting and outgassing, deposition on the surfaces, thermal cycling, and discoloration due to the environmental exposures. The three-dimensional details influence the deposition pattern through the geometry of the vent path, reflections from, and shielding by, the bolt heads, and the elevation of the black anodize aluminum structure above the longeron surface.

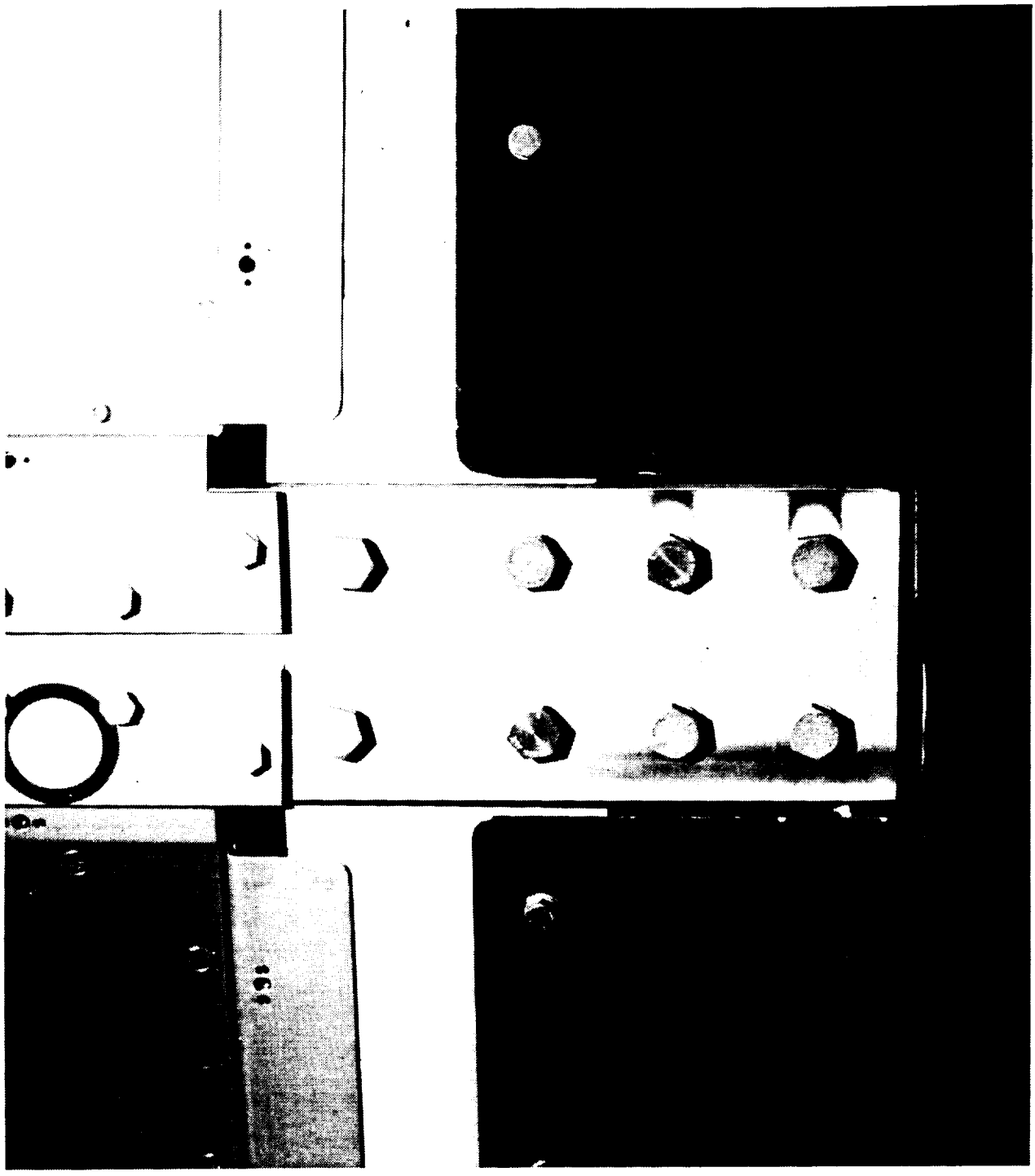

Figure 7.2-4. NASA post-flight photo of contamination deposits on longeron between trays A11 and A12. (Color figure C-15)

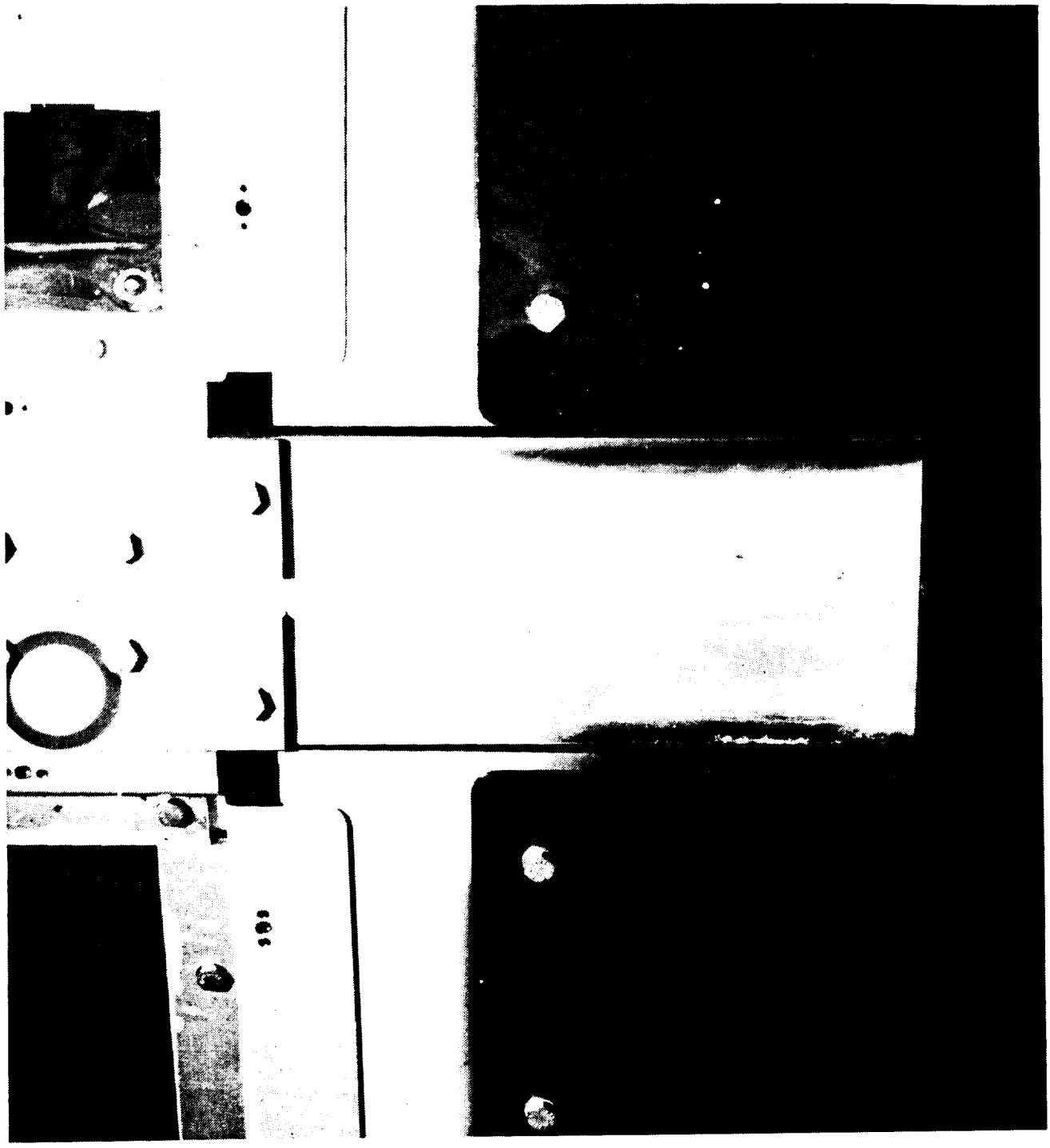

Figure 7.2-5. NASA post-flight photo of contamination deposits on longeron between trays A7 and A8. (Color figure C-16 rotated 90°)

Figures 7.2-6 through 7.2-14 are a series of NASA post-flight photographs showing contamination discoloration patterns due to pre-flight silicone outgassing deposition followed by on-orbit exposure to solar UV. These post-flight photos are all of trays from the leading half of LDEF (rows 7-11). Three of the figures are from tray F11, which contained one of the anodized aluminum thermal balance panels. Only one corner of tray F11 is adjacent to an AO178 tray, but all three corners of the F11 tray show contamination discoloration. Therefore, the source of the darkened contaminated areas is not venting from the AO178 tray. As described in section 6.1, the discolored area of contamination at the tray lips match the width of the tray cover gaskets. It has been suggested that the source of the discoloration on the outside of the trays is outgassed silicone RTV adhesive from experiment AO178. This is not the case. Many of the photographs in figures 7.2-6 through 7.2-14 are taken of corners of trays which were not adjacent to AO178 trays or any other tray which had a source of silicone. The only documented direct exposure to silicone was when the tray covers were in place prior to the flight and after the flight.

Figure 7.2-6 is of tray C7. The patterns of contamination are extremely oriented. Shadowing by the rivets at the bottom of the tray is clearly visible. The post-flight handling covers and gaskets are in place in this photo. These gaskets are made to the same dimensions as the pre-flight gaskets and the match between gasket width and discoloration on the lip is apparent. Several examples, figures 7.2-6 through 7.2-15, are shown to convey the point that discoloration was not due to one specific experiment but rather due to a deposition process which occurred on all trays at the same time (pre-flight) followed by specific on-orbit exposures producing the observed patterns on discoloration.

Figure 7.2-7 is a NASA photo of another corner of tray C7. This location is oriented 90° from the corner in figure 7.2-6 with respect to solar exposure. The discoloration area is minimized in this location.

Figure 7.2-12 is a NASA photo of tray E11. The shadow patterns on the wall to the left in the photo are highly oriented. Note that the two rivets at the bottom left on this surface have distinct shadow patterns but the next rivet does not. The raised surface on the left wall also creates a shadow effect, disrupting the visible contamination plume. The area right at the corner of the tray is substantially darker than the plume along the side of the tray. This area was closest to the source.

Figure 7.2-13 is a NASA photo from tray F11. The darkened areas are not nearly so oriented as in the previous photo.

Figure 7.2-14 is a NASA photo from tray F11. This area is very lightly discolored but like most of the previous photos of tray corners, shows the characteristic discoloration width at the tray lip.

These photos support the conclusion that silicone material outgassed from the tray cover gaskets prior to the flight and that solar exposure darkened these surface over time. This issue has not been investigated thoroughly. All these photos are of leading edge trays which were also subject to some atomic oxygen exposure which would have altered the chemical nature of the films. Trailing edge locations did not show such pronounced patterns.

As a comparison with the contamination on the external tray sides, figure 7.2-15 shows a NASA photo of the interior of a corner of tray D11. This photo shows the pattern from venting of an AO178 tray. The discoloration is extremely localized in this case and is essentially line of sight from the opening at the blanket corner.

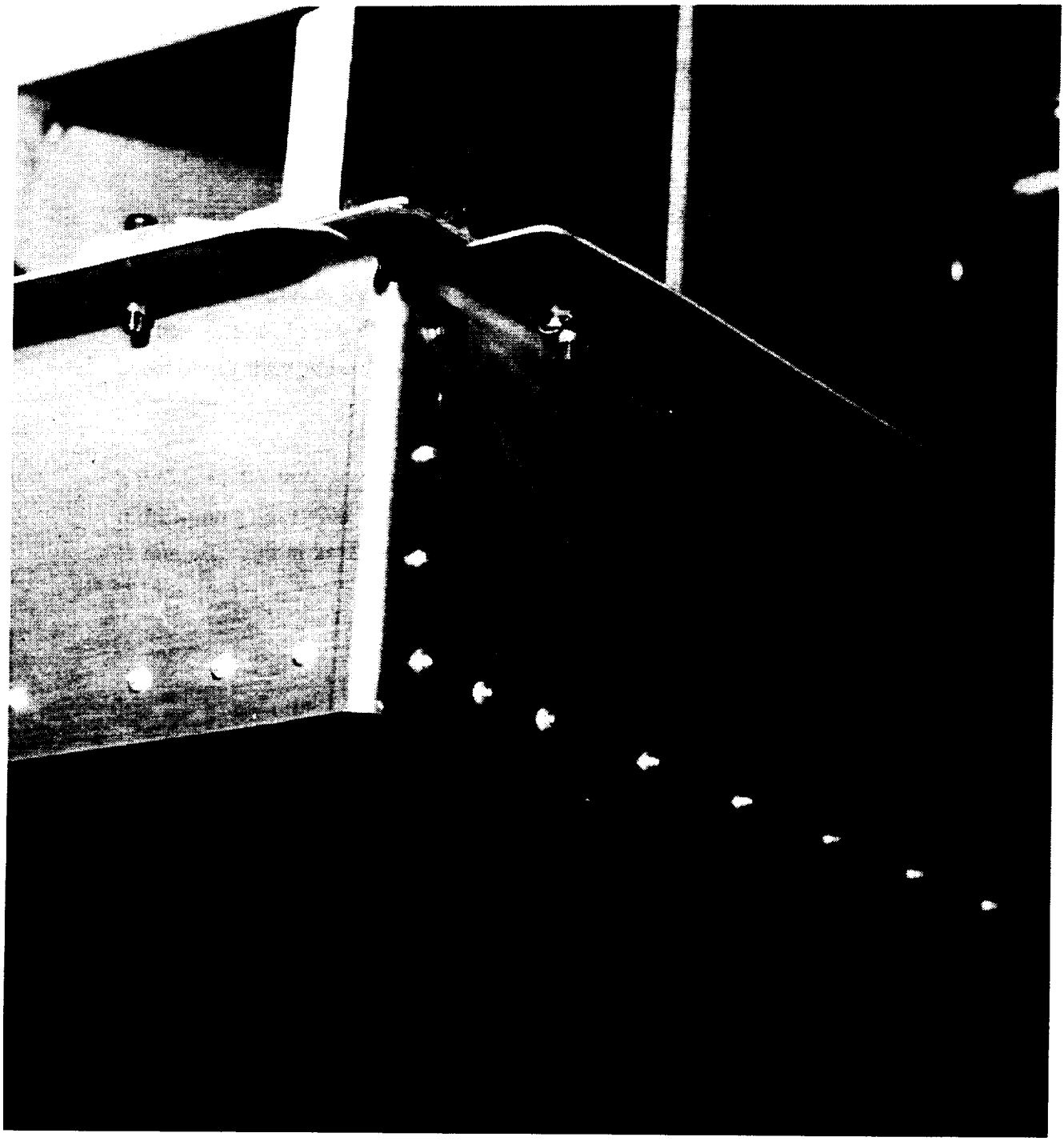

Figure 7.2-6. NASA post-flight photo of exterior of corner of tray C7. (Color figure C-17)

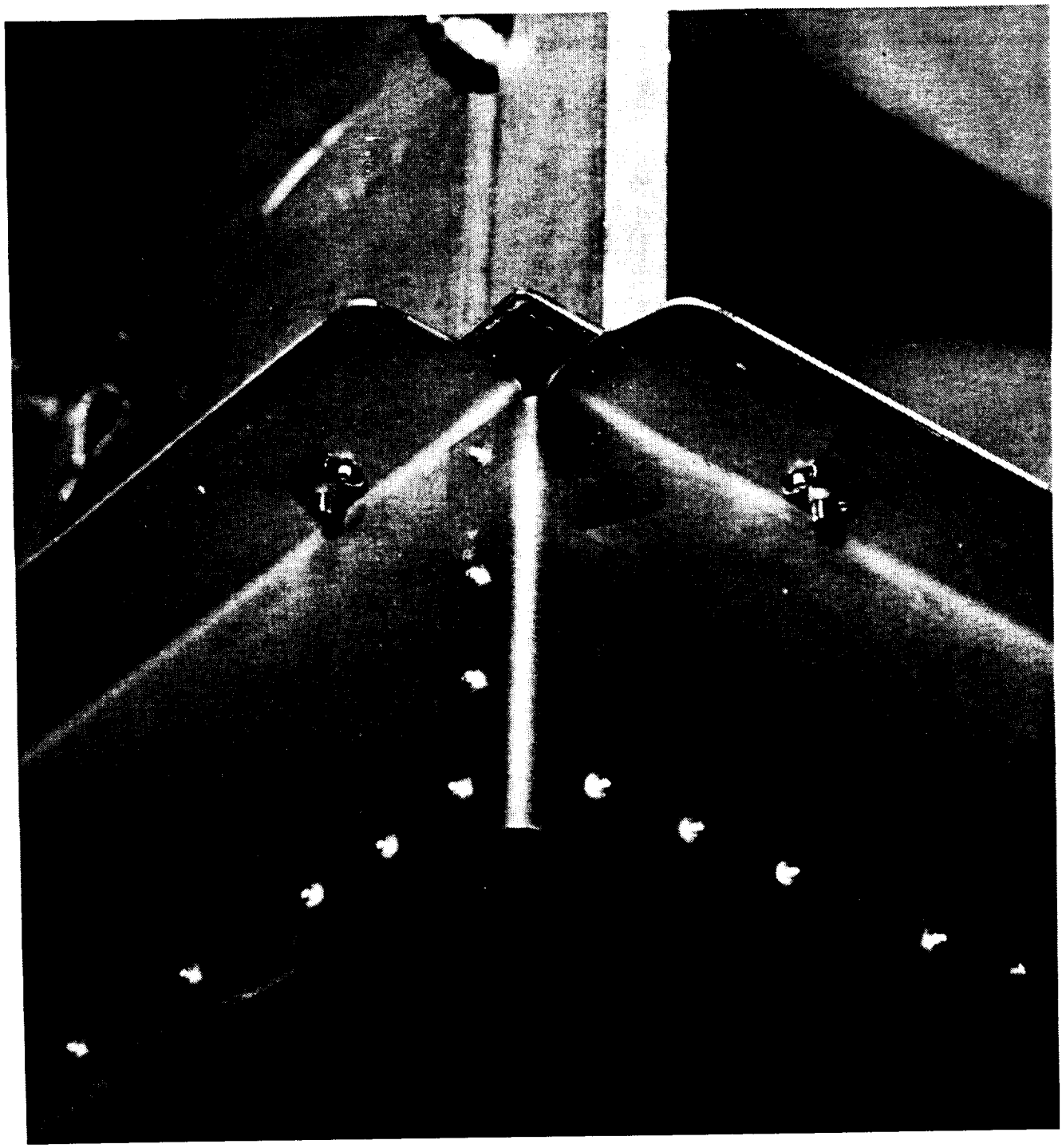

Figure 7.2-7. NASA post-flight photo of exterior of corner of tray C7. (Color figure C-18)

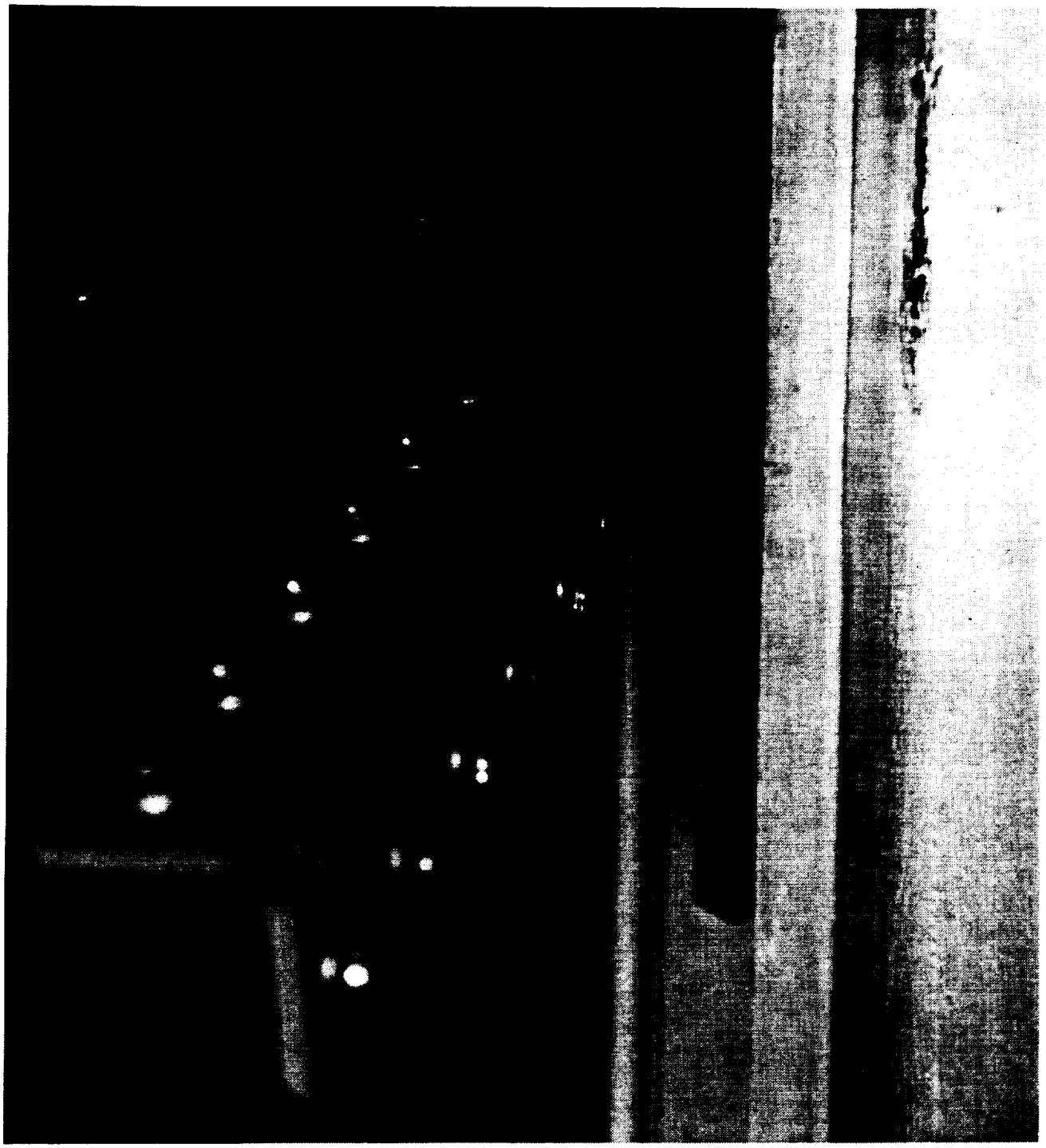

Figure 7.2-8. NASA post-flight photo of exterior of corner of tray D8. (Color figure C-19)

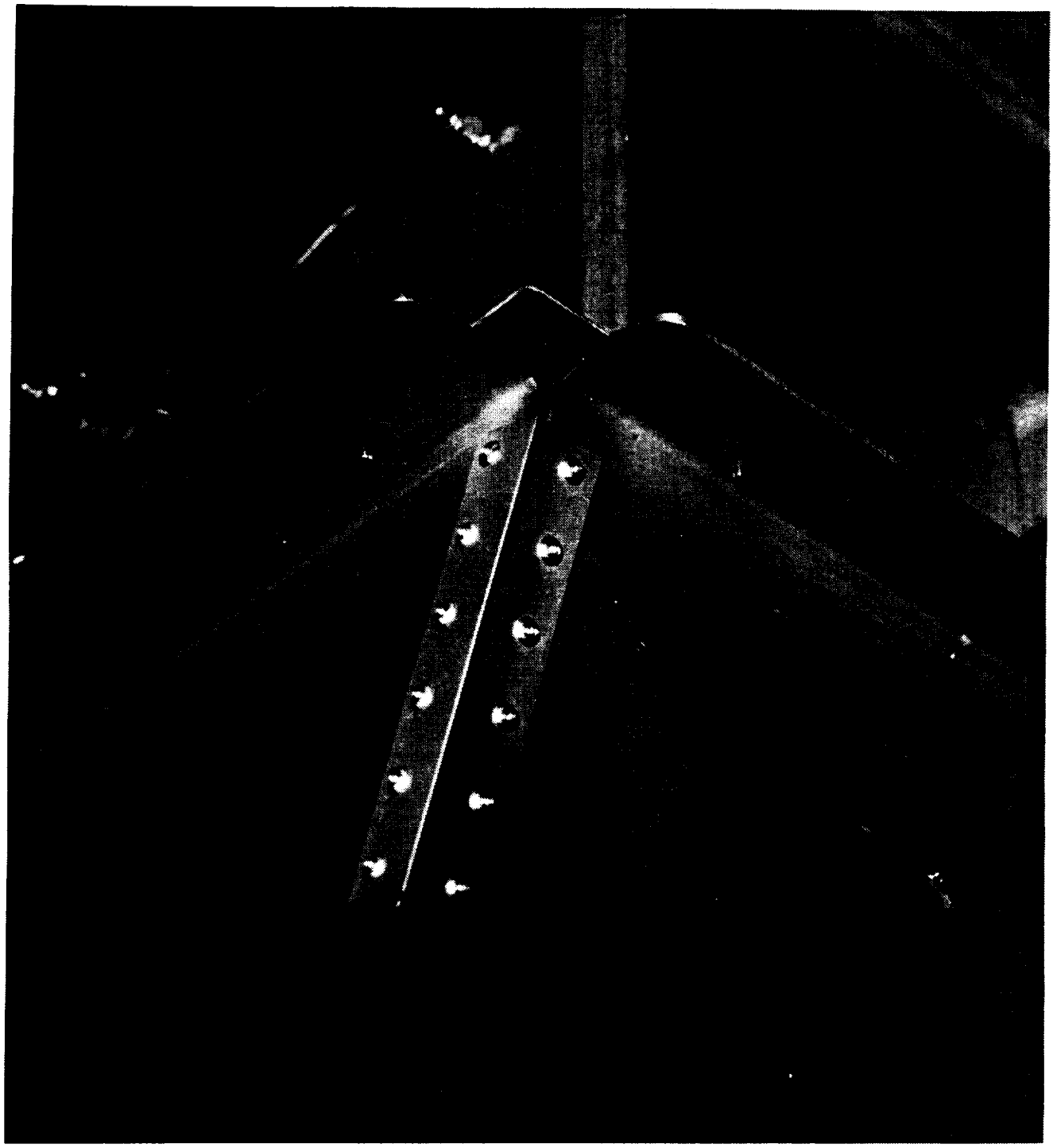

Figure 7.2-9. NASA post-flight photo of exterior of corner of tray F9. (Color figure C-20)

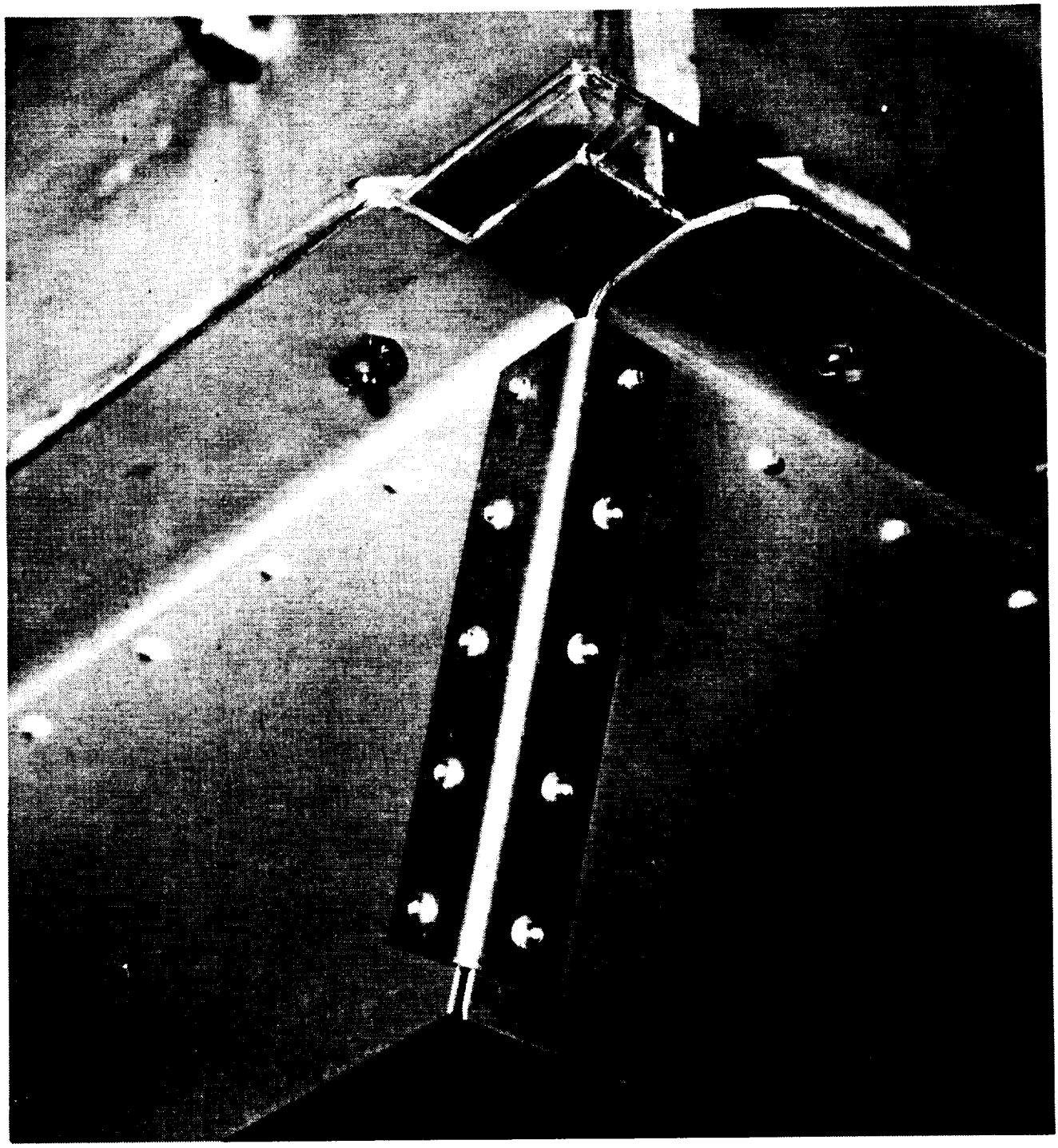

Figure 7.2-10. NASA post-flight photo of exterior of corner of tray C11. (Color figure C-21)

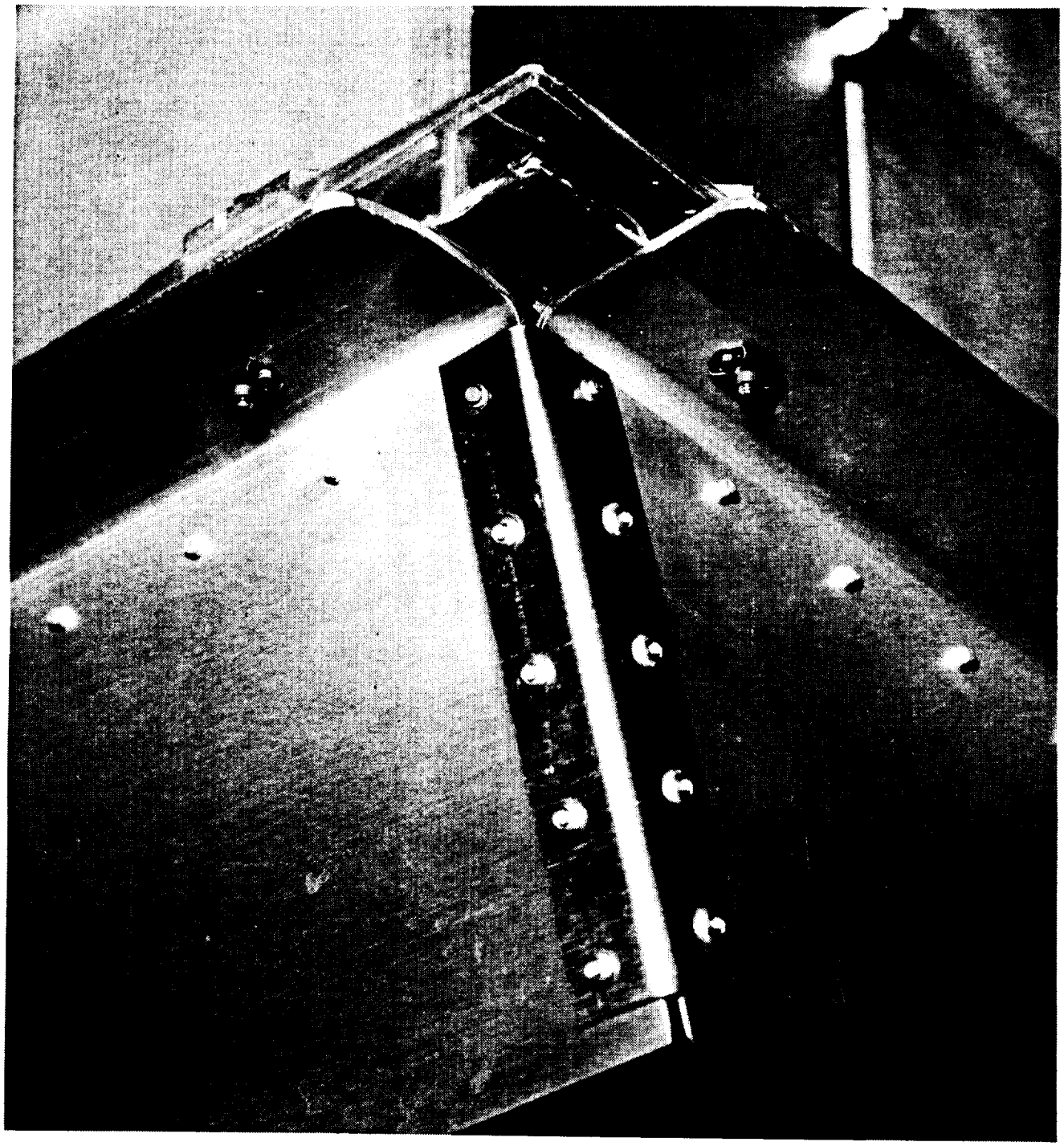

Figure 7.2-11. NASA post-flight photo of exterior of corner of tray C11. (Color figure C-22)

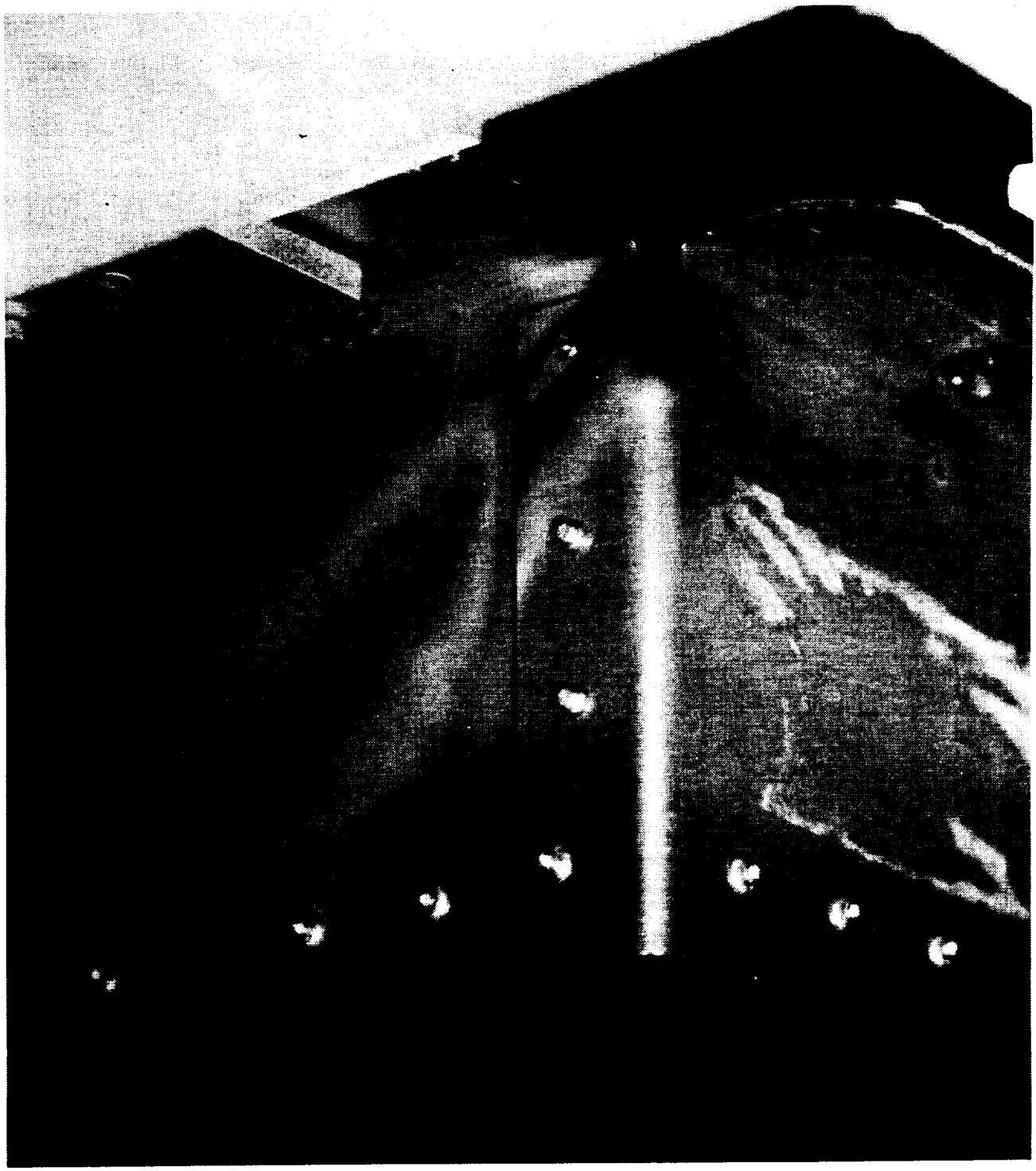

Figure 7.2-12. NASA post-flight photo of exterior of corner of tray F11. (Color figure C-23)

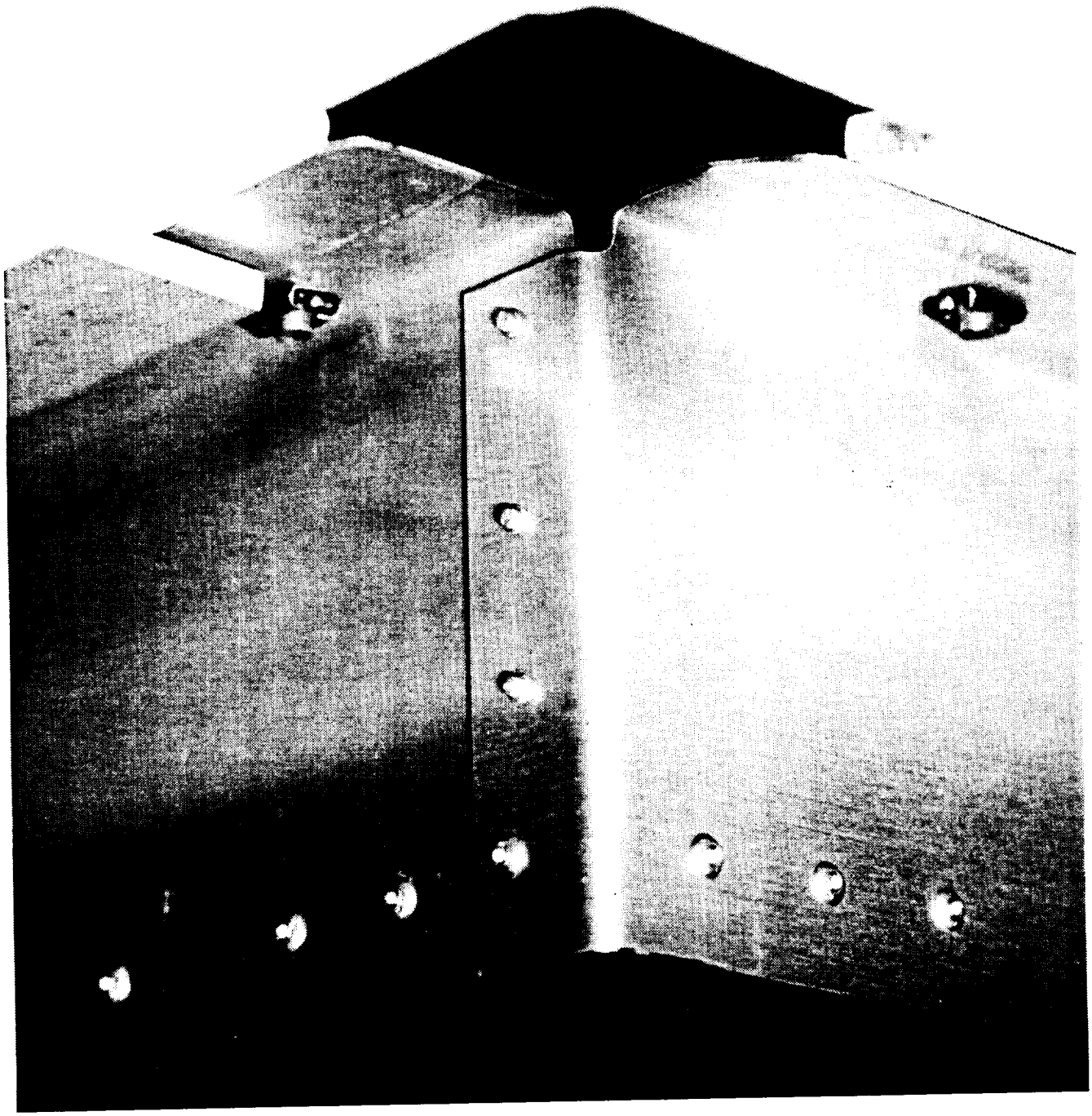

Figure 7.2-13. NASA post-flight photo of exterior of corner of tray F11. (Color figure C-24)

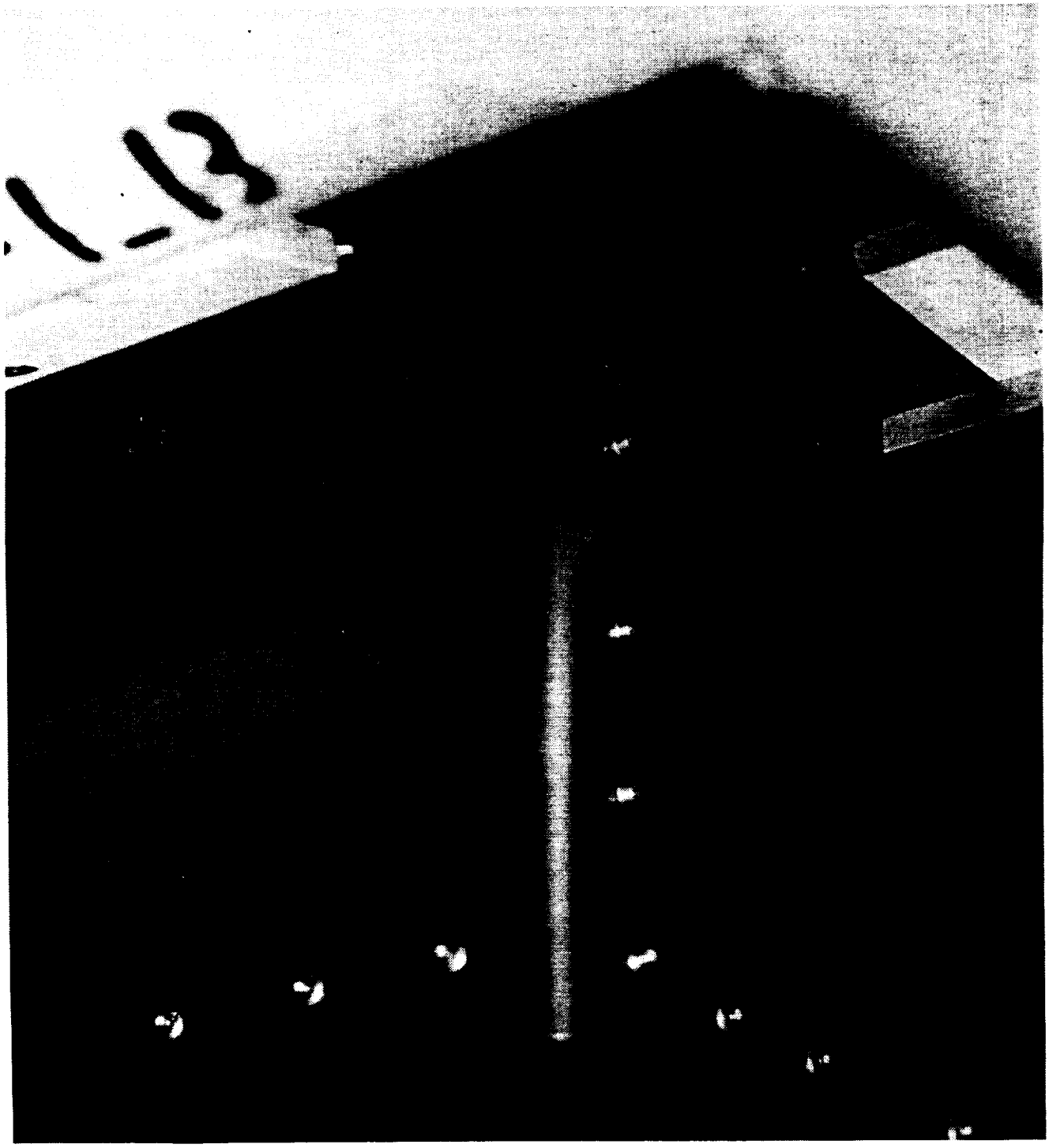

Figure 7.2-14. NASA post-flight photo of exterior of corner of tray F11. (Color figure C-25)

Figure 7.2-15. NASA post-flight photo of outgassing deposits at interior of corner of tray D11. (Color figure C-26)

Figures 7.2-16 and 7.2-17 are photographs showing "L" shaped unanodized aluminum tray clamps from the leading edge. Figure 7.2-18 is a close-up photo of an "L" shaped unanodized trailing edge (C3) tray clamp with nearby anodized clamps, showing the darker color of the unanodized clamp. The appearance of each of the unanodized clamps was essentially unchanged by the flight exposure. These clamps were manufactured to provide extra support for trays C3 and C9. These trays were quite heavy and after the flight certification (vibration) test it was felt the additional support was needed to hold these trays in place. These clamps were not anodized for thermal control because of their relatively small surface area and time constraints. The "L" shaped unanodized tray clamps were manufactured just before the flight.

The leading edge exposed Z306 ring around the A276 paint button in figures 7.2-16 and 7.2-17 is almost completely removed. This erosion is even more severe than the erosion of the Z306 around other leading edge tray clamp paint buttons, such as is shown in figure 7.2-19. A possible explanation is that the temperature cycling on these unanodized clamp surfaces was greater than for the chromic acid anodized (CAA) clamps because of the poorer optical properties of the bare aluminum. The increased temperature relative to the anodized clamps would allow a faster reaction rate of the atomic oxygen with the paint. Any changes to the Z306 on the trailing edge clamps due to solar exposure were concealed by the black pigment in this paint. The chemical structure of the binder may have been altered, but this did not significantly affect the optical properties of the paint. Since these locations saw no atomic oxygen, there was no effective removal mechanism. The A276 paint button on the clamp in 7.2-18 shows the solar UV induced darkening of this paint due to binder damage. For typical trailing edge locations the absorptance of the A276 doubled. The absorptance and emittance values for selected clamps are compared in figure 7.2-20.

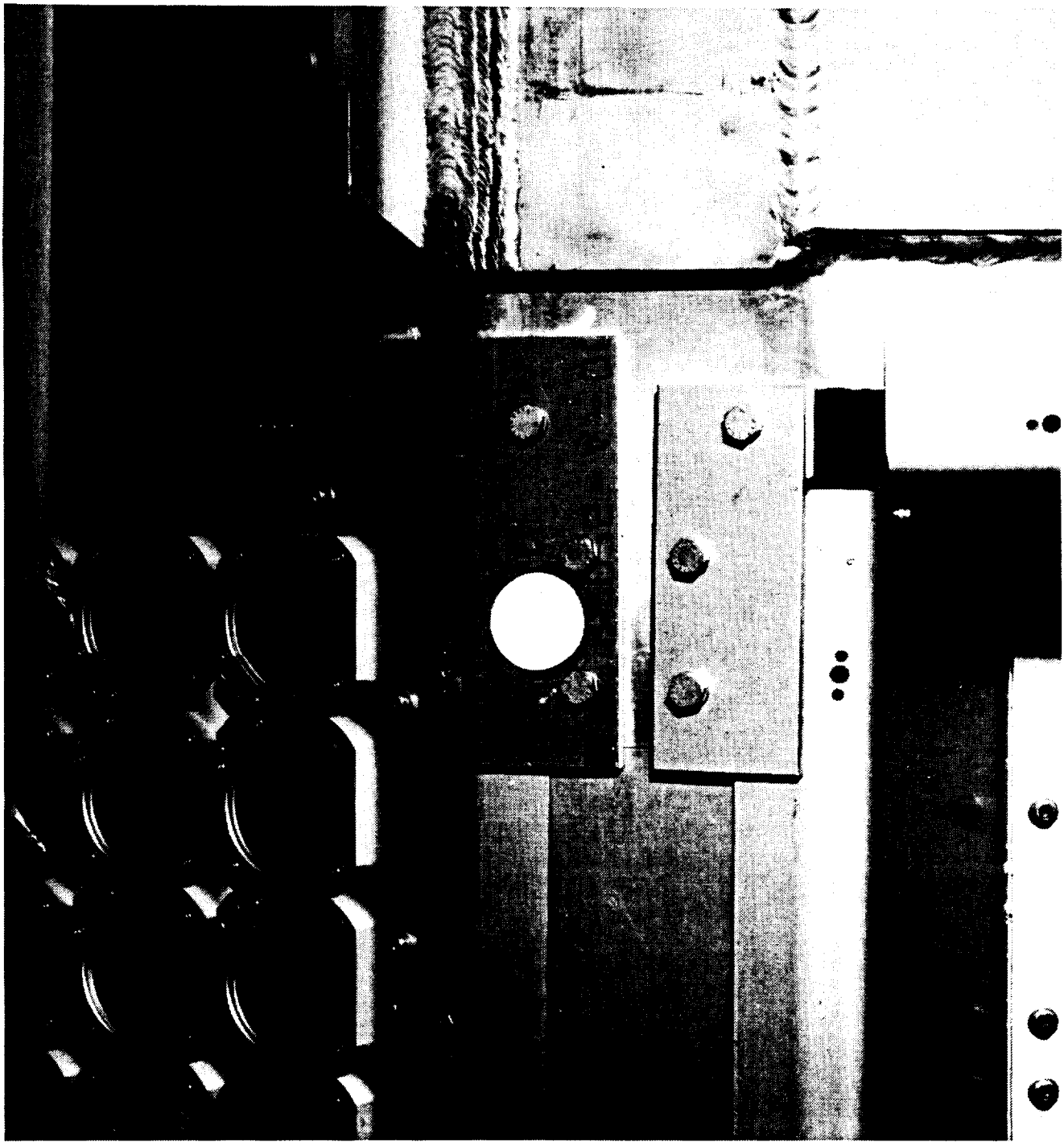

Figure 7.2-16. NASA post-flight photo of leading edge unanodized aluminum tray clamp at space end of C9. (Color figure C-27 rotated 180°)

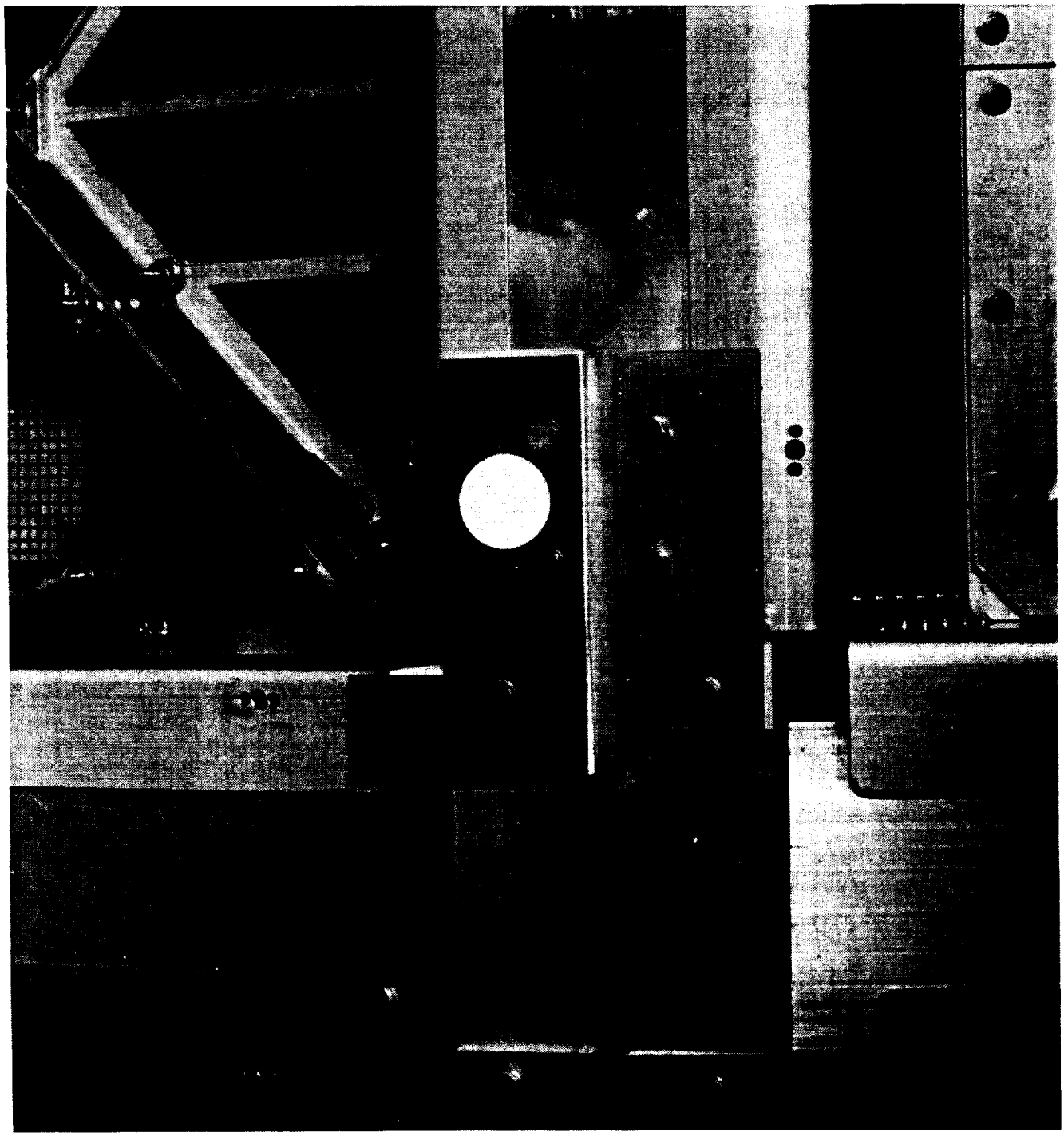

Figure 7.2-17. NASA post-flight photo of leading edge unanodized aluminum tray clamp at Earth end of C9. (Color figure C-28 rotated 90°)

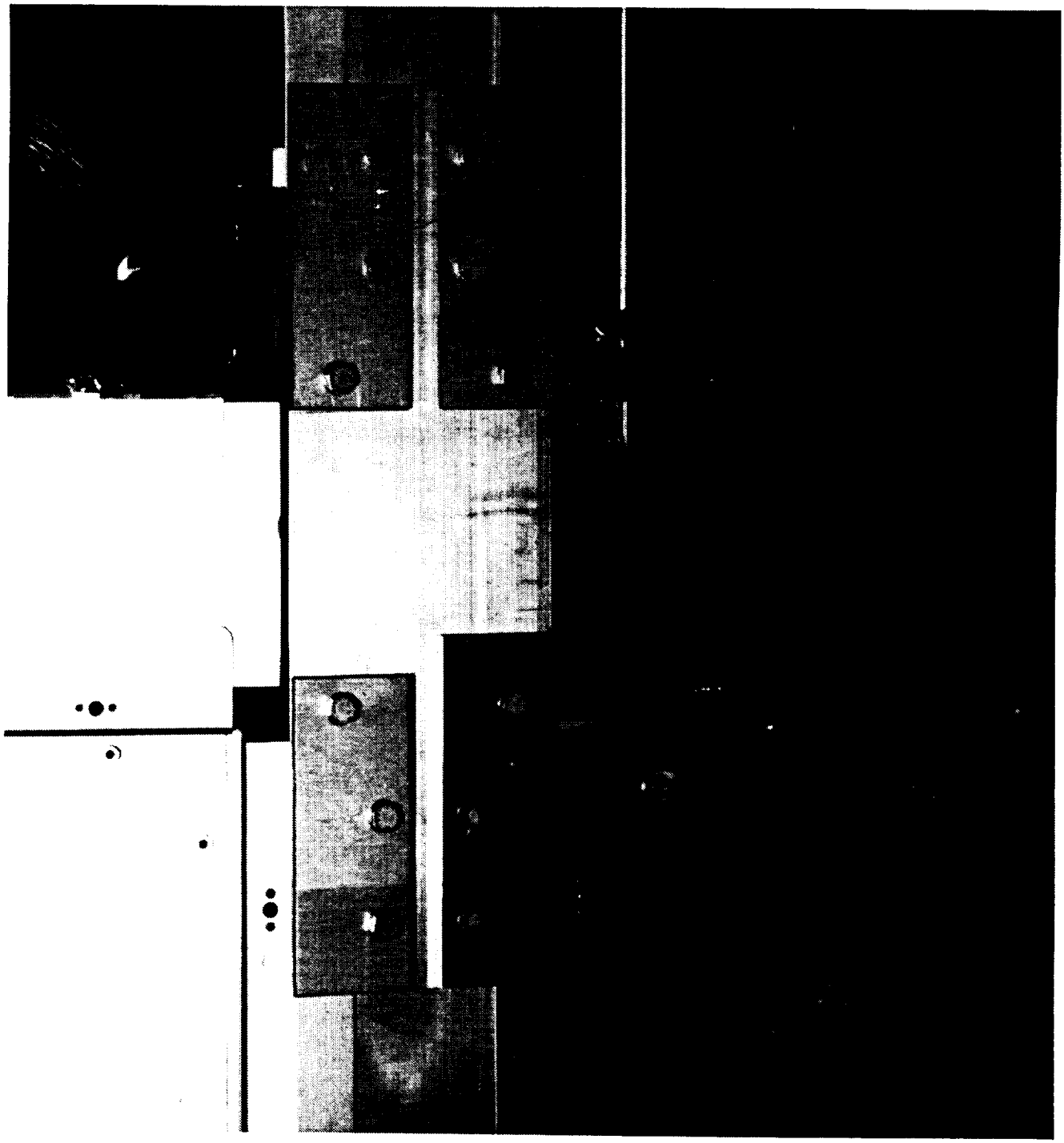

Figure 7.2-18. NASA post-flight photo of trailing edge unanodized aluminum tray clamp on tray C3. (Color figure C-29)

Figure 7.2-19 is a photo showing results of the 69 months exposure on several of the S0069 specimens and nearby hardware. Silicone coated paint specimens, which failed severely on-orbit, are visible on the lower righthand side of the photo. A leading edge paint button with a partially eroded Z306 ring is visible. Comparison with the exposed Z306 ring around the A276 paint buttons shown in figures 7.2-16 and 7.2-17 shows slightly more of the Z306 remains on the anodized tray clamp. A small portion of the silverized Teflon blanket A10, showing a number of impact sites and the associated delaminated areas, can be seen on the left. The area on the A10 tray adjacent to the vent slot in the Ag/FEP blanket shows evidence of deposition of material vented from the inside of the tray.

The failed silicone specimens from S0069 show that components, such as solar cell arrays, protected by thin silicone coatings, may be susceptible to performance degradation due to darkening, or outright failure of the coating.

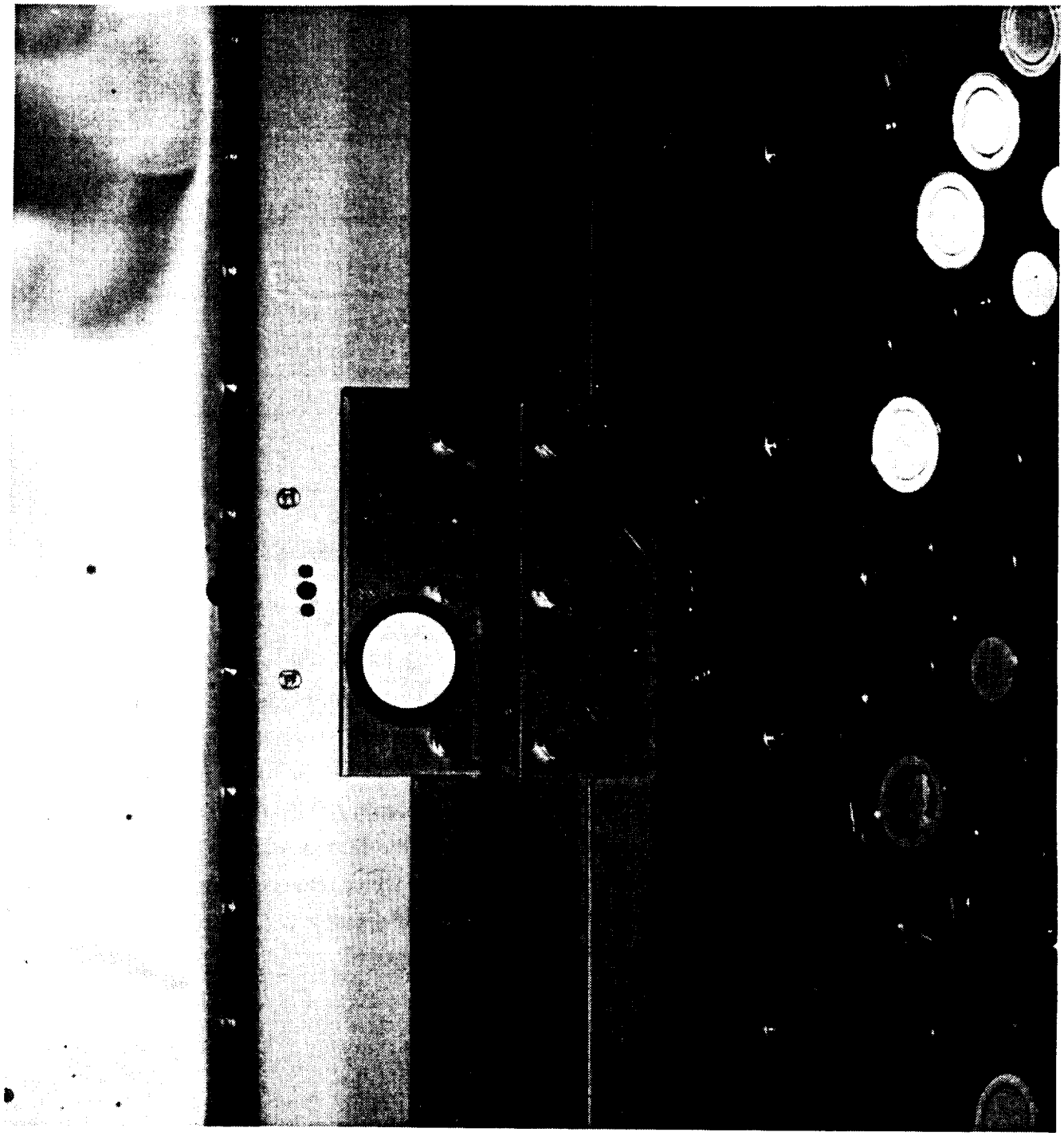

Figure 7.2-19. Close-up of areas of trays A9 and A10 showing environmental effects on a variety of materials. (Color figure C-30)

The absorptance and emittance values for selected clamps are compared in figure 7.2-20.

Sample	Exposure	Surface Treatment	Solar Absorptance	Thermal Emittance
control #4	ground control	CAA	0.32	0.18
C3-5	longeron, rows 3-4	bare	0.74	0.08
C3-5	Back surface, no direct exposure	bare	0.71	0.13
C3-6	longeron, rows 3-4	CAA	0.35	0.14
C9-2	longeron, rows 8-9	CAA	0.33	0.17
C9-7	longeron, rows 9-10	bare	0.69	0.06
C9-7	back surface, no direct exposure	bare	0.72	0.09

Figure 7.2-20. Comparison of optical properties of anodized and unanodized aluminum flown on LDEF.

Figure 7.2-21 is a close-up showing corners of D9 and D10. Several of the thin film material specimens on D9 failed during flight and twisted, partially covering other specimens. This area of tray D9 was directly under a scuff plate and experienced exposure levels of atomic oxygen and solar UV reduced to about 1/3 in comparison with the remaining area of D9. Portions of the aluminized Kapton on AO054 (visible in the lower right hand corner of the photo) failed during flight as the Kapton was eroded by atomic oxygen. The extremely thin vapor deposited aluminum which remained when the Kapton was removed had essentially no mechanical integrity and disintegrated, distributing flakes over other locations. This damage is visible in the photograph.

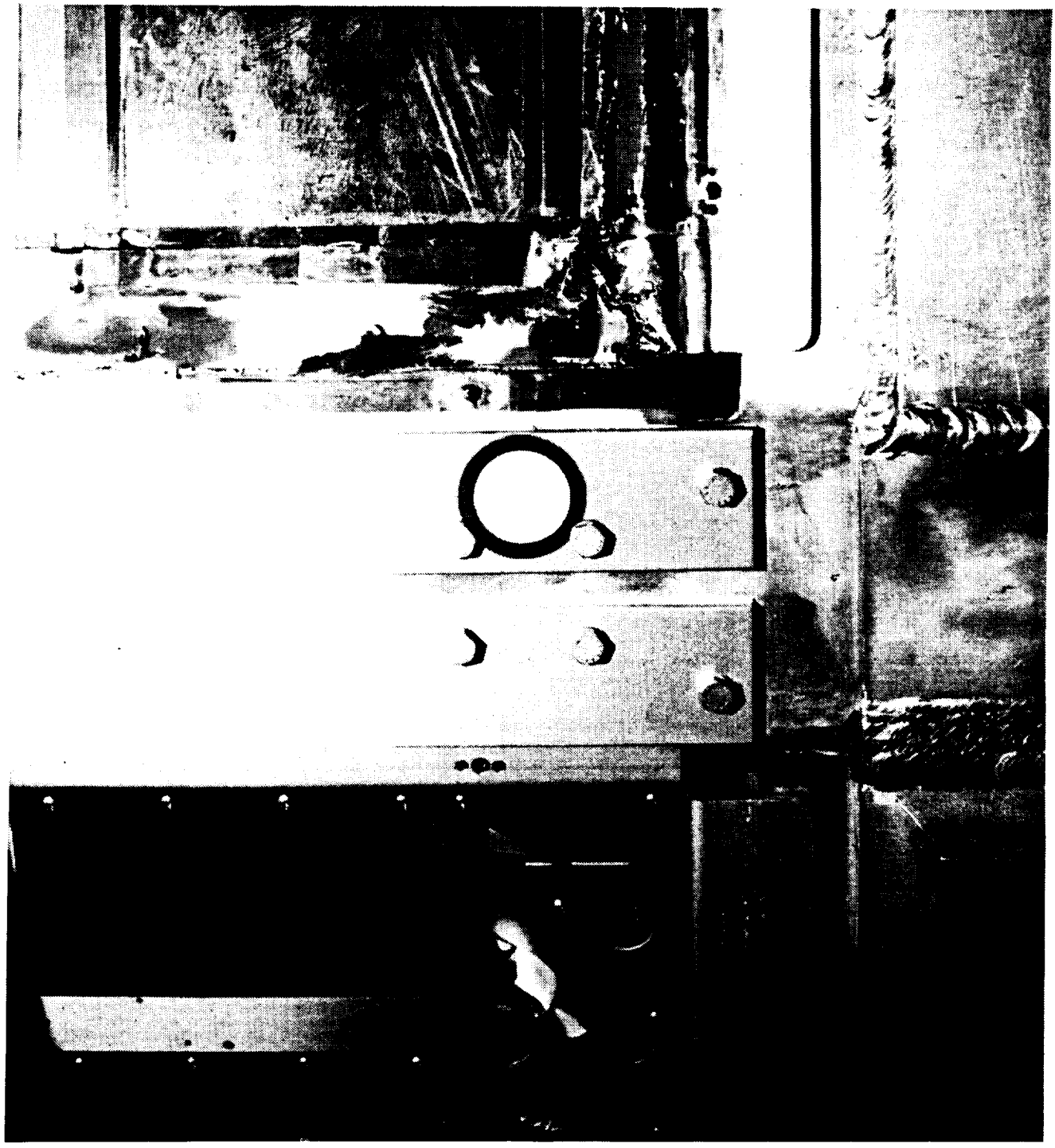

Figure 7.2-21. NASA photo showing close-up of areas on trays D9 and D10. (Color figure C-31)

Figures 7.2-22 and 7.2-23 are photographs showing a leading (longeron between D10 and D11) and a trailing (longeron between C2 and C3) edge location, respectively. The paint button toward the leading edge remained white, but only the pigment remained. The trailing edge location shows a significant color change as the solar UV damaged the surface of the A276 paint binder. The photograph of the trailing edge location also shows rolled-up films of tantalum which failed mechanically during flight. The failure was likely caused by thermal-cycling-induced stresses.

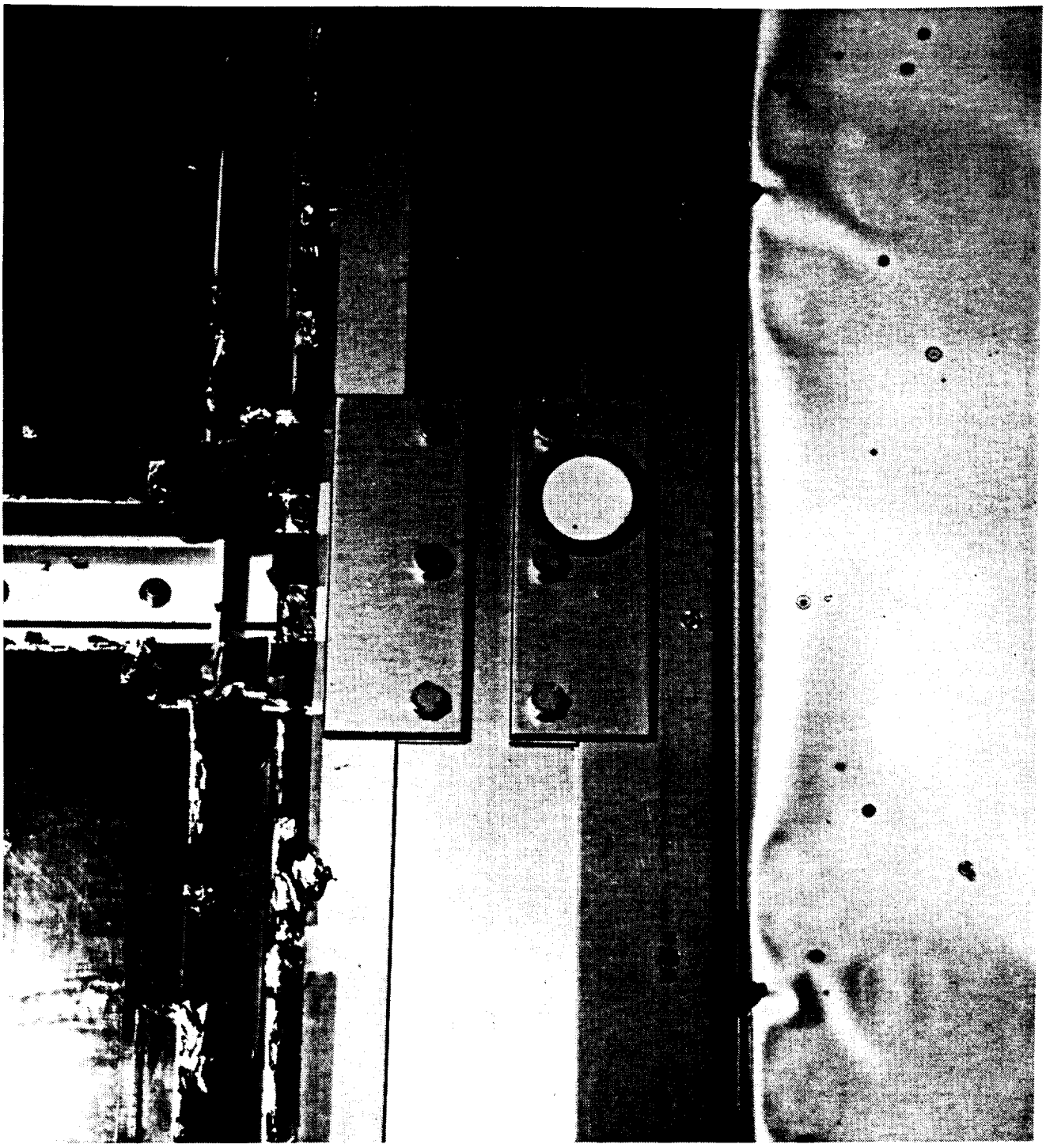

Figure 7.2-22. NASA post-flight photo of leading edge tray clamp with paint button mounted between trays D10 and D11. (Color figure C-32)

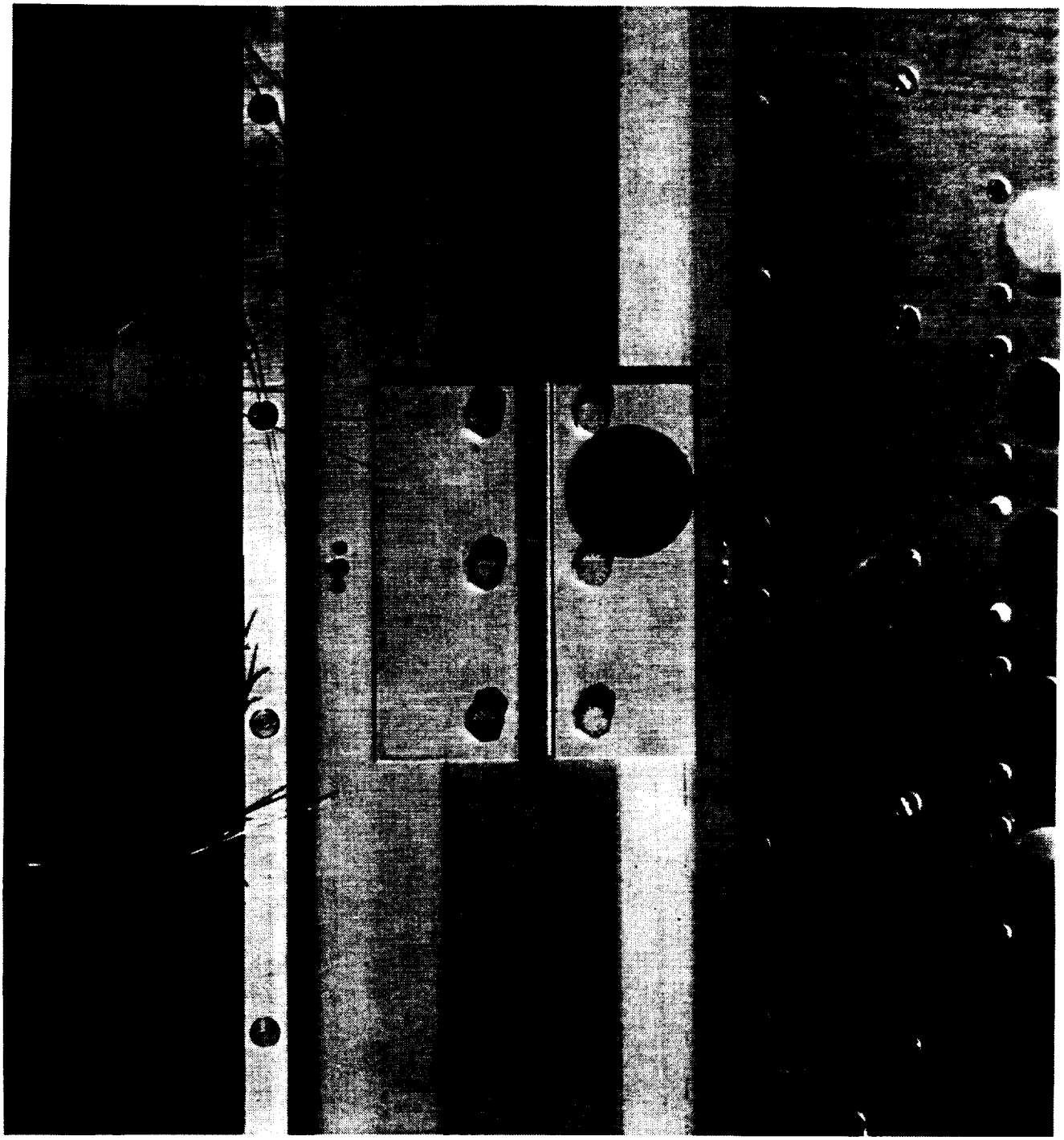

Figure 7.2-23. NASA post-flight photo of trailing edge tray clamp with paint button mounted between trays C2 and C3. (Color figure C-33)

The space end photo in figure 7.2-24 shows the extreme directionality of impingement of atomic oxygen. The top portion of the paint button, shielded from AO, has darkened under UV exposure. The majority is white where it has been attacked by moderate amounts of AO. The ram exposure is a grazing angle incidence from the right. The flag is a decal applied just before the flight.

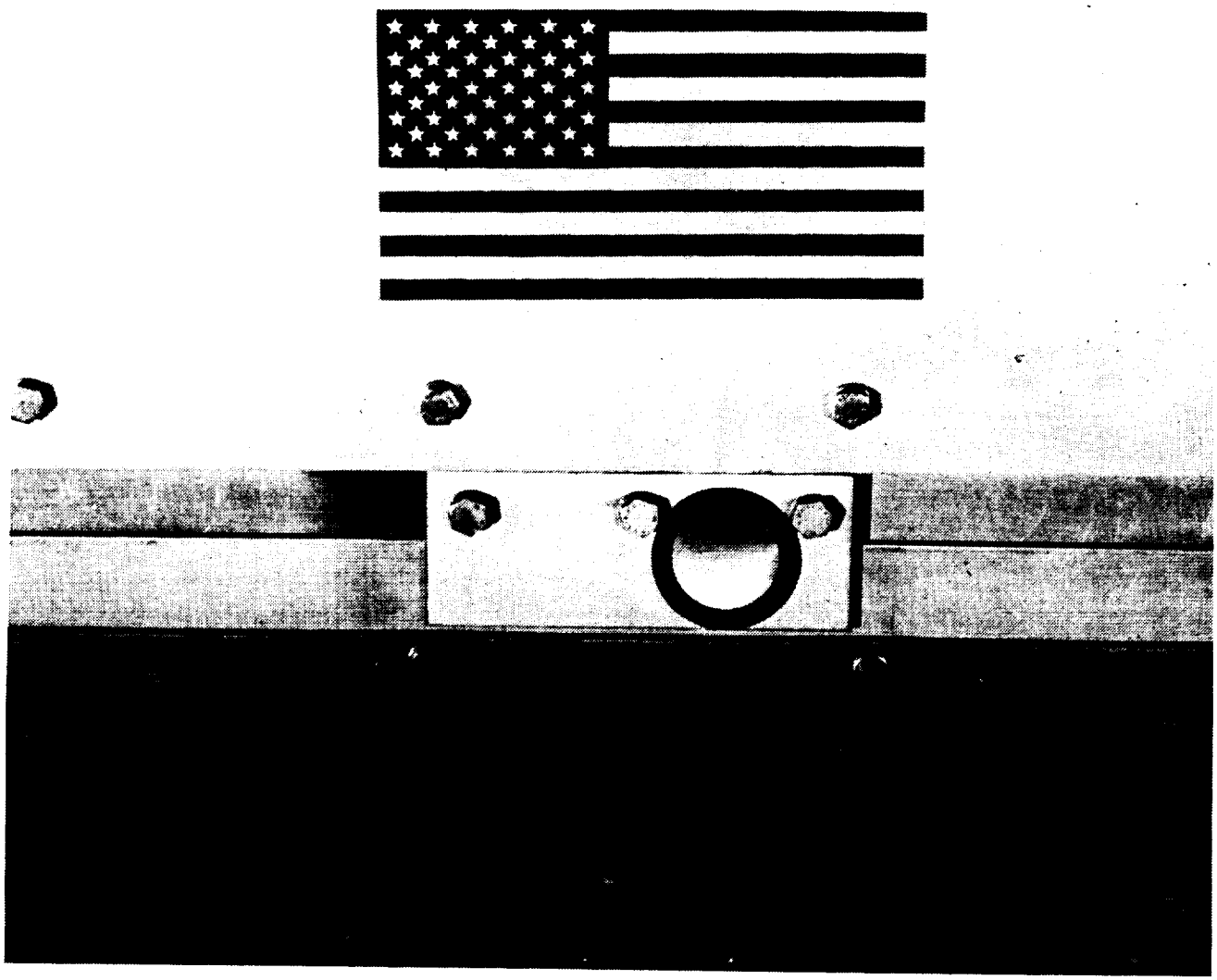

Figure 7.2-24. NASA post-flight photo showing detail of space end of LDEF showing blocking of ram atomic oxygen impingement on a paint button by a tray clamp bolt. (Color figure C-34).

8.0 MATERIALS PERFORMANCE EVALUATIONS

8.1 Silverized Teflon

This material performed its thermal control function under all exposure conditions experienced by the LDEF. The material reflectance changed from essentially specular to essentially diffuse under atomic oxygen exposure. M&D impacts damaged <2% of the area on thermal control blankets from experiment AO178. The silver Inconel layer cracked on adhesive-backed silverized Teflon applied to hardware on trays F9 and A9. The average recession rate of ~ 0.34 10^{-24} atoms/cm^2-sec is much higher than previously reported data from short term Space Shuttle experiments. This higher recession rate is because the UV induced damage is much greater on LDEF than for the relatively short Space Shuttle flights. Once the solar exposure has damaged the structure of the FEP, atomic oxygen is able to attack the polymer backbone. Exposure to solar vacuum ultraviolet (VUV) radiation embrittles the FEP layer, lowering its mechanical properties. Adhesive backed Teflon tape on the M0001 experiment cracked and ripped apart. The solar exposure and thermal cycling together with lack of stress relief areas in the tape are the likely causes of the failure.

8.2 Aluminum

In addition to the large surface area of chromic acid anodized aluminum, bare unanodized aluminum clamps were flown on trays C9, D9, C3, and D3. The optical properties of the unanodized 6061 aluminum, shown in figure 7.2-18, show why anodization is necessary. A polished 6061-T6 specimen flown on tray D3 appears uneffected by its space exposure. Specimens on tray D3, experiment MOOO2, were given extremely thin oxide coatings by the post capture exposure on LDEF. Areas of these same specimens shielded during flight by aluminum plates had oxide coatings from ground exposure about 300-400Å thinner than for exposed areas (ref. 31).

Solar absorptance of anodized aluminum tray clamps A6-3, A9-3 and D12-8 was measured in air and in vacuum, at multiple locations on each clamp. The difference in post-flight absorptance measurements in air and vacuum for each location ranged between 0.007 and 0.001 absorptance units, with the air value always being higher. These differences are within the uncertainty of the measurement.

Figure 8.2-1 is a table of average values of absorptance (α) and emittance (ε) for individual chromic acid anodized aluminum tray clamps, from which the conclusions in the report on anodized aluminum were drawn (ref. 7). On average, slight decreases (typically 0-0.02) in ε were observed on tray clamp exposed surfaces relative to unexposed surfaces on the same clamp. For trailing edge clamps, no change to slight increases (typically 0-0.03) in α were observed for the exposed side of a given clamp relative to the unexposed side of the same clamp. For leading edge locations ($>10^{21}$ atoms/cm^2 fluence of AO) very slight decreases (typically 0.01-0.02) in α were observed on exposed surfaces relative to unexposed surfaces on the same clamp. While the overall average changes appear to be real, they are also small, probably induced by varying contamination layers, and are not significant for engineering considerations.

Specimen	α		ε		Specimen	α		ε	
	front	back	front	back		front	back	front	back
F1-7	0.36	0.35	0.17	0.17	B1-4	0.35	0.35	0.17	0.18
C1-7	0.42	0.34	0.20	0.17	D1-4	0.37	0.33	0.16	0.16
D1-7	0.33	0.31	0.14	0.14	E1-5	0.37	0.35	0.14	0.15
F1-3	0.34	0.33	0.15	0.16	E1-3	0.34	0.34	0.15	0.18
E1-8	0.33	0.33	0.15	0.16	F1-8	0.34	0.34	0.14	0.16
B1-1	0.34	0.34	0.15	0.16	D1-1	0.33	0.33	0.15	0.16
C1-2	0.34	0.34	0.15	0.17	F1-3	0.34	0.33	0.15	0.16
E1-3	0.34	0.34	0.15	0.18					
E2-3	0.34	0.34	0.15	0.17	E2-8	0.34	0.35	0.15	0.16
A2-8	0.36	0.37	0.14	0.15	A2-2	0.34	0.32	0.16	0.17
F2-8	0.35	0.33	0.15	0.16	C2-1	0.39	0.35	0.17	0.17
C2-2	0.35	0.34	0.17	0.16	D2-1	0.35	0.34	0.16	0.16
D2-3	0.35	0.34	0.16	0.17	A2-4	0.34	0.33	0.13	0.15
B2-4	0.34	0.33	0.15	0.15	E2-7	0.36	0.37	0.17	0.18
E2-6	0.38	0.35	0.17	0.18	F2-6	0.36	0.33	0.17	0.16
F2-5	0.35	0.35	0.14	0.15	D2-7	0.36	0.33	0.15	0.15
C2-7	0.33	0.32	0.15	0.15	C2-6	0.34	0.34	0.13	0.15
B2-6	0.36	0.34	0.14	0.14					
E3-8	0.41	0.36	0.18	0.20	C3-2	0.37	0.34	0.16	0.16
A3-5	0.37	0.35	0.18	0.17	E3-3	0.37	0.36	0.15	0.16
E3-6	0.33	0.34	0.14	0.17	F3-2	0.32	0.32	0.14	0.14
F3-6	0.35	0.34	0.15	0.16	F3-3	0.32	0.34	0.15	0.16
B3-5	0.33	0.33	0.14	0.15	C3-6	0.36	0.34	0.13	0.13
A3-8	0.34	0.34	0.13	0.13	A3-7	0.36	0.34	0.16	0.16
B3-2	0.36	0.32	0.15	0.15	E3-1	0.36	0.35	0.14	0.16
F4-2	0.34	0.35	0.15	0.14	B4-2	0.33	0.33	0.13	0.14
B4-4	0.35	0.35	0.14	0.16	C4-2	0.38	0.35	0.16	0.17
E4-2	0.38	0.34	0.16	0.16	B4-7	0.34	0.33	0.15	0.19
D4-6	0.35	0.33	0.16	0.16	C4-5	0.36	0.34	0.15	0.17
D4-8	0.34	0.33	0.15	0.16					
E5-1	0.38	0.37	0.17	0.19	D5-1	0.33	0.35	0.14	0.16

Figure 8.2-1. Post-flight solar absorptance and thermal emittance of selected anodized aluminum tray clamps from LDEF.

Specimen	α		ε		Specimen	α		ε	
	front	back	front	back		front	back	front	back
D5-3	0.33	0.32	0.14	0.15	F5-8	0.35	0.33	0.15	0.17
D5-6	0.37	0.35	0.15	0.17	A5-5	0.37	0.37	0.17	0.16
B5-4	0.36	0.35	0.15	0.17	C5-1	0.33	0.32	0.15	0.16
F5-4	0.34	0.33	0.15	0.17	C5-5	0.36	0.34	0.16	0.17
C5-2	0.36	0.34	0.16	0.17					
F6-4	0.33	0.35	0.15	0.16	E6-8	0.33	0.34	0.15	0.18
E6-1	0.38	0.36	0.17	0.16	E6-3	0.35	0.35	0.17	0.17
A6-2	0.36	0.34	0.17	0.17	A6-3	0.36	0.38	0.18	0.16
C6-1	0.34	0.33	0.15	0.14	C6-2	0.35	0.33	0.17	0.17
F6-1	0.38	0.36	0.16	0.17	B6-1	0.38	0.36	0.15	0.16
E6-6	0.34	0.36	0.16	0.17	D6-7	0.32	0.33	0.15	0.14
C6-5	0.33	0.35	0.15	0.16	B6-5	0.35	0.34	0.14	0.15
B6-7	0.34	0.33	0.14	0.15	F6-6	0.34	0.33	0.13	0.15
D6-6	0.33	0.33	0.13	0.15					
B7-2	0.33	0.34	0.16	0.18	B7-5	0.34	0.34	0.16	0.17
B7-7	0.34	0.34	0.15	0.16	B7-4	0.33	0.33	0.13	0.16
E7-8	0.34	0.33	0.16	0.17	D7-6	0.33	0.34	0.15	0.17
A7-7	0.35	0.33	0.16	0.17	A7-4	0.33	0.35	0.17	0.18
F7-7	0.32	0.33	0.16	0.17	F7-5	0.33	0.34	0.15	0.17
F7-2	0.32	0.33	0.13	0.14	A7-5	0.32	0.34	0.15	0.16
F7-3	0.33	0.34	0.14	0.16	F7-7	0.32	0.33	0.16	0.14
E8-8	0.35	0.35	0.16	0.16	E8-3	0.34	0.34	0.14	0.16
C8-8	0.34	0.36	0.13	0.15	E8-1	0.34	0.34	0.15	0.15
F8-3	0.32	0.33	0.16	0.16	F8-4	0.33	0.34	0.15	0.17
C8-5	0.33	0.35	0.16	0.17	E8-6	0.33	0.33	0.15	0.15
F9-6	0.33	0.34	0.16	0.16	F9-8	0.34	0.34	0.15	0.16
A9-3	0.38	0.36	0.17	0.17	C9-2	0.34	0.35	0.16	0.18
A9-7	0.33	0.33	0.15	0.16	C9-6	0.32	0.33	0.12	0.13
B9-3	0.34	0.37	0.15	0.17	B9-1	0.35	0.35	0.15	0.17
F9-4	0.34	0.34	0.13	0.13	E9-4	0.35	0.35	0.13	0.13
D9-1	0.33	0.33	0.15	0.15	D9-6	0.33	0.34	0.14	0.16

Figure 8.2-1 (continued). Post-flight solar absorptance and thermal emittance of selected anodized aluminum tray clamps from LDEF.

Specimen	α		ε		Specimen	α		ε	
	front	back	front	back		front	back	front	back
E9-3	0.32	0.33	0.14	0.17	B9-7	0.33	0.34	0.15	0.16
E9-2	0.36	0.34	0.13	0.13					
A10-3	0.36	0.36	0.16	0.16	D10-1	0.31	0.33	0.14	0.16
F10-1	0.34	0.35	0.14	0.16	B10-2	0.33	0.35	0.15	0.17
F10-7	0.35	0.35	0.17	0.15	A10-4	0.34	0.33	0.17	0.18
A10-7	0.33	0.35	0.16	0.18	E10-6	0.34	0.36	0.15	0.18
D10-6	0.32	0.33	0.15	0.18	F10-4	0.34	0.33	0.13	0.14
B10-5	0.32	0.38	0.14	0.17	B10-8	0.33	0.33	0.13	0.13
F11-1	0.39	0.35	0.18	0.17	F11-3	0.34	0.36	0.16	0.18
F11-5	0.34	0.37	0.16	0.18	A11-3	0.36	0.36	0.17	0.17
F11-8	0.32	0.34	0.14	0.16	D11-6	0.33	0.35	0.15	0.18
D11-1	0.31	0.33	0.14	0.16	C11-7	0.33	0.33	0.15	0.17
B11-1	0.32	0.33	0.13	0.14	B11-5	0.33	0.35	0.15	0.17
B11-2	0.33	0.34	0.15	0.18					
E12-2	0.35	0.34	0.14	0.14	F12-3	0.34	0.34	0.15	0.16
D12-3	0.32	0.32	0.14	0.15	A12-3	0.32	0.33	0.15	0.17
D12-6	0.33	0.34	0.15	0.17	A12-7	0.32	0.32	0.14	0.16
B12-4	0.33	0.36	0.15	0.18	F12-6	0.34	0.33	0.15	0.18
F12-8	0.33	0.34	0.15	0.16	F12-7	0.15	0.16	0.08	0.08
A12-4	0.33	0.34	0.14	0.16					

Figure 8.2-1 (continued). Post-flight solar absorptance and thermal emittance of selected anodized aluminum tray clamps from LDEF.

8.3 Thermal Control Materials

In addition to the anodized aluminum and Ag/FEP, which together accounted for the large majority of the surface area on the LDEF, several selected white paints, black paints, black anodize coating, and selected highly specific specialty coatings, were flown as specimens or in-service hardware.

Z-93 white paint specimens from both leading and trailing edges were essentially unchanged by the exposure conditions. This result lead to designation of the Z-93 as the baseline white thermal control paint for the International Space Station. S13G/LO used on certain experiment modules darkened under solar UV exposure. This result was expected as significant changes S13G/LO absorptance have been observed on other spacecraft and during ground-based testing.

Polyurethane based A276 (white) and Z-306 (black) Chemglaze paints (ref. 8) showed significant degradation under the range of LDEF exposures: loss of binder from each paint under atomic oxygen attack, loss of pigment in the Z-306 under AO attack, and severe darkening of A276 under solar UV exposure. The white paint used for the paint buttons on the aluminum tray clamps was $1\,^1/_2$ quarts of a Dissler flattener (DX 256) for every $^1/_2$ gallon of A276.

Black D111 paint and SiO_x/nickel coatings performed satisfactorily. Optical properties of an aluminum leaf in epoxy binder used as a coating on the leading edge actually improved over the mission. Absorptance increased due to UV-induced darkening of the binder on trailing edge aluminum leaf coated specimens. Mechanical integrity of the leading edge specimens was compromised but this should not be an in-service problem on spacecraft as long as no physical contact is made with the surface.

A number of panels on the Earth facing end and an area on the McDonnell-Douglas experiment on tray F9 were coated with black chrome plate. Post-flight examination clearly showed areas of discoloration of the black chrome coating. Figure 8.3-1 is a photo of this radiator. Details of an extensive investigation of the F9 radiator are contained in the report on Thermal Control Paints (ref. 8) and a paper from the 2nd Post-Retireval Symposium (ref. 32). Despite considerable effort, including optical property measurements, surface analysis, and thermal modeling, a clear and obvious mechanism to explain the color pattern has not been found. Contamination has been ruled out. The tan areas were shielded by

the aluminum backing from a failed aluminized Kapton blanket. The process which caused the changes is still not understood.

Two black chrome-plated panels from the Earth end, identified as 916-10A and 916-4A, were examined in several locations for comparison with the F9 plate. Figure 8.3-2 shows a NASA on-orbit photo of the Earth end of LDEF, including the black chrome panels of interest. The end panels have small ~4 inch wide sections bent at 90 degrees to the large, Earth-facing part of each panel. The small section on each plate overlays the Earth end intercostal for a particular row and is oriented with respect to the ram direction in the same manner as the particular row. This means that, in addition to the Earth-facing exposure, a continuous range of exposure conditions was experienced around the bend. One edge of panel 916-10A is on row 10, 22° from ram. Figure 8.3-3 shows the relationship between the angle around the bend in the panel, measured from the Earth facing end as 90°, and the angle from ram. Figure 8.3-4 shows the Earth-end panel (916-10A) with black chrome plate finish.

The larger, roughly triangular side of panel 916-4A was Earth facing and received about 3.3×10^{20} atoms/cm^2 fluence of AO and about 4500 ESH solar radiation. The small rectangular side was exposed on row 4, and saw no AO and about 10500 ESH solar radiation. This difference is accentuated by the fact that only a little over 1000 hours on the Earth end was direct solar, while the remainder was Earth-reflected sunlight.

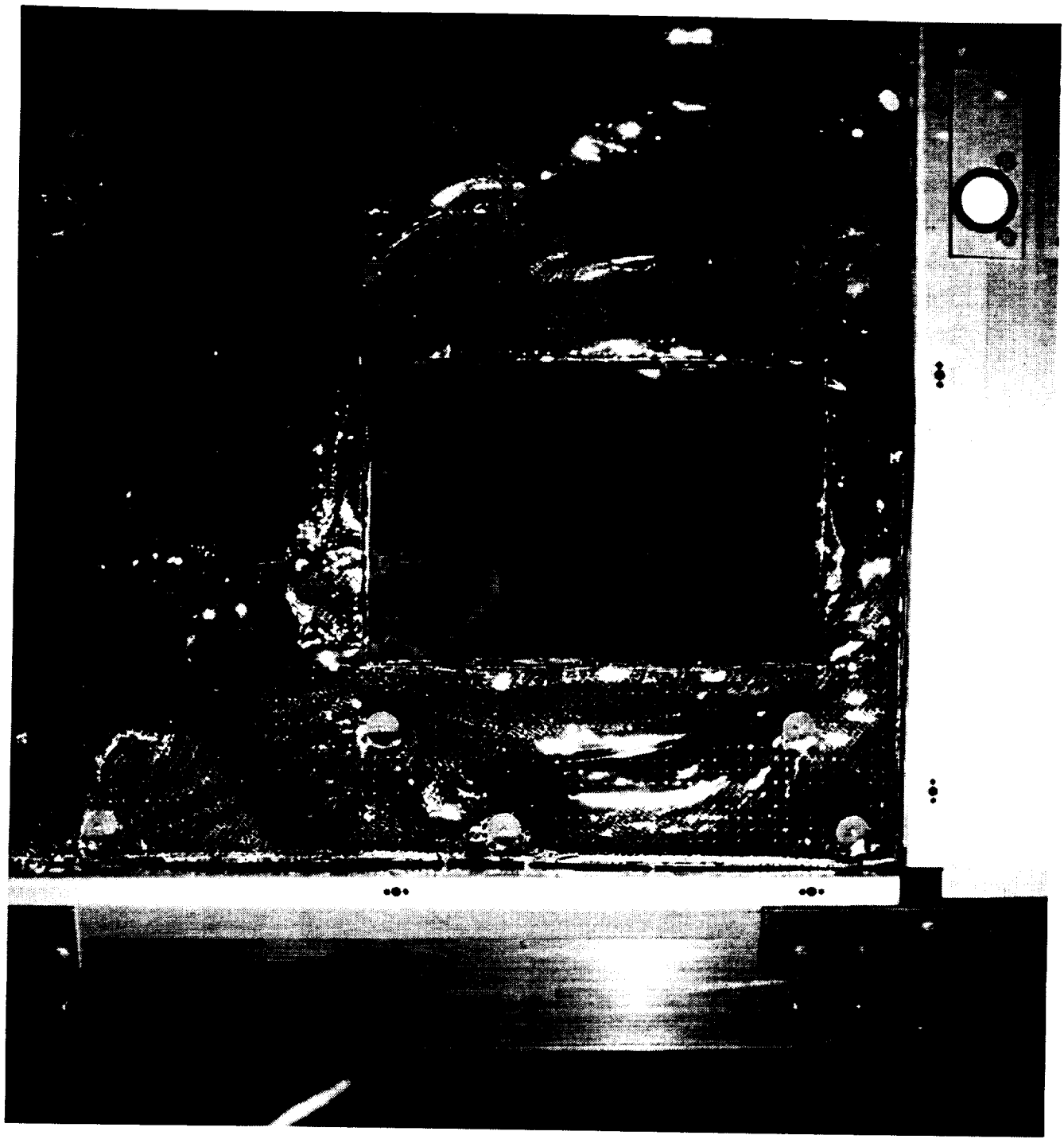

Figure 8.3-1. NASA post-flight photo of radiator panel from tray F9. (Color figure C-35 rotated 90°)

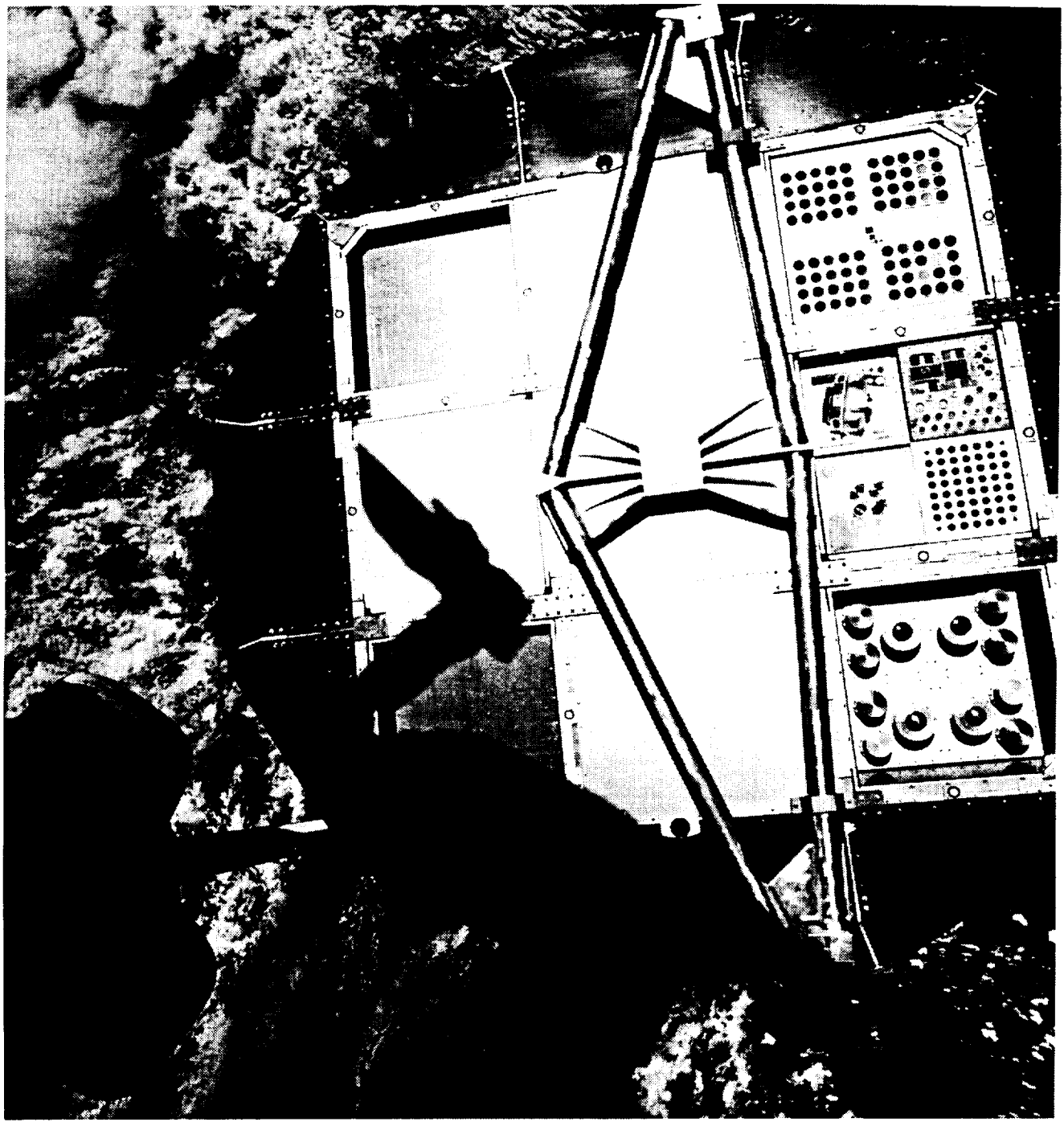

Figure 8.3-2. NASA on-orbit photo of Earth end of LDEF. (Color figure C-36)

Angle around panel curve (deg)	Angle from ram (deg)
0	22
10	24
15	26
20	28
25	33
30	37
35	41
40	45
45	49
50	53
55	58
60	62
65	67
70	71.5
75	76
80	81
90	90.8

Figure 8.3-3. Angle along panel bend correlated with angle from ram for panel 916-10A.

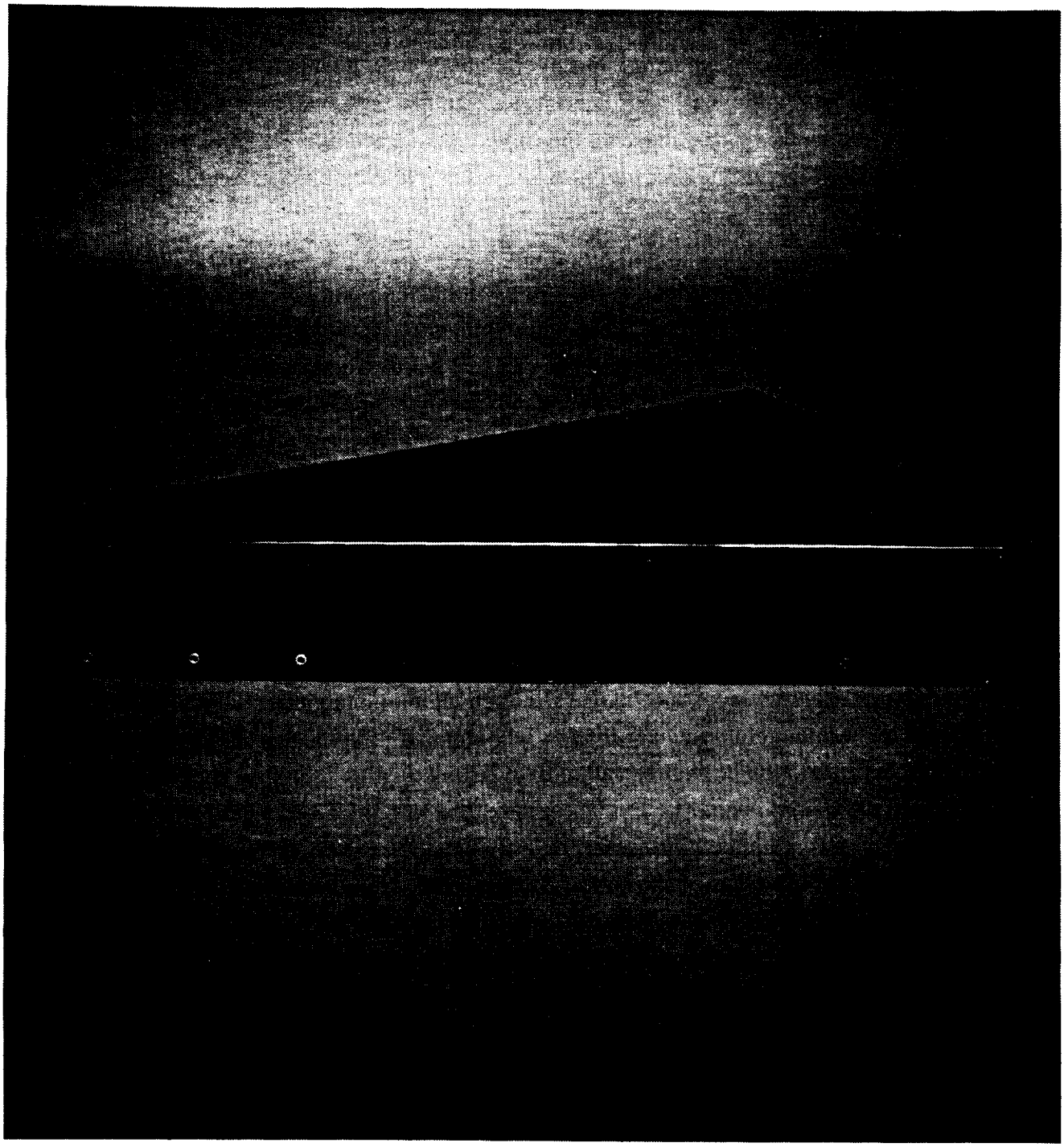

Figure 8.3-4. NASA post-flight photo of panel 916-10A from LDEF Earth end. (Color figure C-37)

In comparison, the higher exposure levels at orientations toward row 4 were primarily from direct solar. The rectangular area on 916-10A was on row 10 and saw 8.4 x 10^{21} atoms/cm^2 AO fluence. The orientation of the curved portion on this panel varied between 22° from ram to 90.8° from ram, with the corresponding variation in AO exposure.
Surface analysis and optical measurements were carried out on specimens from a number of locations on this panel, including the curved portion between the Earth and row four facing areas. The panel surface was a chrome oxide layer over a nickel layer on a 6061-T6 aluminum substrate.

Data on chrome oxide thickness and silicon content were obtained by auger depth profiling at the selected locations on panel 916-4A are reported in figure 8.3-5. A diagram of the locations of this set of samples is shown in figure 8.3-6. The detailed auger spectra are included in appendix B, as are results of surface analysis by ESCA. Samples 1 through 5 were chosen as being representative of different colored areas visible on the surface. Specimens 6, 7, and 8 were chosen to sample the 90° bend in the panel. The row 4 facing part is labeled as the 0° end and the large Earth-facing area is the 90° end. The row 4 facing surface was generally a lighter brown than the Earth-facing surface, although there were streaks of light brown at many locations on the Earth-facing surface. Golden brown areas were visible particularly near the edge of the Earth-facing part of the panel. Several areas of bright blue color were observed on one side (away from the leading edge direction) of the large bolt holes. SEM photographs showed the blue and golden brown areas to be smoother than most of the darker areas on both surfaces. The rougher surfaces seemed to pitted or dented with the pits generally ~10 to 20μm across. The pits did not penetrate the chrome oxide layer on the surface. The analysis area was 300 x 240μm, and thus averaged over many pits. Chrome, carbon, oxygen, and silicon were detected at the surface of each area sampled. The range of silicon was 3.8% to 10.2% of the surface, with an average of 5.9%. The silicon concentration did not seem to be related to the color of the panel surface, the thickness of the chrome oxide layer, or the specimen location on the panel. The sputter rate of silicon is about 160Å/minute and the silicon was generally sputtered away within 1 minute. Small amounts of S, Cl, F, and Na were detected at the surface of some specimens. Specimens were sputtered to a depth of ~4000Å. This depth was sufficient to have sputtered through the chrome oxide layer in all specimens.

Figure 8.3-7 shows the oxide thickness, angle along the bend (from 0° at row 10 to 90° at the Earth-facing surface), angle from ram, and amount of surface silicon in each of a series of specimens taken from the bend region of panel 916-10A. The thinnest oxide layers are

generally in the bend of the panel. This may be an artifact of the application or manufacturing processes rather than an effect of exposure. The darkest brown, dark blue, and light blue areas generally had the thickest oxides. These results are different from earlier work on the black chrome plated coverplate for experiment AO076, located on tray F9. On that surface, the thickest oxide (1770Å) was in a light brown area and the thinest oxide (1200Å) was in a blue area.

Reflectance and emissivity were measured at selected locations on both pieces of black chrome plated hardware. The results are shown in figure 8.3-8. Locations of the samples for these measurements are shown in the diagrams of figures 8.3-9 and 8.3-10. Sample 2 from panel 916-4A and sample 3 from panel 916-10A were chosen because these locations appeared to be representative of the majority of the surface area on the row 4 and row 10 facing areas of these panels, respectively. Sample 1 from each panel was on the Earth-facing piece and each was visually brown. The other measurement locations appeared blue. In spite of the considerable differences in visual appearance the measured optical values for these areas were similar.

Specimen	Oxide thickness (Å)	Si% on surface
#4 brown 0 °	2150	5.8
#4 brown 0 ° (b)	2210	5.4
#7 brown 0 °	2000	6.3
#8 brown 0 °	2040	6.4
#8 brown 6 °	1960	7.2
#7 brown 15 °	1790	5.5
#8 brown 20 °	1940	5.0
#7 brown 30 °	1830	4.7
#8 brown 30 °	1780	5.5
#8 brown 40 °	2000	9.2
#6 brown 45 °	1820	5.0
#7 brown 45 °	1800	4.8
#8 brown 52 °	1980	6.2
#7 brown 60 °	1920	5.0
#8 brown 62 °	2020	5.5
#7 brown 75 °	2030	4.7
#8 brown 75 °	2100	4.4
#7 brown 90 °	2450	10.2
#8 brown 90 °	2310	5.1
#5 dark brown 90·° (b)	2400	7.0
#5 dark brown 90 °	2430	6.2
#2 plume brown 90 ° (b)	2040	8.6
#2 plume brown 90 °	2040	10.2
#2 off plume dark brown 90 ° (b)	2120	6.5
#2 off plume dark brown 90 °	2130	6.1
#3 off plume dark brown 90 °	2120	5.4
#3 blue line between gold brown & dark brown 90 °	2090	4.9
#3 blue line between gold brown & dark brown 90 ° (b)	2140	5.1
#3 golden brown edge 90 °	2020	5.5

Figure 8.3-5. Oxide thickness and percent silicon on surface for selected specimens from panel 916-4A.

Specimen	Oxide thickness (Å)	Si% on surface
#1 golden brown edge 90 ° (c)	2190	
#1 golden brown edge 90 ° (b)	2160	
#1 golden brown edge 90 ° (a)	2270	4.2
#1 dark blue 90 ° (b)	2500	
#1 dark blue 90 °	2510	4.2
#1 light blue 90 °	2560	3.8
#1 light blue 90 ° (b)	2880	

Figure 8.3-5 (continued). Oxide thickness and percent silicon on surface for selected specimens from panel 916-4A.

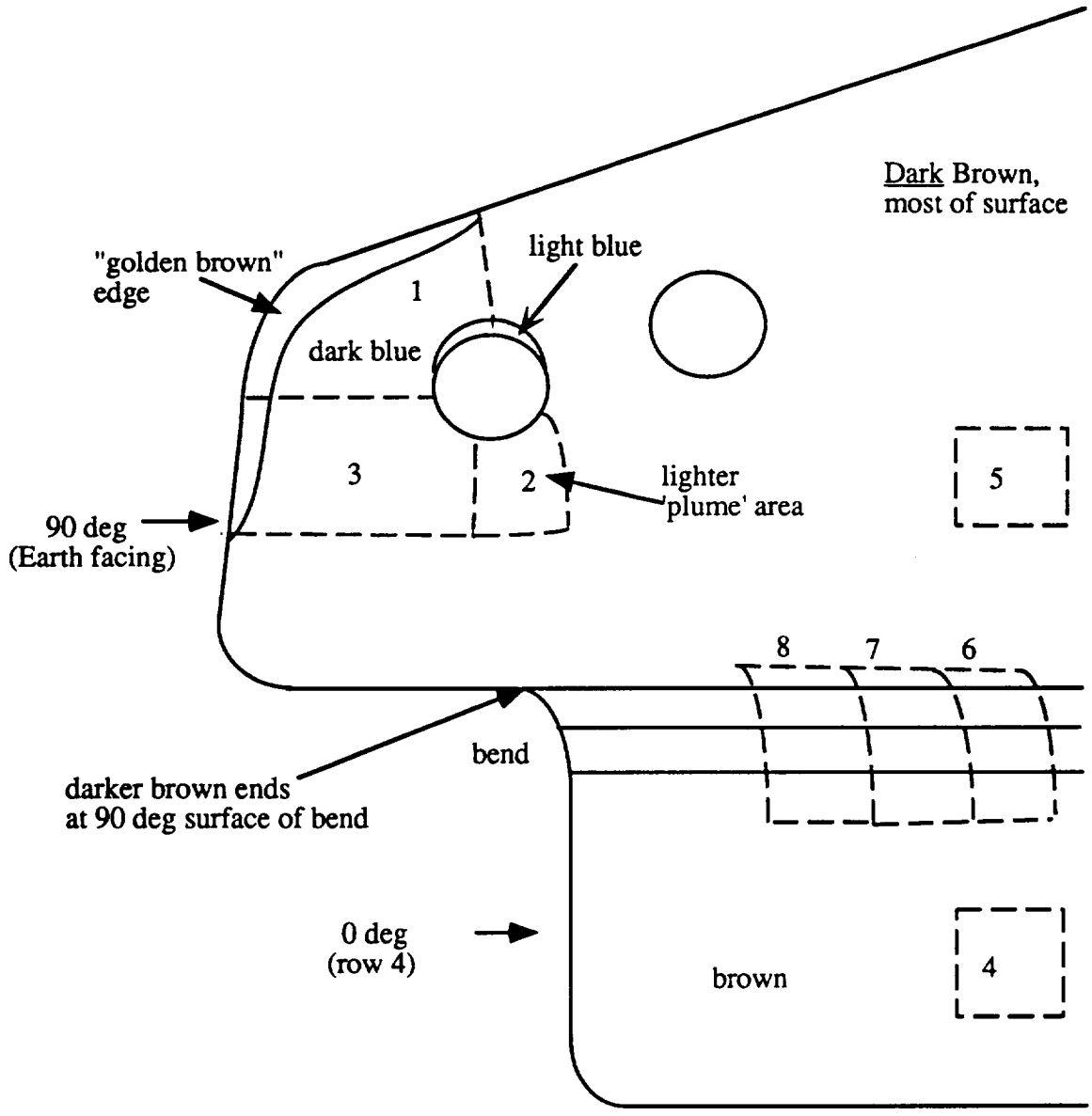

Figure 8.3-6. Diagram of specimens from 916-4A used for % silicon and depth profiles.

Specimen	Angle from ram	Oxide thickness (Å)	Surface Silicon %
#1-0°-a	22°	2290	21.7
#1-0°-b	22°	2220	21.7
#1-5°	22.5°	2330	16.2
#1-18°	28°	2250	9.5
#1-32°	38°	2000	9.1
#1-46°	50°	2400	7.4
#1-59°	61°	2470	10.5
#1-72°	73°	2460	10.8
#1-85°	85°	2480	9.4
#1-90°	90°	2600	11.5
#2-0°-a	22°	2130	22.7
#2-0°-b	22°	2160	21.2
#2-4°	22°	2030	17.4
#2-14°	26°	2000	10.4
#2-25°	33°	1880	8.7
#2-35°	41°	2040	5.5
#2-45°	49°	2260	7.4
#2-56°	59°	2340	4.9
#2-68°	70°	2260	6.7
#2-83°	83.5°	2370	4.9
#2-90°-a	90°	2340	7.6
#2-90°-b	90°	2230	11.7

Figure 8.3-7. Angle from ram, oxide thickness, and surface silicon percent for selected locations on bend in panel 916-10A.

Specimen	Total Normal Reflectance	Emissivity (average)	Absorptance
916-4A-1	0.907, 0.897, 0.897	0.100	0.93
916-4A-2	0.902, 0.901, 0.900	0.099	0.92
916-4A-3	0.910, 0.908. 0.909	0.091	0.94
916-10A-1	0.930, 0.928, 0.931	0.070	0.90
916-10A-2	0.913, 0.911, 0.912	0.088	0.88
916-10A-3	0.936, 0.934, 0.936	0.065	0.89
916-10A-4	0.924, 0.922, 0.920	0.078	0.93

Figure 8.3-8. Measured optical property values for selected locations on black chrome plated aluminum panels.

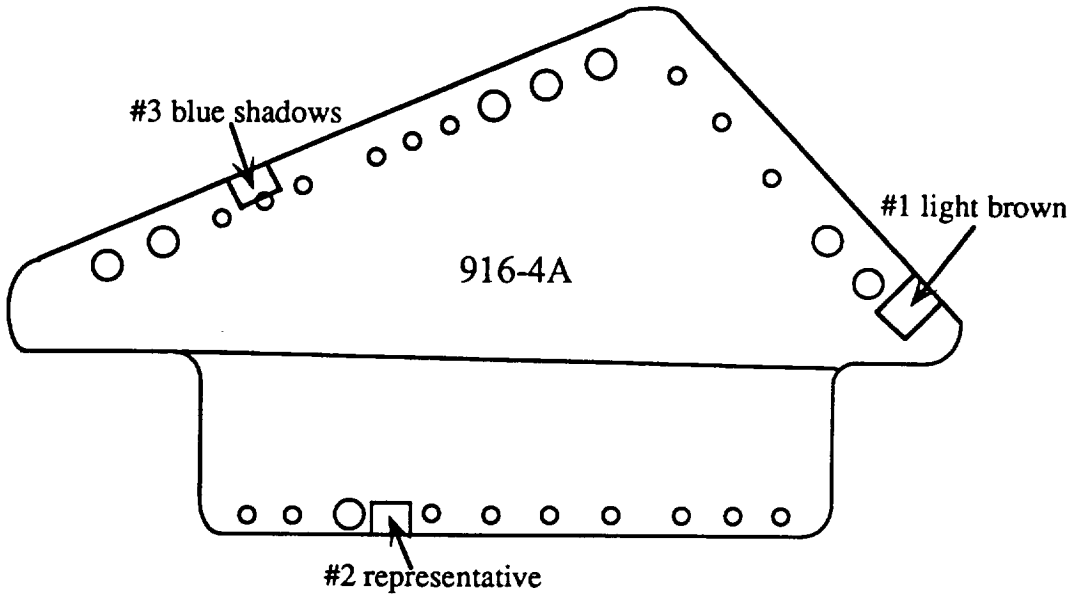

Figure 8.3-9. Specimen locations for optical property measurements on 916-4A.

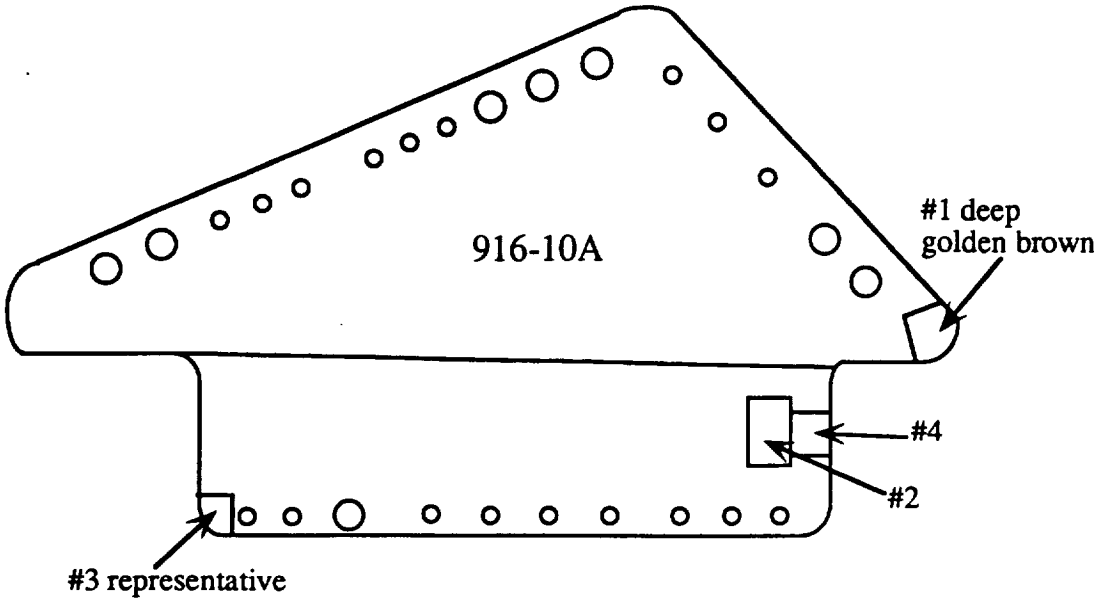

Figure 8.3-10. Specimen locations for optical property measurements on 916-10A.

8.4 Thin Polymeric Films

The increase in the mission duration was catastrophic for many of the thin film specimens and thermal control blankets on the leading edge. Pre-flight material selection included Kapton blankets with thicknesses estimated to be able to withstand a flight of about twice the planned 10-month duration. Aluminized Kapton on the AO076 (row 9) and AO054 (row 10) experiments completely failed after the polymer was removed by atomic oxygen. Thin specimens of weather balloon materials were likewise destroyed.

Kapton on the AO133 experiment, located on the space end, was eroded but not completely removed. Post-flight analysis indicated a recession rate of 1.7×10^{-24} cm^3/atom on this material. The accepted recession rate for Kapton is 3×10^{-24} cm^3/atom, The lower value for this experiment may be due to the fact that the atomic oxygen impinged on the spacecraft surface at a glancing angle in this case. A detailed publication on the mechanical performance of the Kapton and other materials on this experiment is available (ref. 33).

8.5 Composites

Uncoated organic composites recessed under AO exposure, with the resins being eroded faster than the fibers. The leading edge eroded materials suffered some loss of mechanical properties due essentially to reduced cross-sectional areas. Trailing edge specimens suffered no degradation of engineering performance. Extensive on-orbit data on the coefficient of thermal expansion of selected composite materials was obtained on experiment AO180 over the first year of the mission. Coated composites survived well; coatings as thin as 1600Å protected composites on the leading edge from any mass loss. In certain cases, the coatings suffered damage and/or were degraded by the exposure, but in all cases the underlying composite material was undamaged, except for the occasional impact, and suffered no loss in mechanical properties. These findings and other details are covered in the Composite Materials final report (ref. 13).

Selected metal-matrix composites were flown on M0003 to evaluate thermal expansion behavior on-orbit. The Gr/Al performed better than the Gr/Mg. Some thermally induced bending was observed in the Gr/Mg, attributed to the lower thermal conductivity of this material (ref. 34).

8.6 Metals

A variety of metals were flown as specimens and as in-service hardware. A summary of metals findings are included in a separate report on the performance of metals on LDEF (ref 12). Metals varied in their response to the environmental exposures. Gold was unaffected by exposure to LEO. Metals such as copper, aluminum, tungsten, and molybdenum formed thin passivating oxide layers under AO exposure. Silver and osmium were severely attacked by AO, and in some cases completely eroded. Metals were generally unaffected by solar exposure except for deposition of thin contamination layers.

8.7 Adhesives

A wide variety of adhesives and adhesive-like materials were flown on LDEF. The majority of these materials were not part of the experimenters' initial objectives but because of the extended mission time these materials became valuable experiments in themselves. The adhesive and adhesive-like materials flown on LDEF included epoxies and silicones (including lap shear specimens), conformal coatings, potting compounds, and several tapes and transfer films. Most of these materials were used in the fabrication and assembly of experiments, such as bonding thermal control surfaces to other hardware and holding individual specimens in place, similar to applications on other spacecraft. Typically, adhesives were not exposed to solar radiation or atomic oxygen. Only one adhesive system was used in a structural application. The performance of adhesives is documented in a separate report (ref. 16).

Nearly 400 aluminum-backed paint buttons mounted on the tray clamps were attached with MYSTIK aluminum adhesive Tape 740-2L. There were no bonding failures of any of these paint buttons.

Solar cells bonded with Shell EPON 828 were lost during flight; however, this adhesive was used successfully at other locations. FEP and Kapton films attached with RTV debonded. However, this failure may have been due to lack of primer and not the adhesive.

Silicone adhesives also provided many localized sources of outgassed material. This is evidenced by the presence of Si on many analyzed specimens taken from near identified locations of silicone adhesive.

8.8 Seals and Lubricants

A wide variety of seals and lubricants were also flown on LDEF. Like the adhesive specimens, these materials were generally not part of experimenter's initial objectives but because of the extended LDEF mission, also became valuable experiments in themselves. These materials generally performed as required during the flight. Some damage to the EECC seals on the leading edge (rows 8 and 9) was observed. Cetyl alcohol used as a lubricant on numerous bolts essentially evaporated and many of these bolts seized upon attempted removal. A detailed report has been produced for these materials (ref. 9).

8.9 Ceramics-Glasses

Several documents have reported in detail the results of examination of the many optical specimens flown on LDEF. One of the mini-databases developed by the MSIG is exclusively dedicated to optical materials. Issues of concern for most optical materials are scattering induced by even single particulates on the surface, thin molecular film contamination lowering the transmission through the glass, and catastrophic damage due to meteoroid or debris impacts.

Ceramic materials, such as Si_3N_4, were essentially inert to the environmental exposure with the exception of some darkening on the surface due to contamination layers (ref. 35).

8.10 Shielded Hardware

A report on the condition of selected hardware from the interior of LDEF has been published (ref. 1). Hardware from the interior generally appeared in excellent condition during post-flight examination. Contamination deposits were found on a number of materials. Outgassing data was obtained for heat shrink tubing, velcro, and RTV silicone adhesive from numerous locations.

9.0 ENVIRONMENTS MODELING OF SELECTED HARDWARE

Atomic oxygen and solar UV exposure are two of the primary contributors to degradation of spacecraft materials in the low Earth orbit environment. Three sets of computer programs have been developed to model the low Earth orbit space environment. Two of these sets of programs model atomic oxygen exposure to spacecraft surfaces and one models solar exposure to spacecraft surfaces. The first atomic oxygen program set calculates direct fluence to unshielded spacecraft surfaces. The second program set models the atomic oxygen fluxes to spacecraft surfaces which may shadow or reflect atomic oxygen to one another. Neither atomic oxygen model accounts for atomic oxygen density buildup due to scattering from surfaces.

The solar exposure program models solar exposure to spacecraft surfaces from both direct solar exposure and Earth-reflected solar exposure, as well as from exposure reflected from one surface to another. The following paragraphs give an overview of the capabilities of these codes.

9.1 FLUXAVG

The direct atomic oxygen exposure model FLUXAVG (ref. 36) calculates atomic oxygen exposure to unshielded surfaces on satellites such as LDEF, which have fixed orientation with respect to heading direction in orbit and with respect to the center of the Earth. Inputs to FLUXAVG include mission start and end dates, surface orientation, a file of solar and geomagnetic data, and a file of orbit data including conventional orbital elements, satellite drag coefficient, area, and mass.

FLUXAVG employs several features which lead to accurate modeling of atomic oxygen fluxes and fluences on satellite surfaces. Atomic oxygen is an ideal gas with a Maxwell-Boltzman velocity distribution. A function has been derived which gives the flux on a surface as a function of surface orientation with respect to the ram direction, atomic oxygen density and kinetic temperature, and satellite velocity relative to the atmosphere. When a satellite moves through such a gas, the flux received by satellite surfaces is highly dependent on surface orientation. For a typical low Earth orbit satellite, the flux on a surface parallel to the ram direction is approximately 5% of the flux on a surface facing ram and the flux on a trailing surface is many orders of magnitude lower. It is assumed that the Earth's atmosphere (including atomic oxygen) co-rotates with the Earth. Because of this

the satellite velocity and surface orientation relative to the atmosphere depend on orbit inclination and position on orbit. Atomic oxygen density and temperature depend on solar and geomagnetic activity, altitude, latitude, longitude, date, and time of day. The standard NASA MSIS-86 atmospheric model (ref. 37) calculates atomic oxygen density and temperature using these factors. Flux on satellite surfaces for long missions is usually calculated for a number of short periods throughout the mission. These fluxes are used to calculate fluence for the mission. For short missions, the fluxes may be calculated continuously throughout the mission. A modified version of the short-term orbit propagation routine ASAP (ref. 38) calculates satellite position and calls the MSIS-86 atmospheric model to calculate atomic oxygen density and temperature at a representative number of positions on orbit for short periods. A modified version of the long-term orbit propagation routine LOP (ref. 39) propagates the orbit over long periods to provide orbital elements for the start of ASAP calculations. When all fluxes have been calculated for a mission, fluences on satellite surfaces are calculated.

Outputs from FLUXAVG for times throughout the mission include fluxes and fluences for each surface, for true ram and parallel to ram surfaces, average, maximum, and minimum atomic oxygen densities, temperatures, satellite altitudes, absolute satellite speed, and satellite speed relative to the atmosphere. All outputs are written to a standard (printer) output file and to a mission file. The mission file is set up to be convenient for extraction of data by auxiliary codes.

9.2 SHADOWV2

The microenvironment atomic oxygen exposure program SHADOWV2 (ref. 40) calculates total atomic oxygen fluxes on surfaces of satellites such as LDEF, which have fixed orientation with respect to heading direction on orbit and to the center of the Earth. The total flux predictions include contributions from primary and scattered (both specular and diffuse reflected, and absorbed) atomic oxygen fluxes on surfaces. Because it is computationally impractical to calculate these fluxes at a large number of positions on orbit as is done in FLUXAVG, event average atomic oxygen density, temperature, and satellite speed relative to the atmosphere are used as representative conditions. Complicated satellite surfaces are constructed from simple geometric surfaces.

After reading input, SHADOWV2 calculates a table of directional fluxes (flux per steradian as a function of angle off average ram direction) based on the Maxwell-Boltzman velocity distribution and average satellite speed relative to the atmosphere. Rays are traced from points on the satellite surfaces. The atomic oxygen flux is accumulated from the rays which are unblocked. Atomic oxygen is Monte Carlo scattered from surfaces based on their surface properties for atomic oxygen scattering (specular and diffuse reflection, surface reaction, and recombination). If reflection occurs, the ray is propagated until it is removed from consideration by surface reaction or recombination or until it no longer strikes any surface. Scattered fluxes on surfaces are accumulated.

9.3 SOLSHAD

The microenvironment solar exposure program SOLSHAD (ref. 41) calculates primary and Earth-reflected direct and reflected solar exposure in cumulative Equivalent Sun Hours (ESH) to complex satellite surfaces for satellites in circular orbit with fixed orientation to heading direction on orbit and to the center of the Earth. Somewhat elliptic orbits may be approximated as circular with little loss in accuracy. Inputs to SOLSHAD include event start and end dates, simple circular orbit specification (if desired, exposure calculations can be limited to a portion of an orbit), number of Sun/satellite positions, and structure geometry. Geometry inputs are identical between SOLSHAD and SHADOWV2.

Solar exposure calculations start by randomly selecting a date and time during the event (this determines the Sun position) and the satellite position on orbit. If the Earth does not block the satellite from the Sun, rays are traced from each grid point on the structure toward the Sun. If adjacent satellite structure does not block the ray, solar exposure is accumulated at the grid point. In similar manner to SHADOWV2, the ray is Monte Carlo scattered until it is absorbed or leaves the structure. Scattered solar exposure is accumulated. Earth-reflected solar exposure is calculated in similar manner for each Sun position by ray tracing from each point on the satellite toward a grid of points on the part of the surface of the Earth which is Sunlit and in view of the satellite. The solar exposure calculation is completed when all Sun/satellite positions have been considered (several thousand Sun/satellite positions are typically used because the accuracy of the solar exposure calculation is proportional to one over the square root of the number of Sun/satellite positions).

Atomic oxygen fluences in atoms/cm^2 and solar exposure in cumulative equivalent Sun hours have been modeled for selected LDEF hardware. Figure 9.3-1 lists the hardware modeled. Atomic oxygen exposure has been modeled using SHADOWV2 (ref. 5). Solar exposure has been modeled using SOLSHAD Version 1.0 (ref. 41).

Hardware	AO Exposure	Solar Exposure	Filename Root
S0069 Row 9A thermal control surfaces experiment	√	√	S0069
LDEF FEP blanket fold row 6 toward row 7	√	√	CODAR6
LDEF FEP blanket fold row 7 toward row 6	√	√	CODAR7
M0001 space end NRL cosmic ray experiment	√	√	M0001
Tray D-11 copper ground strap	√		D11CU
Tray F-9 angle bracket	√		F9
Tray D-11 FEP blanket fold at tray edge toward row 10	√		D11BLA
Tray B-7 FEP blanket fold at longeron toward row 8	√		B7BLAN
Tray C-5 FEP blanket fold near tray edge		√	C5BLAN
Tray D-1 FEP blanket fold near row 2 edge		√	D1BLAN
C-9 scuff plate	√	√	C9SCU
Space end tray clamp H-12 with three bolts	√		CLAMP
B-9 Environment Exposure Control Canister (EECC) Experiment Tray	√	√	B9EECC
C-2 Environment Exposure Control Canister (EECC) Experiment Tray	√	√	C2EECC
E-3 Environment Exposure Control Canister (EECC) Experiment Tray	√	√	E3EECC
D-4 Environment Exposure Control Canister (EECC) Experiment Tray	√	√	D4EECT
D-8 Environment Exposure Control Canister (EECC) Experiment Tray	√	√	D8EECT

Figure 9.3-1. LDEF AO and Solar Exposures Modeled.

9.4 Computer Model Sample Output

An example of the 3-D output of the computer model is shown in figure 9.4-1. This figure shows the scuff plate and surrounding area at location C9. The computer program is capable of modeling complex surfaces. The variation in solar exposures highlighted in figure 9.4-1 shows the significance of structural details influencing the exposure level. Similar diagrams for both atomic oxygen and solar exposure levels have been produced for each of the LDEF surfaces modeled. These results are being prepared for publication in a separate document.

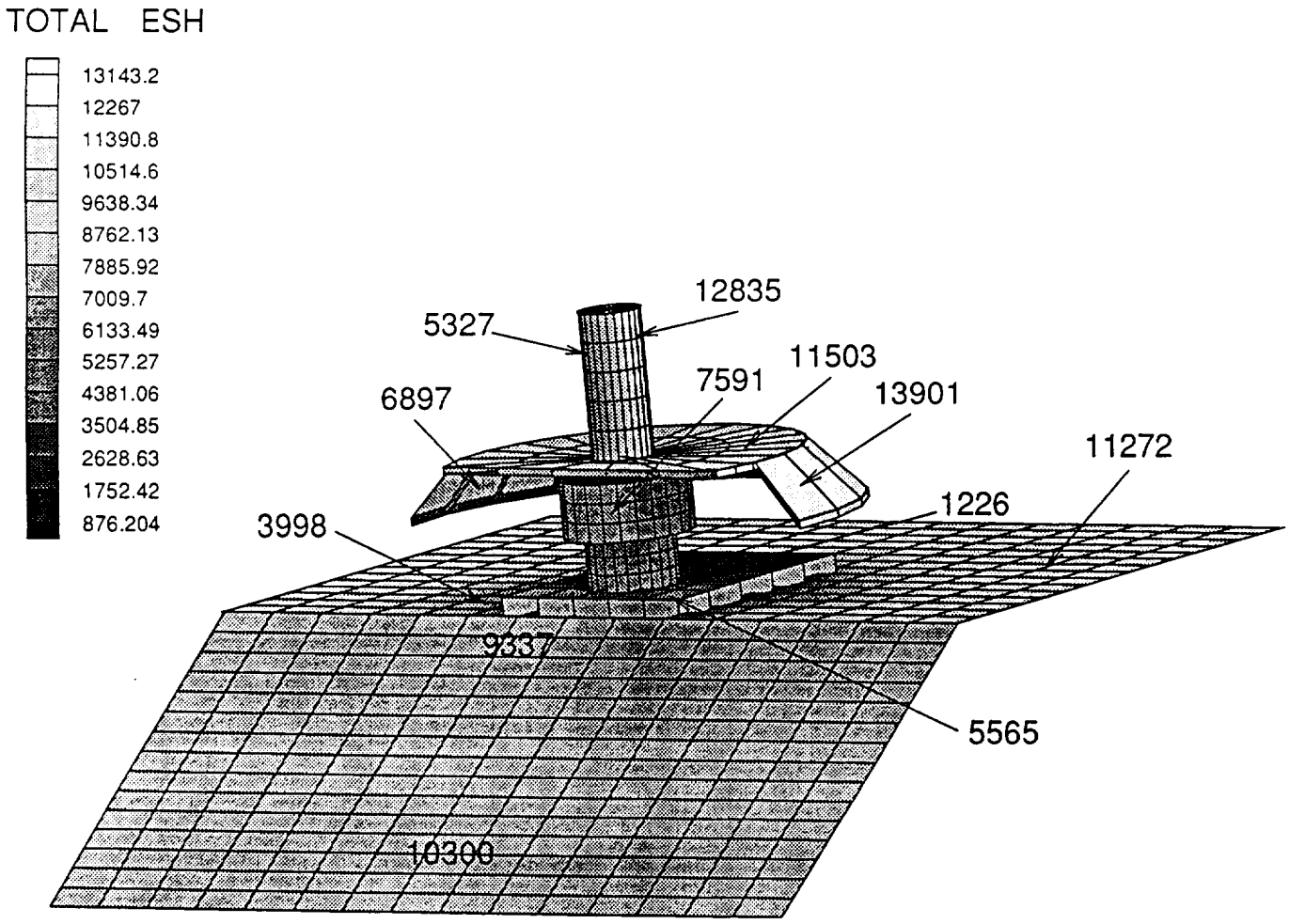

Figure 9.4-1. Output of computer code showing solar exposure levels on and around the scuff plate from location C9.

10.0 DATA FROM SELECTED EXPERIMENTS

10.1 M0003 - Space Environmental Effects on Spacecraft Materials

This experiment was located on trays D9, D8, D3, and D4. Cadmium-plated steel bolts used on the Boeing part of the M0003 experiment (tray D3) were examined post-flight for effects of exposure. The cadmium plate thickness on bolts was measured using an x-ray fluorescence method (ASTM B567/568). The surfaces of the bolts were also examined at 200X magnification for visible changes as compared to control specimens. Thickness measurements indicated that the bolts still have cadmium plating in excess of that required by fastener standard specification. No visible indications of cadmium sublimation or other adverse effects were observed by microscopy. No cadmium volatilized from these bolts as a result of prolonged vacuum exposure, probably due to their chromate conversion coated finish, and the low operating temperatures on tray D3 during the LDEF mission.

10.2 M0001 - Heavy Ions in Space

This experiment was on the space end of LDEF. Tapes holding thermal control blankets on detector stacks for the Naval Research Laboratory experiment were split approximately along a 90° bend in each tape where it was bonded around the edge of an aluminum mounting container holding the lexan detector plates. The failed edge of each tape had the appearance of a brittle failure, which would not be expected for fresh FEP, except possibly at very low temperatures. Thermal cycling and UV-induced damage were the likely reasons for this failure, rather than any low temperatures.

10.3 S0109 - Fiber Optic Data Transmission Experiment

The S0109 experiment was examined because of the large amount of fluid contamination it contained. This experiment had a liquid flow across part of the outer surface of its thermal shield when the LDEF was first rotated in the SAEF II building at KSC in February, 1990. Samples taken at that time were identified as trioctylphosphate which is used as a plasticizer and a flame retardant in vinyl resins. Only the fiber optic bundles, Valtec MG05 40030-01, employed a PVC sheath. This material was identified as the probable source of the outgassed material.

The source of the outgassing appeared to be the inside of the experiment since brown stains could be seen all around the thermal shield. Outgassed products which deposited on the outside of the tray during flight had turned dark brown and appeared to be dry. Certain material found within the tray was still fluid and a several mil quantity was present. The greatest amounts were found on the top surfaces of the fiberglass brackets used to support the aluminum sheet metal sunshield. Lesser quantities were visible on the floor and walls of the cavity as interference fringes. The likely sequence of events which led to the flowing of material across the outside thermal control surface during deintegration in SAEF-II is moisture absorption by the trioctylphosphate while row 12 remained on the "top" side of the LDEF assembly and transport structure. The liquid flowed the first time the LDEF was rotated in SAEF-II. Although the liquid was an artifact of recovery since material which remained in space would not have been exposed to moisture, there was substantial on-orbit outgassing of this material.

Based on the shadowing patterns, particularly that of the large sunshield bracket, the source of the outgassing appeared to be the fiber coil sheathed with the PVC. The PVC sheath, which was attached to the connectors with heat-shrink tubing, showed considerable shrinkage. At one connector, the sheath had pulled out of the heat-shrink tubing and was retracted approximately 1/2 inch from the end of the heat-shrink tubing.

10.4 AO175 - Evaluation of Long-Duration Exposure on Composites

The aluminum frame holding the individual composite panels within trays A1 and A7 was treated with a chemical film per MILC5541-class1A. This is an alodining process. Comparison of pre- and post-flight photographs show that this coating discolored during flight. However, the extent of discoloration could not be quantified because no preflight measurements on the frames were carried out.

10.5 Atomic Oxygen-Resistant Coatings Experiment Mounted on S1001 Tray

Kapton and FEP strips, coated with a variety of coatings selected to provide protection from atomic oxygen, were flown on trays F9, F12, and H1. Figures 10.5-1 through 10.5-3 show the sample layout on each of these trays. Optical properties data for these specimens were obtained by Ms. Wanda Peters of McDonnell-Douglas and Mr. Lon Kauder of Goddard Space Flight Center. These data have been provided for inclusion in this report and are reproduced in figure 10.5-4.

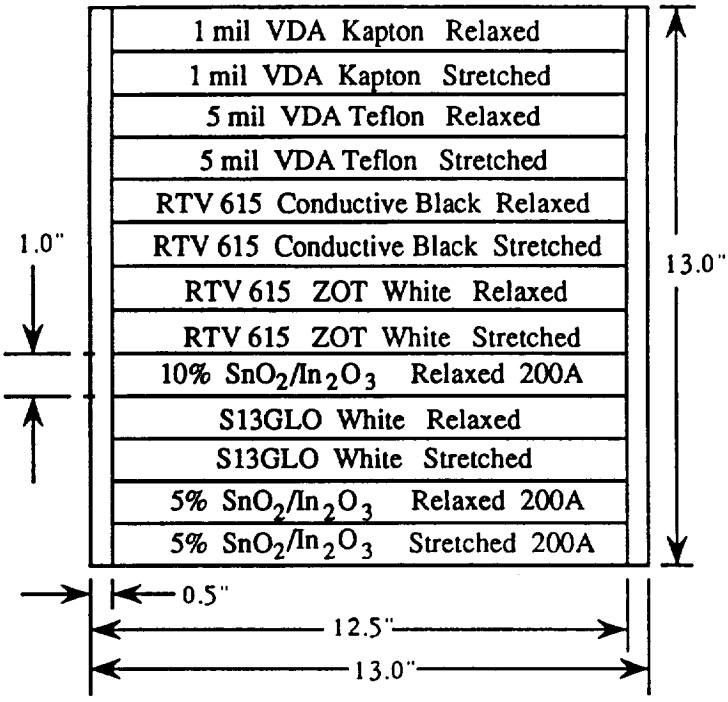

Figure 10.5-1 Sample panel configuration for AO coatings flown on S1001, tray F9.

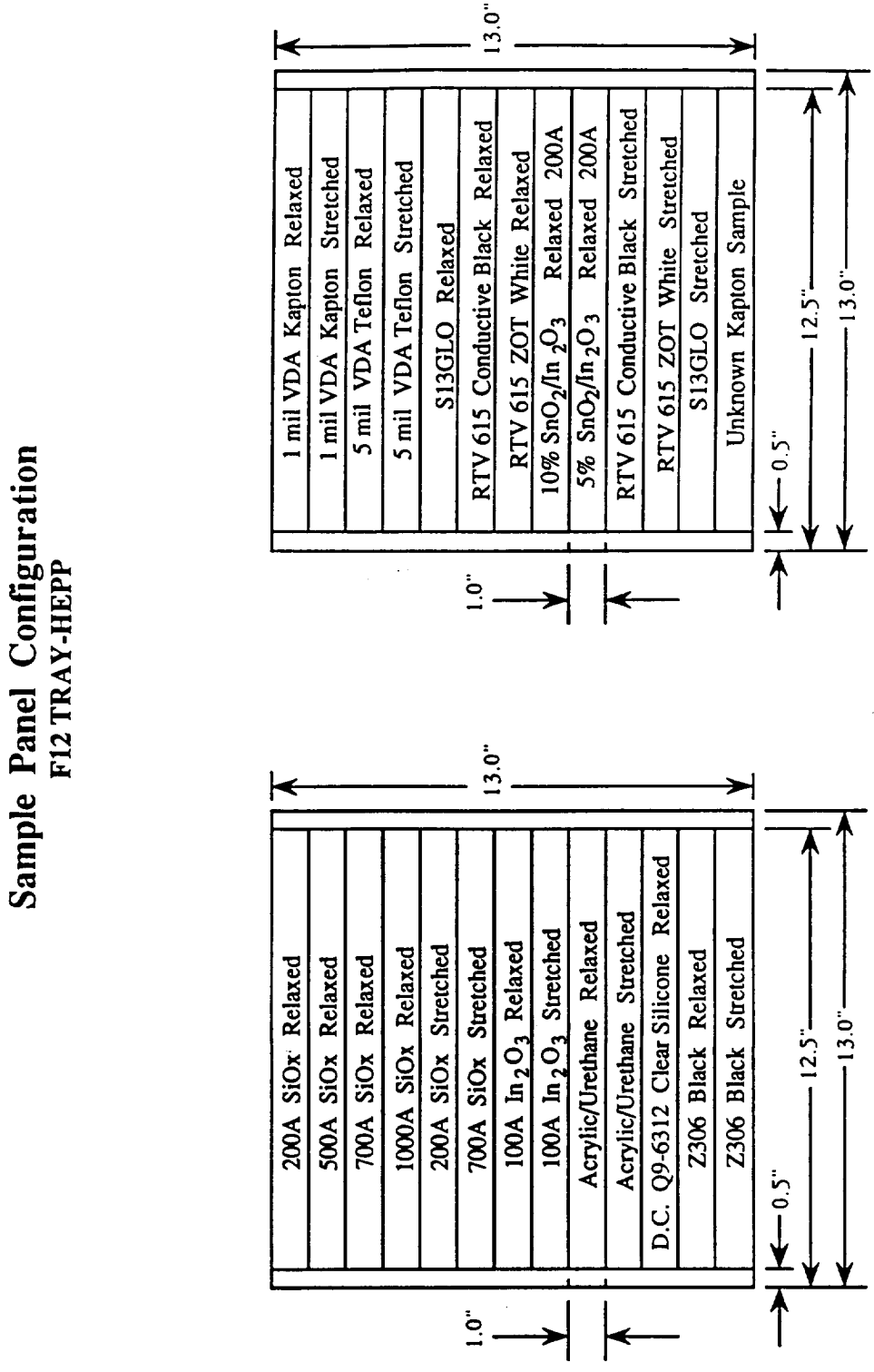

Figure 10.5-2 Sample panel configuration for AO coatings flown on S1001, tray F12.

Sample Panel Configuration
H1 TRAY- POWER

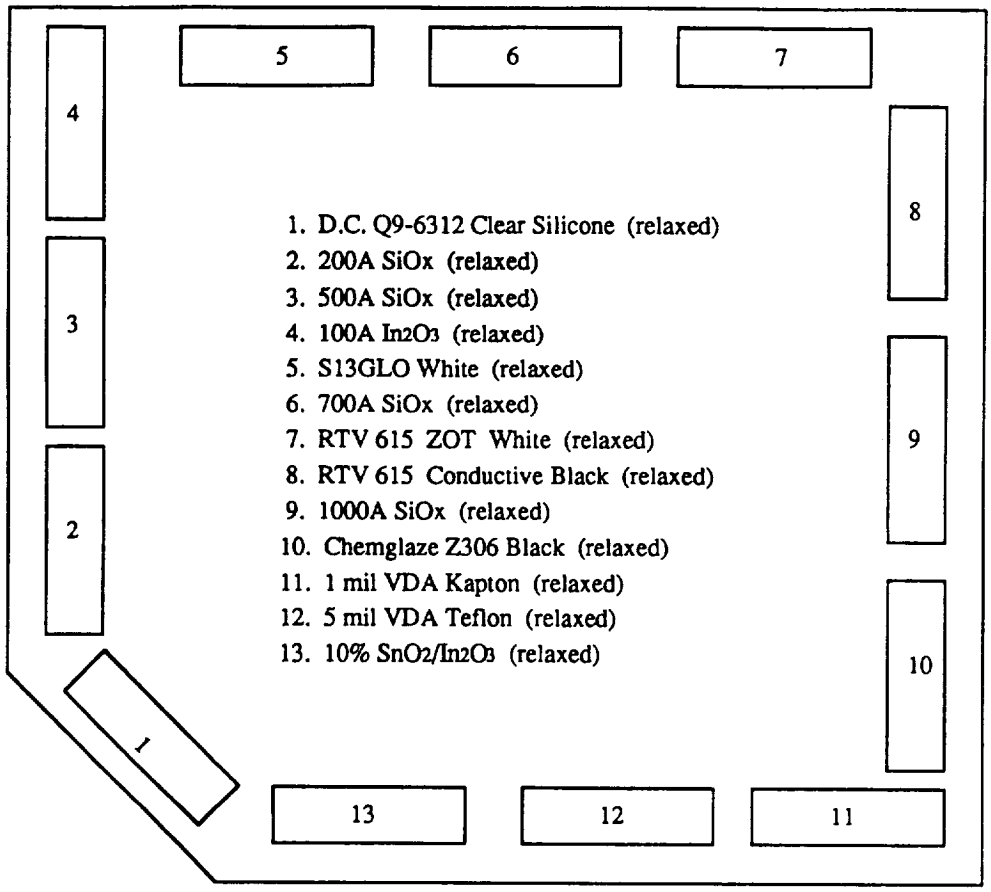

Figure 10.5-3 Sample panel configuration for AO coatings flown on S100, tray H1.

SAMPLE	SUBSTRATE	TEST DATE	ORIGIN	MEASURED MATERIAL	APPLICATION	A	E	COMMENTS
Vapor Deposited Aluminum (VDA)	Teflon 5 mil	3/14/90	LDEF Control	Aluminum	relaxed	0.088	0.02	
Vapor Deposited Aluminum (VDA)	Teflon 5 mil	3/14/90	LDEF Control	Teflon	relaxed	0.147	0.803	
Vapor Deposited Aluminum (VDA)	Teflon 5 mil	3/7/90	F9	Aluminum	stretched	0.144	0.115	Al side exposed to atomic oxygen. Highly degraded.
Vapor Deposited Aluminum (VDA)	Teflon 5 mil	3/7/90	F9	Teflon	stretched	0.189	0.818	Teflon cloudy and glossy in appearance.
Vapor Deposited Aluminum (VDA)	Teflon 5 mil	3/7/90	F9	Wiped Aluminum	stretched	0.12	0.775	Looks transparent with small traces of Al remaining.
Vapor Deposited Aluminum (VDA)	Teflon 5 mil	3/15/90	F12	Aluminum	relaxed	0.133	0.093	Very similar in appearance to the control sample.
Vapor Deposited Aluminum (VDA)	Teflon 5 mil	3/15/90	F12	Teflon	relaxed	0.205	0.829	Cloudy and milky in appearance.
Vapor Deposited Aluminum (VDA)	Teflon 5 mil	3/15/90	F12	Aluminum	stretched	0.132	0.09	Same as VDA Teflon F12 relaxed in appearance.
Vapor Deposited Aluminum (VDA)	Teflon 5 mil	3/15/90	F12	Teflon	stretched	0.183	0.811	Same as VDA Teflon F12 relaxed in appearance.
Vapor Deposited Aluminum (VDA)	Teflon 5 mil	4/26/90	H1	Teflon	relaxed	0.162	0.807	Sample appearance similar to the control sample.
Vapor Deposited Aluminum (VDA)	Teflon 5 mil	4/26/90	H1	Aluminum	relaxed	0.146	0.048	Sample appearance similar to the control sample.
S13GLO White Paint	Aluminized Kapton	3/12/90	LDEF Control		relaxed	0.155	0.899	
S13GLO White Paint	Aluminized Kapton	3/12/90	F9		stretched	0.416	0.878	Flat (no curling), dirty biege/tan in color (two-tone).
S13GLO White Paint	Aluminized Kapton	3/12/90	F9		relaxed	0.422	0.878	Same as F9 S13GLO (S) on appearance and color.
S13GLO White Paint	Aluminized Kapton	3/14/90	F12		stretched	0.397	0.89	Biege in color (one-tone), lighter in color than F12 S13GLO (R).
S13GLO White Paint	Aluminized Kapton	3/14/90	F12		relaxed	0.407	0.886	Light brown/dark tan in color, uniformed one-tone.
S13GLO White Paint	Aluminized Kapton	4/23/90	H1		relaxed	0.471	0.889	Gradient color of white at the top, brown, and tan towards the bottom.
RTV 615 ZOT White Paint	Aluminized Kapton 1/3 mil	3/13/90	LDEF Control		relaxed	0.229	0.87	
RTV 615 ZOT White Paint	Aluminized Kapton 1/3 mil	3/13/90	F9		relaxed	0.469	0.852	Biege/tan in color, curling along the edges.
RTV 615 ZOT White Paint	Aluminized Kapton 1/3 mil	3/13/90	F9		stretched	0.492	0.845	Same as F9 ZOT White (R).
RTV 615 ZOT White Paint	Aluminized Kapton 1/3 mil	3/14/90	F12		stretched	0.316	0.858	Off-white in color, curling along the edges.
RTV 615 ZOT White Paint	Aluminized Kapton 1/3 mil	3/14/90	F12		relaxed	0.331	0.86	Off-white in color, curling along the edges.
RTV 615 ZOT White Paint	Aluminized Kapton 1/3 mil	4/23/90	H1		relaxed	0.397	0.859	Gradient color of white, biege, and tan. Darkest portion in the middle.
RTV 615 Conductex Black Paint	Aluminized Kapton 1/3 mil	3/14/90	LDEF Control		relaxed	0.965	0.897	
RTV 615 Conductex Black Paint	Aluminized Kapton 1/3 mil	3/14/90	F9		relaxed	0.966	0.871	Curling along the edges.
RTV 615 Conductex Black Paint	Aluminized Kapton 1/3 mil	3/14/90	F9		stretched	0.958	0.862	Curling along the edges.
RTV 615 Conductex Black Paint	Aluminized Kapton 1/3 mil	3/14/90	F12		relaxed	0.951	0.882	Curling along the edges.
RTV 615 Conductex Black Paint	Aluminized Kapton 1/3 mil	3/14/90	F12		stretched	0.944	0.881	Curling along the edges.
RTV 615 Conductex Black Paint	Aluminized Kapton 1/3 mil	4/23/90	H1		relaxed	0.945	0.9	Flat, similar to control in appearance.
Z306 Black Paint	Aluminized Kapton 1/3 mil	3/16/90	F12		stretched	0.949	0.91	Detached from border, curled slightly towards center position tape.
Z306 Black Paint	Aluminized Kapton 1/3 mil	3/16/90	F12		stretched	0.943	0.9	Flat portion of the sample located next to the center position tape.
Z306 Black Paint	Aluminized Kapton 1/3 mil	3/16/90	F12		relaxed	0.946	0.905	Curled similar to Z306 Black (stretched).
Z306 Black Paint	Aluminized Kapton 1/3 mil	4/24/90	H1		relaxed	0.943	0.899	Sample was flat.

Figure 10.5-4 Results of optical properties measurements for AO coatings flown on S1001 where A is absorptance (α) and E is emittance (ε).

SAMPLE	SUBSTRATE	TEST DATE	ORIGIN	MEASURED MATERIAL	APPLICATION	A	B	COMMENTS
200A 10% SnO2/In203	Aluminized Kapton 1/2 mil	3/13/90	F9		relaxed	0.345	0.586	Has a dull sheen appearance, no longer golden and glossy.
200A 10% SnO2/In203	Aluminized Kapton 1/2 mil	3/13/90	F12		relaxed	0.313	0.6	The golden color remains, but it is not as glossy in appearance.
200A 10% SnO2/In203	Aluminized Kapton 1/2 mil	4/26/90	H1		relaxed	0.345	0.638	The sample is golden and glossy in appearance.
200A 5% SnO2/In203	Aluminized Kapton 1/2 mil	3/13/90	F9		relaxed	0.349	0.586	Has a dull sheen appearance, no longer golden and glossy.
200A 5% SnO2/In203	Aluminized Kapton 1/2 mil	3/13/90	F9		stretched	0.36	0.59	Has several ripes in the longitudinal direction, dull appearance.
200A 5% SnO2/In203	Aluminized Kapton 1/2 mil	3/13/90	F12		relaxed	0.313	0.596	The golden color remains, but it is not as glossy in appearance.
200A SiOx	Aluminized Kapton 1/2 mil	3/19/90	LDEF Control		relaxed	0.337	0.56	Golden and glossy in appearance.
200A SiOx	Aluminized Kapton 1/2 mil	3/19/90	F12		relaxed	0.356	0.568	Similar to the control in appearance.
200A SiOx	Aluminized Kapton 1/2 mil	3/19/90	F12		stretched	0.368	0.563	Similar to the control in appearance.
200A SiOx	Aluminized Kapton 1/2 mil	4/25/90	H1		relaxed	0.356	0.58	Similar to the control in appearance.
500A SiOx	Aluminized Kapton 1/2 mil	3/19/90	LDEF Control		relaxed	0.33	0.565	Golden and glossy in appearance.
500A SiOx	Aluminized Kapton 1/2 mil	3/19/90	F12		relaxed	0.34	0.567	Similar to the control in appearance.
500A SiOx	Aluminized Kapton 1/2 mil	4/25/90	H1		relaxed	0.367	0.593	Similar to the control in appearance.
700A SiOx	Aluminized Kapton 1/2 mil	3/19/90	LDEF Control		relaxed	0.322	0.569	Golden and glossy in appearance.
700A SiOx	Aluminized Kapton 1/2 mil	3/19/90	F12		relaxed	0.321	0.564	Similar to the control in appearance.
700A SiOx	Aluminized Kapton 1/2 mil	3/19/90	F12		stretched	0.338	0.576	Similar to the control in appearance.
700A SiOx	Aluminized Kapton 1/2 mil	4/25/90	H1		relaxed	0.357	0.596	Similar to the control in appearance.
1000A SiOx	Aluminized Kapton 1/2 mil	3/19/90	LDEF Control		relaxed	0.331	0.58	Golden and glossy in appearance.
1000A SiOx	Aluminized Kapton 1/2 mil	3/19/90	F12		relaxed	0.342	0.568	Similar to the control in appearance.
1000A SiOx	Aluminized Kapton 1/2 mil	4/25/90	H1		relaxed	0.404	0.607	Similar to the control in appearance.
100A In203	Aluminized Kapton 1/2 mil	3/21/90	LDEF Control		relaxed	0.341	0.569	Golden and glossy in appearance.
100A In203	Aluminized Kapton 1/2 mil	3/21/90	F12		relaxed	0.34	0.549	Has a dull sheen appearance, no longer glossy.
100A In203	Aluminized Kapton 1/2 mil	3/21/90	F12		stretched	0.335	0.561	Has a dull sheen appearance, no longer glossy.
100A In203	Aluminized Kapton 1/2 mil	4/25/90	H1		relaxed	0.367	0.589	Similar to control sample in appearance.
Vapor Deposited Aluminum (VDA)	Kapton 1 mil	3/1/90	Control	Kapton	relaxed	0.347	0.653	Golden and glossy.
Vapor Deposited Aluminum (VDA)	Kapton 1 mil	4/26/90	F12	Kapton	relaxed	0.353	0.569	Similar to control sample in appearance.
Vapor Deposited Aluminum (VDA)	Kapton 1 mil	4/26/90	F12	Kapton	stretched	0.338	0.571	Similar to control sample in appearance.
Vapor Deposited Aluminum (VDA)	Kapton 1 mil	4/26/90	H1	Kapton	relaxed	0.35	0.594	Similar to control sample in appearance.
Acrylic/Urethane	Aluminized Kapton 1/2 mil	3/26/90	LDEF Control		relaxed	0.361	0.865	
Acrylic/Urethane	Aluminized Kapton 1/2 mil	3/26/90	F12		relaxed	0.4	0.852	Slight sheen, but not as glossy as the control.
Acrylic/Urethane	Aluminized Kapton 1/2 mil	3/22/90	F12		stretched	0.384	0.832	Slight sheen, but not as glossy as the control.

Figure 10.5-4(continued). Results of optical properties measurements for AO coatings flown on S1001.

SAMPLE	SUBSTRATE	TEST DATE	ORIGIN	MEASURED MATERIAL	APPLICATION	A	E	COMMENTS
D. C. 93-500 Clear Silicone	Aluminized Kapton 1/2 mil	4/27/90	F12		relaxed	0.413	0.826	Golden in color, wrinkled and fragile in appearance.
D. C. 93-500 Clear Silicone	Aluminized Kapton 1/2 mil	4/27/90	H1		relaxed	0.366	0.788	Golden in color, wrinkled and fragile in appearance.
Silver Teflon	Teflon 5 mil	3/7/90	Control	Silver	relaxed	0.094	0.804	
Silver Teflon (BO3 front/top)	Teflon 5 mil	3/22/90	F12	Silver	relaxed	0.29	0.826	Sample colors are bronze/gray/silver, this portion is silver.
Silver Teflon (BO3 front/bottom)	Teflon 5 mil	3/22/90	F12	Silver	relaxed	0.548	0.864	Sample colors are bronze/gray/silver, this portion is gray/bronze.
Silver Teflon (BO2 front/top)	Teflon 5 mil	3/22/90	F12	Silver	relaxed	0.164	0.798	Sample colors are bronze/silver, this portion is silver.
Silver Teflon (BO2 front/bottom)	Teflon 5 mil	3/22/90	F12	Silver	relaxed	0.226	0.796	Sample colors are bronze/silver, this portion is light bronze.

NOTE: ALL COATINGS WITH ALUMINIZED KAPTON AS A SUBSTRATE ARE APPLIED TO THE KAPTON SIDE.

Figure 10.5-4(continued). Results of optical properties measurements for AO coatings flown on S1001.

11.0 DATABASES

Electronic databases containing results for studies of treated aluminum, silverized Teflon, and thermal control paints have been constructed. A companion database documenting the exposure levels to each space environment factor as a function of location was also made. These databases contain information available through the 2nd Post-Retrieval Symposium. An additional database covering optical materials, funded through both the Systems and the Materials Special Investigation Groups, is complete through the 3rd Post-Retrieval Symposium. These databases are available as part of the user's guide (ref. 17) in both IBM compatible and MacIntosh™ versions that run on a Filemaker Pro™ software. Experimenters' conclusions, observations, and essential data are provided for these subject areas.

12.0 SUMMARY AND CONCLUSIONS

12.1 Atomic Oxygen Recession Rates

Thin polymeric films had recession rates similar to short term rates obtained from Space Shuttle data. The recession rate for FEP obtained from LDEF measurements (~0.34 x 10^{-24} atoms/cm^2) is substantially greater than values obtained from Space Shuttle data (ref. 42-44) and Lockheed's LEO measurements (ref. 45). The complete removal of Kapton from leading edge locations, while not quantitative, is consistent with the average erosion rate obtained from shuttle data (~3.0 x 10^{-24} atoms/cm^2). The low value obtained for the space end exposed Kapton (~1.7 X 10^{-24} atoms/cm^2) from experiment AO133, may be due to the extreme atomic oxygen impingement angle. Attempts have been made to determine an angular dependence on the FEP erosion rates. However, uncertainty in the measurements due to as-manufctured thickness variability as well as uncertainties in the MSIS86 predicted atomic oxygen density make the data inconclusive. Organic composites recessed at rates averaging about 10^{-24} atoms/cm^2. Resin typically recessed three times as fast as the graphite fibers.

12.2 Materials Selection Lessons

The original prioritization of non-experimenters' hardware included aluminum, silverized Teflon, A276 and Z306 polyurethane paints, copper, and selected composites as high priority items for examination. These materials are in current use on spacecraft and are candidates for selection on future designs. These material types were also found in multiple locations on LDEF, allowing development of performance characteristics as a function of exposure conditions.

12.3 Comparison with Results from other Flights

An extensive set of data exists from a series of materials experiments flown as part of certain Space Shuttle missions (refs. 42-44). Long term data on the performance of thermal control materials exists for the SCATHA experiment (ref. 46), flown at geosynchronous altitudes, for ML-101 (ref. 47), and for the Solar Maximum Recovery Mission (ref. 48). Performance data for FEP, Kapton, and SiO_x coatings on Kapton has also been published for a Lockheed flight experiment lasting about 105 days in LEO (ref. 45). LDEF results confirmed the linear recession of organic materials with atomic oxygen

fluence. The optical performance of Ag/FEP agreed with the Solar Max results. Both FEP and Tetrafluoro-ethylene (TFE) showed recession rates greater than rates determined from Space Shuttle flights. This result is evidence that the degradation mechanisms for fluorinated materials and organics are different, with the fluorinated materials requiring creation of damage sites before atomic-oxygen-induced degradation may occur. Data from the Lockheed flight reference above support this conclusion. Low Earth orbit data from a variety of flight experiments has been compiled into a materials selection guide (ref. 49). Rules of thumb for spacecraft designers have been developed and included in the guide.

13.0 REFERENCES

1. H.A. Smith, K.M., Nelson, D. Eash, and H.G. Pippin, "Analysis of Selected Materials Flown on Interior Locations of the Long Duration Exposure Facility," NASA Contractor Report 4586 (April 1994).

2. LDEF-69 Months in Space First Post-Retrieval Symposium, NASA CP 3134, Part 2, Kissimmee, Florida, June 2-8, 1991, A.S. Levine, ed.

3. LDEF Materials Workshop '91, NASA CP 3162, Parts 1 and 2, NASA Langley Research Center, Hampton, Virginia, November 19-22, 1991, B.A. Stein and P.R. Young, eds.

4. LDEF-69 Months in Space Second Post-Retrieval Symposium, NASA CP 3194, Part 3, San Diego, California, June 1-5, 1992, A.S. Levine, ed.

5. LDEF Results for Spacecraft Applications, NASA CP 3257, Huntsville, Alabama, October 27-28, 1992, A.F. Whitaker and J. Gregory, eds.

6. LDEF-69 Months in Space Third Post-Retrieval Symposium, NASA CP 3275, Williamsburg, Virginia, November 1-5, 1993, A.S. Levine, ed.

7. W.L. Plagemann, "Space Environmental Effects on the Integrity of Chromic Acid Anodized Coatings," NASA Contractor Report 191468 (May 1993).

8. J.L. Golden "Results of the Examination of LDEF Polyurethane Thermal Control Coatings," NASA Contractor Report 4617 (July 1994).

9. H.W. Dursch, B.K. Keough, and H.G. Pippin, "Evaluation of Seals and Lubricants Used on the Long Duration Exposure Facility," NASA Contractor Report 4604 (June 1994).

10. R.J. Bourass and J.R. Gillis, "Atomic oxygen exposure of LDEF experiment trays," NASA Contractor Report 189627 (May 1992).

11. H.W. Dursch, W.S. Spear, E.A. Miller, G.L. Bohnhoff-Hlavacek, and J. Edelman, "Analysis of Systems Hardware Flown on LDEF-Results of the Systems Special Investigation Group," NASA Contractor Report 189628 (April 1992).

12. H.G. Pippin "Effects of Space Exposure on Metals Flown on the Long Duration Exposure Facility," NASA Contractor Report 4662 (May 1995).

13. P. George, H.W. Dursch, and H.G. Pippin, "Composite Materials Flown on the Long Duration Exposure Facility," NASA Contractor Report 4657 (April 1995).

14. H.G. Pippin, "Analysis of Silverized Teflon Thermal Control Material Flown on the Long Duration Exposure Facility," NASA Contractor Report 4663 (May 1995).

15. R. J. Bourassa and J. R. Gillis, "Solar Exposure of LDEF Experiment Trays," NASA Contractor Report 189554 (February 1992).

16. H.W. Dursch, B.K. Keough, and H.G. Pippin, "Evaluation of Adhesive Materials Used on the Long Duration Exposure Facility," NASA Contractor Report 4646, March 1995.

17. G. Bohnhoff-Hlavacek, "LDEF Mini-Data Base Users Guide-MacIntosh version," NASA Contractor Report 4656 (May 1995) and "LDEF Mini-Data Base Users Guide-IBM Compatible PC Computer version," NASA Contractor Report 4655 (May 1995).

18. L.G. Clark, W.H. Kinard, D.J. Carter, and J.L. Jones, "The Long Duration Exposure Facility (LDEF): Mission 1 experiments," NASA-SP-473, 1984.

19. T.H. See, M.A. Allbrooks, D.R. Atkinson, C.G. Simon, and M. Zolensky, "Meteoroid and Debris Impact Features Documented on the Long Duration Exposure Facility, A Preliminary Report," Publication #84, JSC #24608 (1990).

20. G. L. Smith, D. Rutan, and T. D. Bess, Atlas of Albedo and Absorbed Solar Radiation Derived From Nimbus 7 Earth Radiation Budget Data Set - November 1978 to October 1985, NASA Reference Publication 1231 (1990).

21. Earth Albedo and Emitted Radiation, NASA Space Vehicle Design Criteria (Environment), NASA SP-8067 (July 1971).

22. A. S. Jursa, Ed., Handbook of Geophysics and the Space Environment, p. 1-4, Air Force Geophysics Laboratory (1985).

23. T.W. Armstrong and B.L Colborn, "Radiation Model Predictions and Validation Using LDEF Satellite Data," LDEF-69 Months in Space Second Post-Retrieval Symposium, NASA CP 3194, Part 1, San Diego, California, June 1-5, 1992, p. 207.

24. W.M. Berrios, "Use of the LDEF's Thermal Measurement System for the Verification of Thermal Models," LDEF-69 Months in Space First Post-Retrieval Symposium, NASA CP 3134, Part 1, Kissimmee, Florida, June 2-8, 1991, pp. 69-83.

25. E.R. Crutcher and W.W. Wascher, "Particle Types and Sources Associated with LDEF," LDEF-69 Months in Space First Post-Retrieval Symposium, NASA CP 3134, Part 1, Kissimmee, Florida, June 2-8, 1991, pp. 101-120.

26. E.R. Crutcher, L.S. Nishimura, K.J. Warner, and W.W. Wascher, "Migration and Generation of Contaminants from Launch Through Recovery: LDEF Case History," LDEF-69 Months in Space First Post-Retrieval Symposium, NASA CP 3134, Part 1, Kissimmee, Florida, June 2-8, 1991, pp. 121-140.

27. J.P. Wightman and H.L. Grammer, "Surface Characterization of LDEF Materials," Final Technical Report, Grant NAG1-1186, NASA CR-194519, Sept 1990-Oct 1993.

28. M. Lee, W.D. Rooney, and J.B. Whiteside, "An XPS Study of Space-Exposed Polyimide Film," LDEF-69 Months in Space Second Post-Retrieval Symposium, NASA CP 3194, Part 3, San Diego, California, June 1-5, 1992, p. 957.

29. W.K. Stuckey, G Radhakrishnan, and D. Wallace, "Post-Flight Analyses of the Crystals from the M0003-14 Quartz Crystal Microbalance Experiment," LDEF-69 Months in Space Second Post-Retrieval Symposium, NASA CP 3194, Part 3, San Diego, California, June 1-5, 1992, p. 1269.

30. W.K. Stuckey, "An Overview of the On-orbit Contamination of the Long Duration Exposure Facility (LDEF)," LDEF Results for Spacecraft Applications, NASA CP 3257, Huntsville, Alabama, October 27-28, 1992, p. 533

31. J.S. Brodkin, L.C. Sengupta, W. Franzen, and P.L. Sagalyn, "Surface Characterization of Metal Plates Exposed to Atomic Oxygen in Space," Thin Solid Films, 234, 1993, pp.512-517.

32. J.L. Golden, "Selected Results for LDEF Thermal Control Coatings," LDEF-69 Months in Space Second Post-Retrieval Symposium, NASA CP 3194, Part 3, San Diego, California, June 1-5, 1992, p. 1099.

33. J.B. Whiteside, E. Kamykowski, W.D. Rooney, R. Schulte, and M. Stauber, J. of Spacecraft and Rockets, vol. 31, no. 5, Oct. 1994, pp. 860-865.

34. G. Steckel, " LDEF-69 Months in Space Second Post-Retrieval Symposium, NASA CP 3194, Part 3, San Diego, California, June 1-5, 1992, p. 987,

35. H.G. Pippin, O. Mulkey, J. Verzemnieks, E. Miller, S.G. Hill, and H.W. Dursch, "Survey of Results from the Boeing Module on the M0003 Experiment on LDEF," LDEF-69 Months in Space First Post-Retrieval Symposium, NASA CP 3134, Part 1, Kissimmee, Florida, June 2-8, 1991, p. 1109.

36. R.J. Bourassa, P.E. Gruenbaum, J .R. Gillis, C. R. Hargraves, "Operation of the Computer Model for Direct Atomic Oxygen Exposure of Earth Satellites for FLUXAVG Version 2.0," Memorandum 9-5571-SGH-94-002, Boeing Defense & Space Group, January 26, 1994.

37. A. E. Hedin,."MSIS-86 Thermospheric Model," *J. Geophys. Res.* **92**, 4649-4662 (1987).

38. J. H. Kwok, "The Artificial Satellite Analysis Program (ASAP)," Version 2.0, JPL, COSMIC PROGRAM #NPO-17522, April 20, 1987.

39. J. H. Kwok, "The Long-term Orbit Predictor (LOP)," JPL, COSMIC PROGRAM #NPO-17052, June 30, 1986.

40. R. J. Bourassa, J.R. Gillis, P.E. Gruenbaum, "Operation of the Computer Model for Microenvironment Atomic Oxygen Exposure for SHADOWV2", Boeing Defense & Space Group, February 24, 1995.

41. J.R. Gillis, R.J. Bourassa, P.E. Gruenbaum, "Operation of the Computer Model for Microenvironment Solar Exposure for SOLSHAD Version 1.0," Boeing Defense & Space Group, February 24, 1995.

42. L.J. Leger, J.T. Visentine, and J.F. Kuminecz, "Low Earth Orbit Atomic Oxygen Effects on Surfaces," AIAA-84-0548, AIAA 22rd Aerospace Sciences Meeting, January 9-12, 1984, Reno, Nv.

43. A.F. Whitaker, S.A. Little, R.J. Harwell, D.B. Griner, and R.F. DeHaye, "Orbital Atomic Oxygen Effects on Thermal Control and Optical Materials-STS-8 Results," AIAA-85-0416, AIAA 23rd Aerospace Sciences Meeting, January 14-17, 1985, Reno, Nv.

44. "Atomic Oxygen Effects Measurements for Shuttle Mission STS-8 and 41-G," NASA Technical Memorandum 100459, Volume 1, J. Visentine, ed., (September 1988).

45. P.W. Knopf, R.J. Martin, R.E. Damman, and M. McCargo, "Correlation of Laboratory and Flight Data for the Effects of Atomic Oxygen on Polymeric Materials," AIAA 20th Thermophysics Conference, Williamsburg, Va., June 19-21, 1985.

46. R.A. Winn, "ML-101 Thermal Control Coatings: Five Year Space Exposure," Technical Report AFML-TR-78-99, July 1978.

47. D.F. Hall and A.A. Fote, "10 Year Performance of Thermal Control Coatings at Geosynchronous Altitude," AIAA 91-1325, AIAA 26th Thermophysics Conference, June 24-26, 1991, Honolulu, Hawaii.

48. Proceedings of the SMRM Degradation Study Workshop, 408-SMRM-79-0001, Goddard Space Flight Center, May 9-10, 1985, Greenbelt, Maryland.

49. E. M. Silverman, "Space Environmental Effects on Spacecraft: LEO Materials Selection Guide," NASA Contractor Report 4661, Parts 1 and 2, (1995).

Appendix A

Surface Analysis Measurements on Selected LDEF Hardware

This appendix contains results of measurements made with a portable BRDF instrument on areas of selected tray clamps and on a piece of silverized Teflon from blanket C8.

Duplicate reflectance and scattering measurements were made at several locations on each of the specimens. The purpose for these measurements was to determine if any correlation could be made between the BRDF measurements and ESCA determination of silicon percents at these locations. The range of silicon values was not sufficient to develop a good correlation.

For the silverized Teflon sample, a set of measurements 2.0" from the edge were made with the instrument rotated at different orientations with respect to the specimen. This was to see if the oriented surface texturing significantly influenced the measured specular reflectance. Differences of a few percent were noted. The initial orientation was chosen randomly and identified by the bolt pattern holding the casing for the instrument. The long section of this piece is approximately 1.1" in width. Between 0.8 and 0.9 inches from the edge of the blanket is the beginning of the area exposed to atomic oxygen.

Sample: H6-11

Location #	% Reflectance (Specular)	BRDF Measurements 0 deg	50 deg
1	14.0	0.144	0.0264
	14.1	0.136	0.0249
2	6.5	0.225	0.0391
	8.0	0.214	0.0355
3	18.6	0.172	0.0315
	18.5	0.138	0.0301
4	14.1	0.181	0.0373
	12.3	0.197	0.0378
5	14.7	0.181	0.0409
	14.7	0.181	0.0409
	14.7	0.168	0.0396
6	17.6	0.178	0.0391
	18.0	0.203	0.0387
7	18.0	0.149	0.0360
	18.6	0.147	0.0355
8	15.3	0.152	0.0292
	14.4	0.160	0.0297
9	15.4	0.157	0.0364
	17.2	0.144	0.0351
10	12.6	0.153	0.0342
	12.0	0.192	0.0337
11	17.5	0.132	0.0247
	16.0	0.134	0.0310
12	13.3	0.157	0.0324
	15.0	0.154	0.0306
13	14.0	0.157	0.0306
	14.1	0.170	0.0310

Figure A-1. Specular reflectance and BRDF measurements for selected locations on space end tray clamp H6-11.

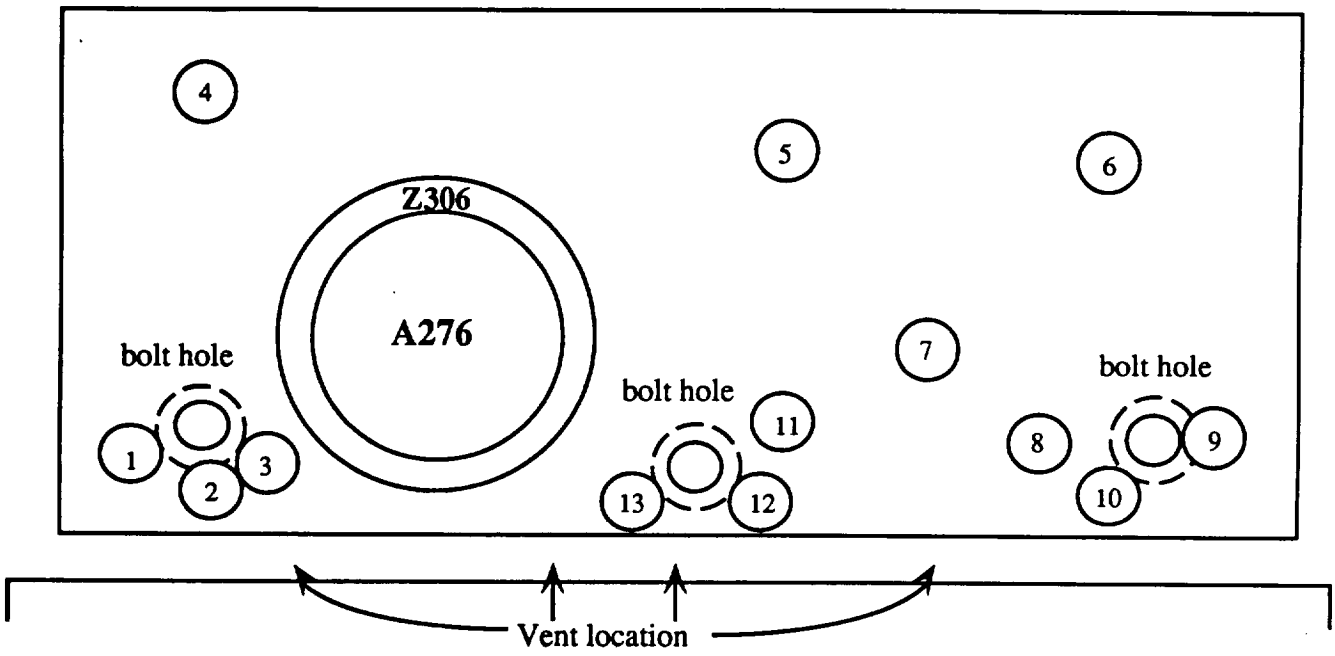

Figure A-2. H6-11 Tray clamp showing BRDF, reflectance, and surface analysis locations.

Sample: G6-5

Location #	% Reflectance (Specular)	BRDF Measurements 0 deg	50 deg
1	16.6	0.175	0.0306
	17.5	0.162	0.0297
2	15.9	0.167	0.0297
	15.7	0.156	0.0279
3	16.3	0.175	0.0292
	15.9	0.200	0.0315
4	16.0	0.178	0.0319
	15.2	0.175	0.0319
5	13.3	0.158	0.0391
	15.0	0.144	0.0297
6	10.2	0.172	0.0391
	9.8	0.178	0.0427
7	15.3	0.181	0.0328
	15.2	0.162	0.0319
8	19.4	0.168	0.0315
	19.5	0.160	0.0301
9	16.6	0.156	0.0292
	16.2	0.163	0.0301
10	16.0	0.167	0.0310
	14.3	0.175	0.0319
11	16.5	0.149	0.0274
	15.7	0.153	0.0283

Figure A-3. Specular reflectance and BRDF measurements for selected locations on Earth end tray clamp G6-5.

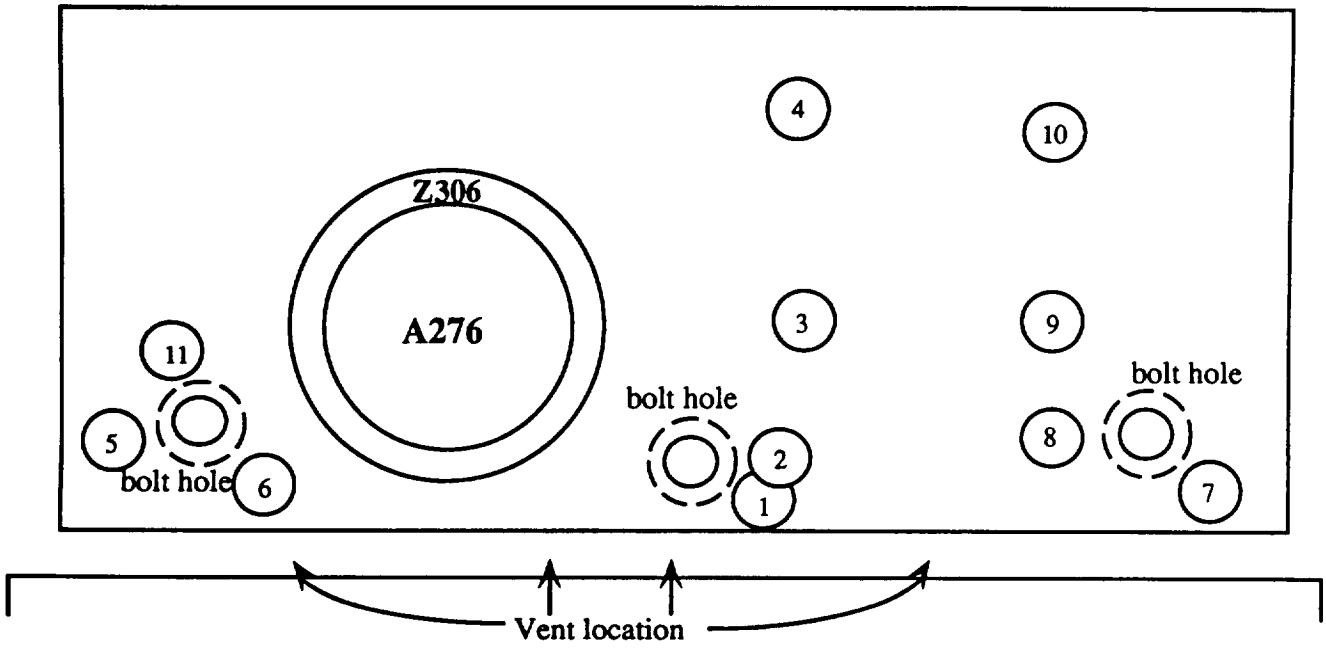

Figure A-4. G6-5 Tray clamp showing BRDF, reflectance, and surface analysis locations.

Sample: F6-8

Location #	% Reflectance (Specular)	BRDF Measurements 0 deg	50 deg
1	15.3	0.175	0.0283
	14.4	0.162	0.0279
2	13.1	0.200	0.0283
	14.0	0.183	0.0270
3	16.3	0.163	0.0264
	16.3	0.175	0.0288
4	16.7	0.181	0.0279
	15.6	0.192	0.0283
5	15.2	0.157	0.0270
	15.3	0.154	0.0266
6	16.0	0.165	0.0274
	16.0	0.164	0.0274
7	16.7	0.165	0.0274
	16.6	0.168	0.0270
8	15.6	0.175	0.0285
	15.6	0.172	0.0283
9	10.4	0.134	0.0269
	12.6	0.141	0.0273
10	9.1	0.151	0.0301
	9.8	0.146	0.0301
11 (device unsteady)	8.8	0.159	0.0333
	12.3	0.147	0.0270
	7.6	0.145	0.0841
12	12.7	0.178	0.168
	12.6	0.168	0.0306

Figure A-5. Specular reflectance and BRDF measurements for selected locations on tray clamp F6-8.

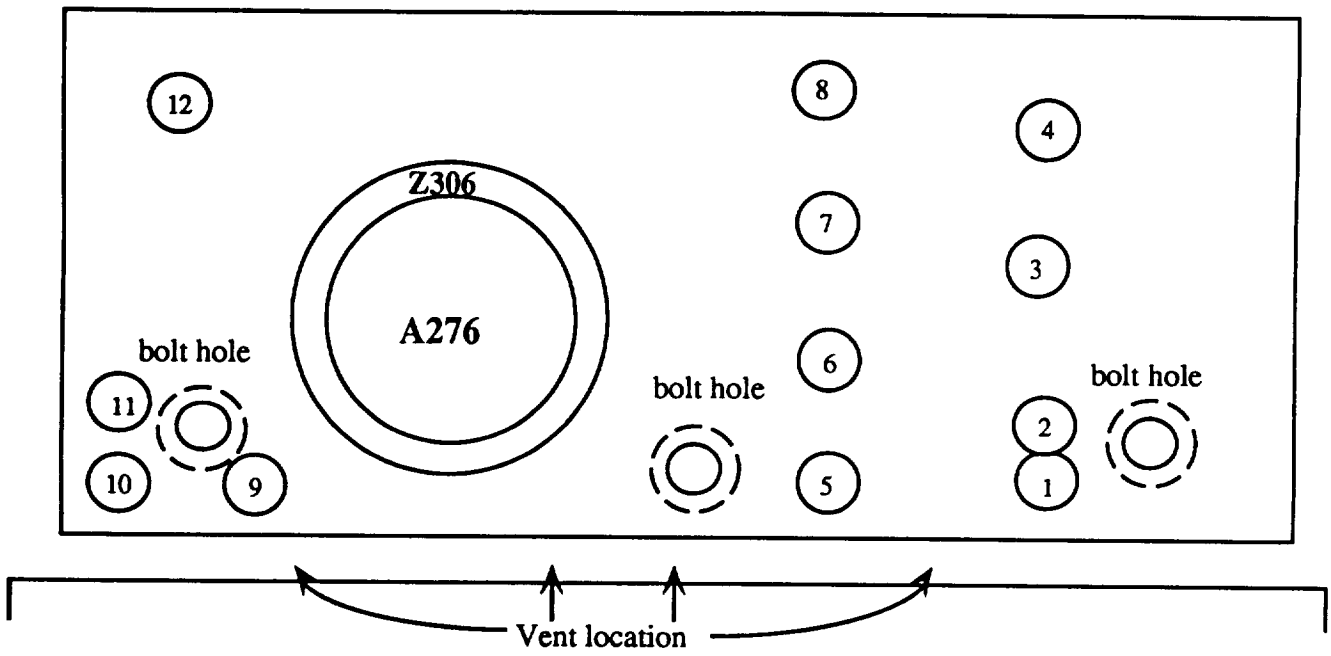

Figure A-6. F6-8 Tray clamp showing BRDF, reflectance, and surface analysis locations.

Sample: H7-2

Location #	% Reflectance (Specular)	BRDF Measurements 0 deg	50 deg
1	6.7	0.247	0.0373
	7.8	0.264	0.0346
2	5.2	0.256	0.0418
	5.3	0.222	0.0441
3	4.8	0.103	0.0306
	7.6	0.140	0.0355
	8.3	0.160	0.0351
4	8.9	0.222	0.0378
	5.2	0.217	0.0436
5	6.3	0.247	0.0400
	7.3	0.253	0.0423
6	12.4	0.152	0.0267
	12.1	0.153	0.0273
7	10.1	0.175	0.0279
	10.0	0.178	0.0283
8	5.4	0.256	0.0508
	6.3	0.256	0.0472
9	10.8	0.169	0.0292
	10.7	0.189	0.0306
10	11.4	0.217	0.0355
	11.3	0.195	0.3280
11	11.1	0.181	0.0270
	11.1	0.200	0.0285
12	11.4	0.165	0.0274
	11.5	0.181	0.0264
13	11.5	0.165	0.0263
	11.4	0.186	0.0273
14	11.0	0.233	0.0292
	11.1	0.197	0.0288
15	10.5	0.169	0.0274
	10.1	0.208	0.0279
	10.1	0.164	0.0306

Figure A-7. Specular reflectance and BRDF measurements for selected locations on tray clamp H7-2.

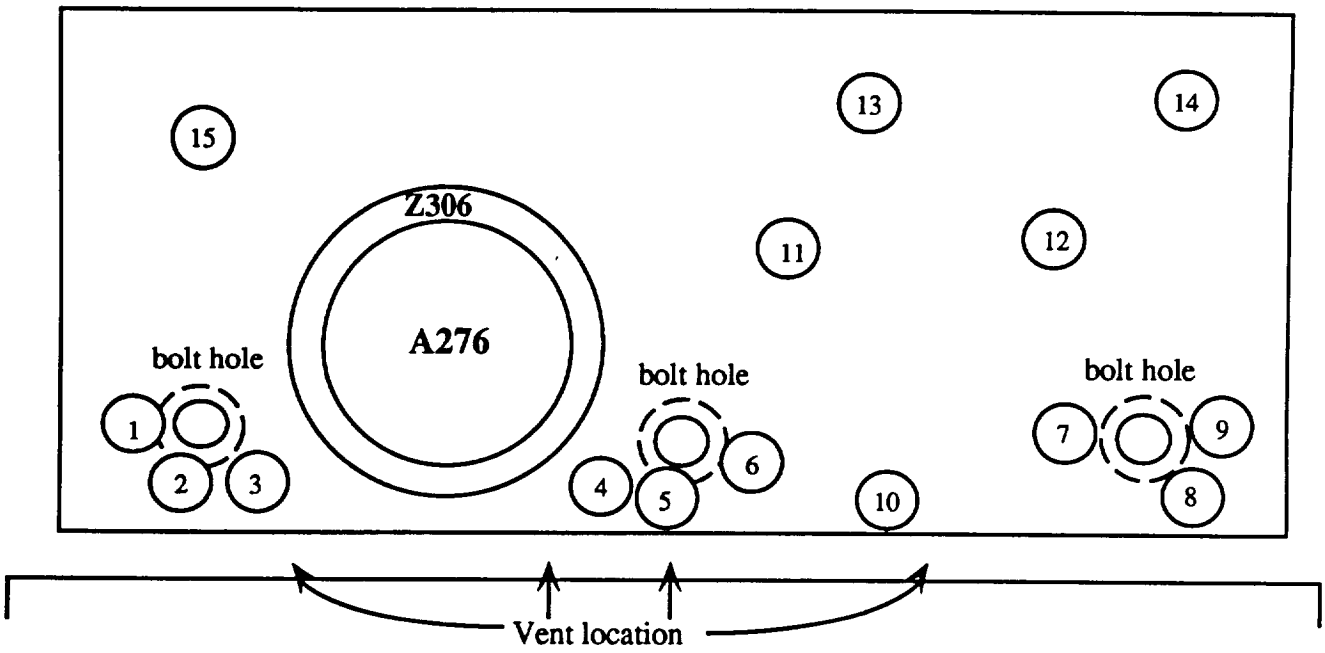

Figure A-8. H7-2 Tray clamp showing BRDF, reflectance, and surface analysis locations.

Sample: Silverized Teflon Blanket C8

Distance from unexposed edge (inches)	% Reflectance (Specular)	BRDF Measurements 0 deg	50 deg
2.0	22.2	0.453	0.0625
2.0	22.1	0.453	0.0625
2.0 (instrument at 180 deg to initial orientation)	27.9	0.336	0.0598
	28.3	0.333	0.0593
2.0 (instrument at 90 deg to initial orientation)	24.4	0.275	0.0728
	24.4	0.281	0.0728
2.0 (instrument at 270 deg to initial orientation)	26.4	0.483	0.0459
	26.4	0.483	0.0459
2.0 (instrument returned to initial orientation)	24.8	0.417	0.0593
1.8	26.7	0.431	0.0575
	25.8	0.436	0.0580
1.6	18.0	0.536	0.0616
	18.2	0.533	0.0616
1.4	9.8	too high	0.0692
	9.5	too high	0.0692
1.3	12.8	0.542	0.0643
	12.8	0.542	0.0643
1.2	26.1	0.406	0.0521
	27.0	0.460	0.0521
1.1	32.4	0.392	0.0490
	32.4	0.392	0.0490
1.0	40.2	0.278	0.0355
	39.7	0.278	0.0355
0.9	43.4	0.0879	0.0119
	42.9	0.0887	0.0119
0.8	68.5	0.0511	0.0896
	71.7	0.0483	0.00896
0.7	74.4	0.0275	0.00544
	74.4	0.0272	0.00544

Figure A-9. Specular reflectance and BRDF measurements for selected locations on silverized teflon blanket from tray location C8.

Sample: Silverized Teflon Blanket C8

Distance from unexposed edge (inches)	% Reflectance (Specular)	BRDF Measurements 0 deg	50 deg
0.6	78.5	0.0214	0.00463
	78.1	0.0214	0.00463
0.4	76.2	0.0225	0.00679
	75.3	0.0225	0.00679
0.2	89.5	0.0231	0.00436
	89.5	0.0228	0.00436
0.2 (instrument at 90 deg to initial orientation)	81.7	0.0289	0.00445
	81.7	0.0289	0.00445
0.3 (highly contaminated area)	84.4	0.0283	0.00566
	84.4	0.0282	0.00566
Ground Control Specimen	84.4	0.0282	0.00477
	84.9	0.0283	0.00477
Ground Control Specimen (instrument at 90 deg to initial orientation)	90.9	0.0175	0.00432

Figure A-9 (continued). Specular reflectance and BRDF measurements for selected locations on silverized teflon blanket from tray location C8.

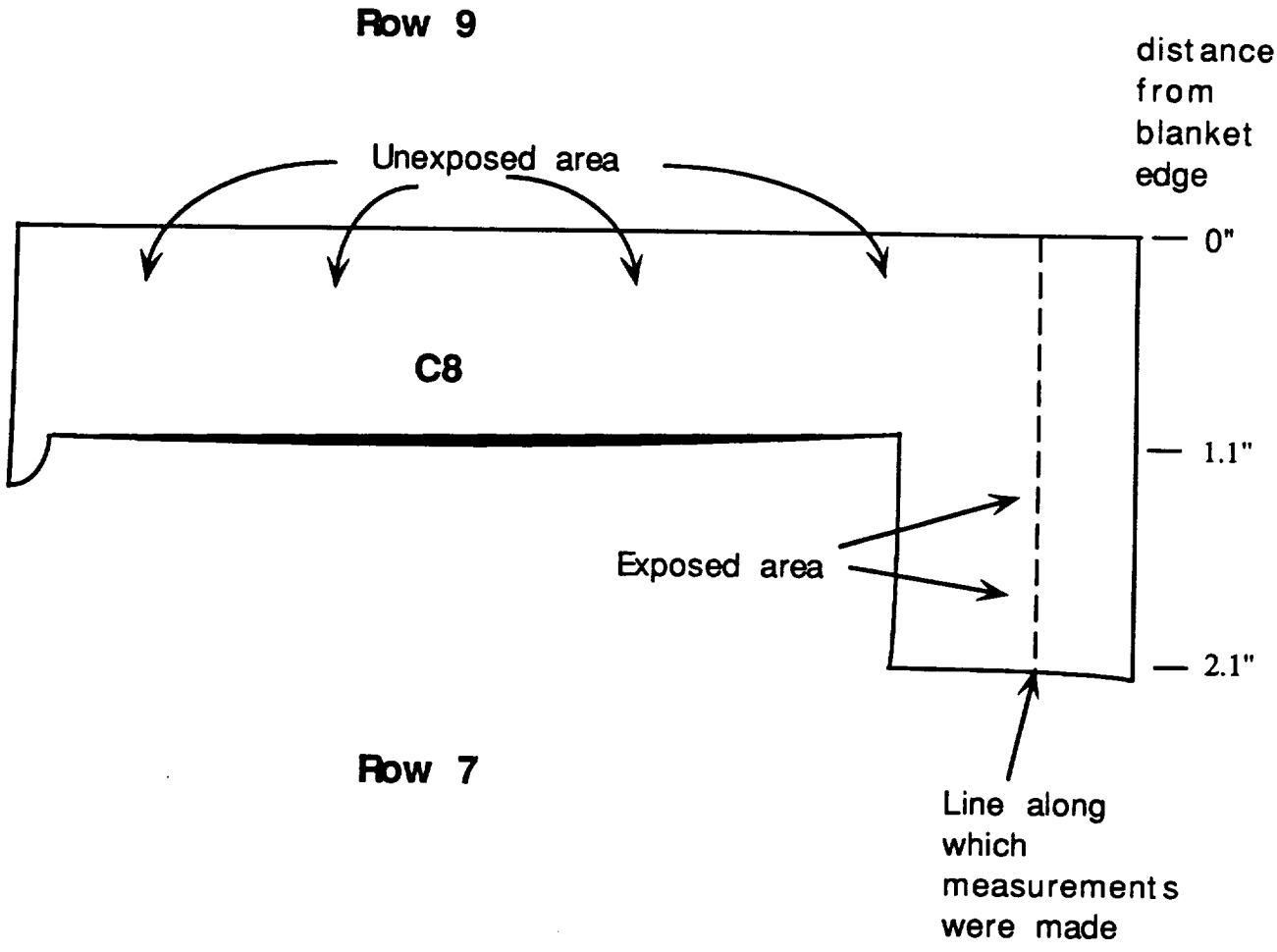

Figure A-10. Edge piece of C8 Ag/FEP blanket showing line along which BRDF and reflectance measurements were made.

Appendix B

Auger Spectra for Selected Areas from Black Chrome Plated Aluminum Panels from Earth end of LDEF.

The locations in the figure titles are from locations on panel 916-4A, shown in figure B-1 (identical to figure 8.3-6), and panel 916-10A, shown in figure B-2 (similar to figure 8.3-10), respectively. The locations on panel 916-10A used for auger measurements are marked as #1-auger and #2-auger to distinguish these locations from areas used for ESCA measurements. Locations of ESCA measurements in figure 8.3-10 are numbered 1, 2, 3, and 4. These are the same areas where optical property measurements were made. The terms "light" and "dark" brown, "light plume area," and "light" and "dark" blue, are notations to indicate the visible appearance of the areas where the measurements were made. Spectra which have no indication of color were essentially uniformly black.

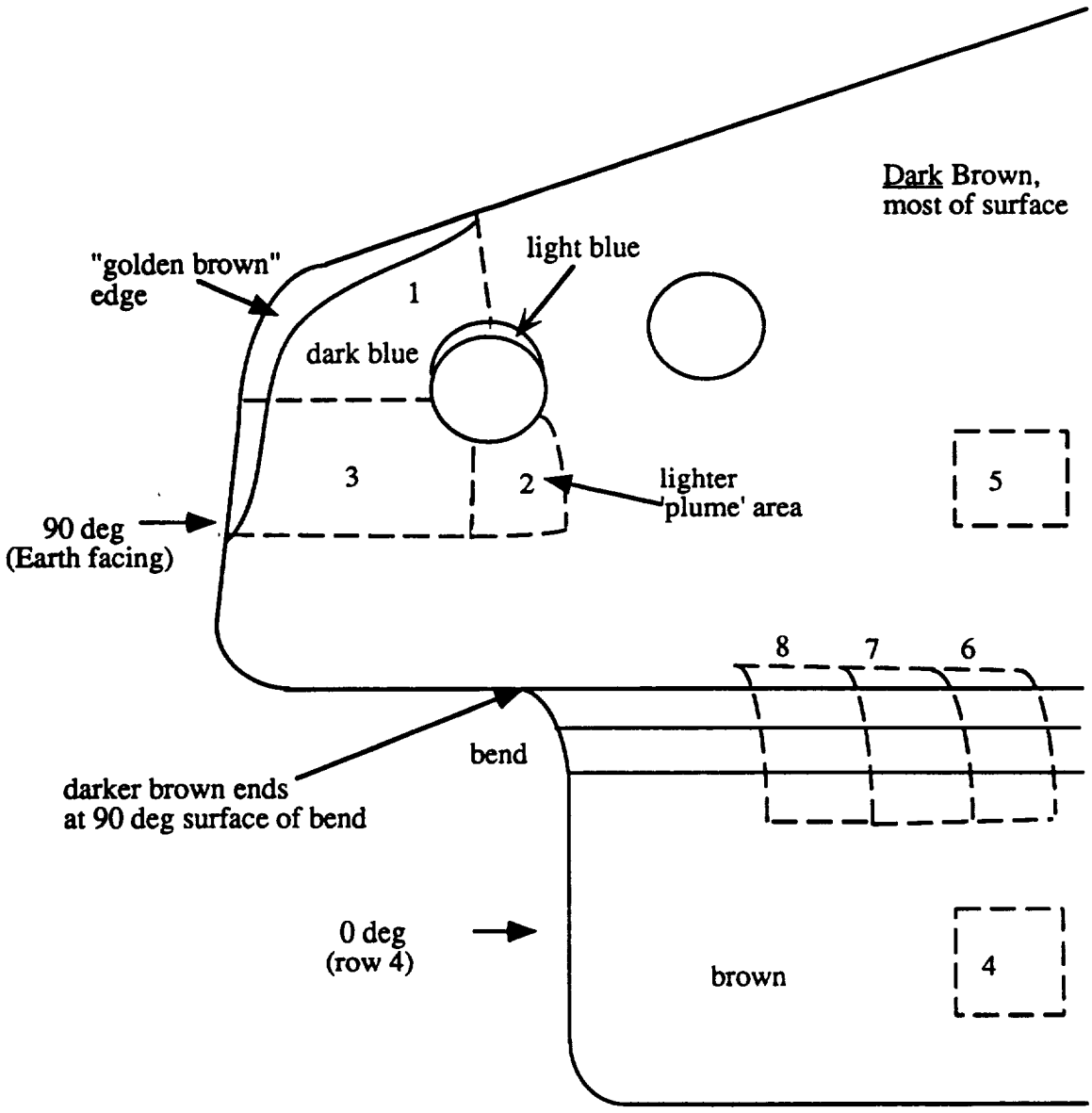

Figure B-1. Specimen locations for ESCA and auger measurements on panel 916-4A.

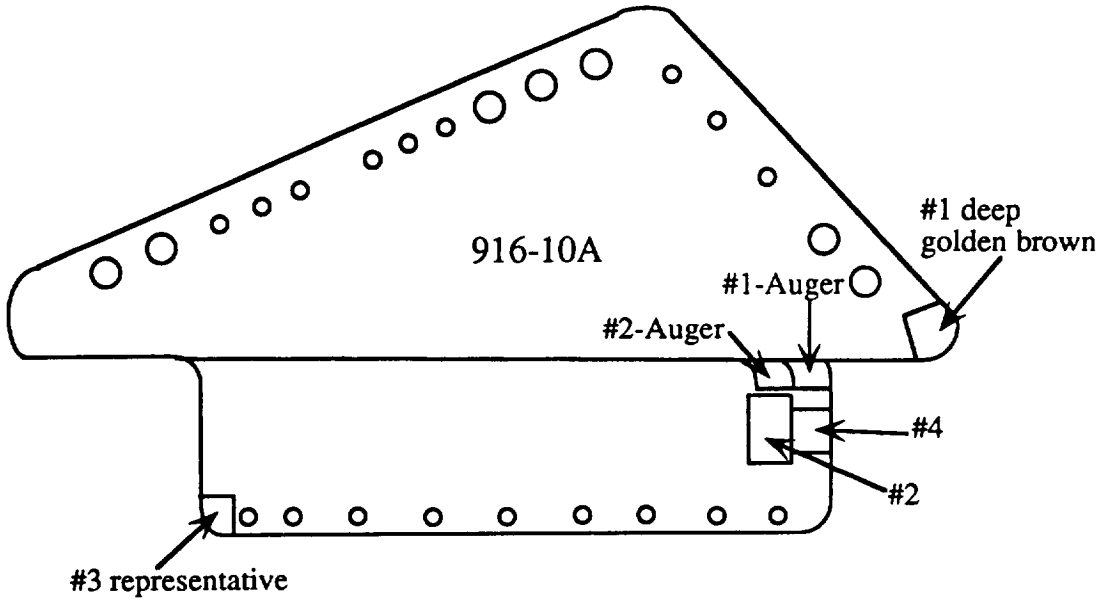

Figure B-2. Specimen locations for ESCA and Auger measurements on panel 916-10A.

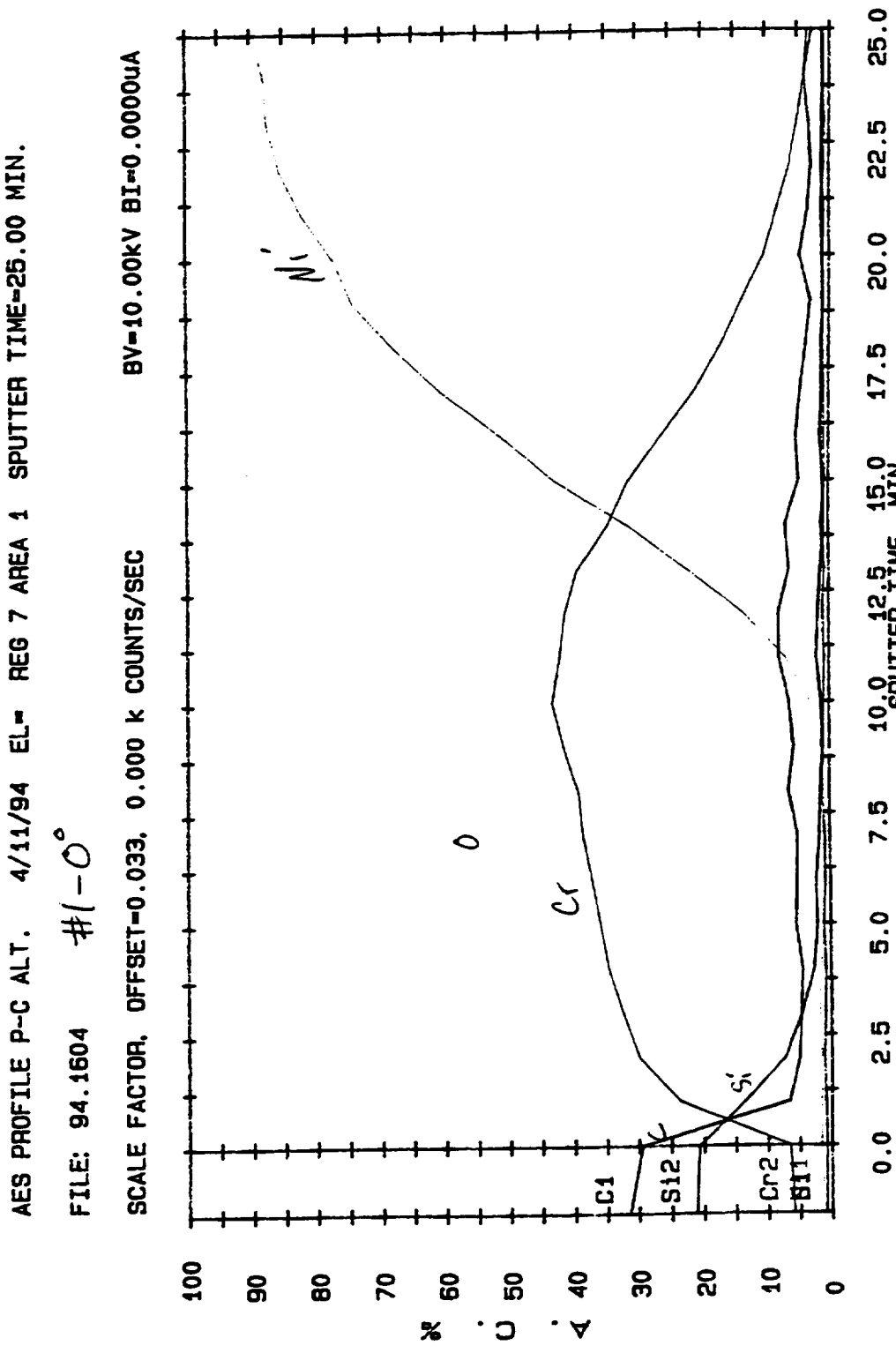

Figure B-3. Auger spectrum from location #1 (0 deg) of panel 916-10A.

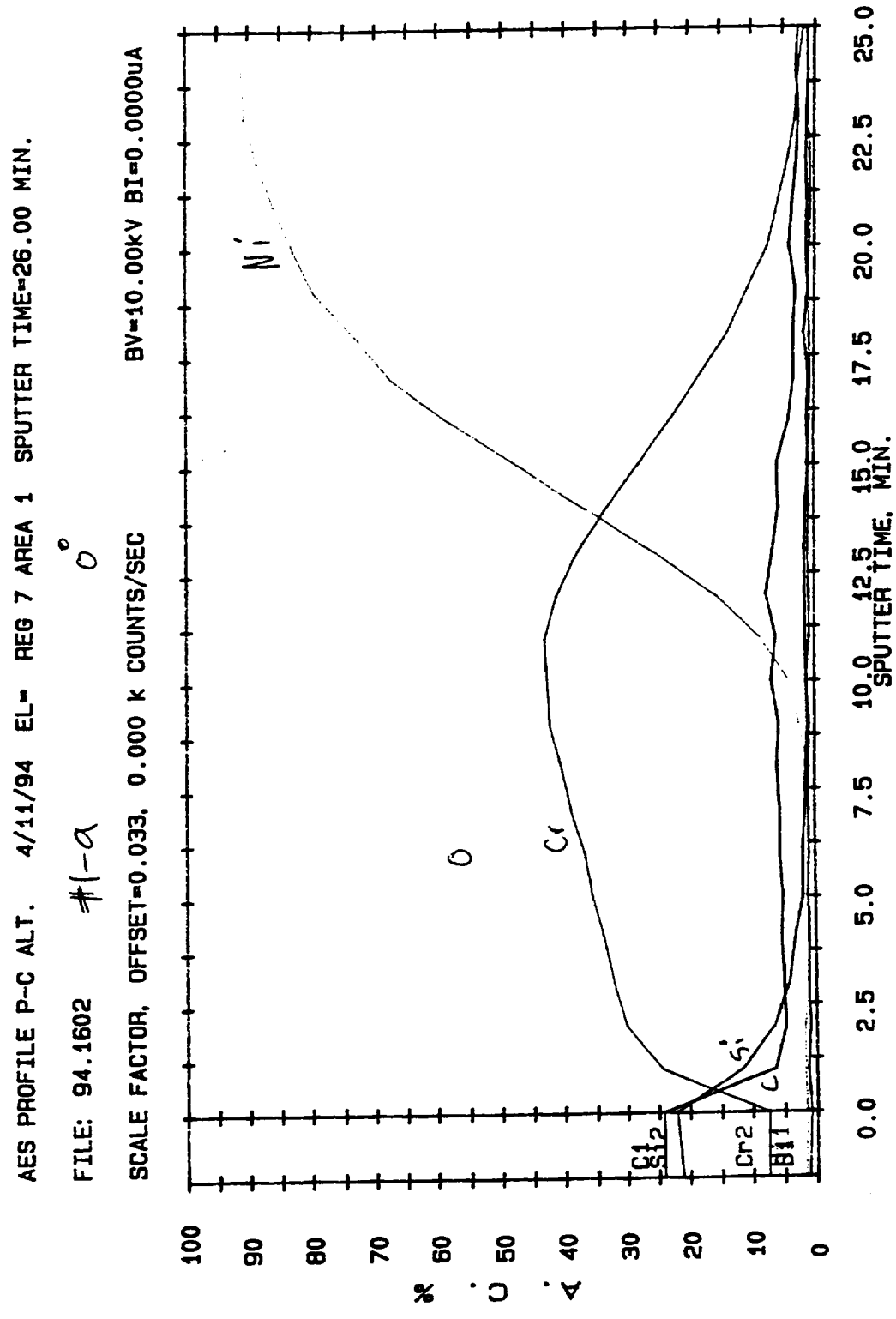

Figure B-4. Auger spectrum from location #1-a (0 deg) of panel 916-10A.

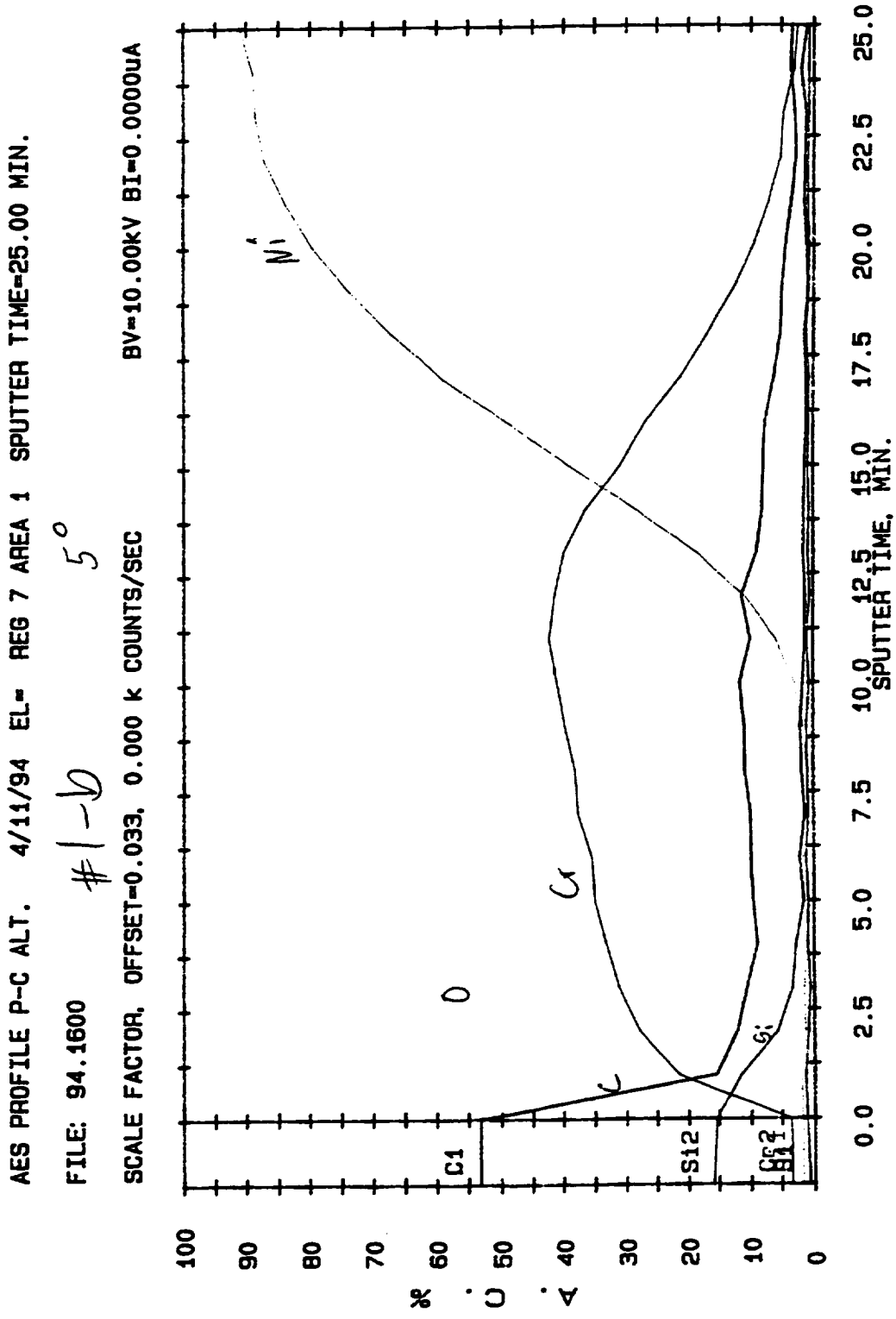

Figure B-5. Auger spectrum from location #1-b (5 deg) of panel 916-10A.

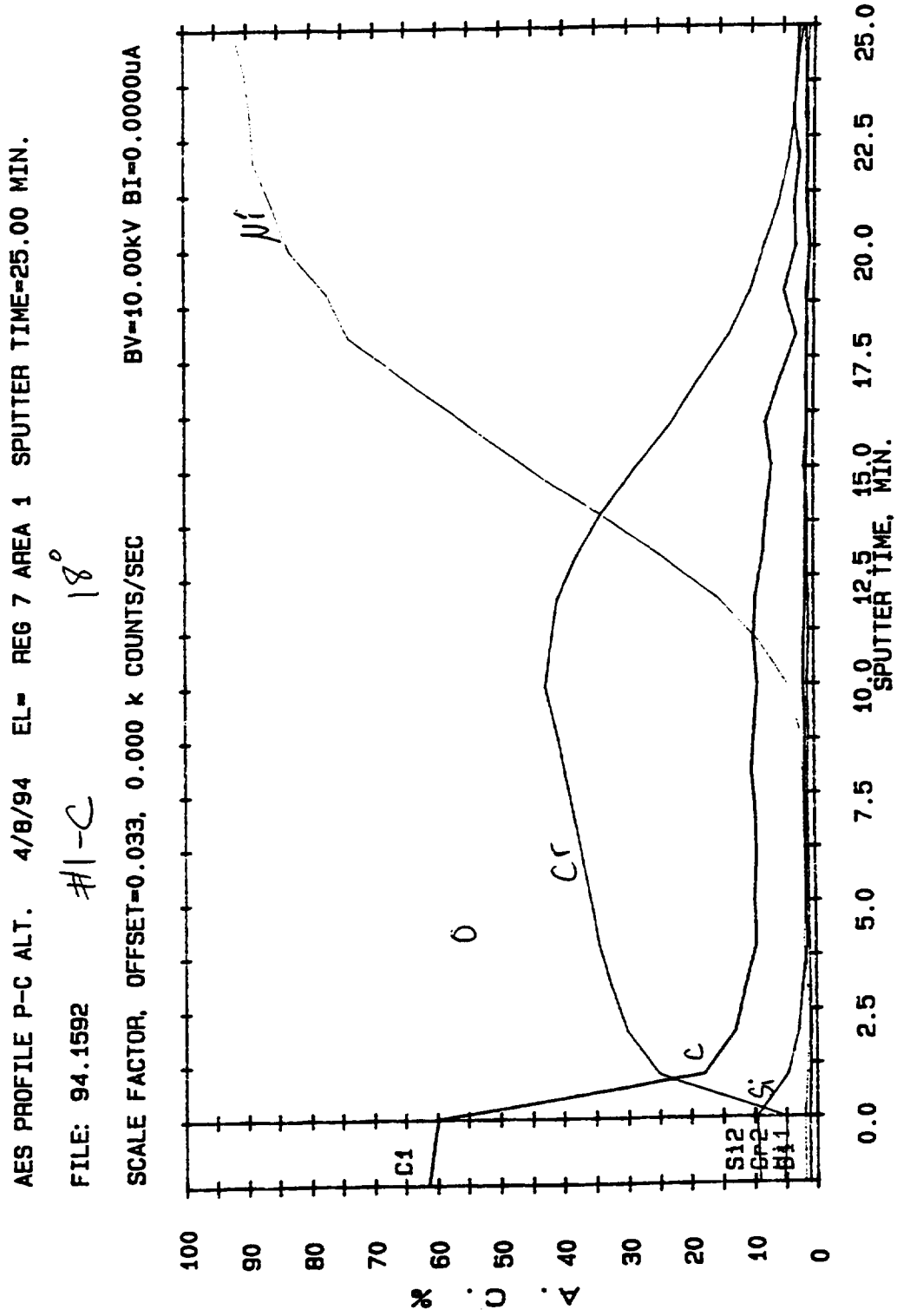

Figure B-6. Auger spectrum from location #1-c (18 deg) of panel 916-10A.

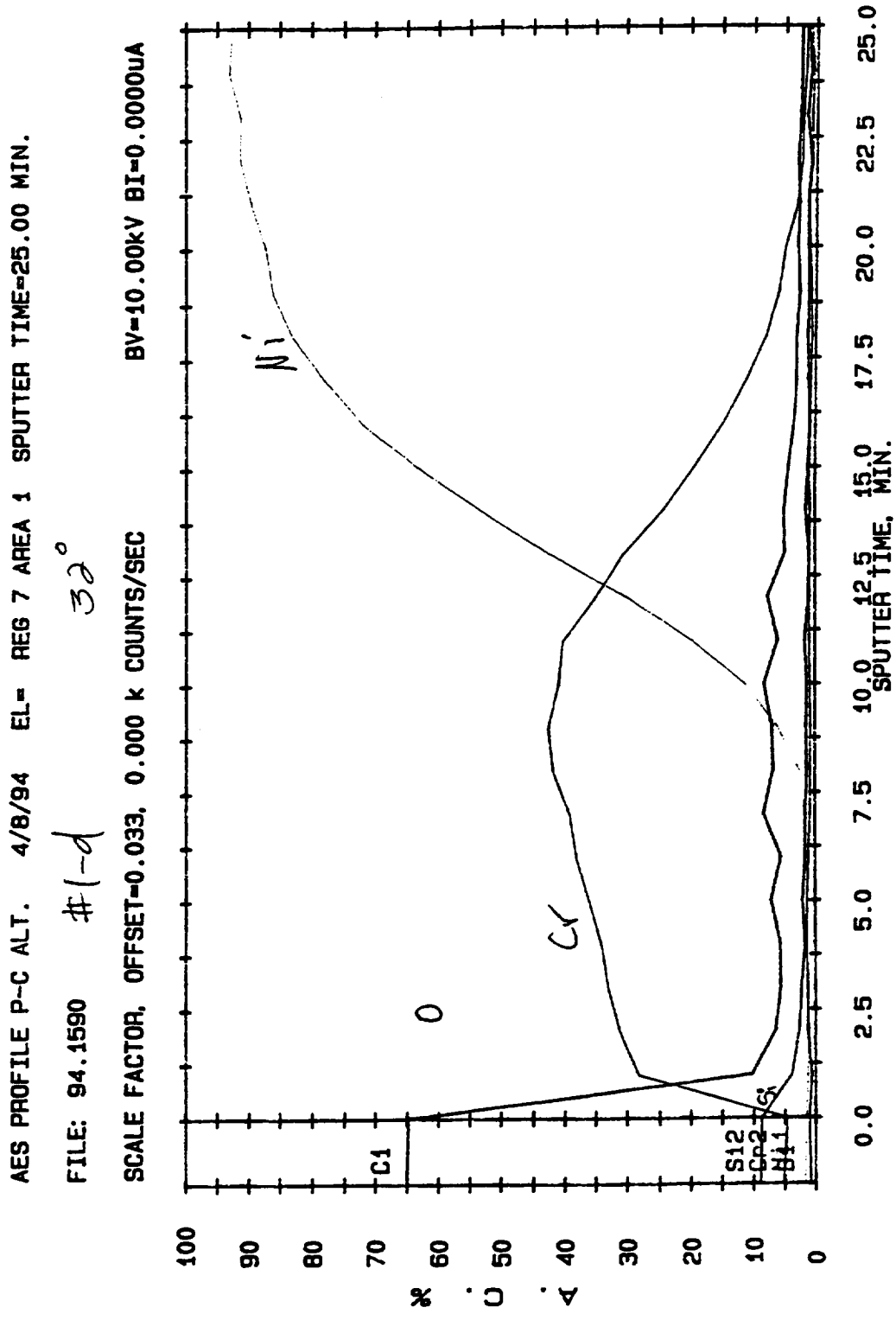

Figure B-7. Auger spectrum from location #1-d (32 deg) of panel 916-10A.

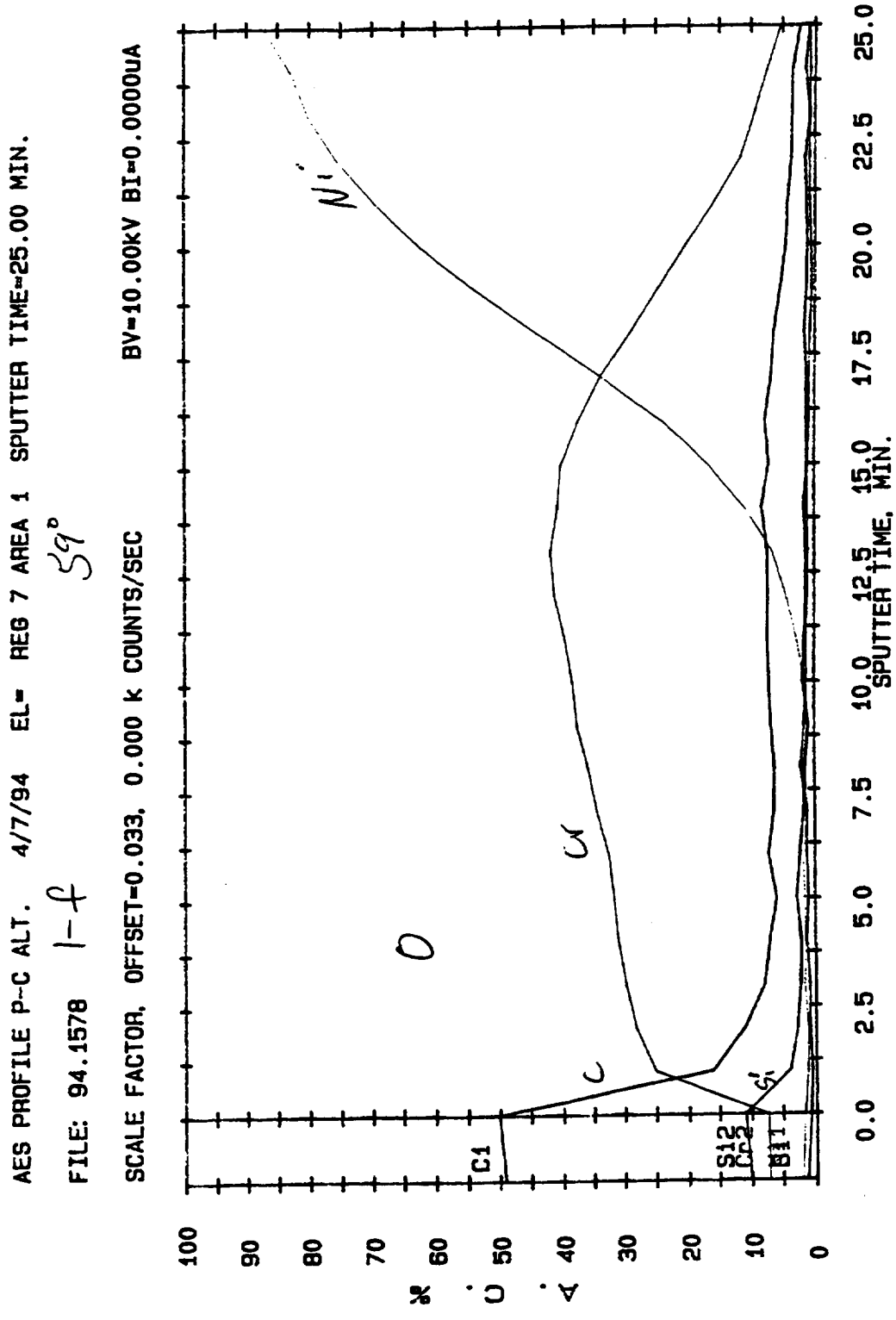

Figure B-8. Auger spectrum from location #1-f (59 deg) of panel 916-10A.

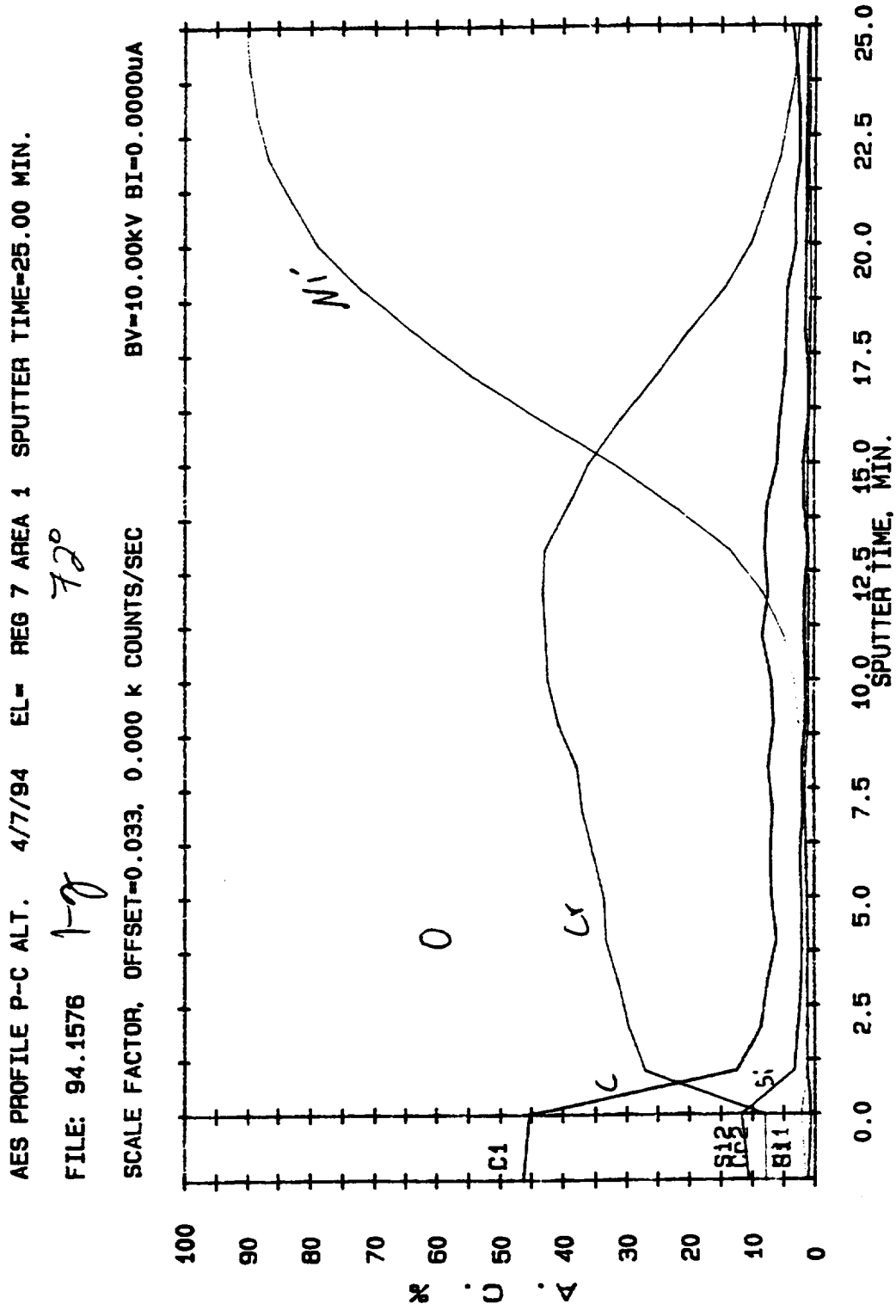

Figure B-9. Auger spectrum from location #1-g (72 deg) of panel 916-10A.

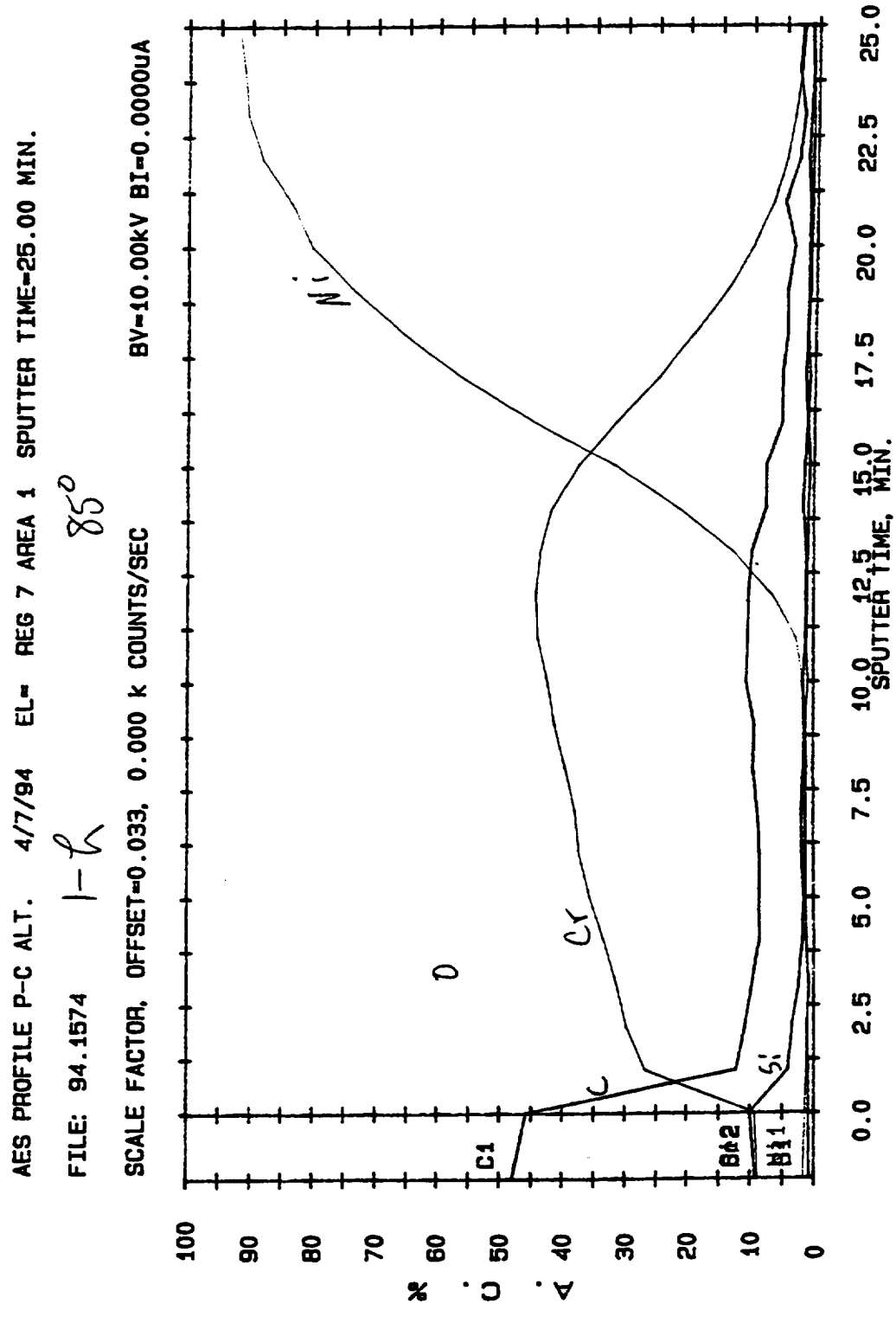

Figure B-10. Auger spectrum from location #1-h (85 deg) of panel 916-10A.

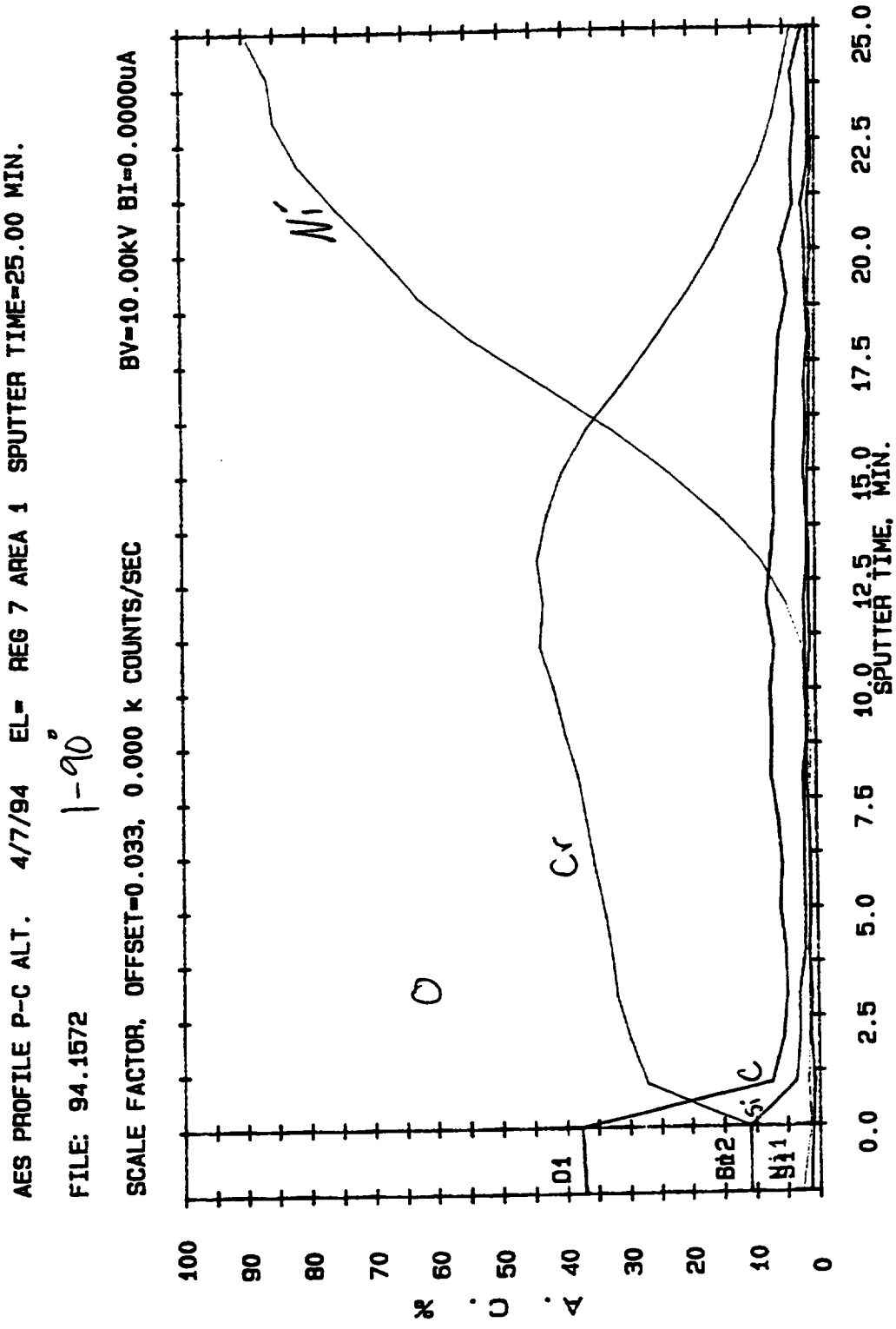

Figure B-11. Auger spectrum from location #1 (90 deg) of panel 916-10A.

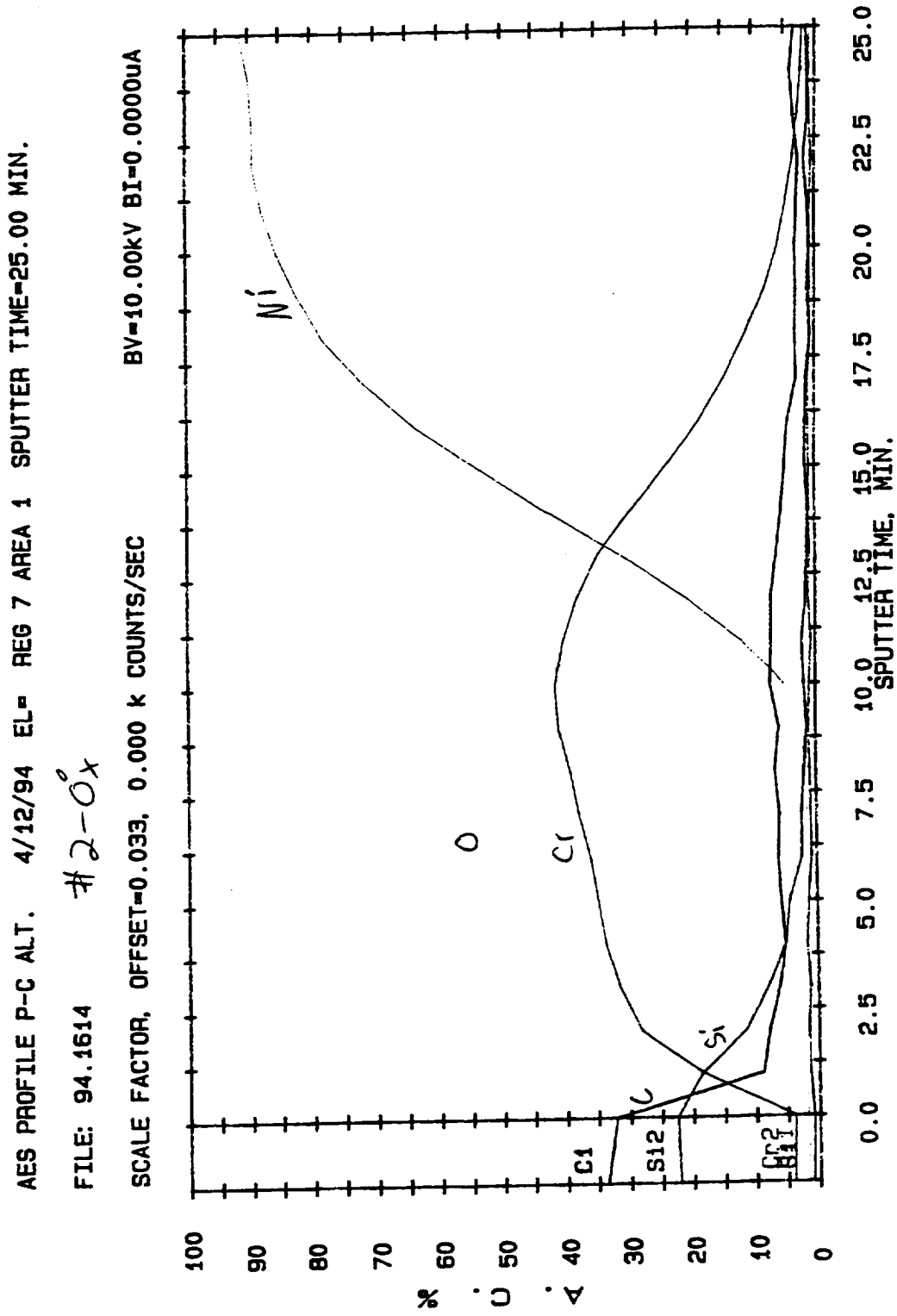

Figure B-12. Auger spectrum from location #2 (0 deg) of panel 916-10A.

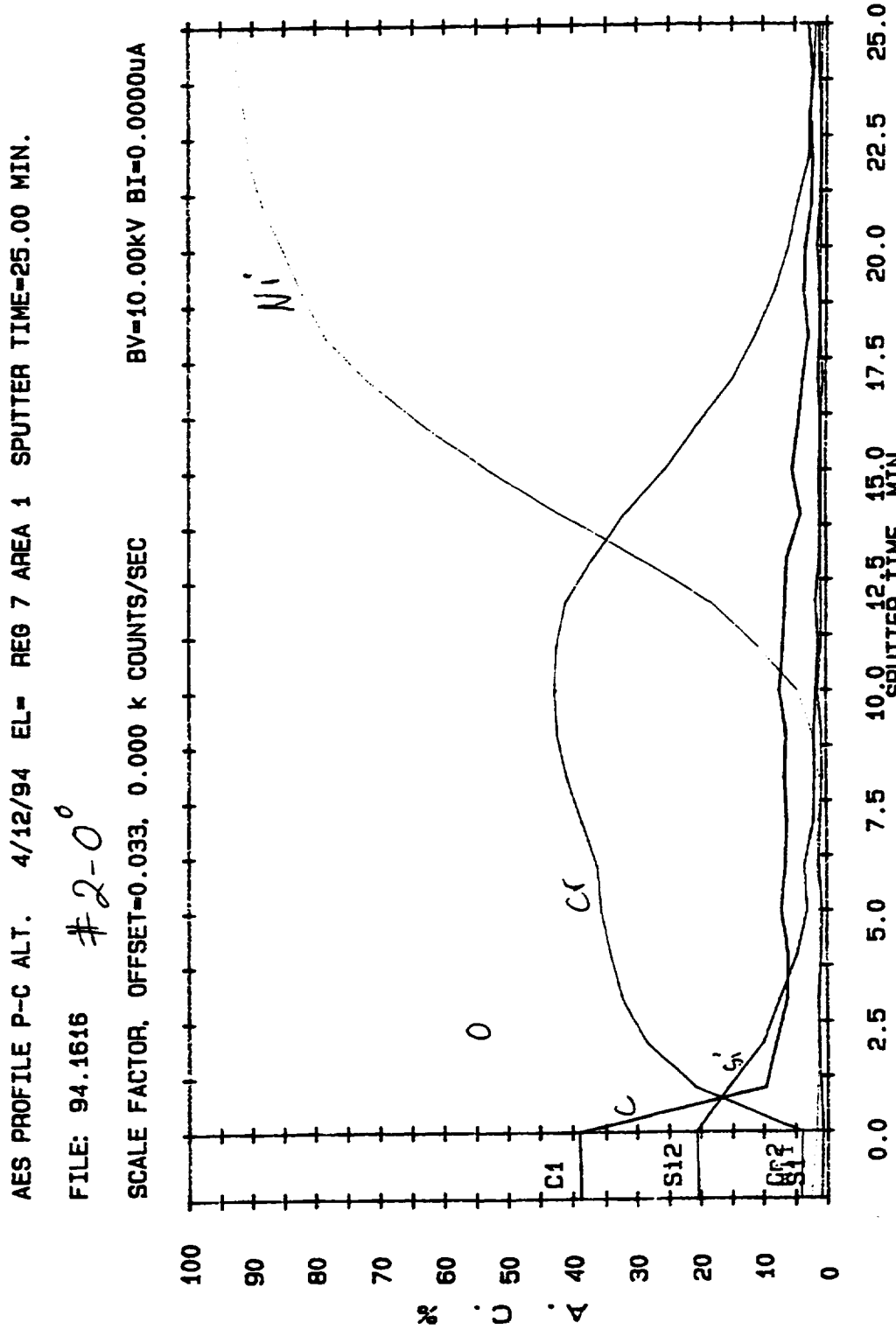

Figure B-13. Auger spectrum from location #2 (0 deg) of panel 916-10A.

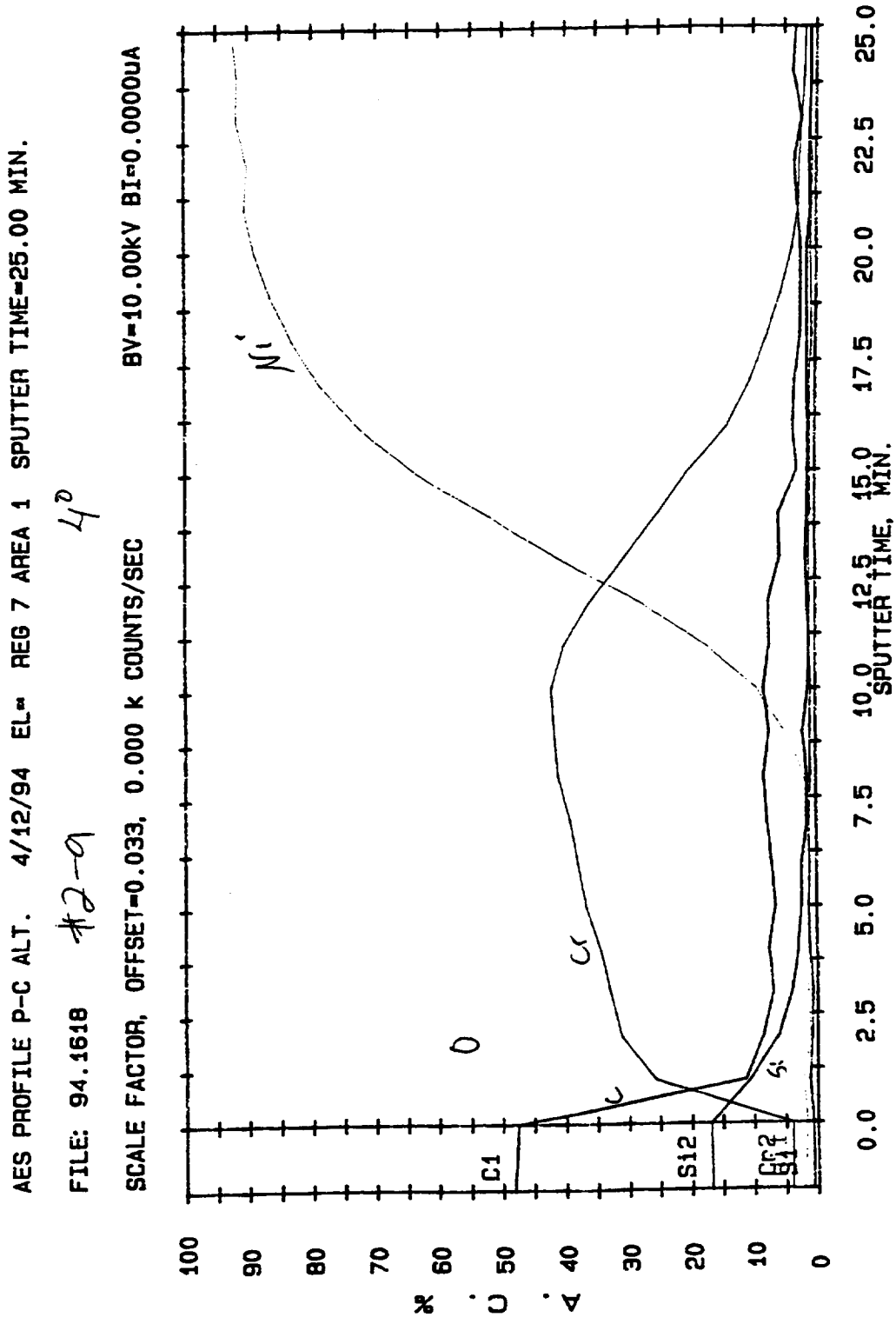

Figure B-14. Auger spectrum from location #2-a (4 deg) of panel 916-10A.

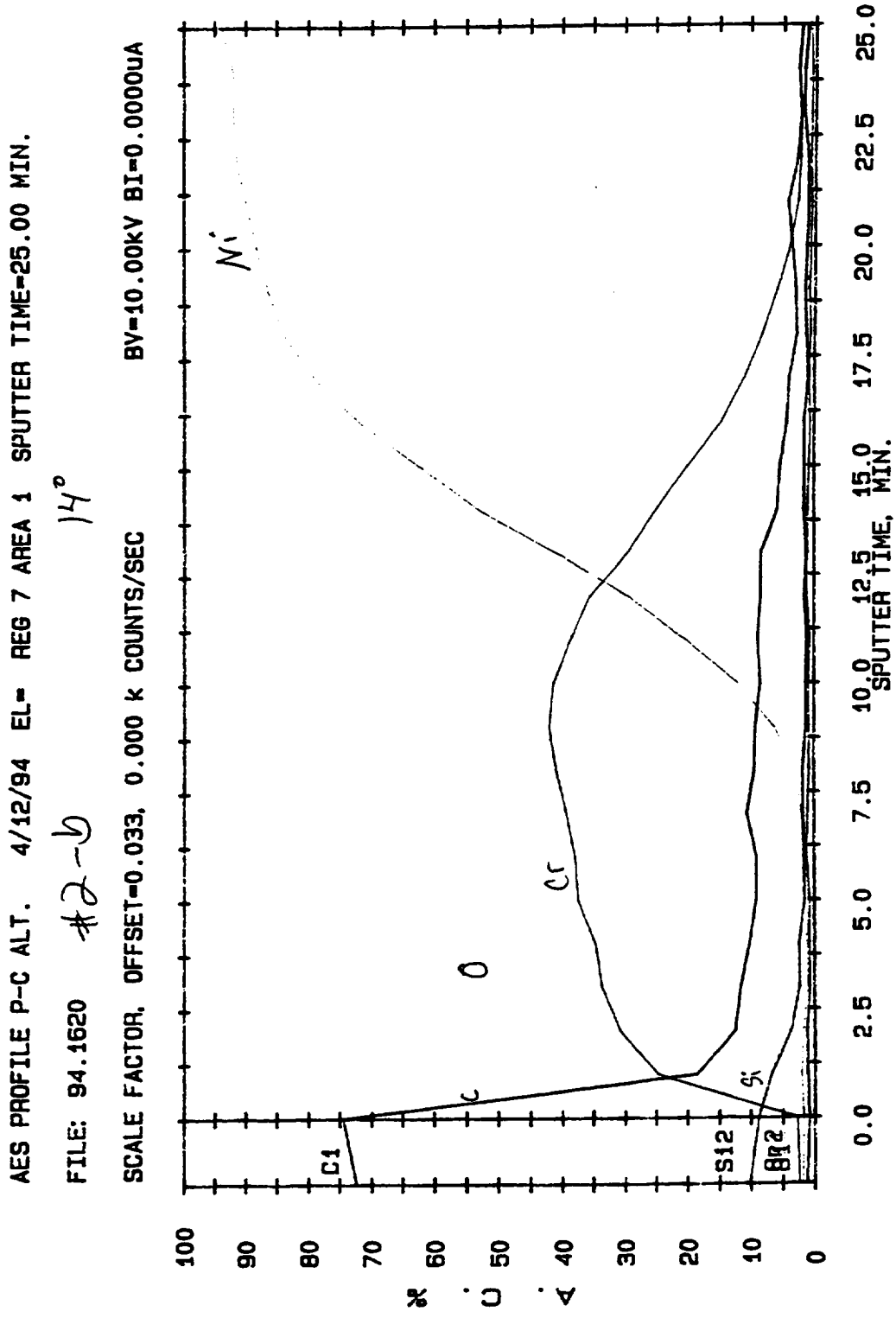

Figure B-15. Auger spectrum from location #2-b (14 deg) of panel 916-10A.

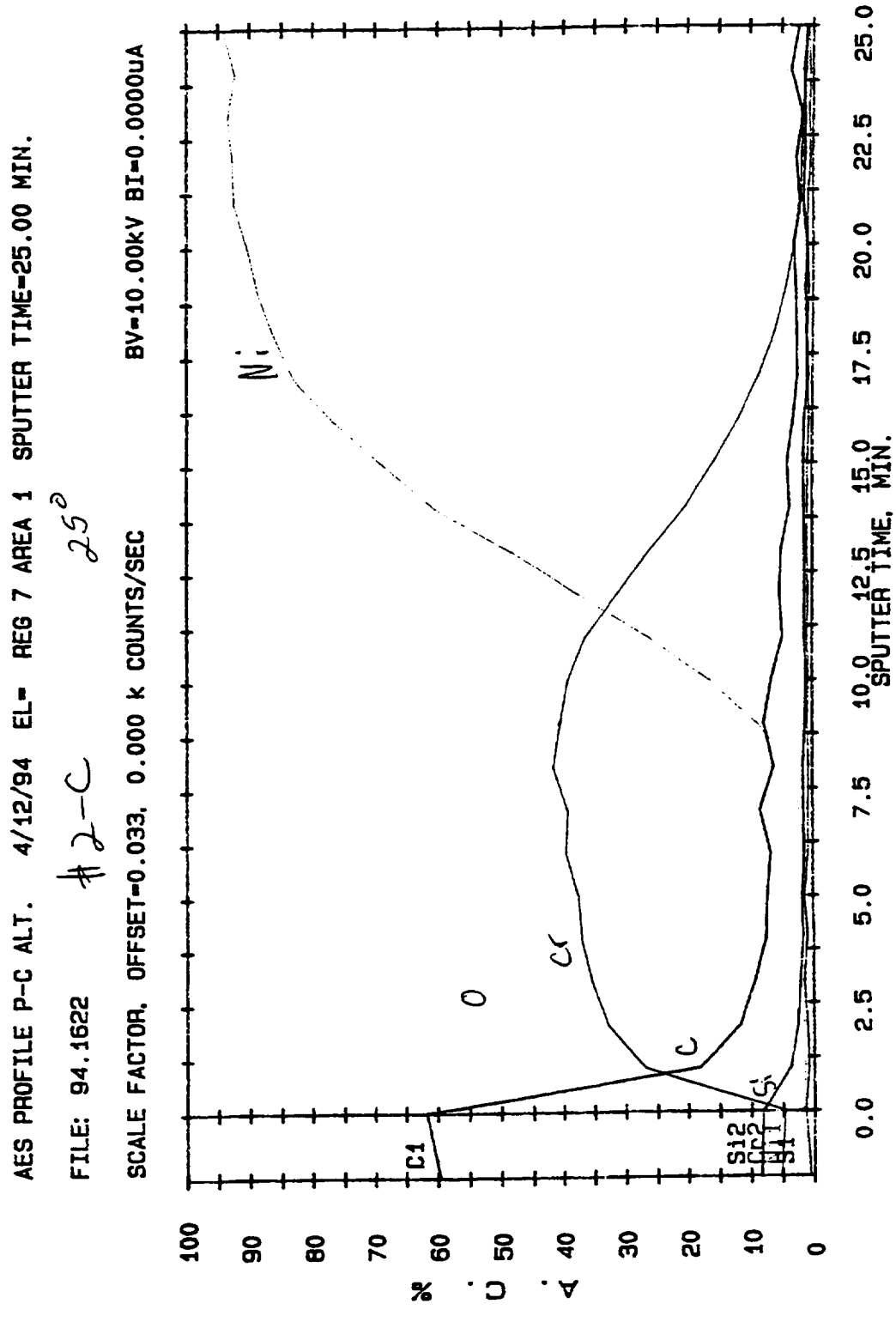

Figure B-16. Auger spectrum from location #2-c (25 deg) of panel 916-10A.

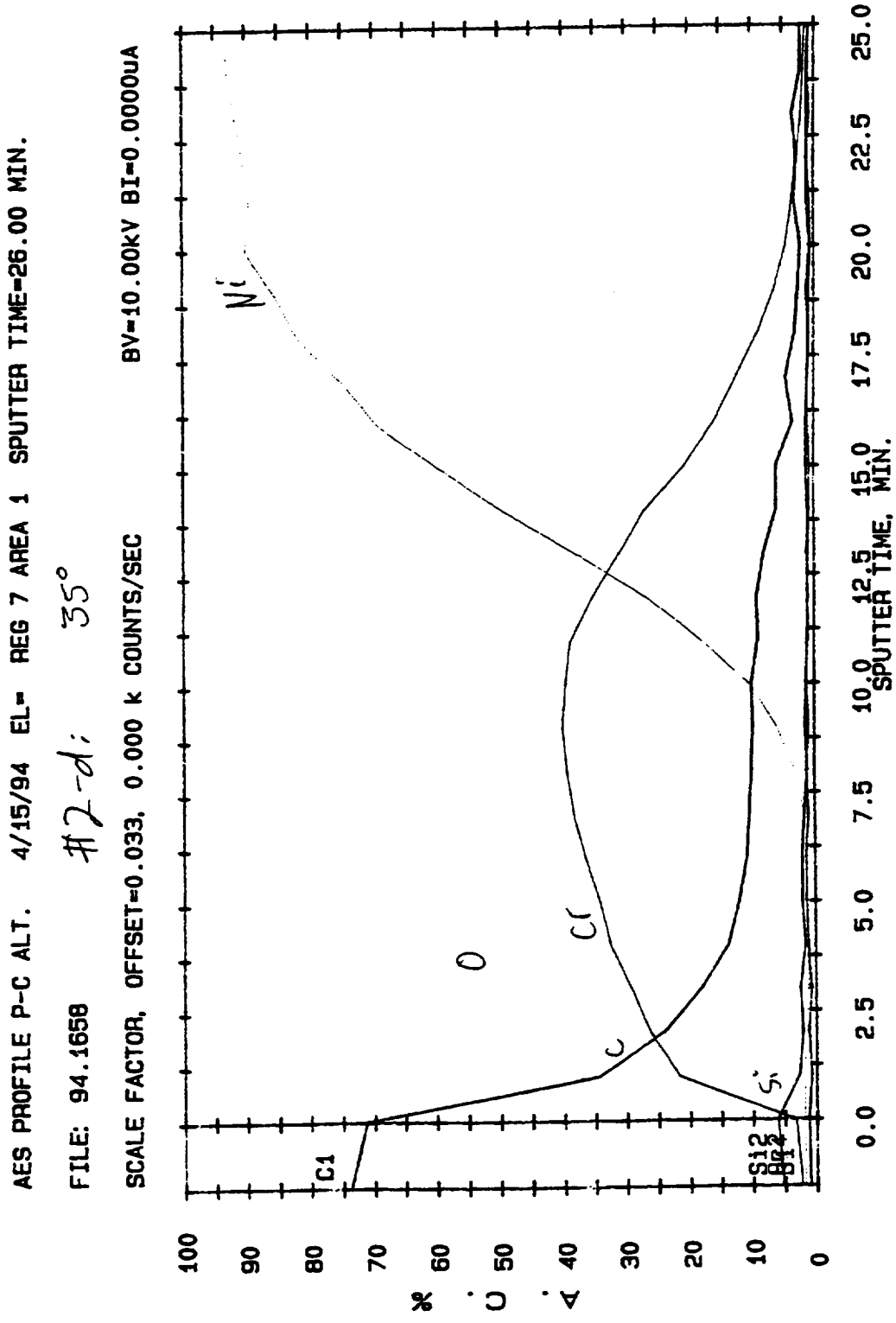

Figure B-17. Auger spectrum from location #2-d (35 deg) of panel 916-10A.

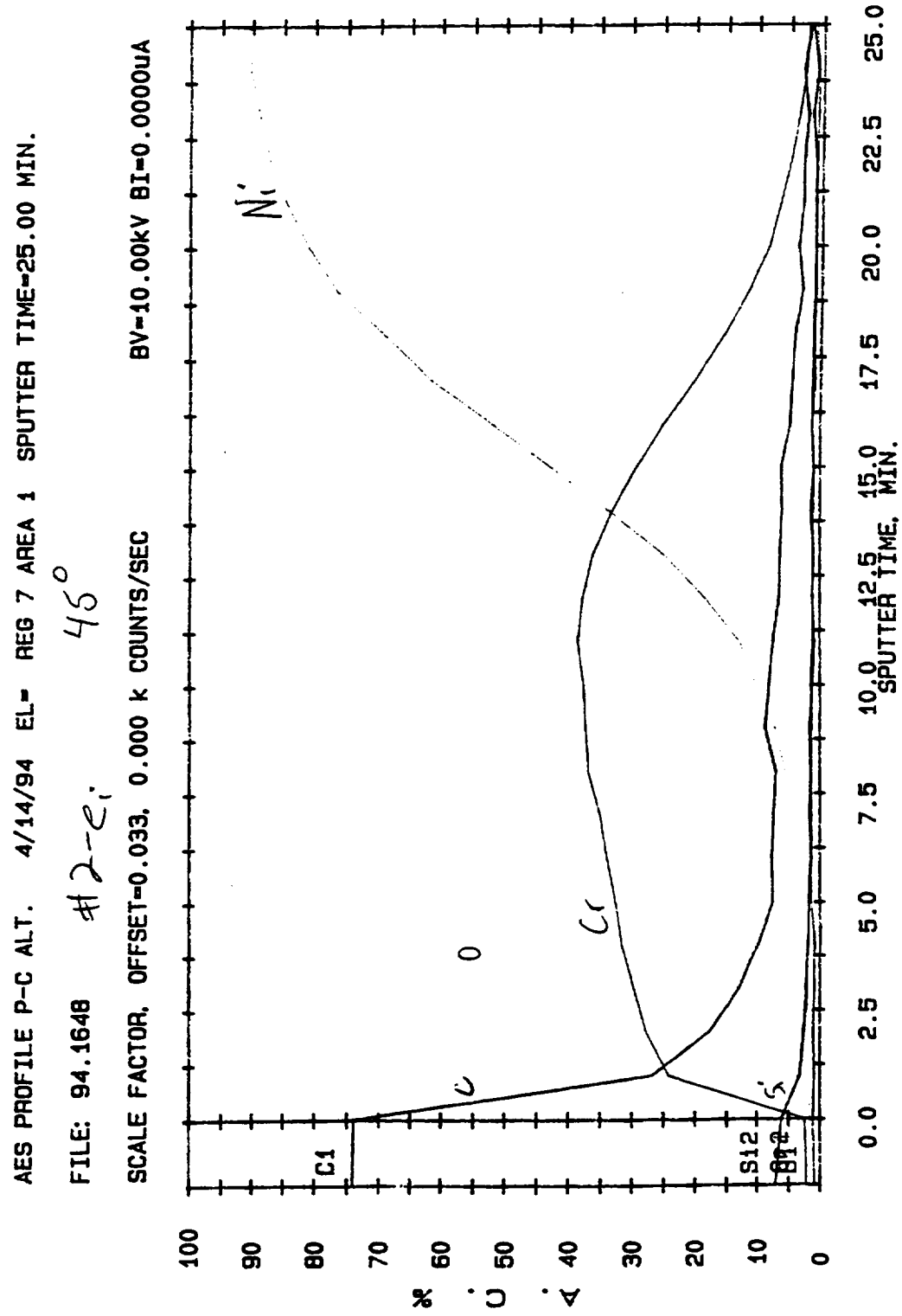

Figure B-18. Auger spectrum from location #2-e (45 deg) of panel 916-10A.

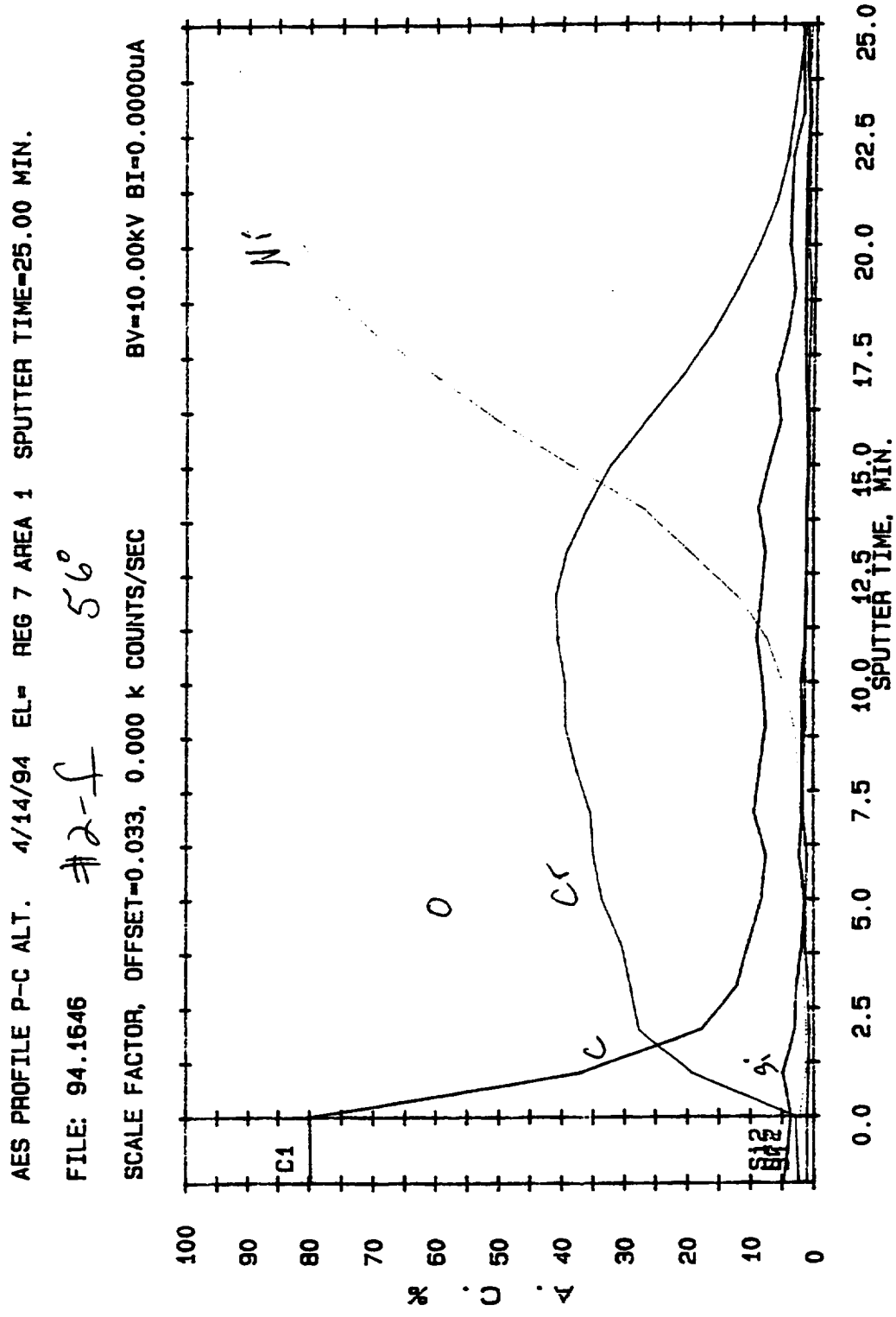

Figure B-19. Auger spectrum from location #2-f (56 deg) of panel 916-10A.

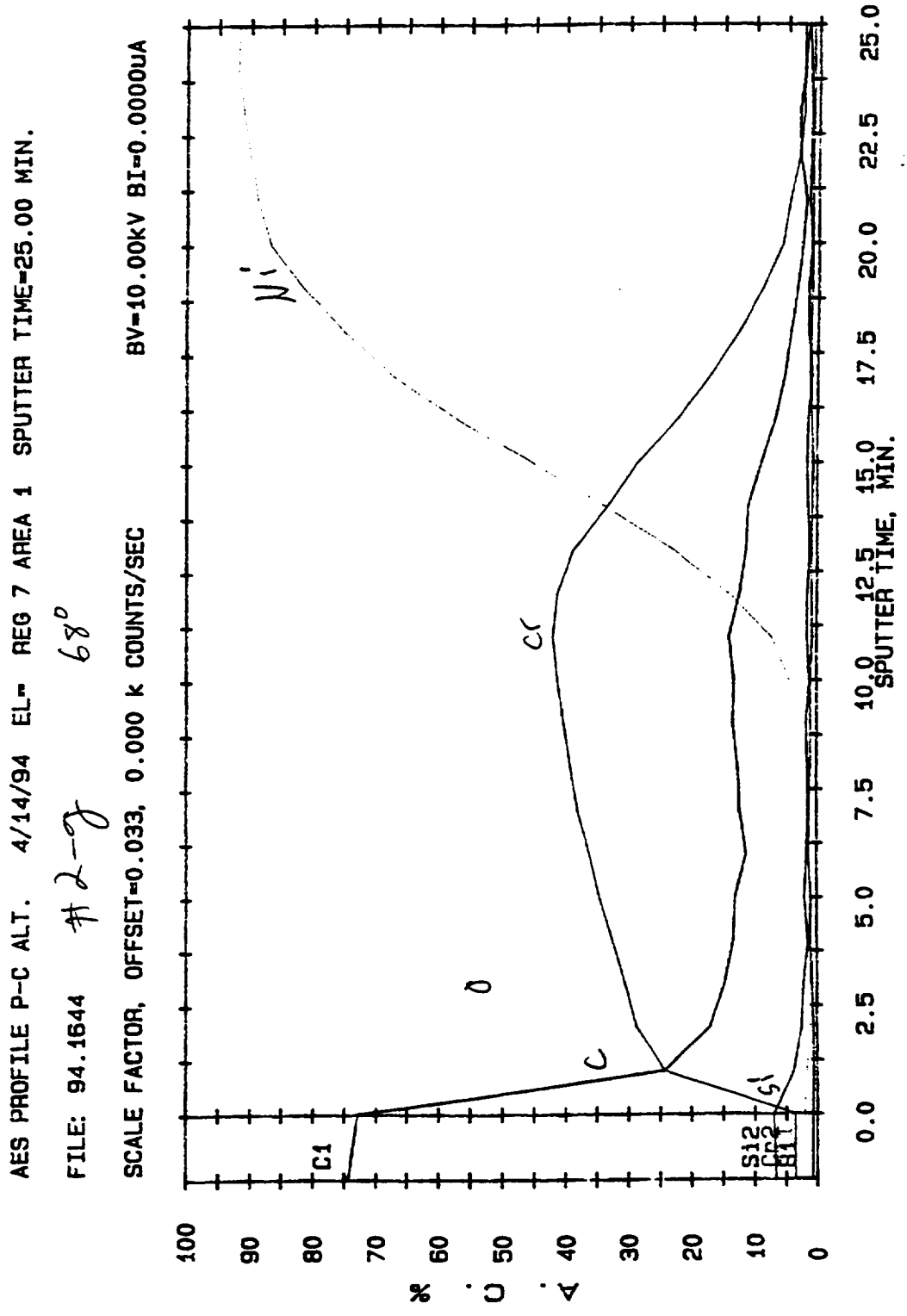

Figure B-20. Auger spectrum from location #2-g (68 deg) of panel 916-10A.

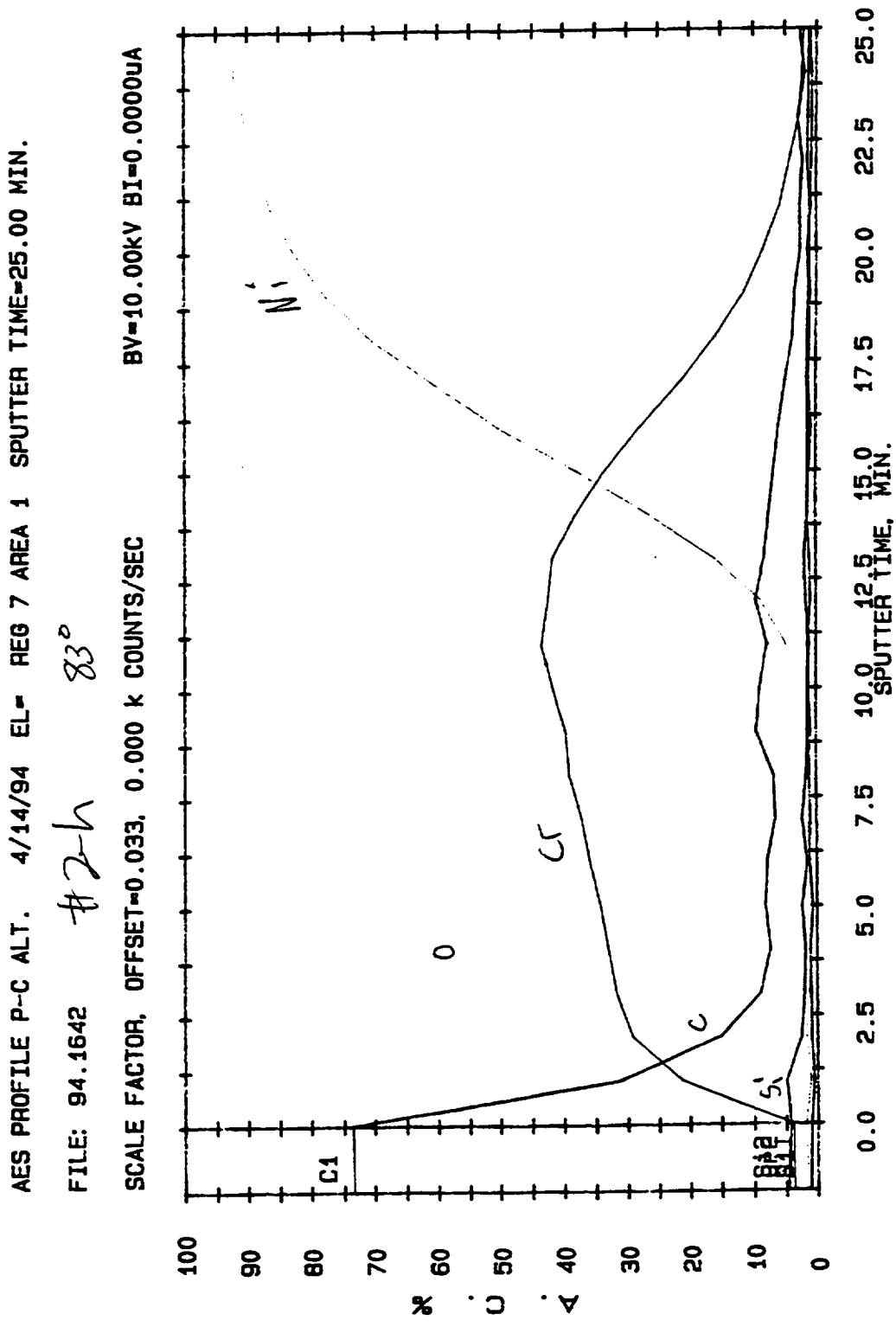

Figure B-21. Auger spectrum from location #2-h (83 deg) of panel 916-10A.

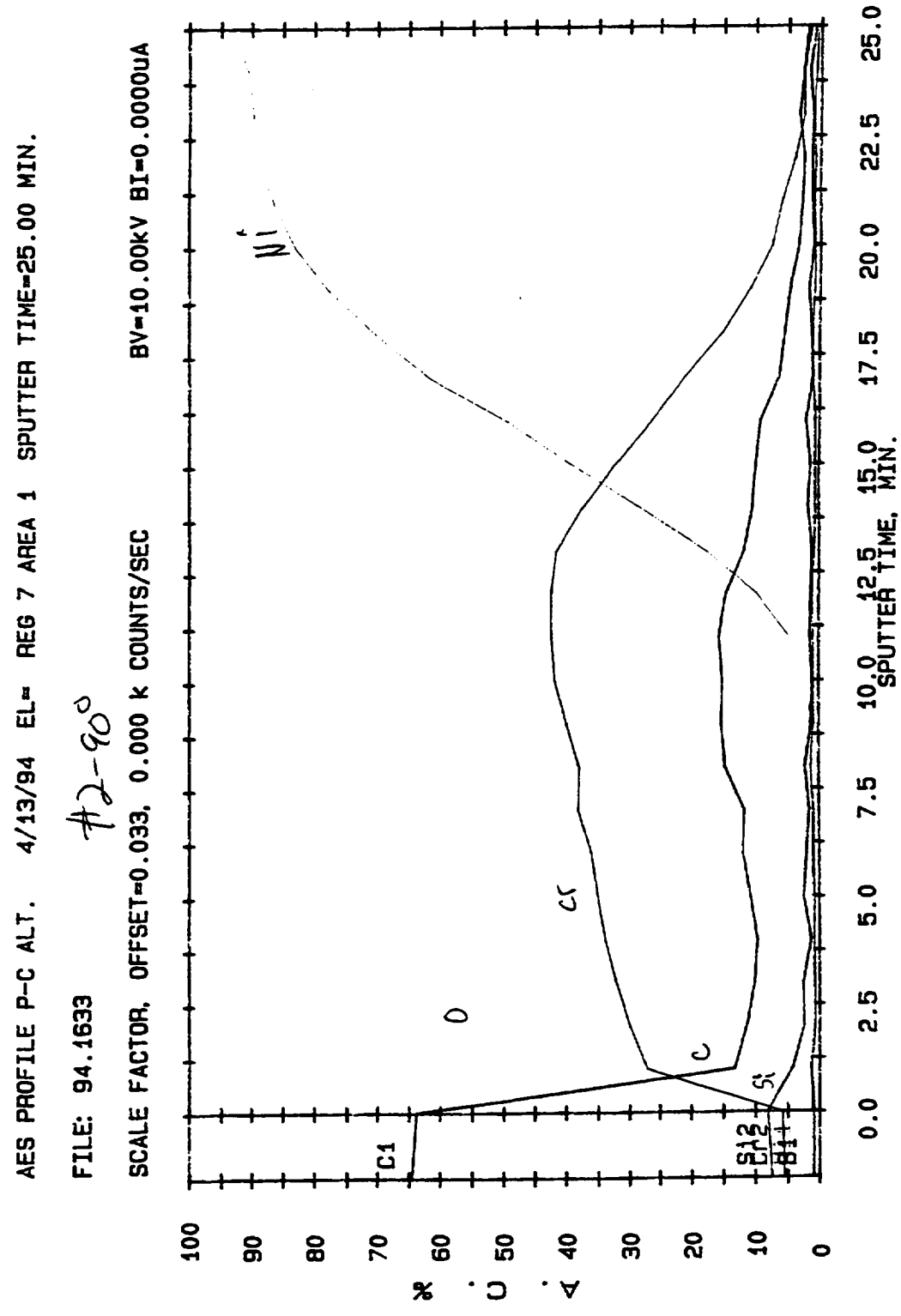

Figure B-22. Auger spectrum from location #2 (90 deg) of panel 916-10A.

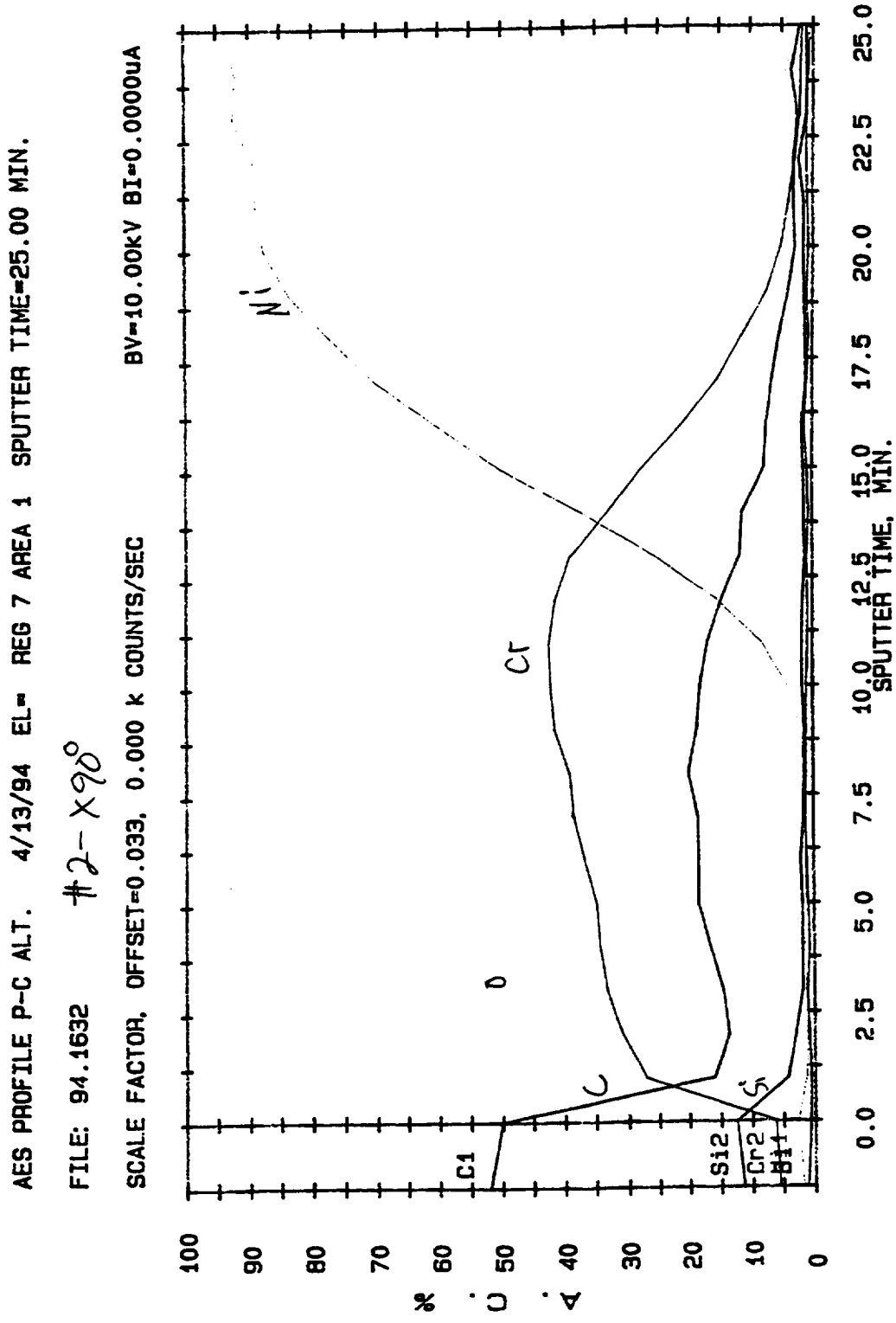

Figure B-23. Auger spectrum from location #2x (90 deg) of panel 916-10A.

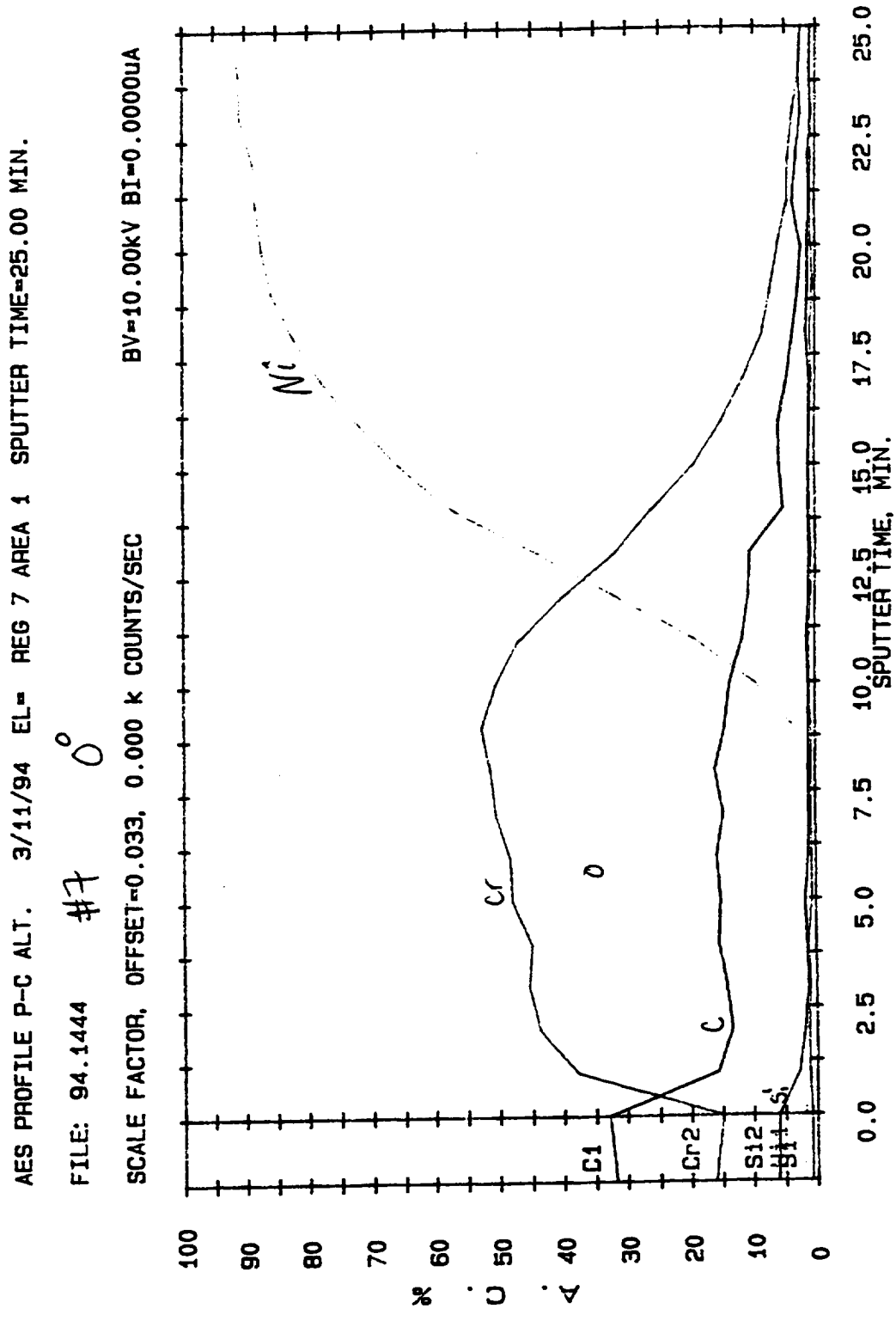

Figure B-24. Auger spectrum from location #7 (0 deg) of panel 916-4A.

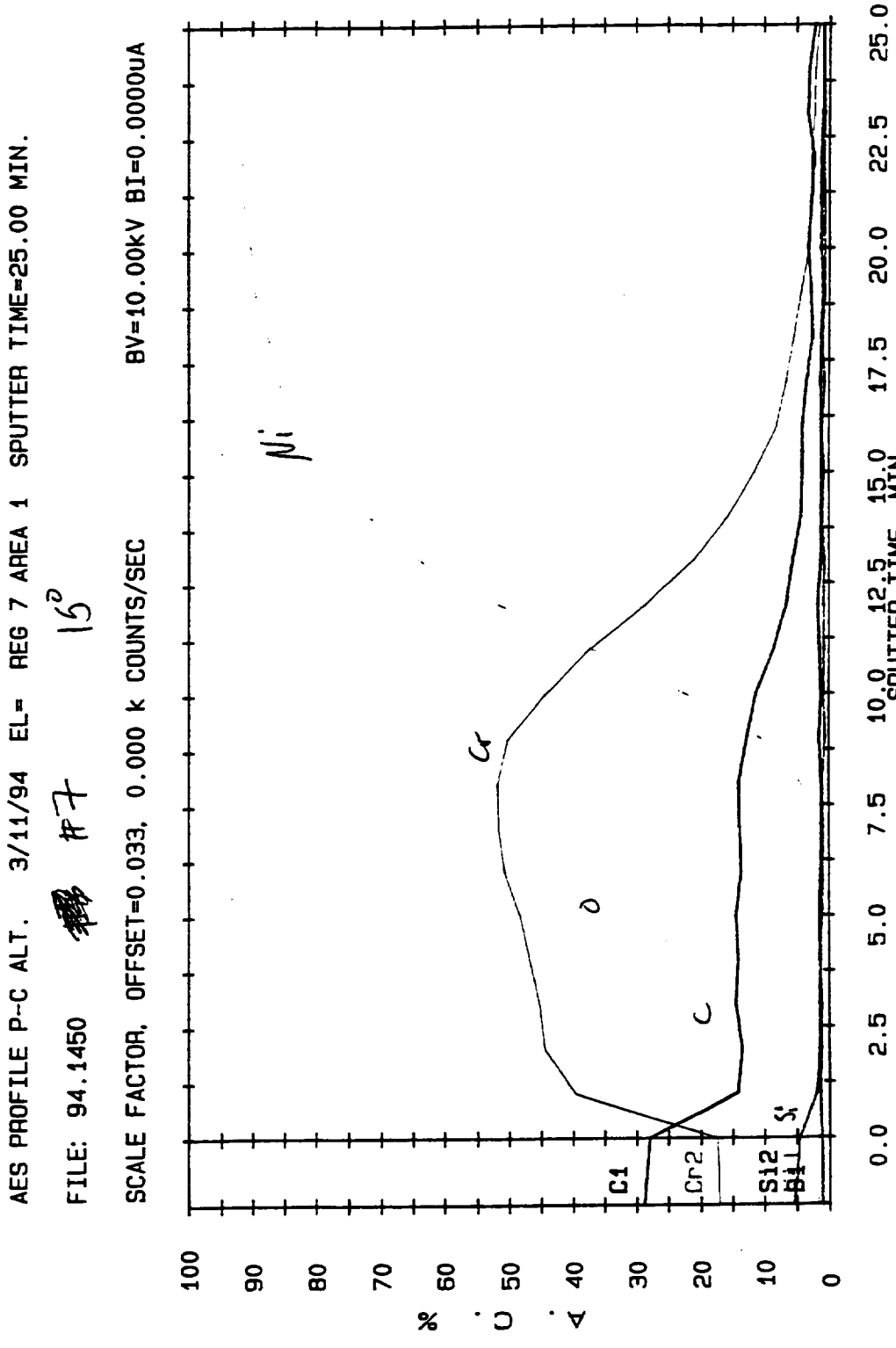

Figure B-25. Auger spectrum from location #7 (15 deg) of panel 916-4A.

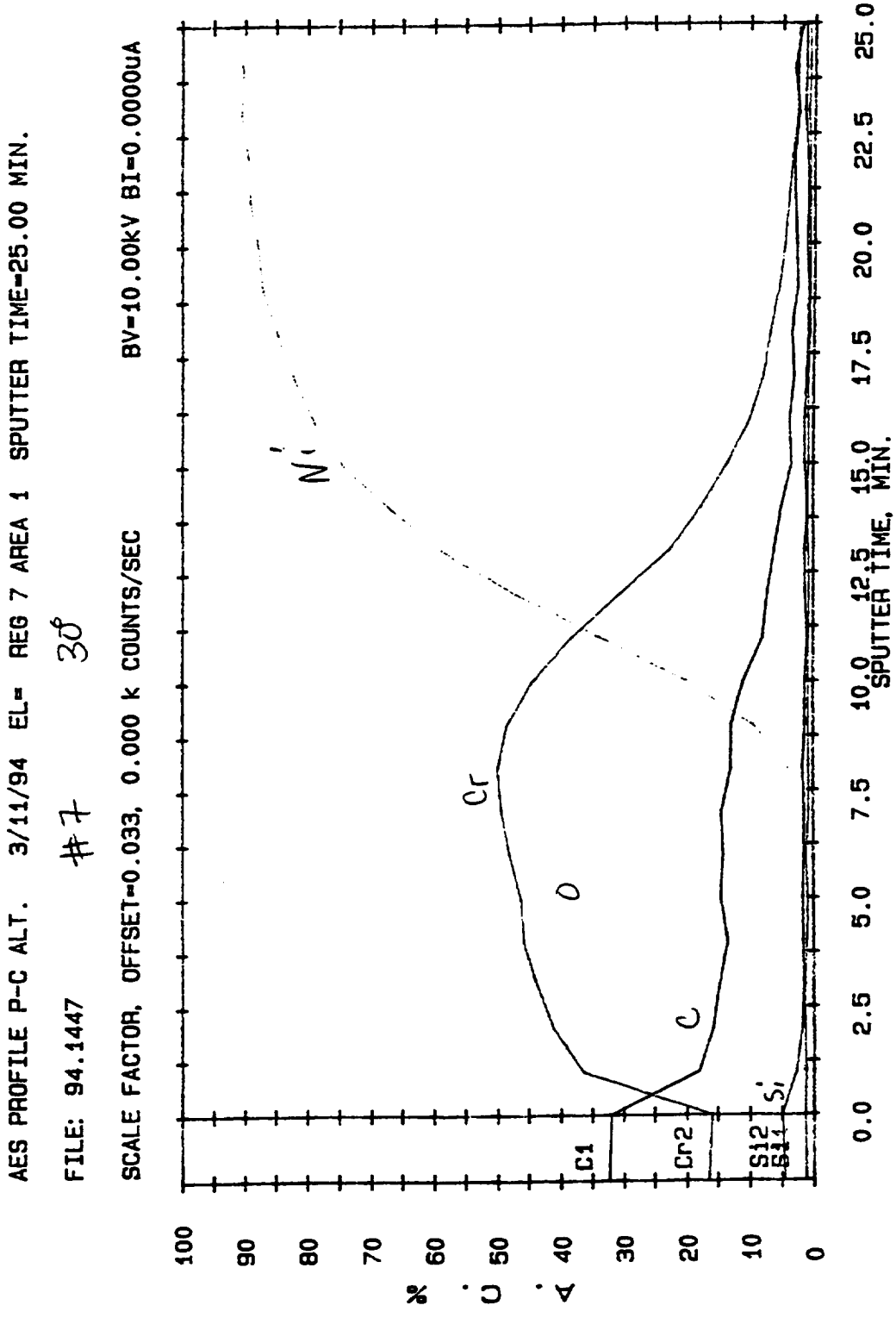

Figure B-26. Auger spectrum from location #7 (30 deg) of panel 916-4A.

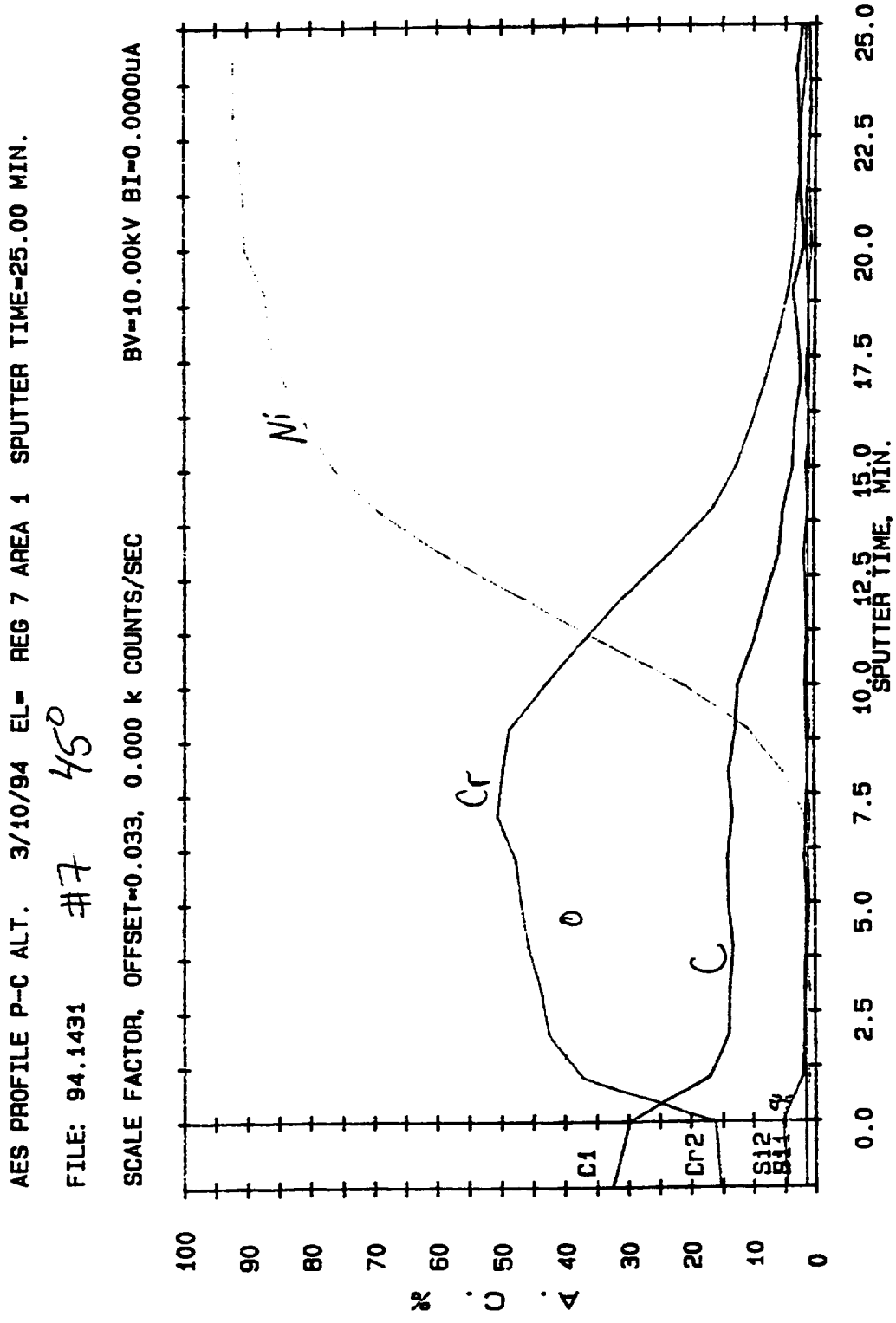

Figure B-27. Auger spectrum from location #7 (45 deg) of panel 916-4A.

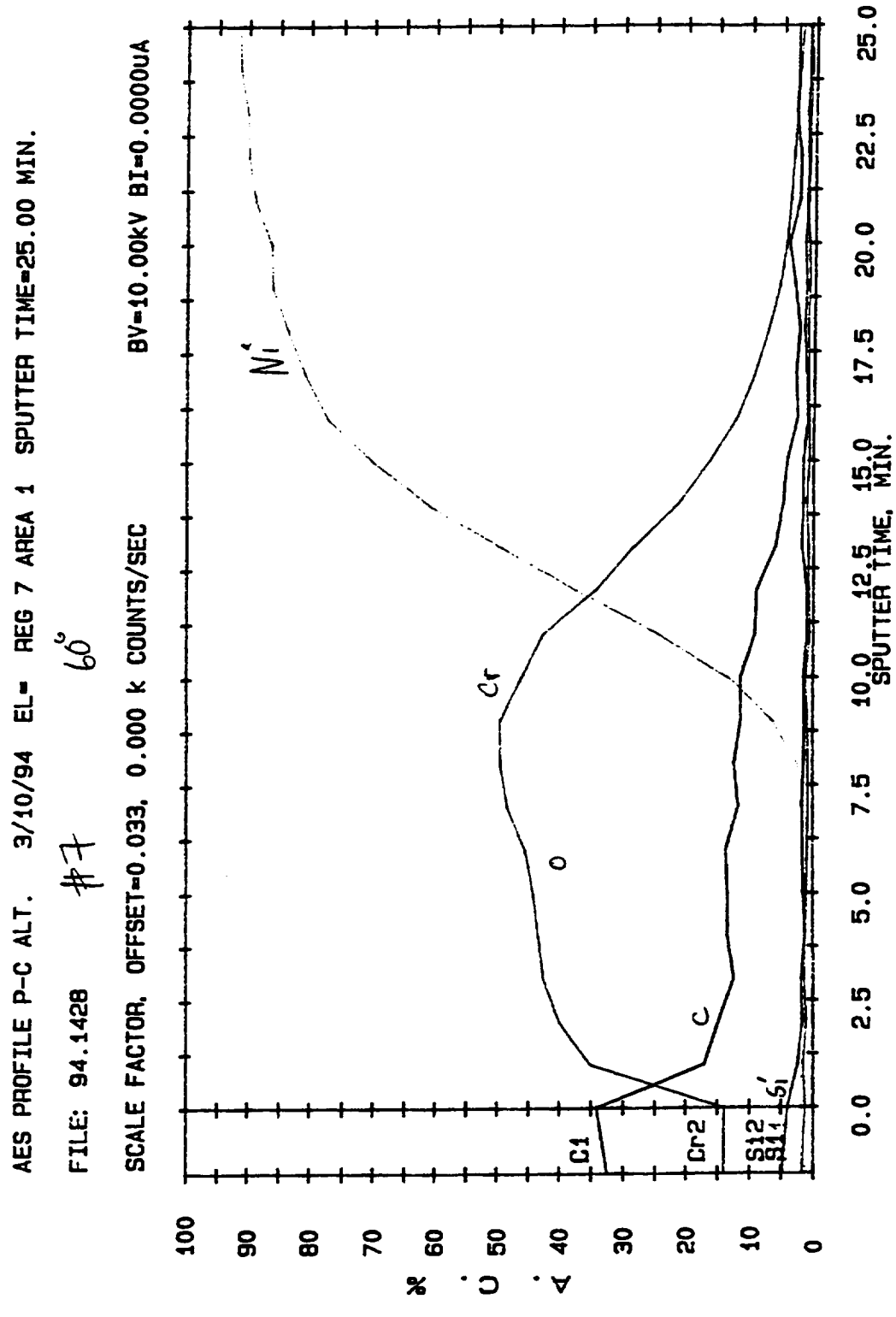

Figure B-28. Auger spectrum from location #7 (60 deg) of panel 916-4A.

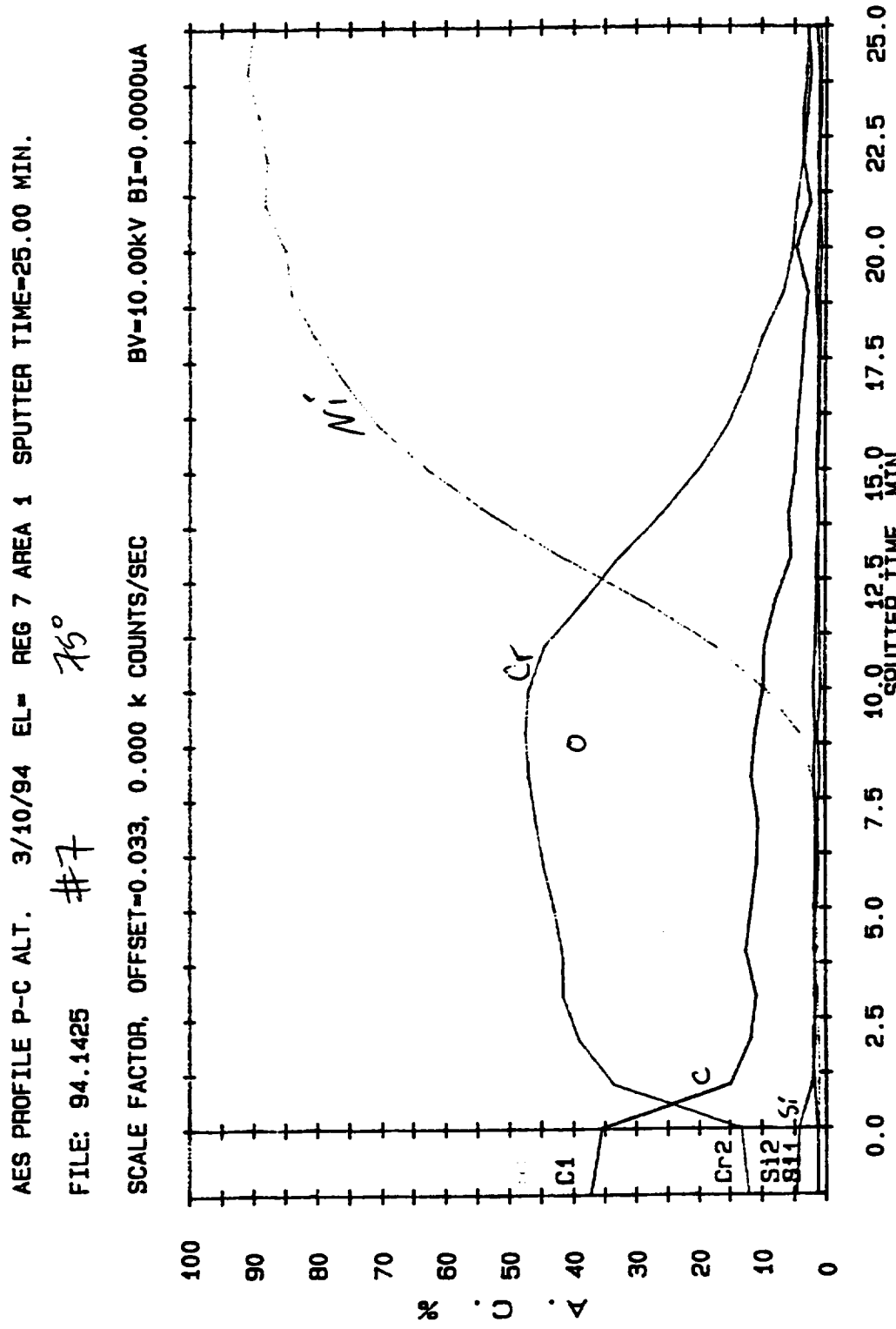

Figure B-29. Auger spectrum from location #7 (75 deg) of panel 916-4A.

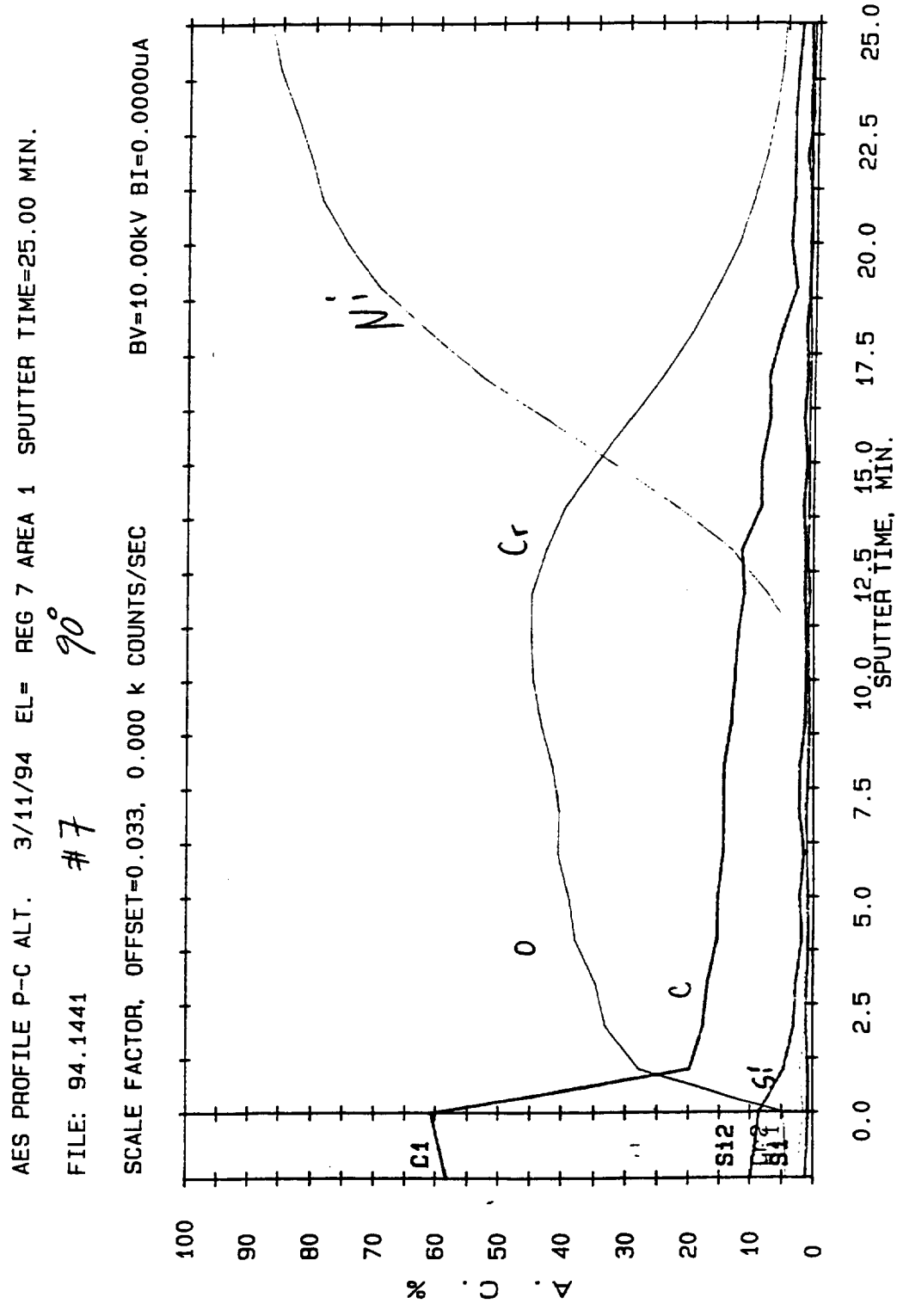

Figure B-30. Auger spectrum from location #7 (90 deg) of panel 916-4A.

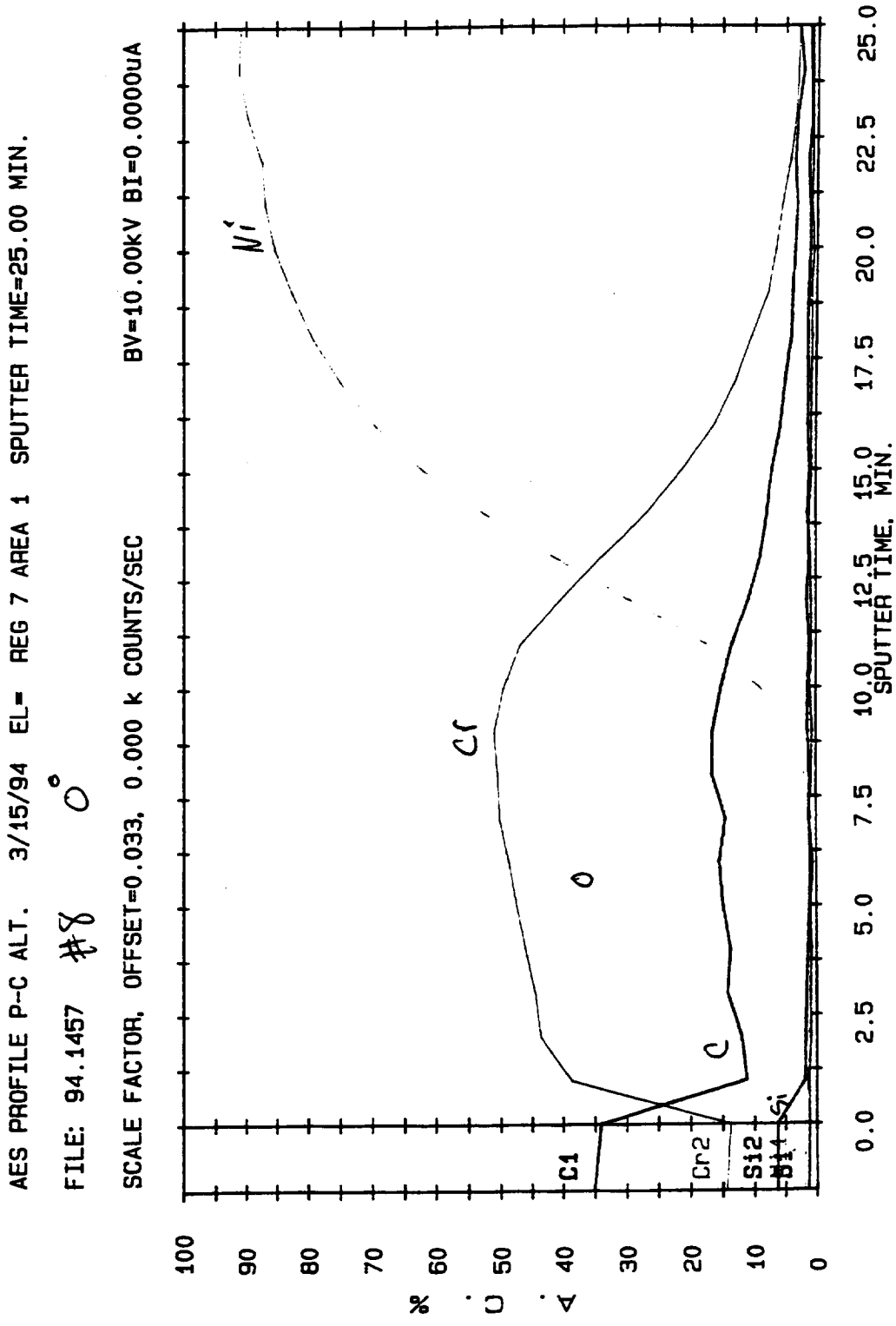

Figure B-31. Auger spectrum from location #8 (0 deg) of panel 916-4A.

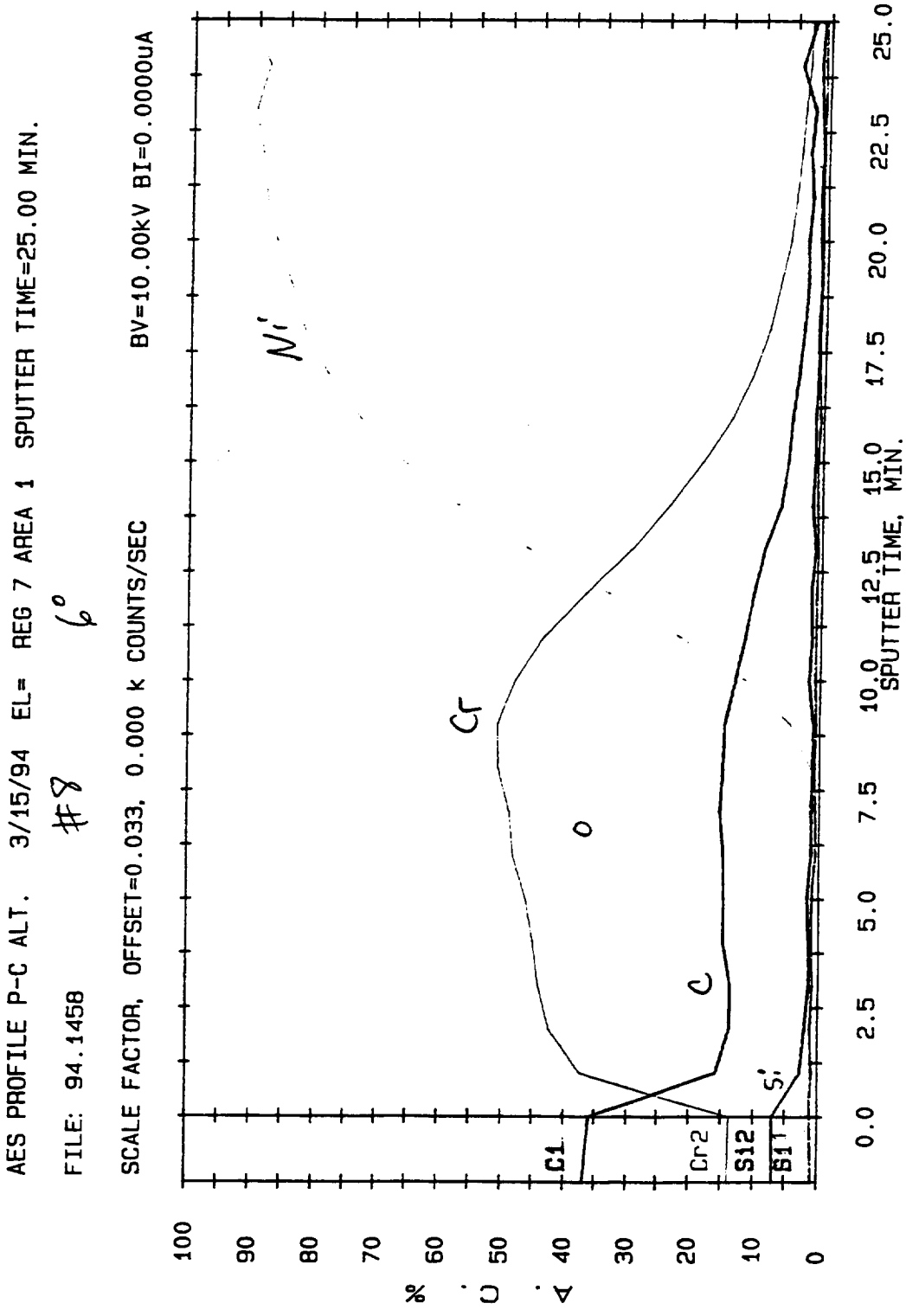

Figure B-32. Auger spectrum from location #8 (6 deg) of panel 916-4A.

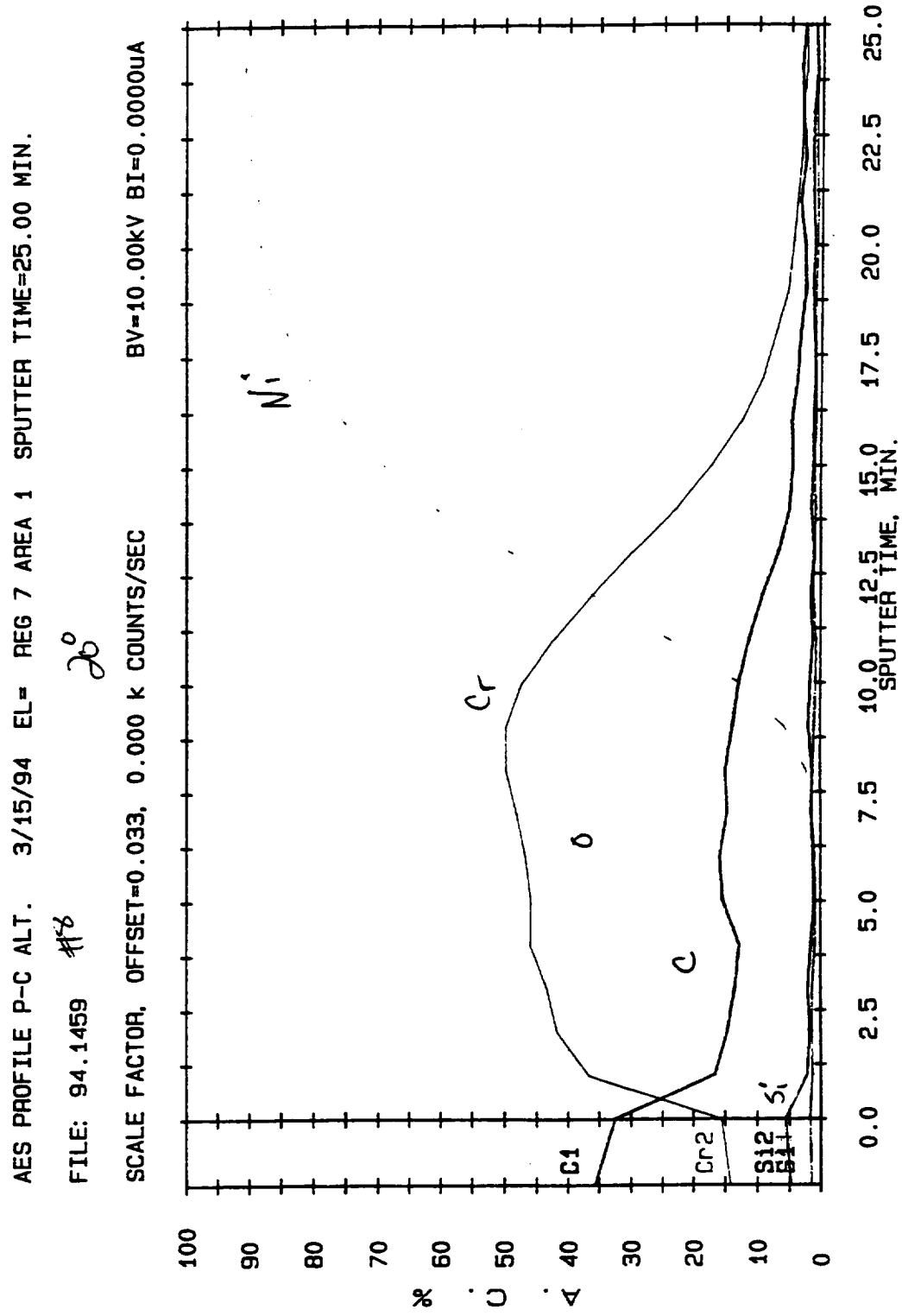

Figure B-33. Auger spectrum from location #8 (20 deg) of panel 916-4A.

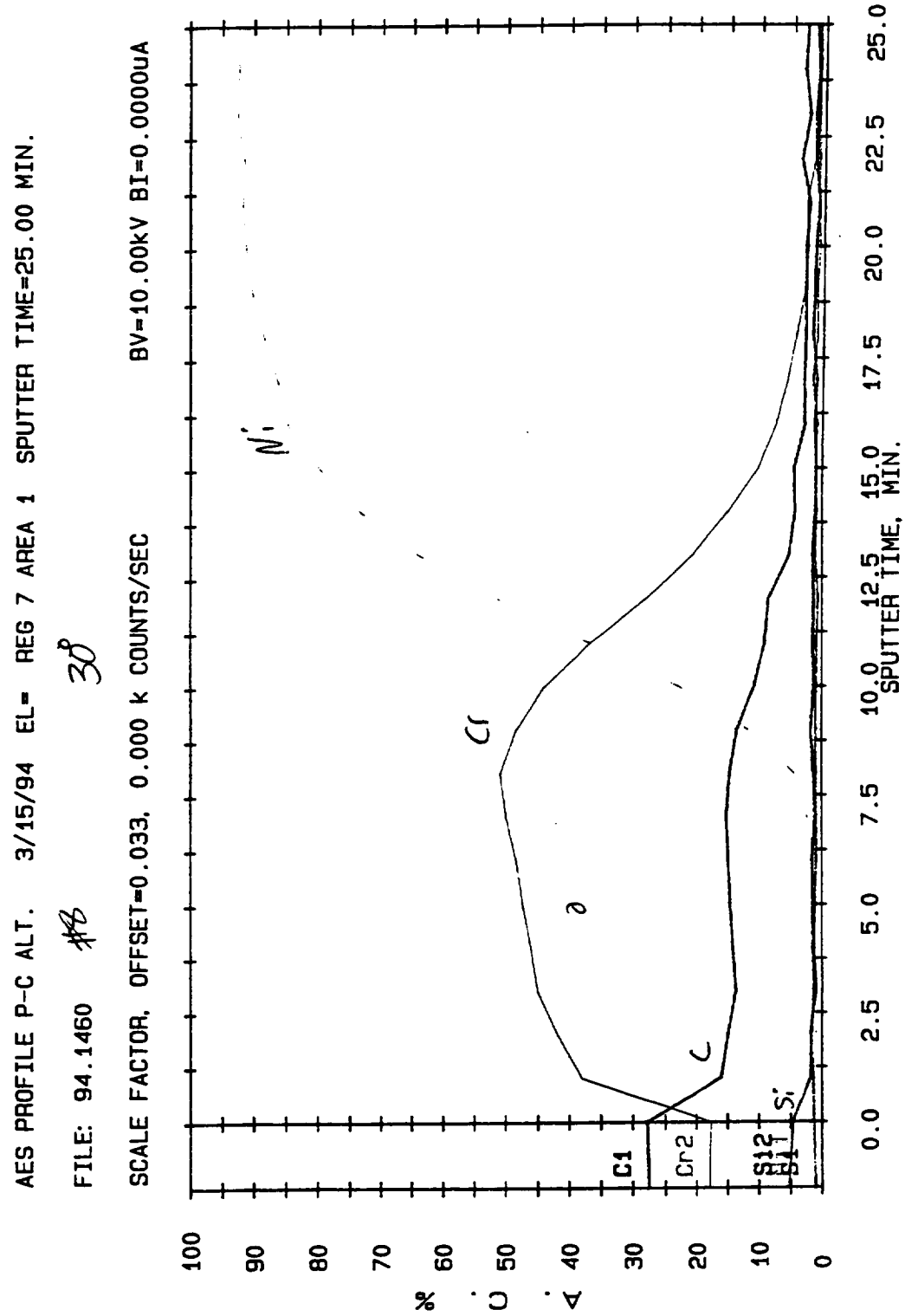

Figure B-34. Auger spectrum from location #8 (30 deg) of panel 916-4A.

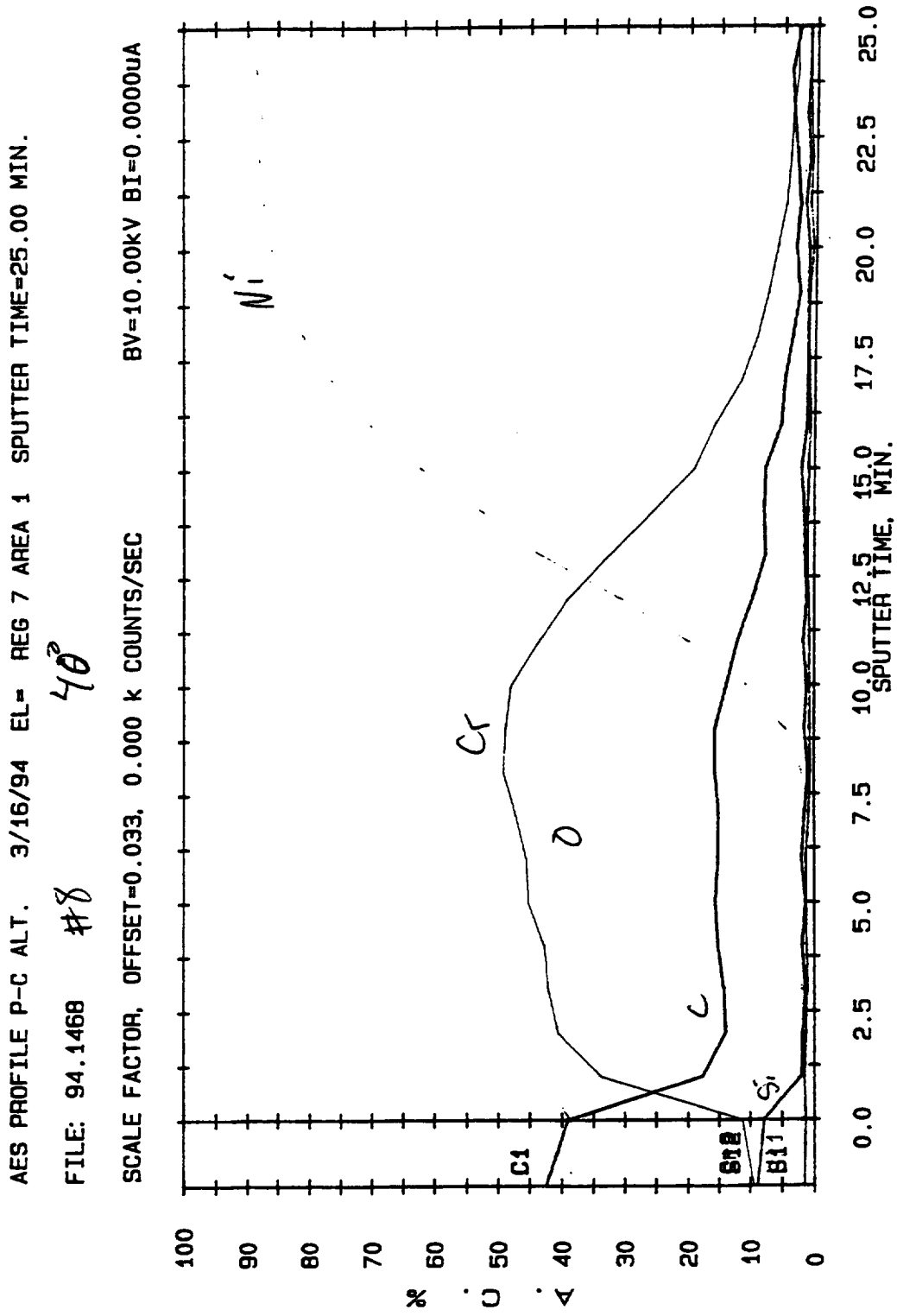

Figure B-35. Auger spectrum from location #8 (40 deg) of panel 916-4A.

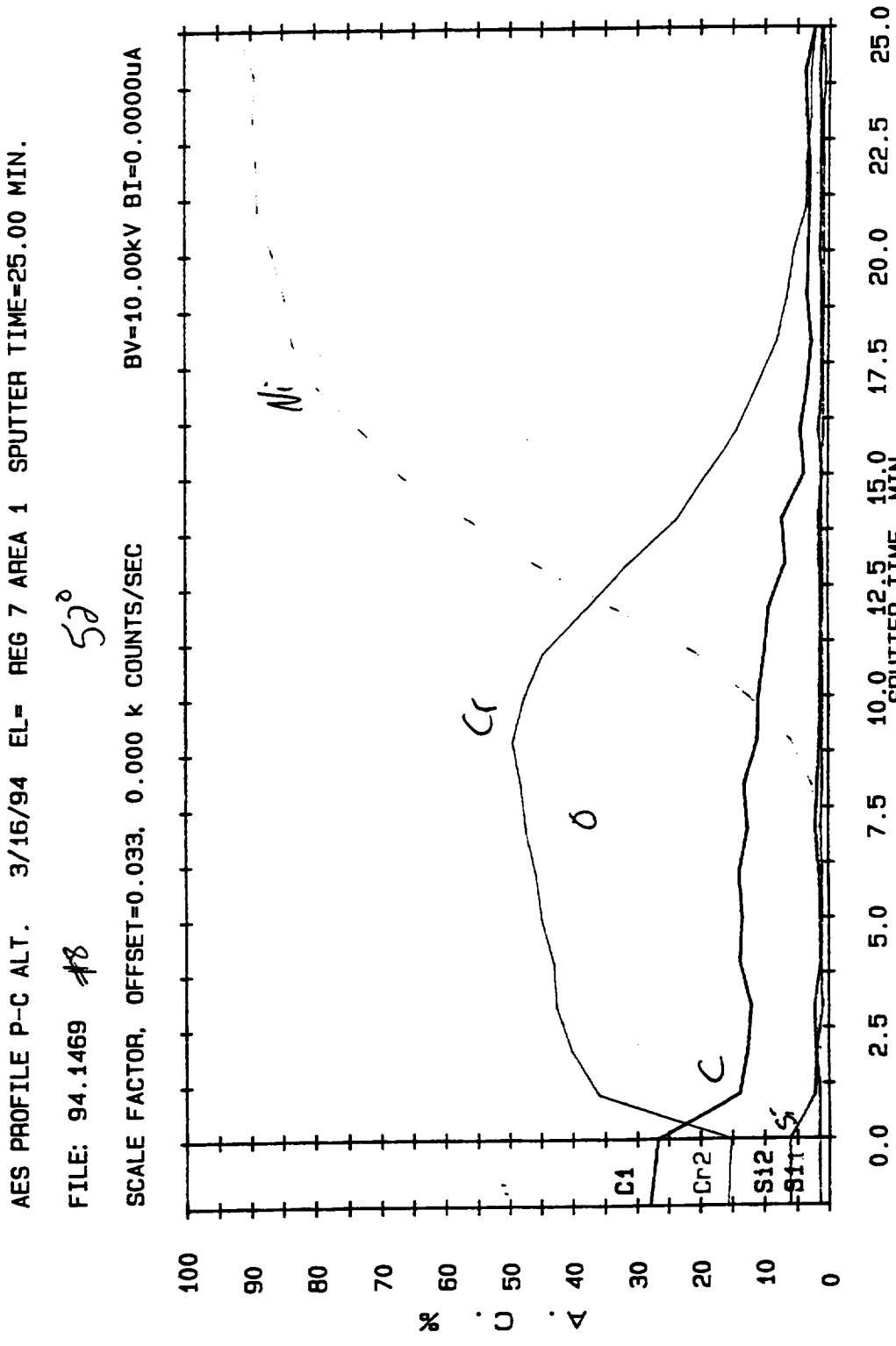

Figure B-36. Auger spectrum from location #8 (52 deg) of panel 916-4A.

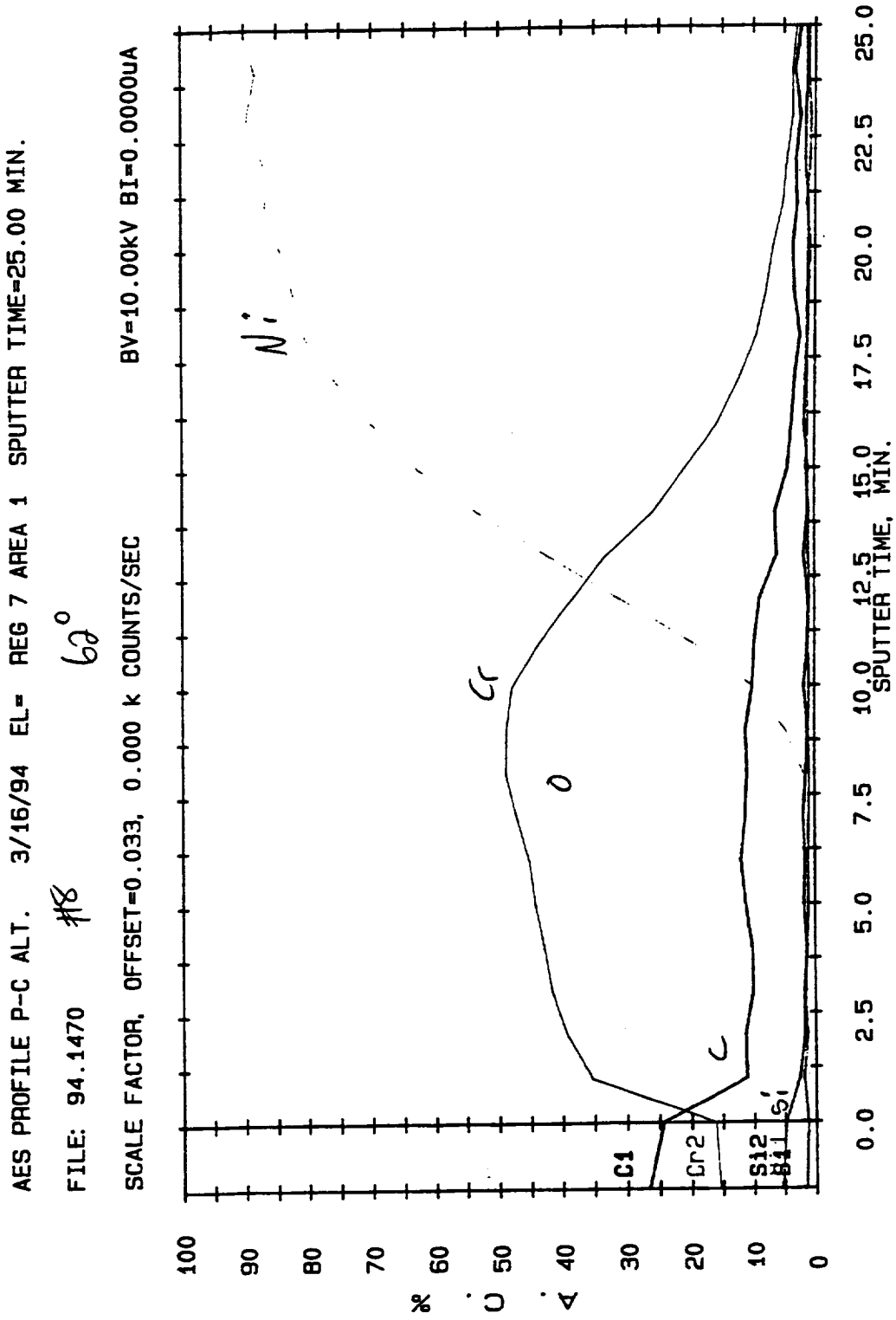

Figure B-37. Auger spectrum from location #8 (62 deg) of panel 916-4A.

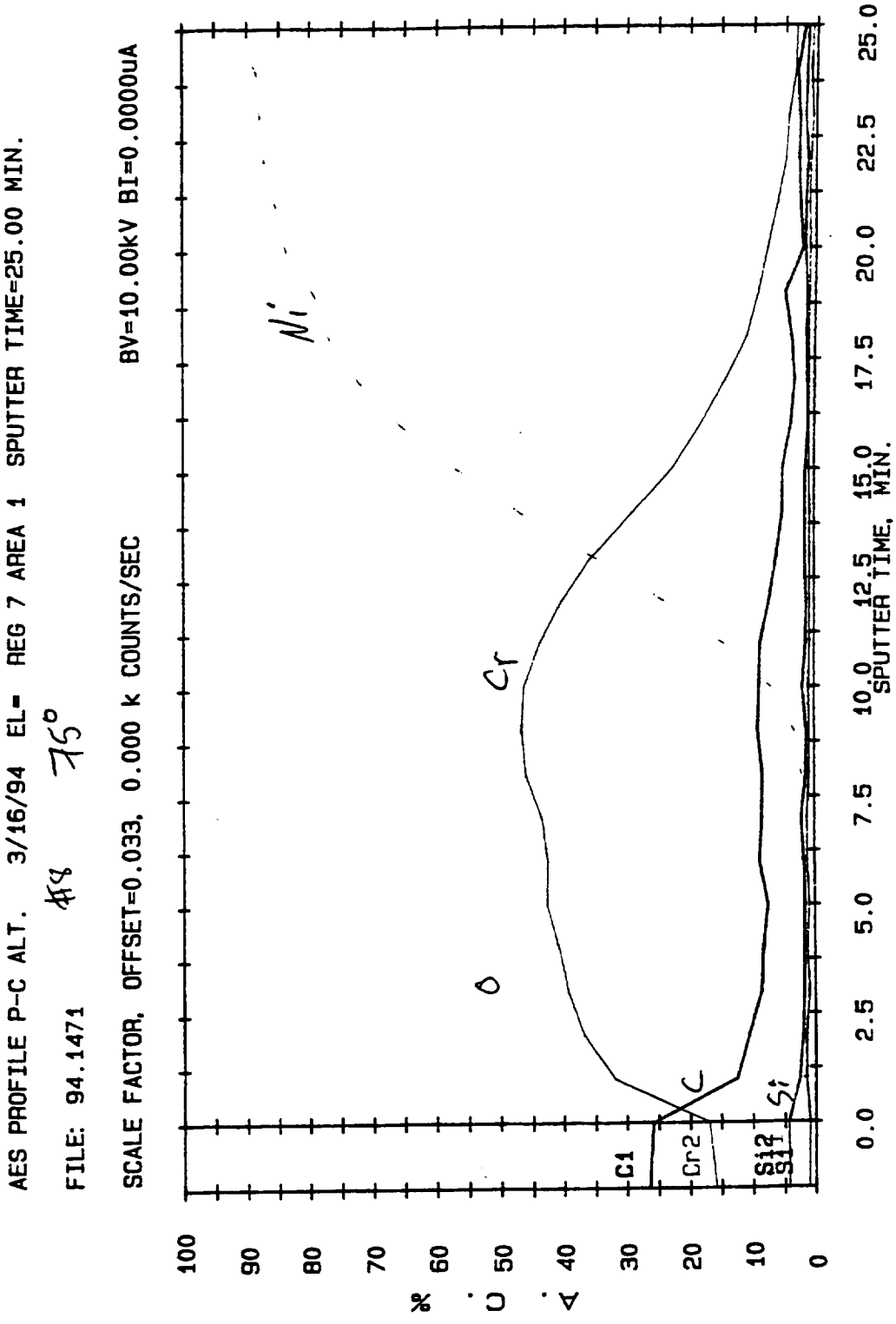

Figure B-38. Auger spectrum from location #8 (75 deg) of panel 916-4A.

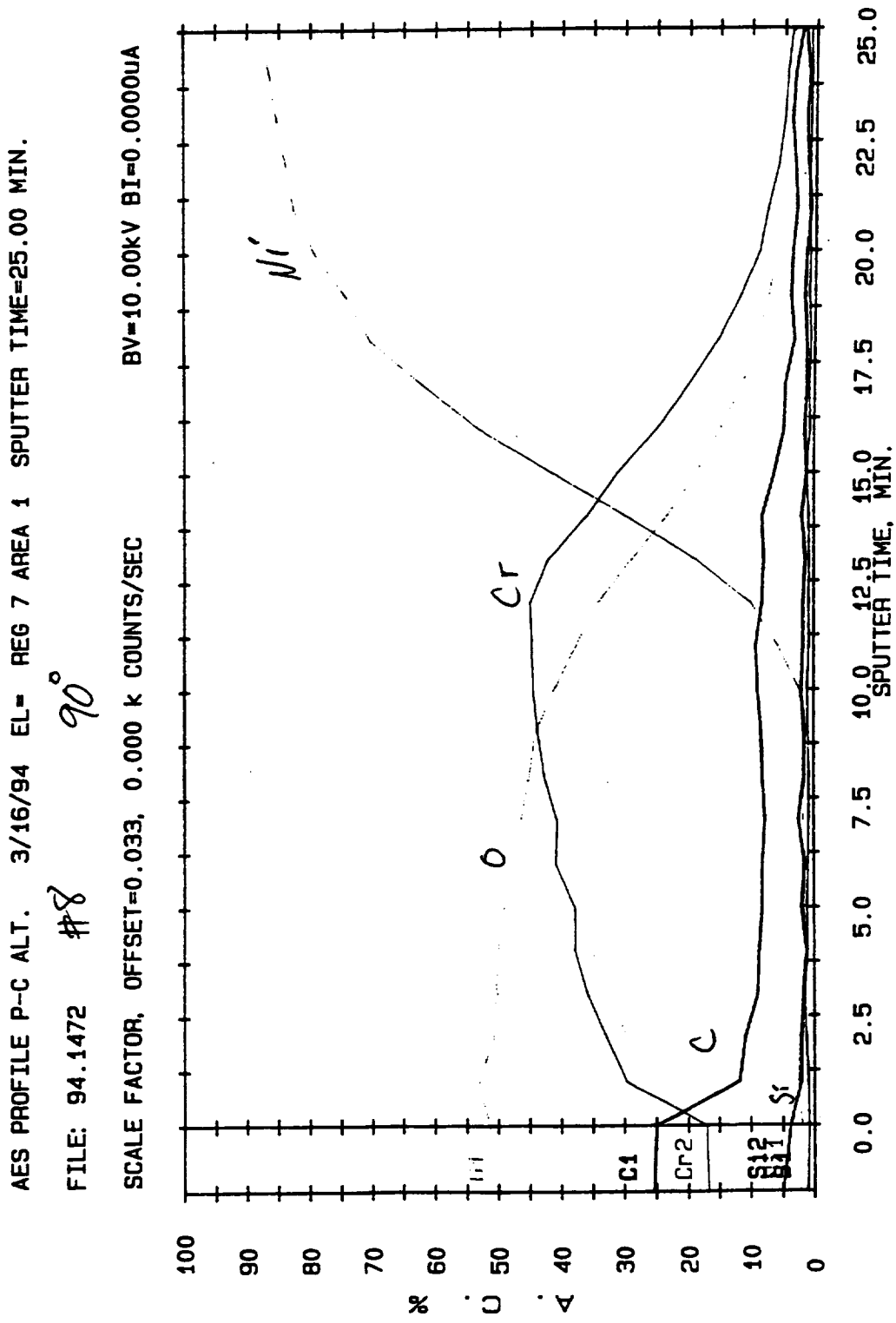

Figure B-39. Auger spectrum from location #8 (90 deg) of panel 916-4A.

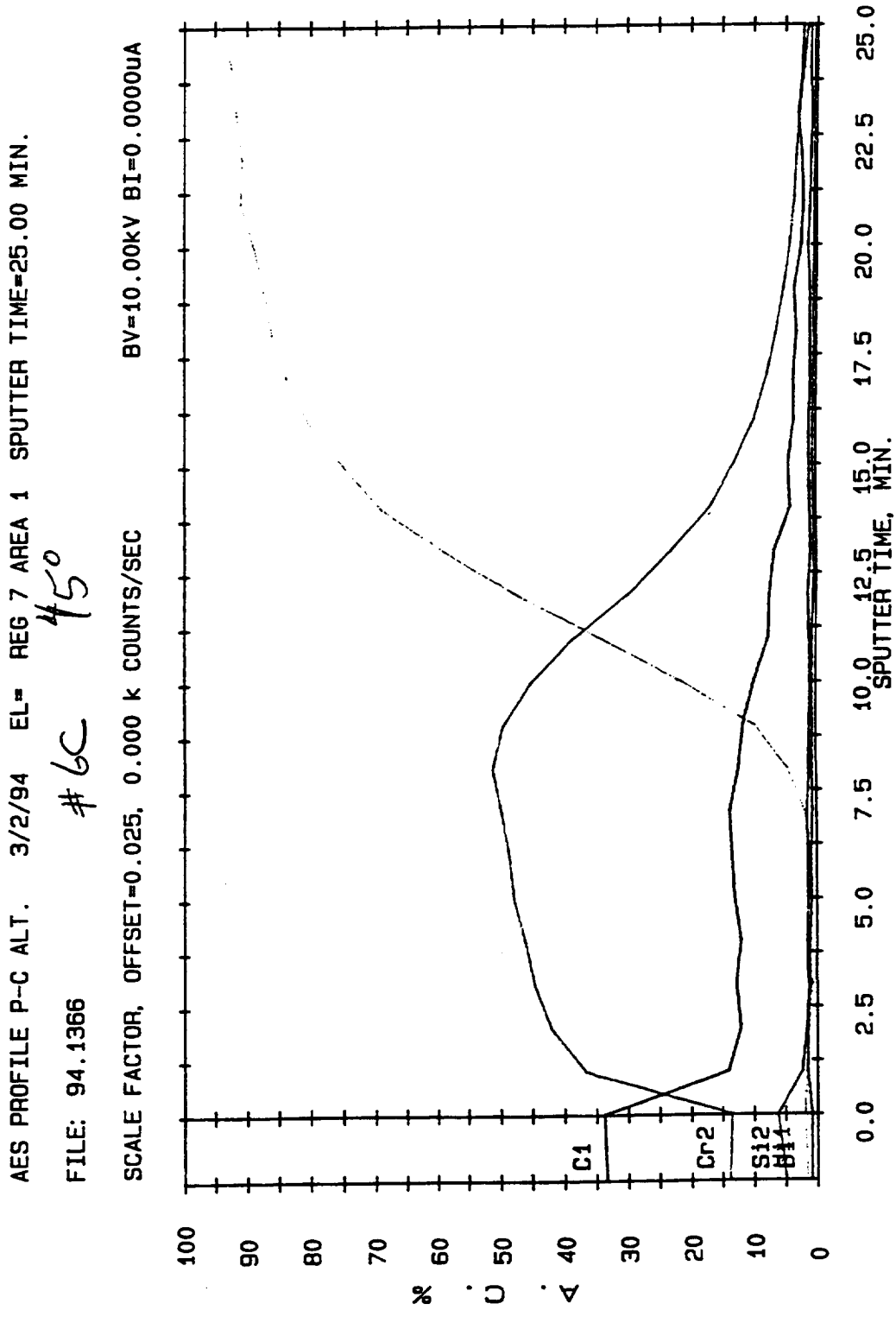

Figure B-40. Auger spectrum from location #6-c (45 deg) of panel 916-4A.

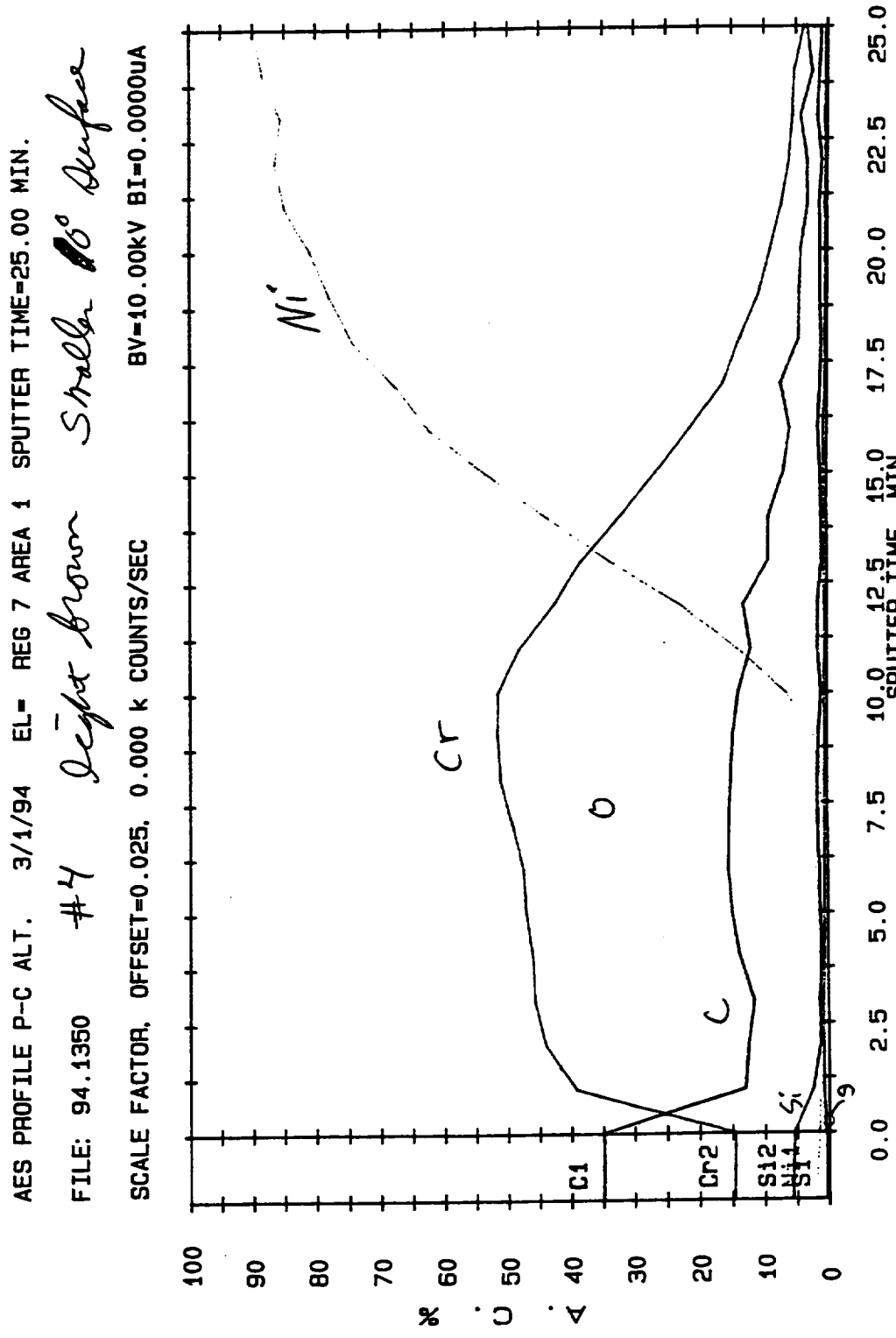

Figure B-41. Auger spectrum from location #4 (light brown) of panel 916-4A.

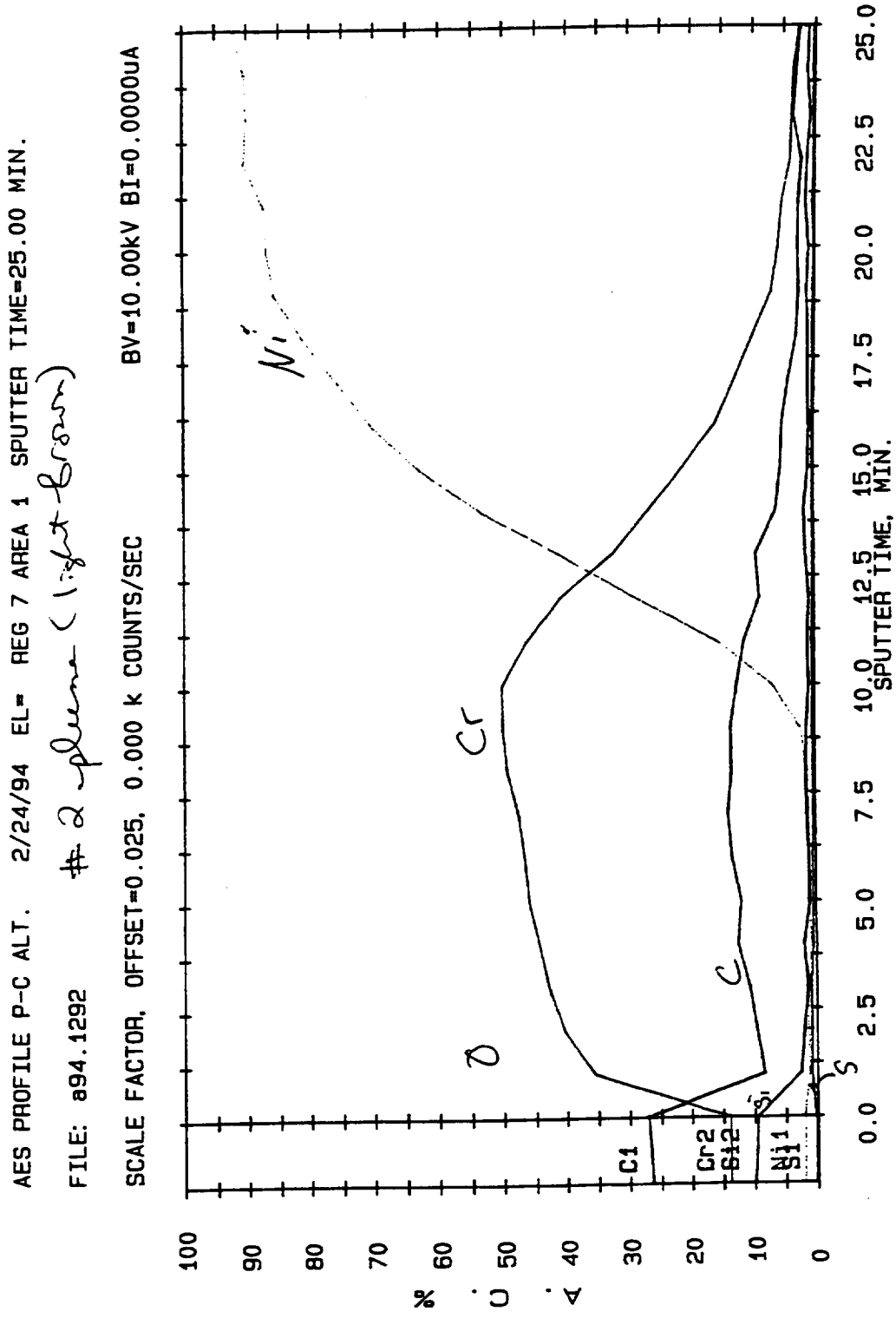

Figure B-42. Auger spectrum from location #2 (light brown plume area) of panel 916-4A.

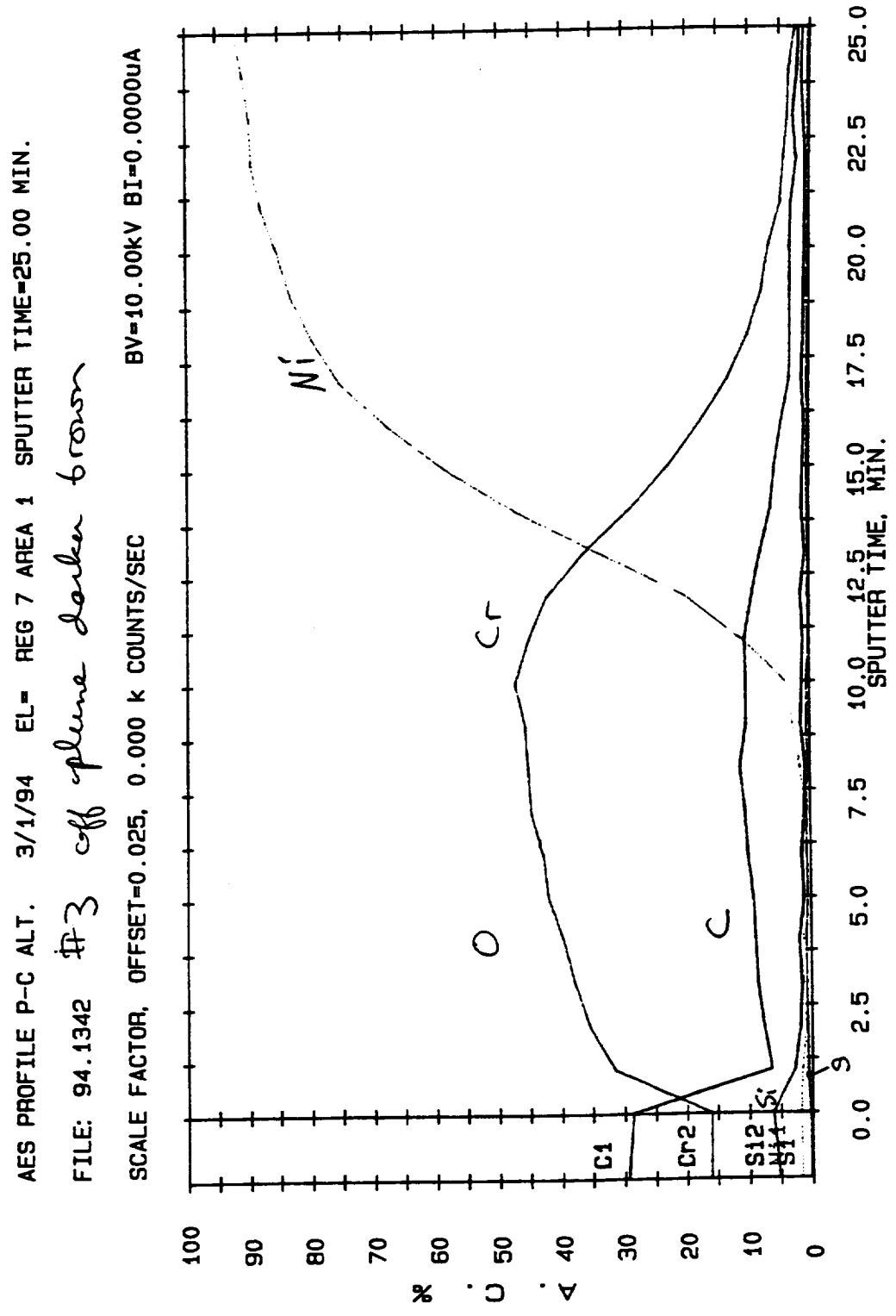

Figure B-43. Auger spectrum from location #3 (darker bown) of panel 916-4A.

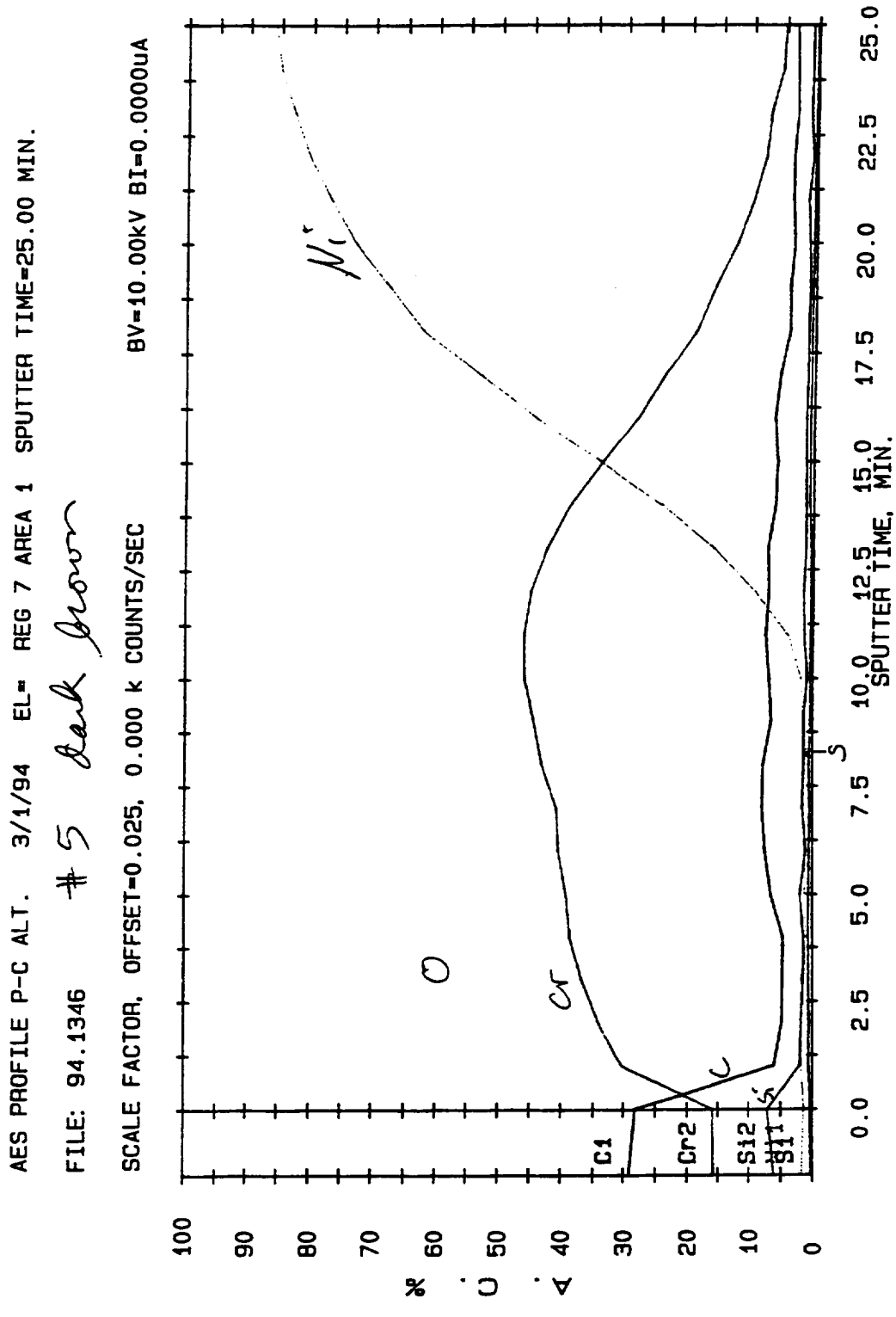

Figure B-44. Auger spectrum from location #5 of panel 916-4A.

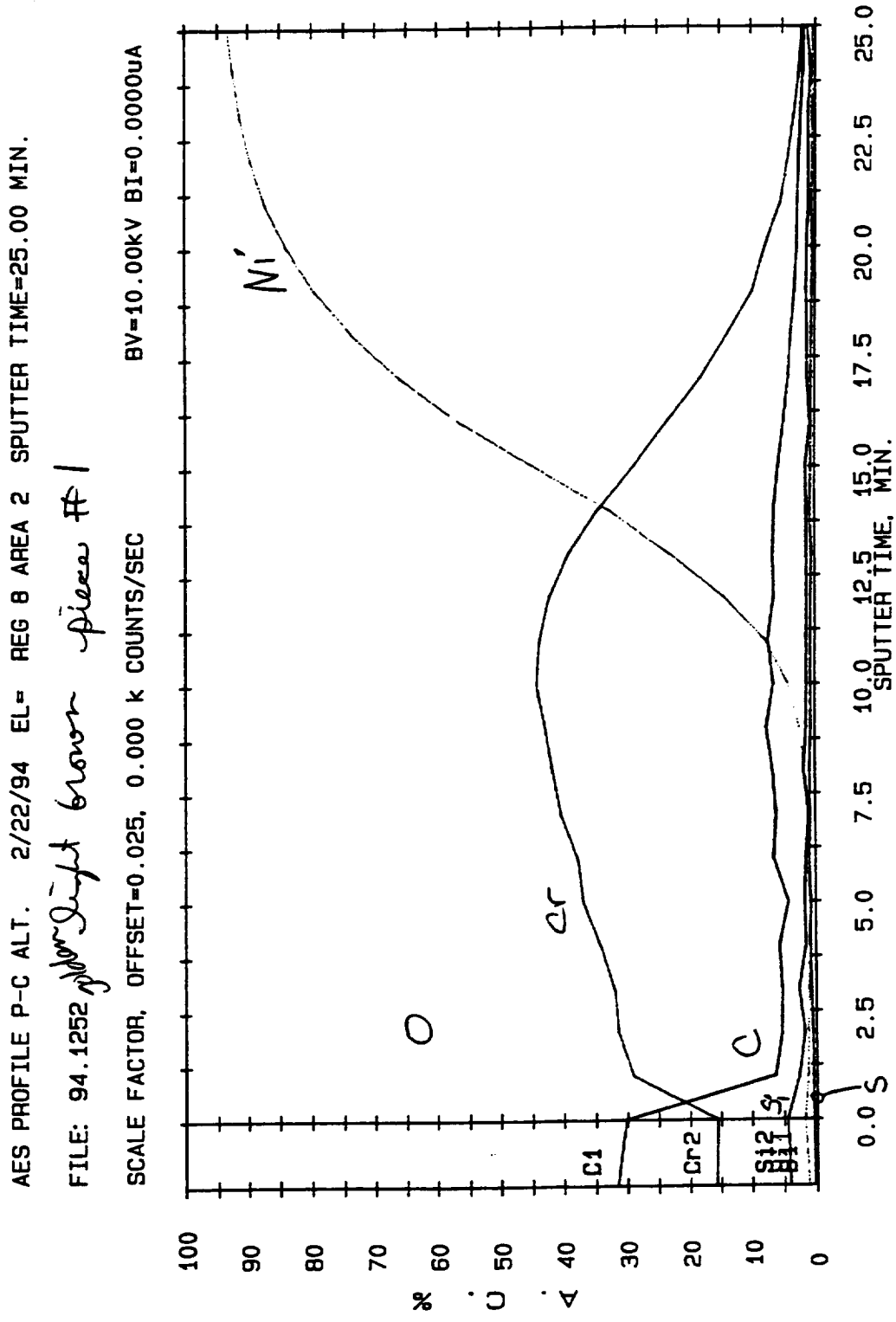

Figure B-45. Auger spectrum from location #1 (light brown piece) of panel 916-4A.

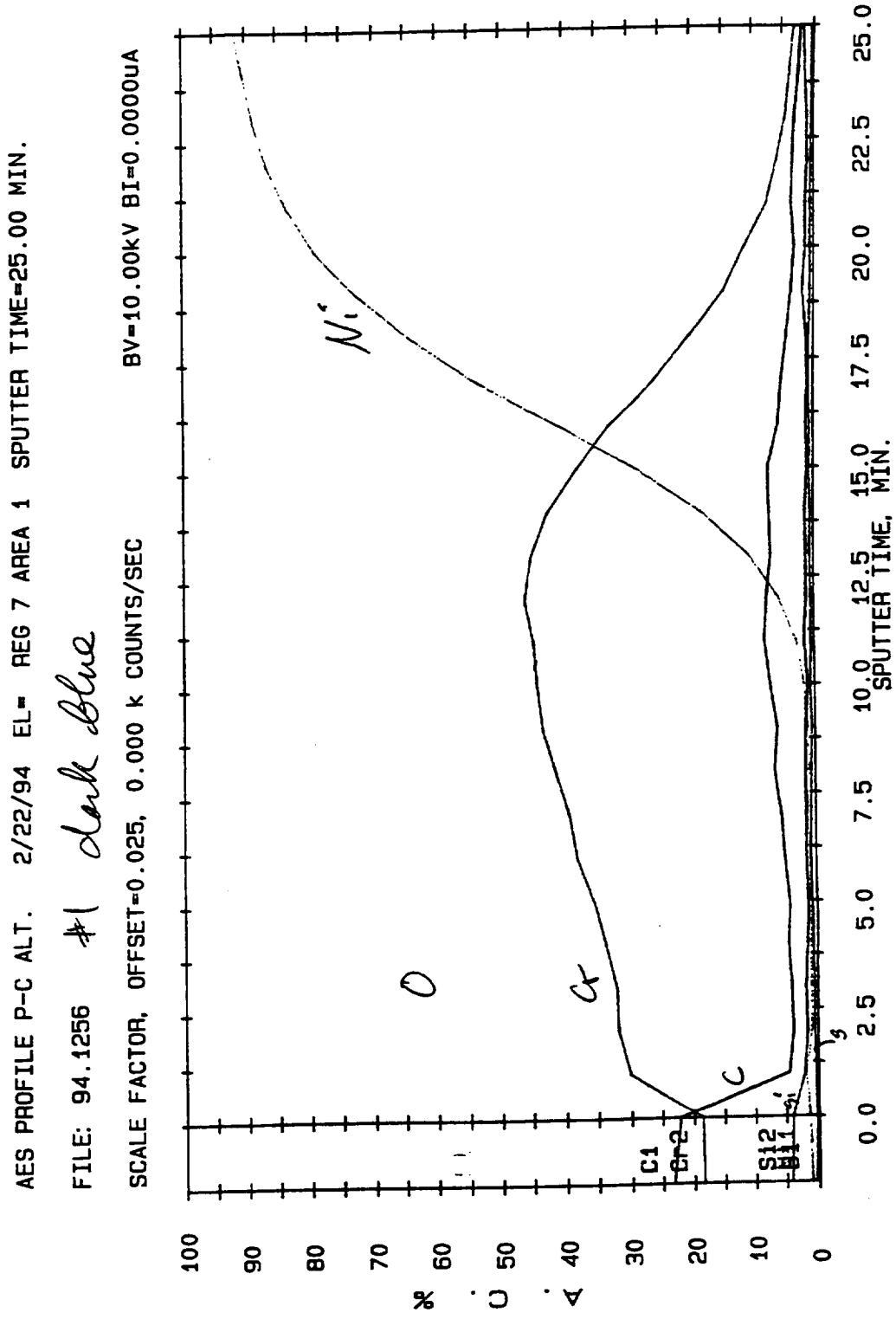

Figure B-46. Auger spectrum from location #1 (dark blue) of panel 916-4A.

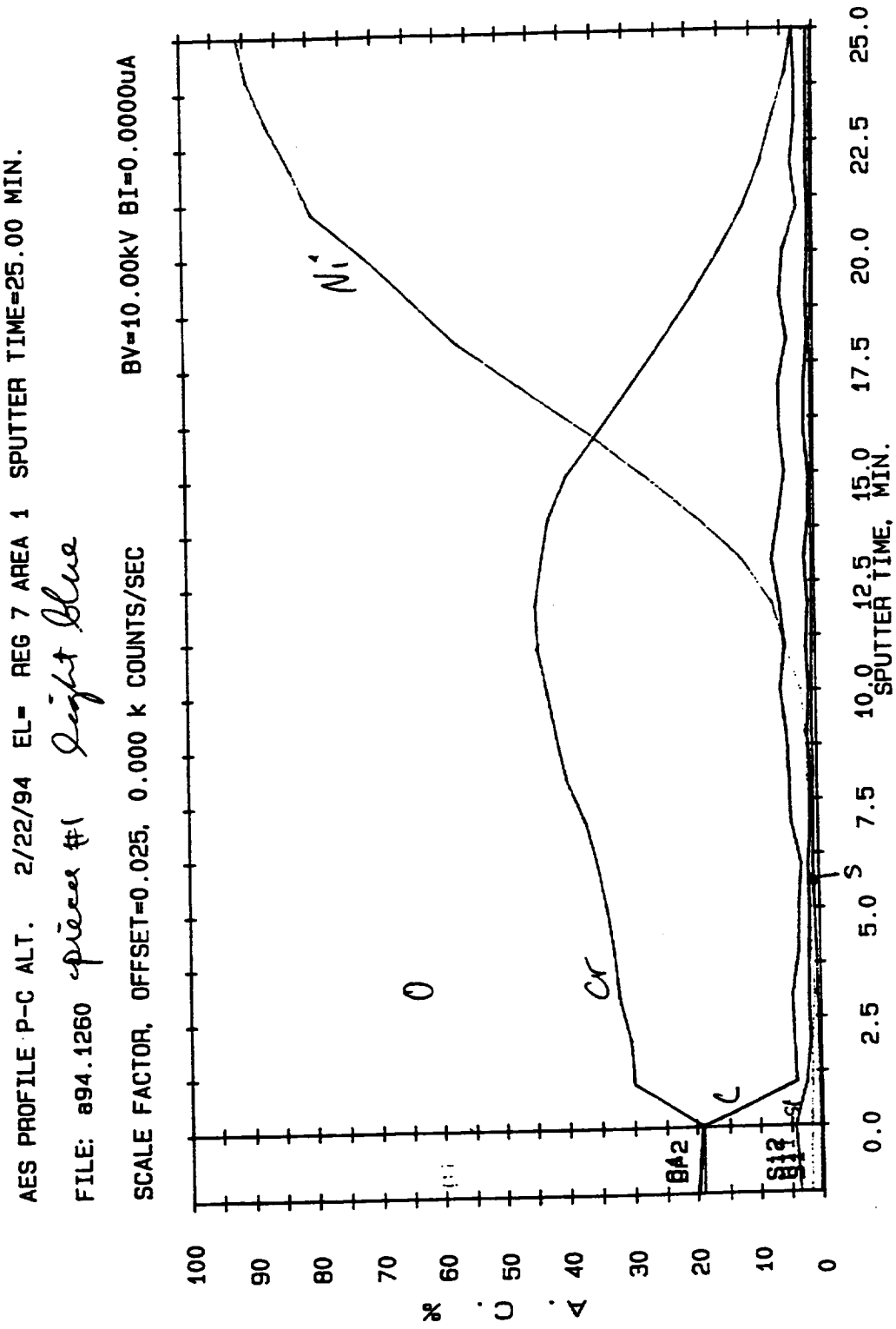

Figure B-47. Auger spectrum from location #1 (light blue) of panel 916-4A.

Surface Elemental Percentages

Panel, specimen #	Angle around bend	Element				
		Carbon	Oxygen	Chromium	Silicon	Nickel
916-4, 8	0	36.30	42.44	14.83	6.43	
	6	37.85	40.68	14.30	7.18	
	20	36.80	43.62	14.56	5.01	
	30	27.69	50.76	16.03	5.53	
	40	44.11	36.93	9.78	9.18	
	52	28.72	48.97	16.09	6.21	
	62	28.60	47.40	18.49	5.50	
	75	27.54	51.62	16.44	4.40	
	90	26.25	51.34	17.27	5.14	
916-4,7	0	32.71	44.32	16.64	6.63	
	15	29.59	47.41	17.54	5.47	
	30	33.17	45.21	16.92	4.69	
	45	33.52	45.75	15.93	4.80	

Figure B-48. Surface elemental analysis results for selected locations on panel 916-4A.

Surface Elemental Percentages

Panel, specimen #	Angle around bend	Element				
		Carbon	Oxygen	Chromium	Silicon	Nickel
916-4,7	60	33.62	46.85	14.52	5.02	
	75	38.31	44.65	12.32	4.72	
	90	60.45	24.81	4.51	10.24	
916-4,4,light brown	0	34.95	42.26	14.65	5.70	2.00
916-4,4,brown	0	35.31	43.14	16.20	5.35	
916-4,5,dark brown	90	29.07	47.03	15.74	6.06	1.77
916-4,5,dark brown (b)	90	26.01	50.59	16.40	7.00	
916-4,2,plume (light brown)	90	26.29	47.51	13.81	9.94	2.12
916-4,2, plume (b)	90	40.46	39.83	11.14	8.57	
916-4,2, off plume	90	38.58	41.98	12.92	6.52	
916-4,2, off plume (dark brown)	90	38.71	41.30	13.85	6.14	

Figure B-48 (continued). Surface elemental analysis results for selected locations on panel 916-4A.

Surface Elemental Percentages

Panel, specimen #	Angle around bend	Element					
		Carbon	Oxygen	Chromium	Silicon	Nickel	
916-4,3, off plume darker brown	90	29.45	47.14	16.06	5.32	1.72	
916-4,3, golden brown edge	90	39.98	41.17	13.36	5.49		
916-4,3, blue line	90	21.90	54.83	18.40	4.87		
916-4,3, blue line (b)	90	32.84	46.21	15.81	5.14		
916-4,1, light brown edge	90	31.56	47.05	15.64	4.10	1.28	
916-4,1, dark blue	90	23.24	52.49	18.41	4.14	1.19	
916-4,1, light blue	90	19.79	55.40	18.86	3.67	1.93	
916-4,6c	90	33.37	45.46	13.77	4.91	1.53	

Figure B-48 (continued). Surface elemental analysis results for selected locations on panel 916-4A.

Appendix C

Color versions of NASA Photographs

Figure C-15. NASA post-flight photo of contamination deposits on longeron between trays A11 and A12.

Figure C-16. NASA post-flight photo of contamination deposits on longeron between trays A7 and A8.

Figure C-17. NASA post-flight photo of exterior of corner of tray C7.

Figure C-18. NASA post-flight photo of exterior of corner of tray C7.

Figure C-19. NASA post-flight photo of exterior of corner of tray D8.

Figure C-20. NASA post-flight photo of exterior of corner of tray F9.

Figure C-21. NASA post-flight photo of exterior of corner of tray C11.

Figure C-22. NASA post-flight photo of exterior of corner of tray C11.

Figure C-23. NASA post-flight photo of exterior of corner of tray F11.

Figure C-24. NASA post-flight photo of exterior of corner of tray F11.

Figure C-25. NASA post-flight photo of exterior of corner of tray F11.

Figure C-26. NASA post-flight photo of outgassing deposits at interior of corner of tray D11.

Figure C-27. NASA post-flight photo of leading edge unanodized aluminum tray clamp at space end of C9.

Figure C-28. NASA post-flight photo of leading edge unanodized aluminum tray clamp at Earth end of C9.

Figure C-29. NASA post-flight photo of trailing edge unanodized aluminum tray clamp on tray C3.

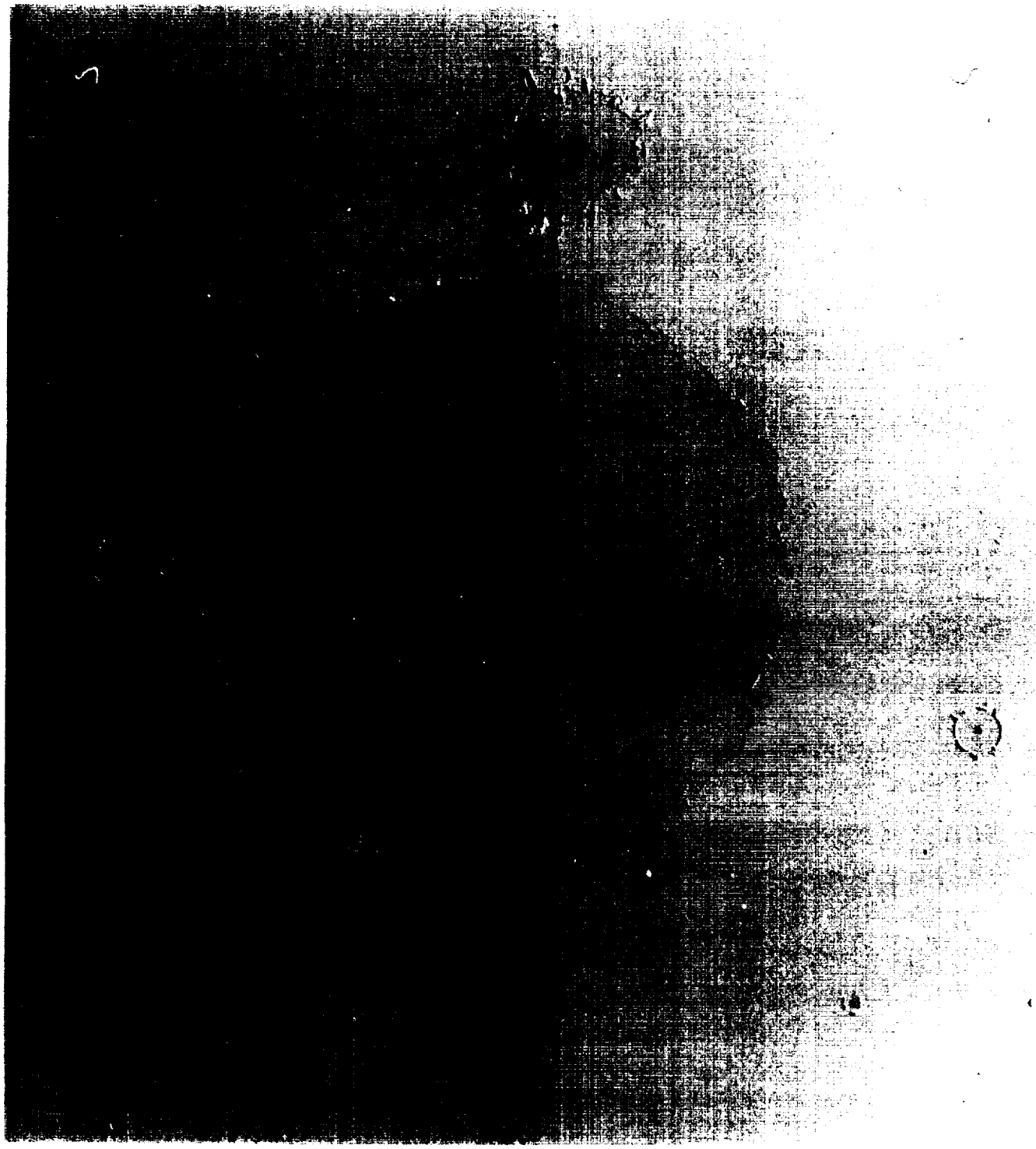

Figure C-1. Painted composite panel from A0038 with impacts visible on one of the white painted areas.

Figure C-2. NASA on-orbit photo of thermal control blanket on tray C8, also showing the unanodized tray clamp on C9.

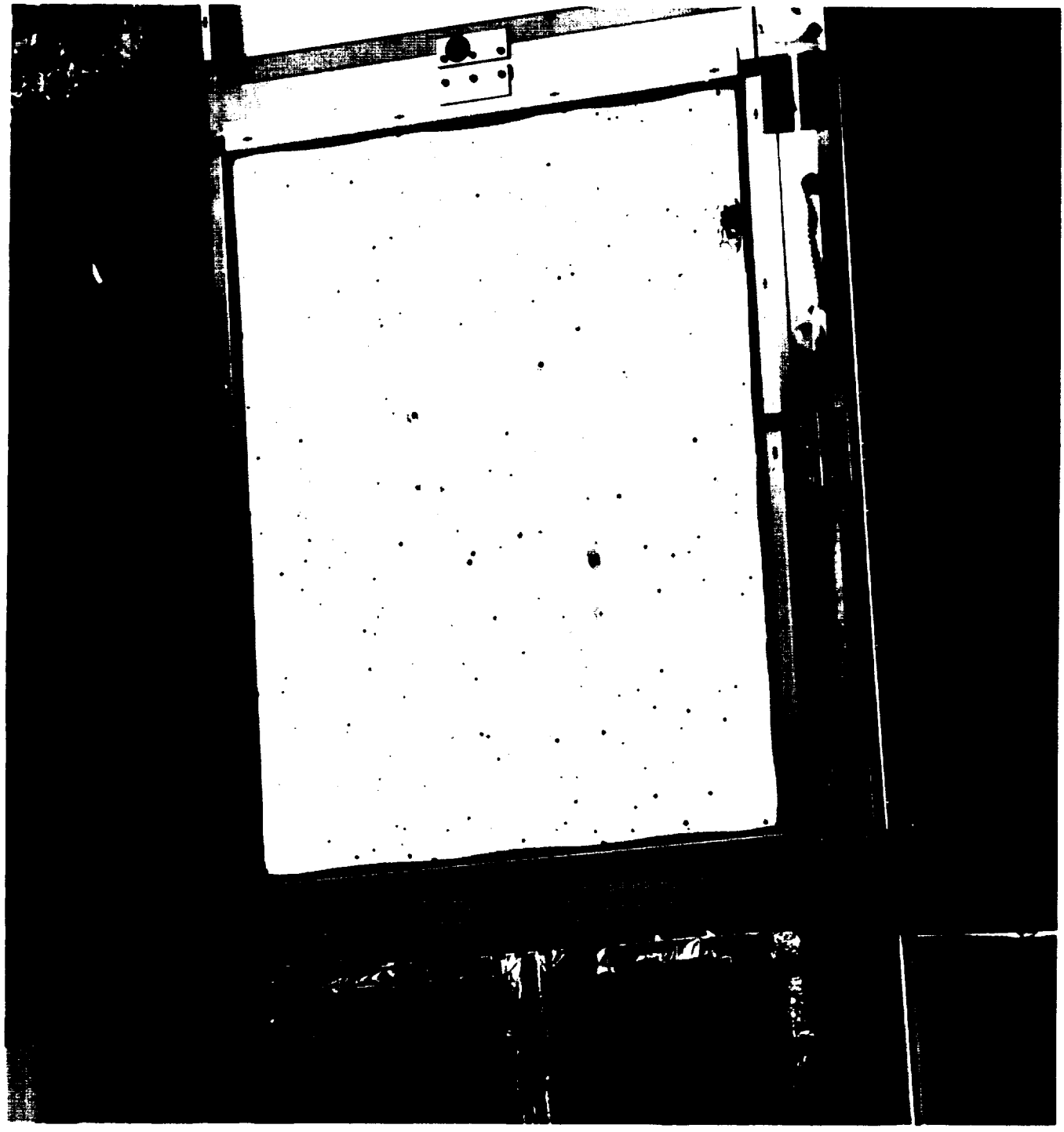

Figure C-3. NASA on-orbit photo of tray E10 showing large impacts on areas supported by velcro.

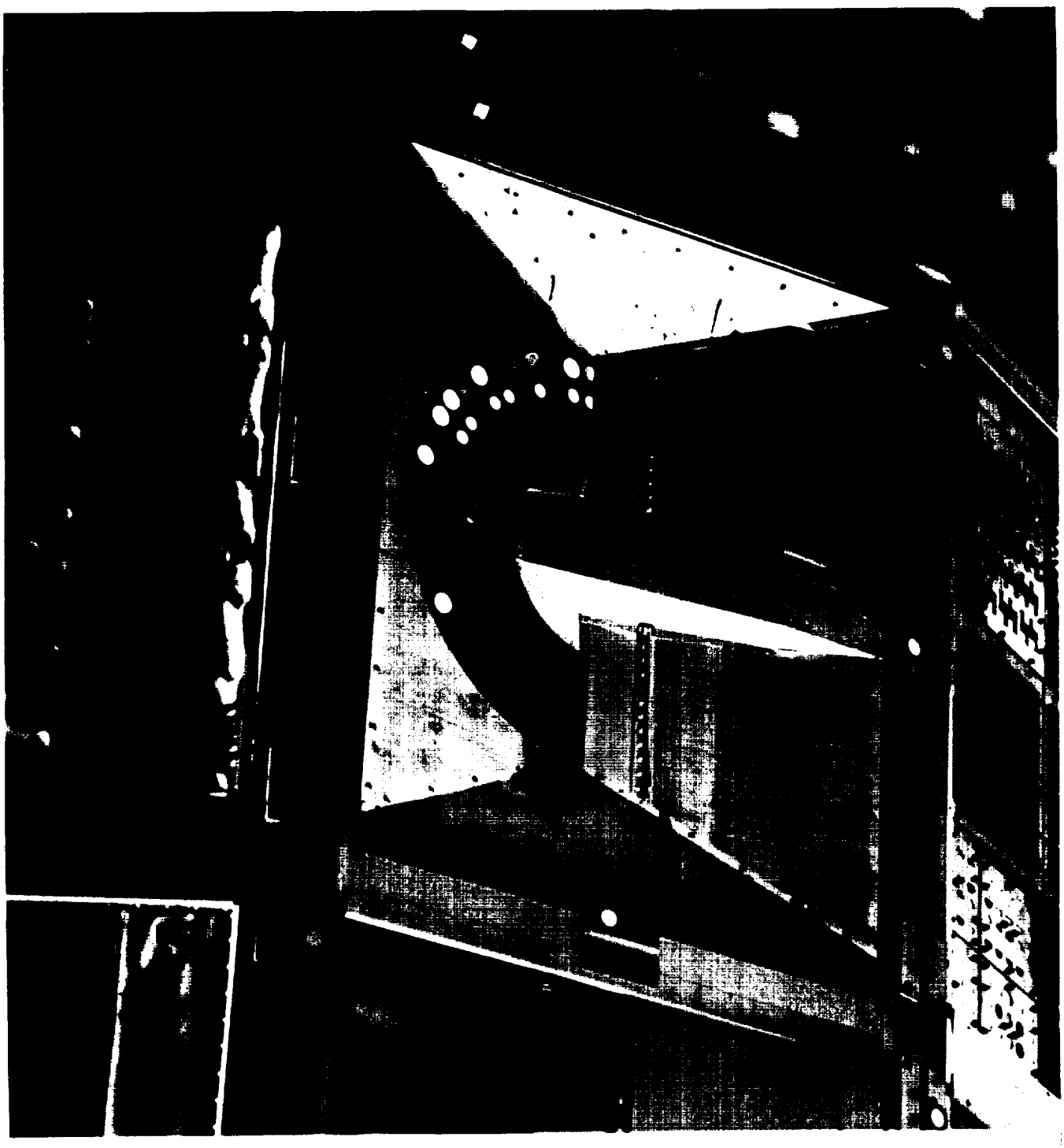

Figure C-4. NASA on-orbit photo of tray A9, containing experiment SO069

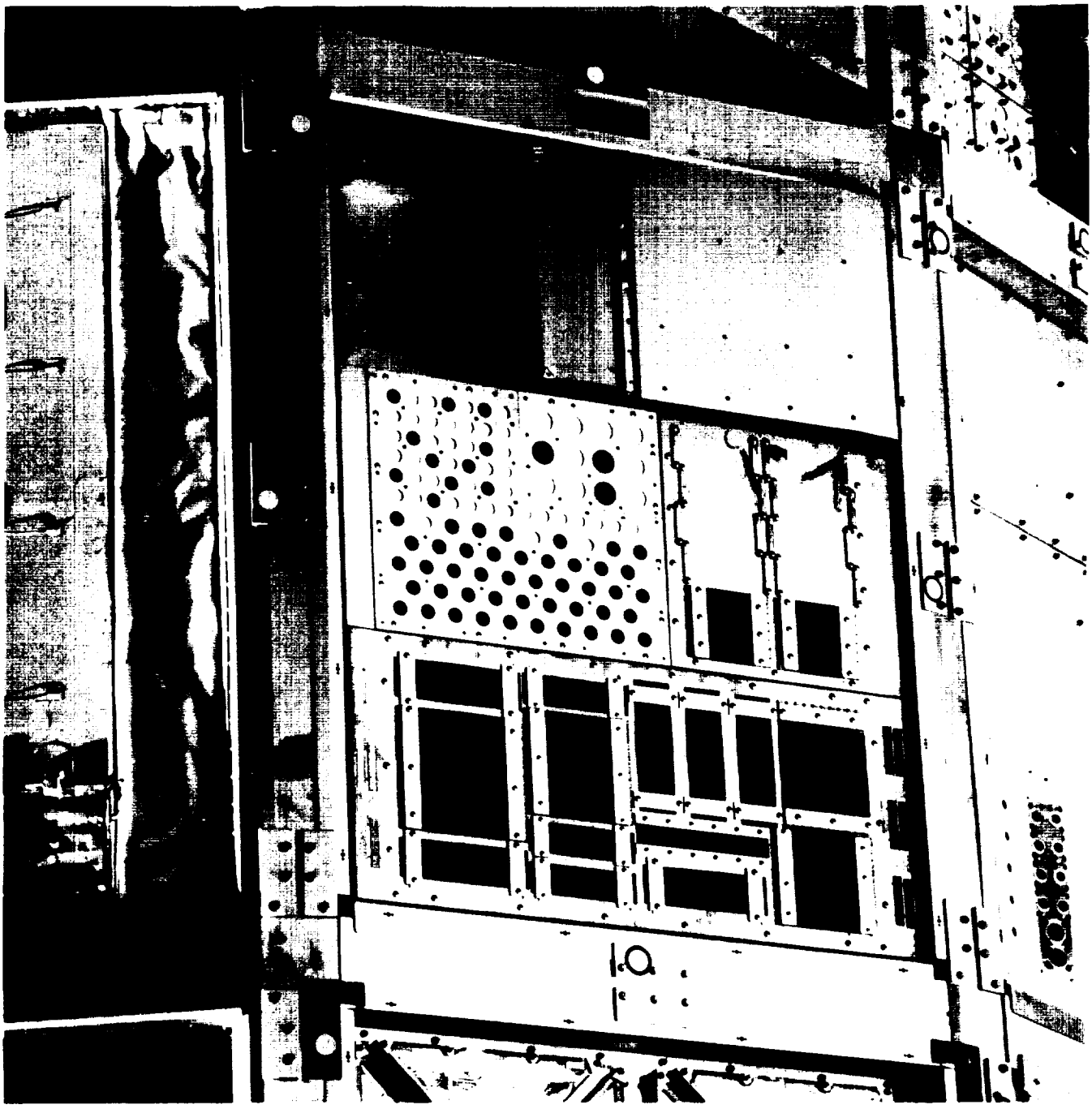

Figure C-5. NASA on-orbit photo of experiments on tray B9, including the closed EECC.

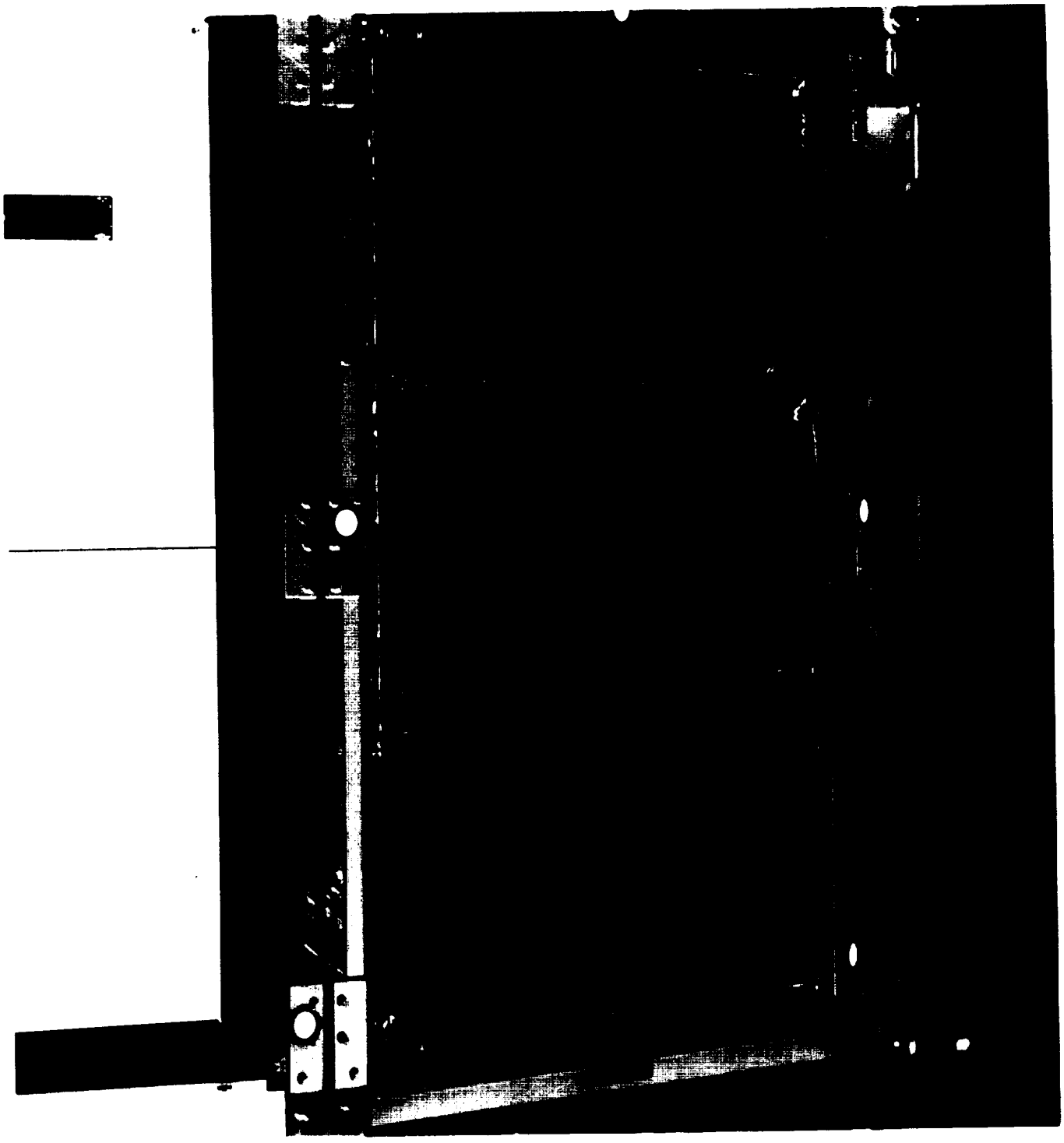

Figure C-6. NASA on-orbit photo of experiment AO175 composite panels on tray A7.

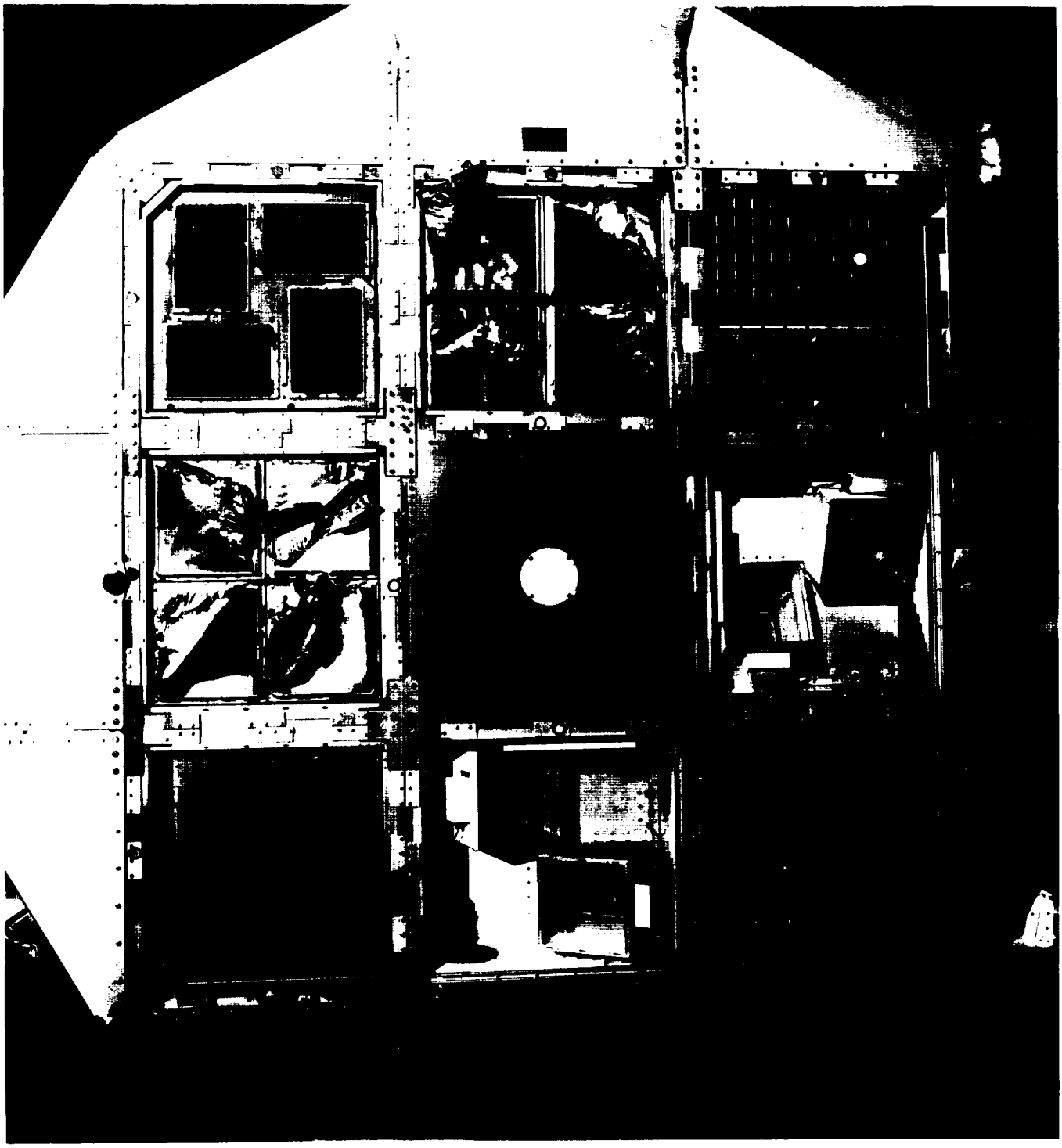

Figure C-7. NASA on-orbit photo of M0001 experiment modules on space end.

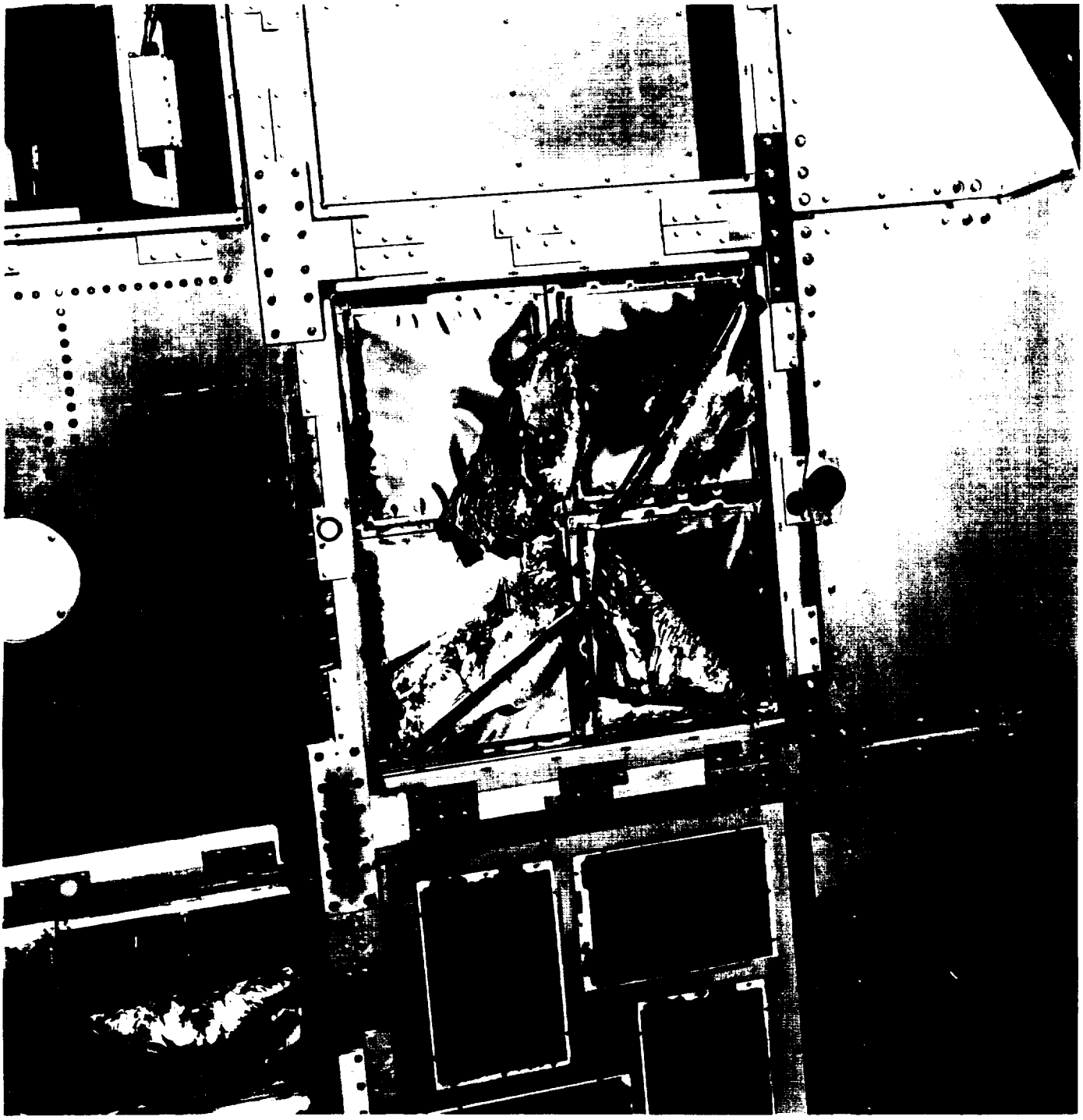

Figure C-8. NASA on-orbit close-up photo of failed thermal control blankets on space end.

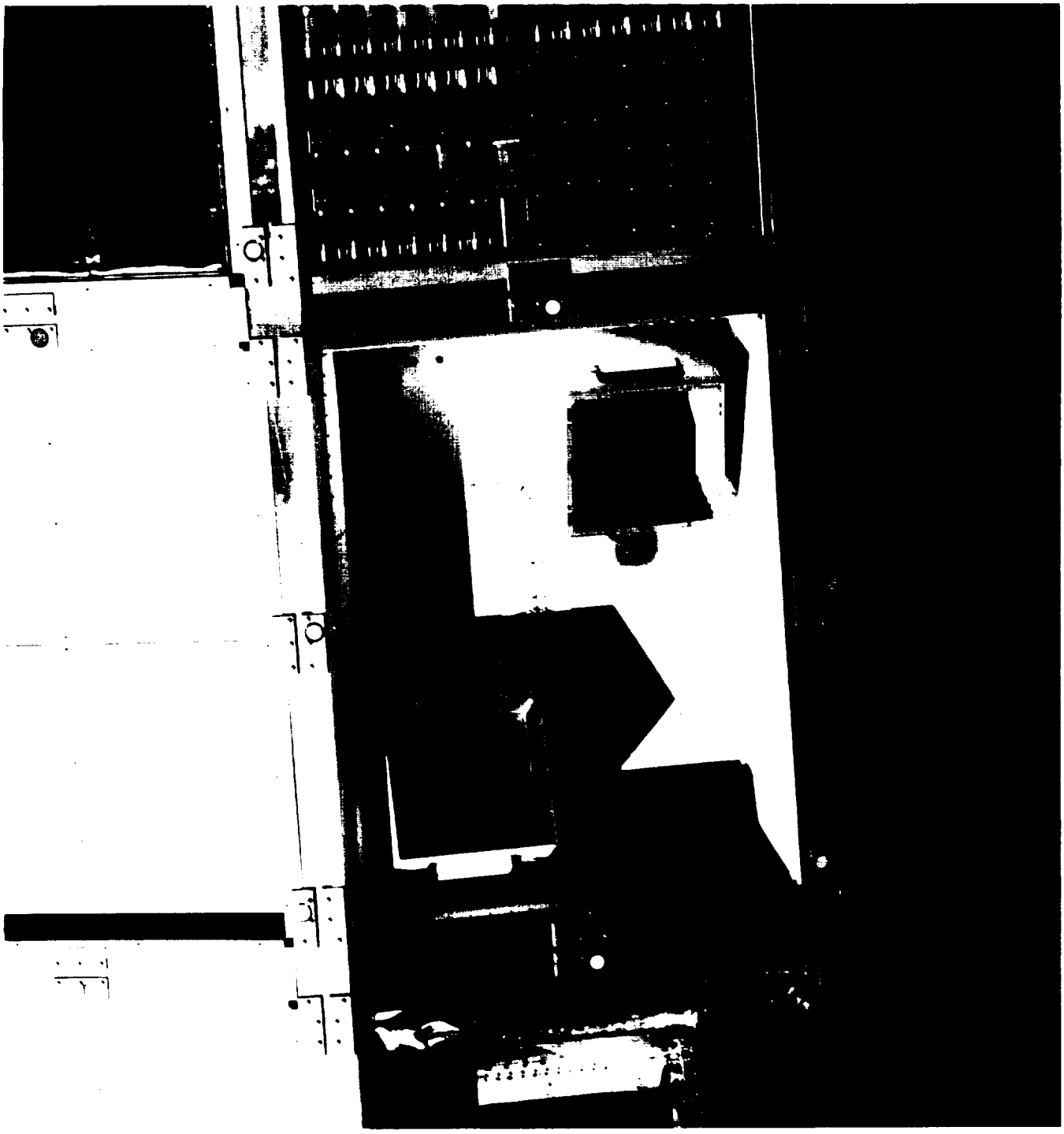

Figure C-9 NASA on-orbit photo of tray E12, showing experiment A0038.

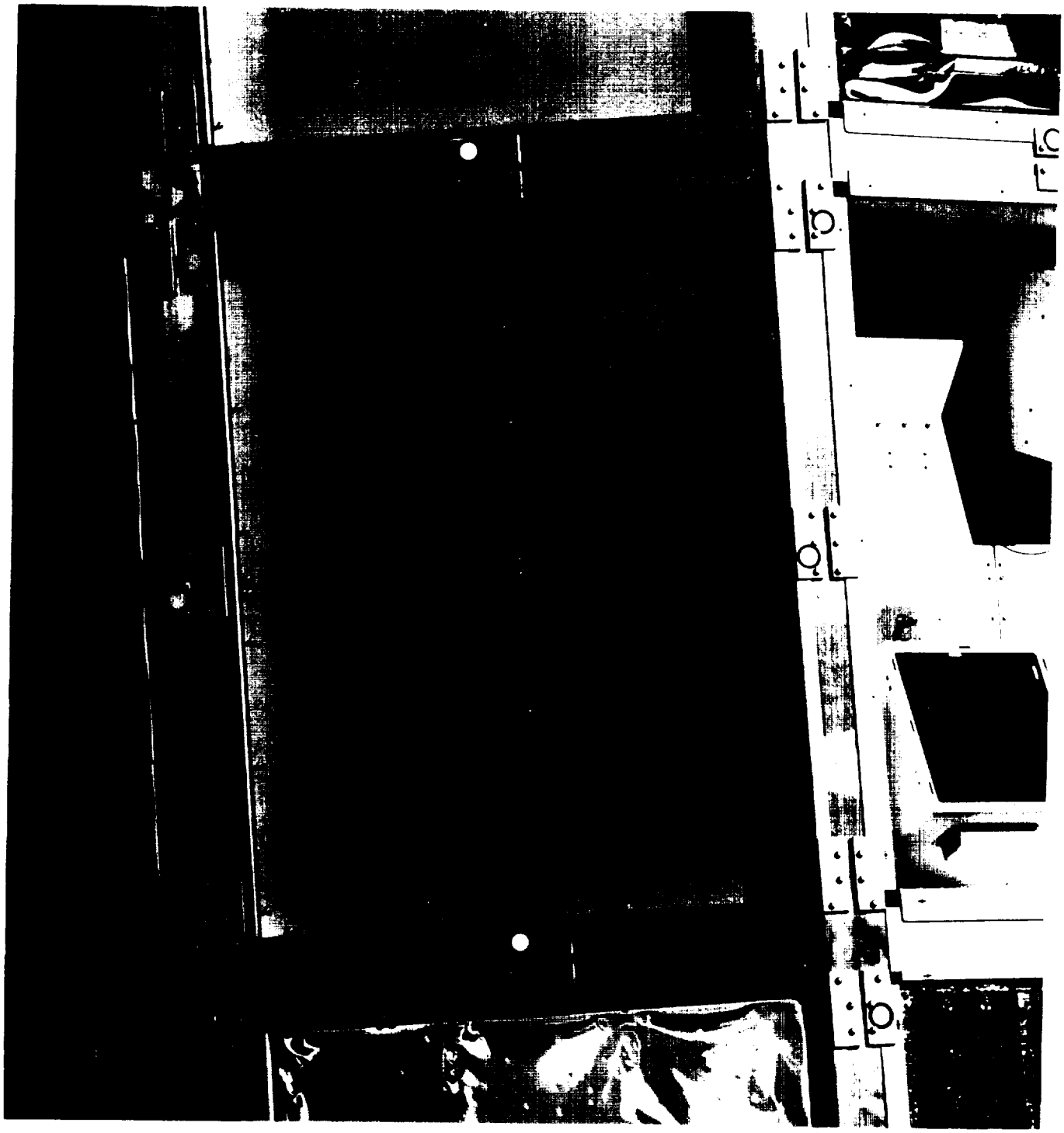

Figure C-10 NASA on-orbit photo showing debris particles on the wire grid of the interstellar gas experiment cameras.

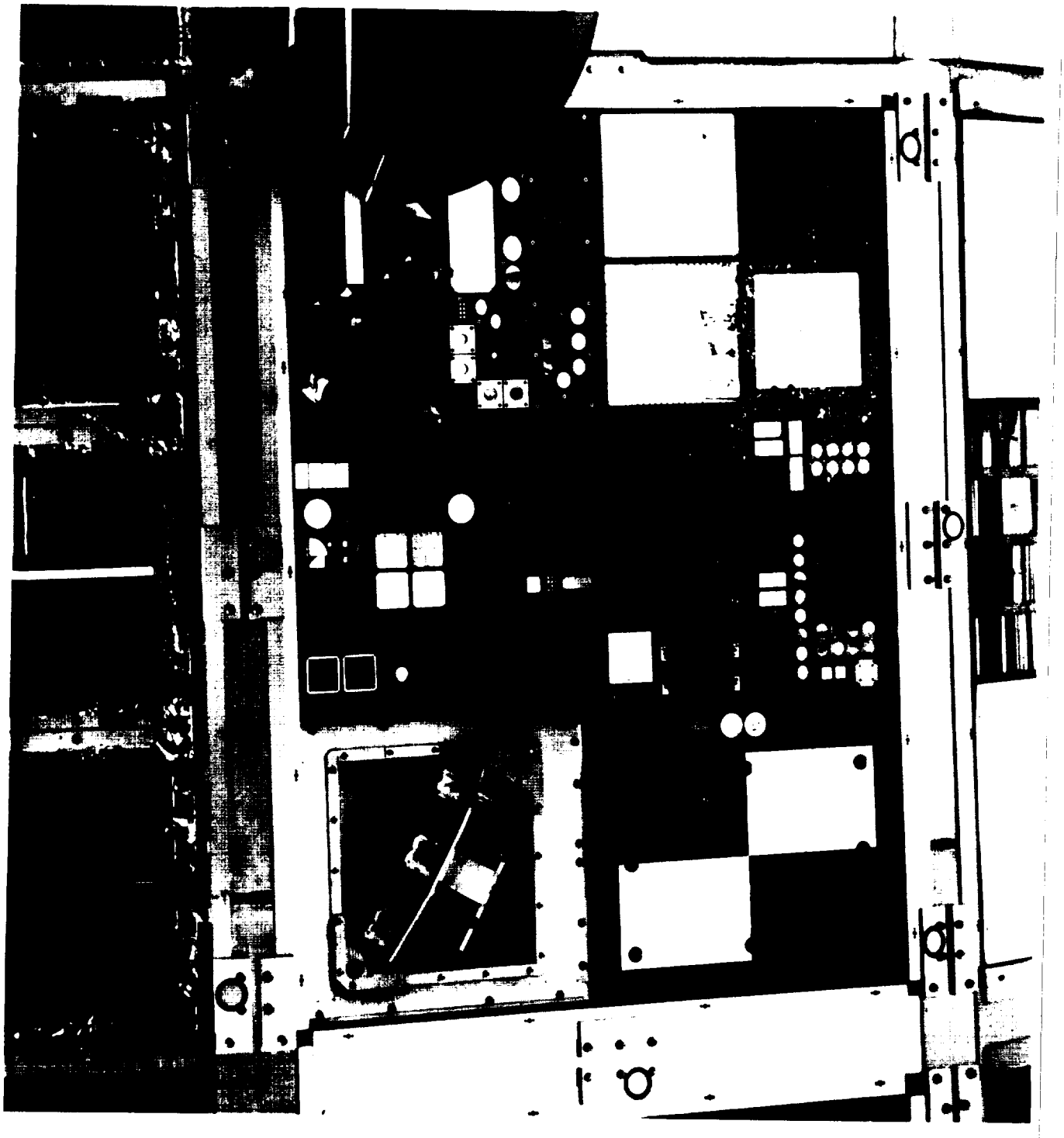

Figure C-11. NASA on-orbit photo showing debris on tray D9.

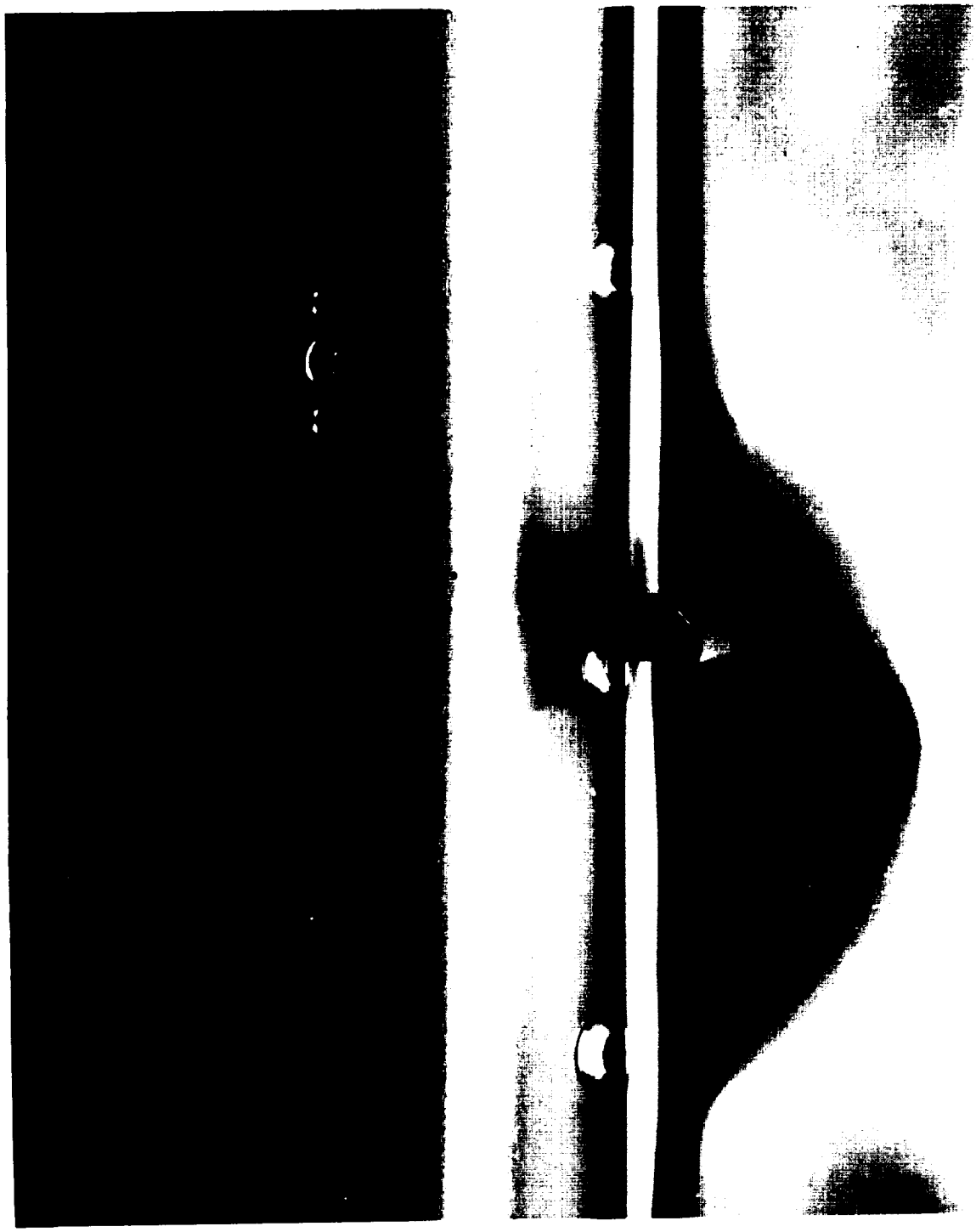

Figure C-12. Photo of the edge of tray C11, showing contamination deposits.

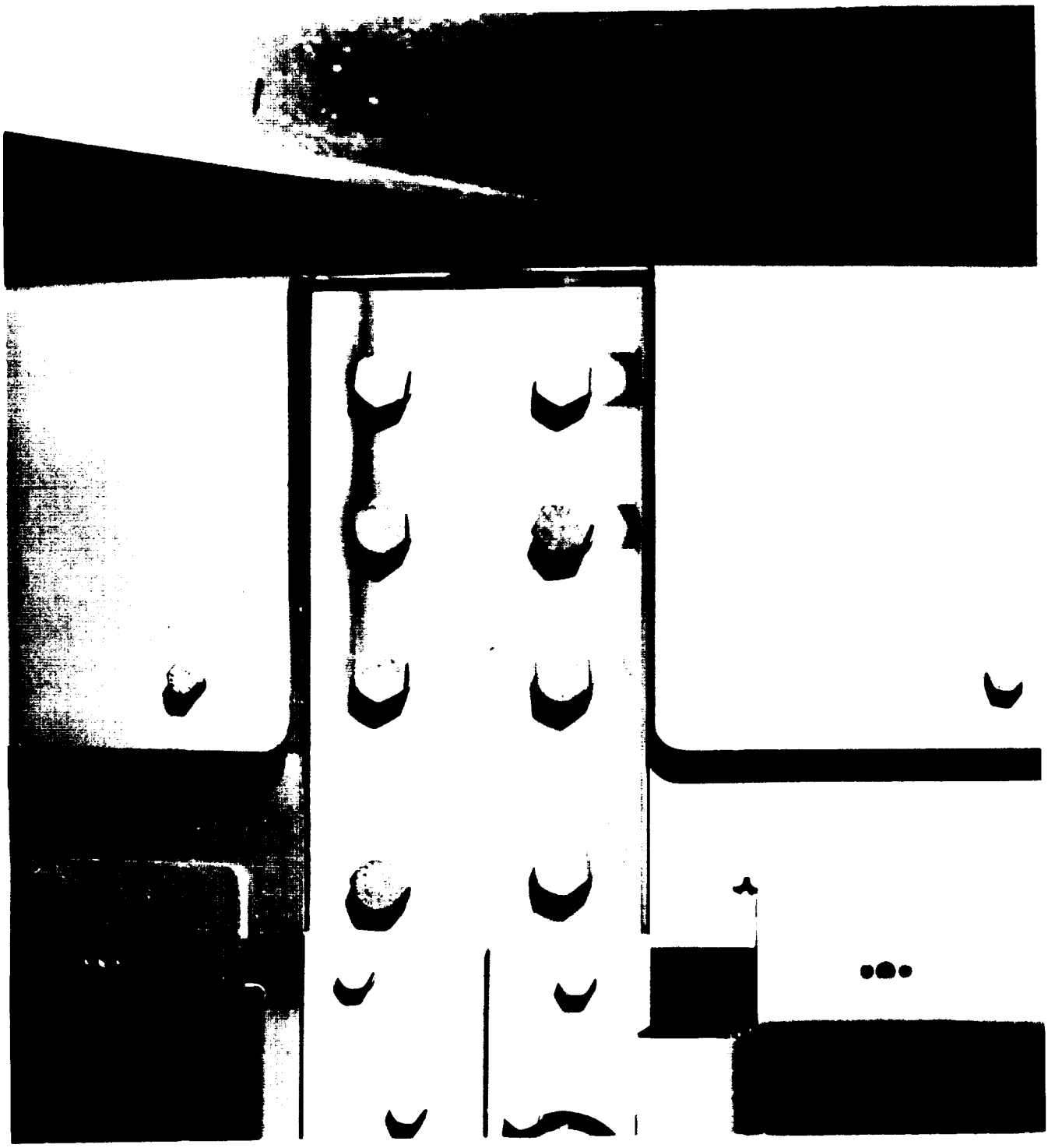

Figure C-13. NASA post-flight photo of contamination deposits on longeron between trays F11 and F12.

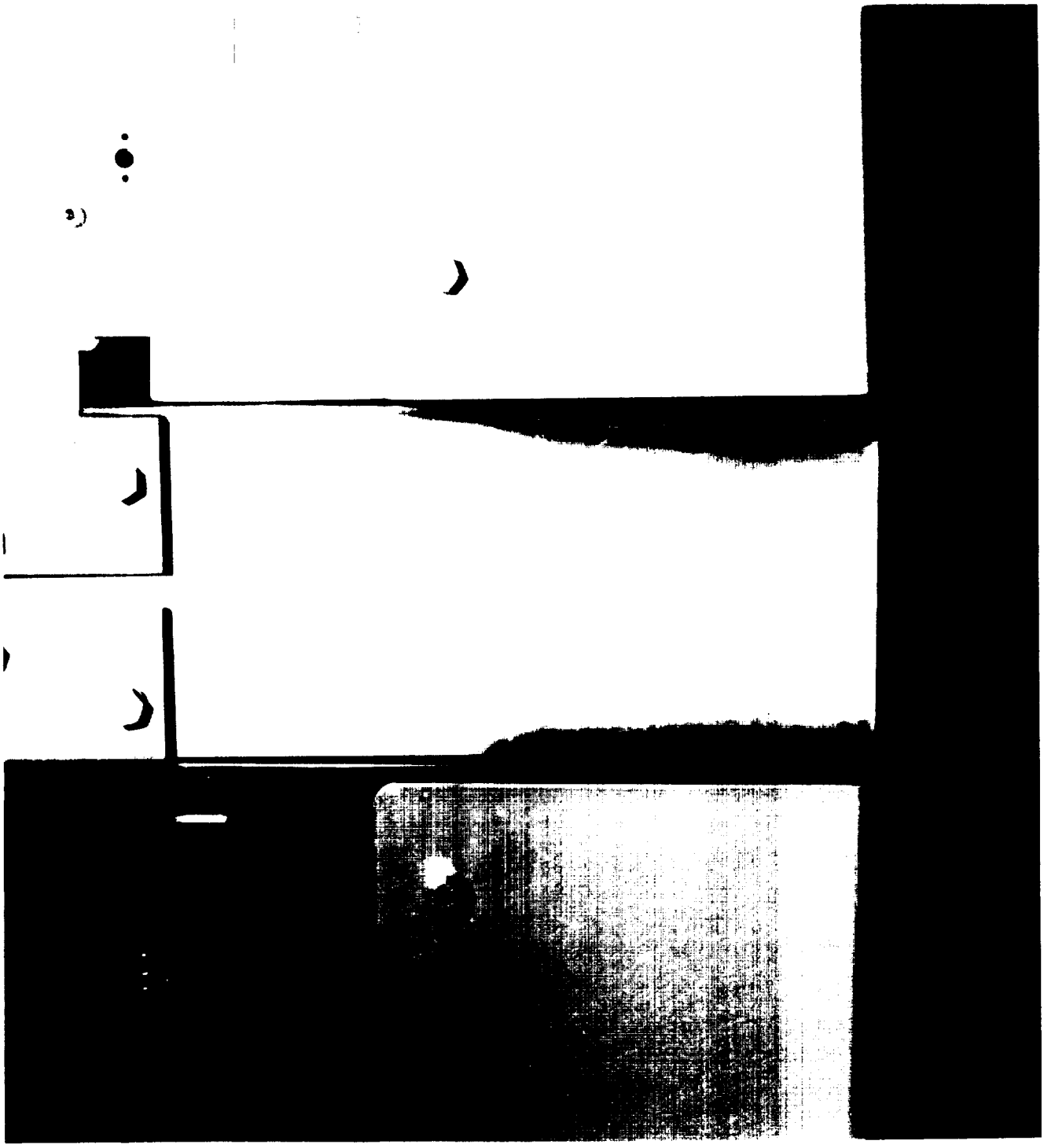

Figure C-14. NASA post-flight photo of contamination deposits on longeron between trays F10 and F11.

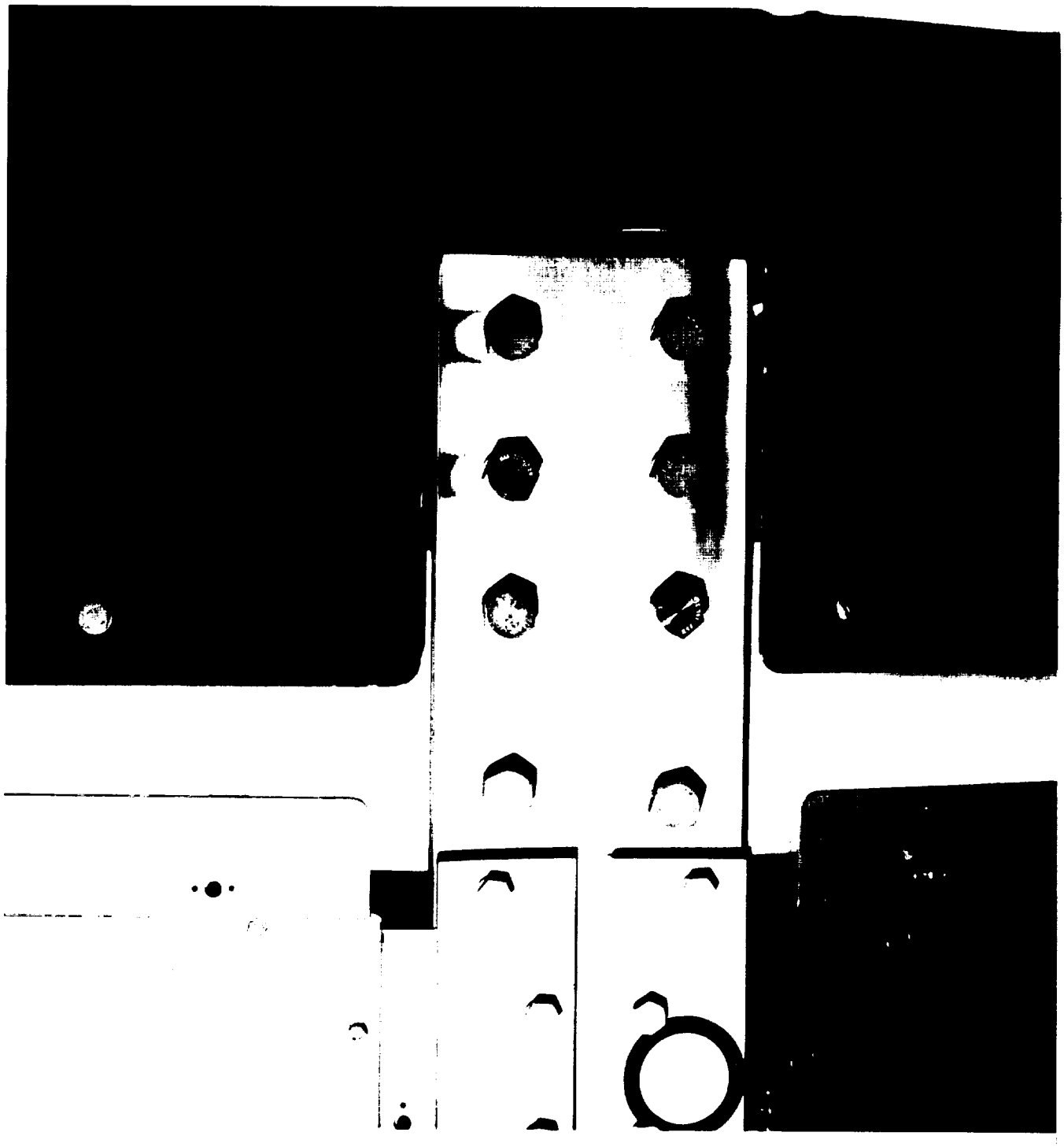

Figure C-15. NASA post-flight photo of contamination deposits on longeron between trays A11 and A12.

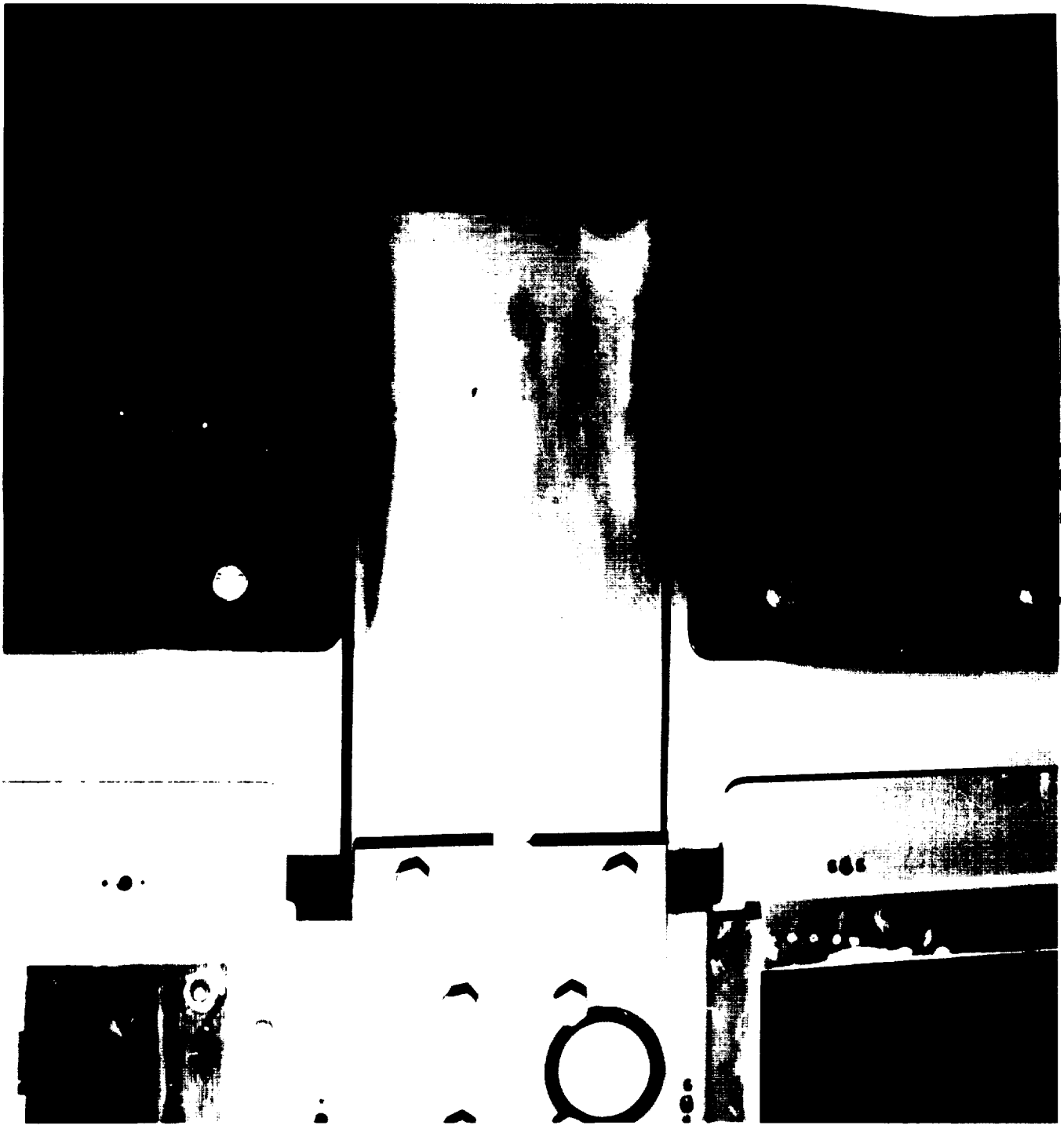

Figure C-16. NASA post-flight photo of contamination deposits on longeron between trays A7 and A8.

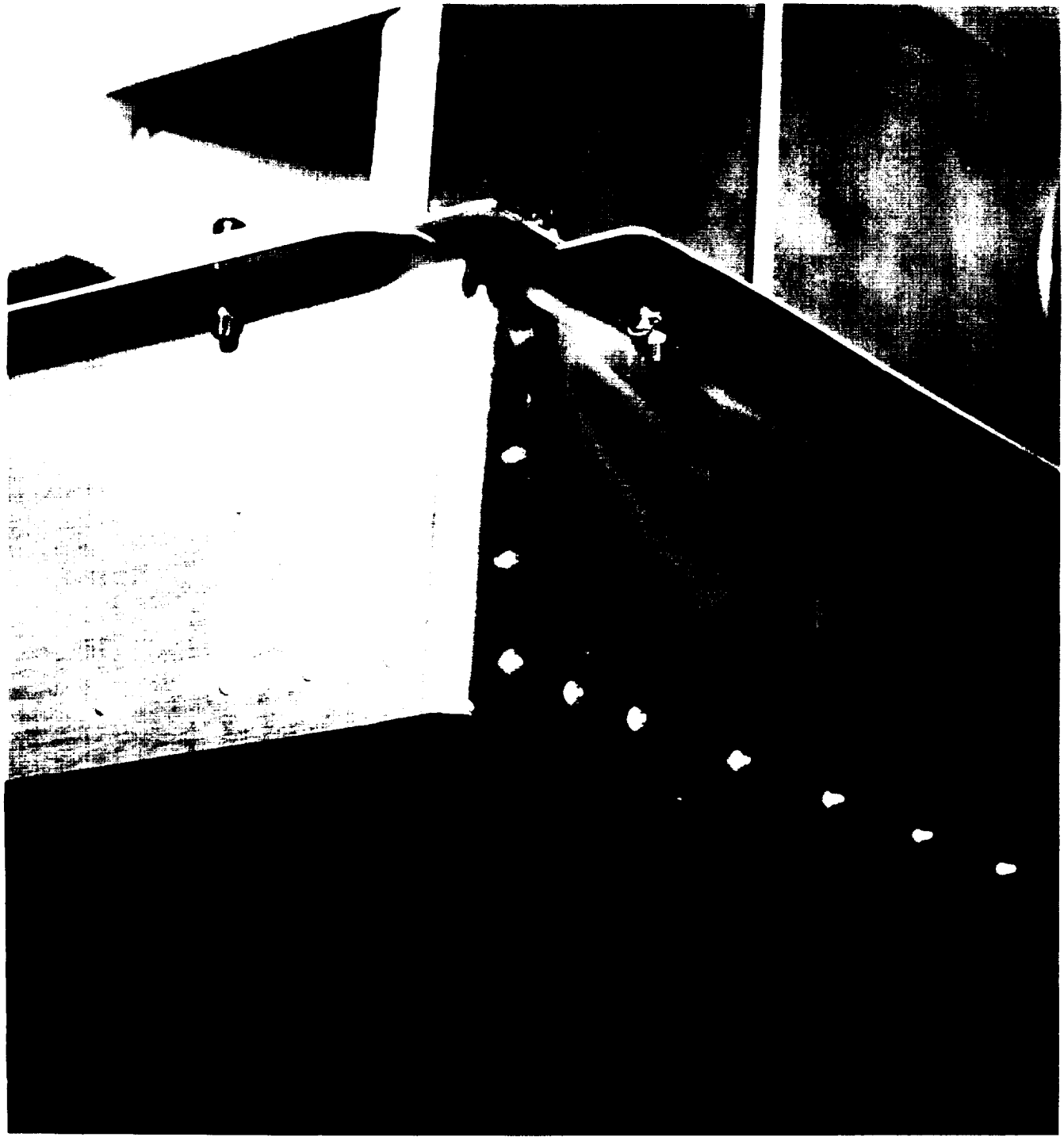

Figure C-17. NASA post-flight photo of exterior of corner of tray C7.

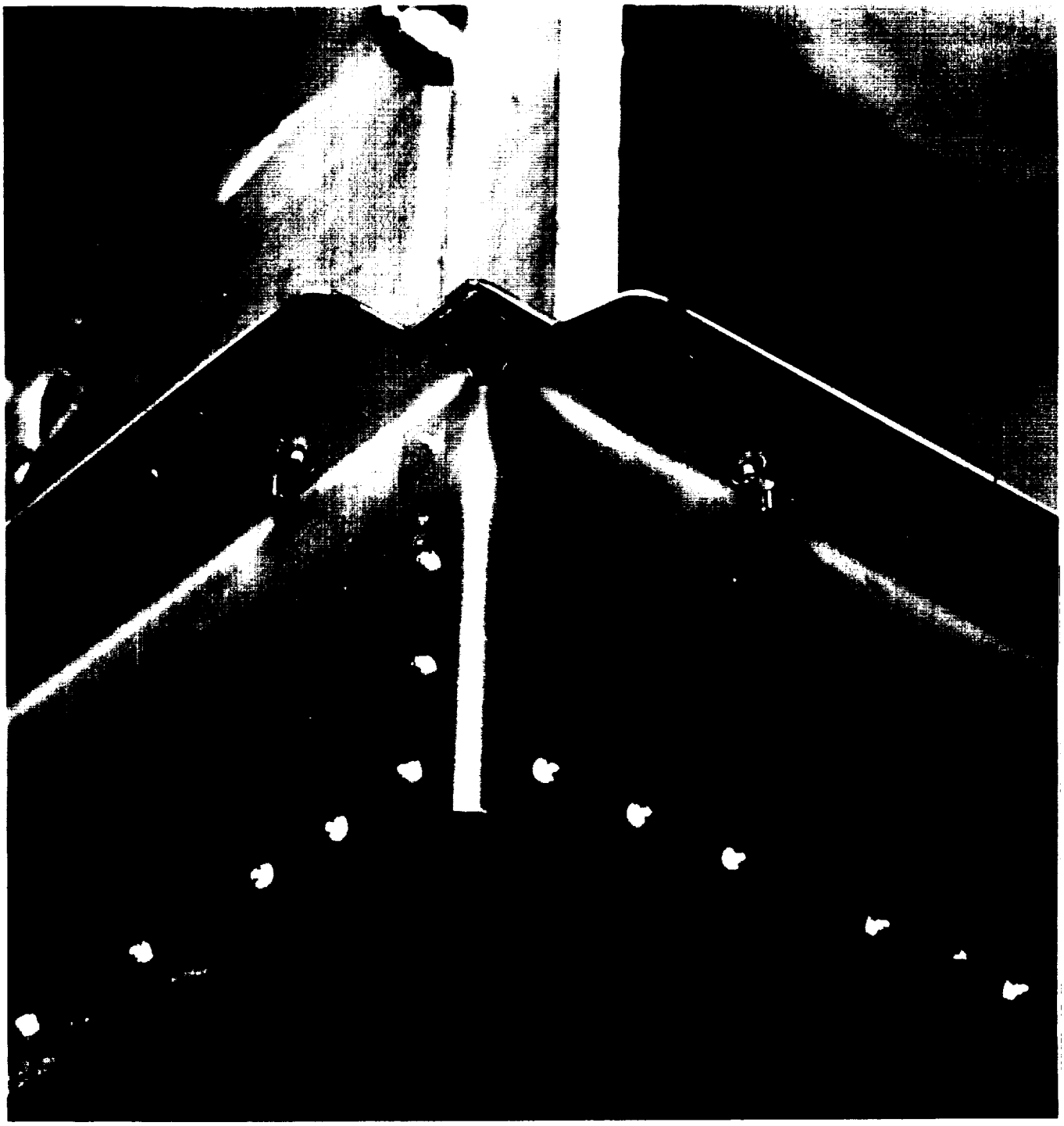

Figure C-18. NASA post-flight photo of exterior of corner of tray C7.

Figure C-19. NASA post-flight photo of exterior of corner of tray D8.

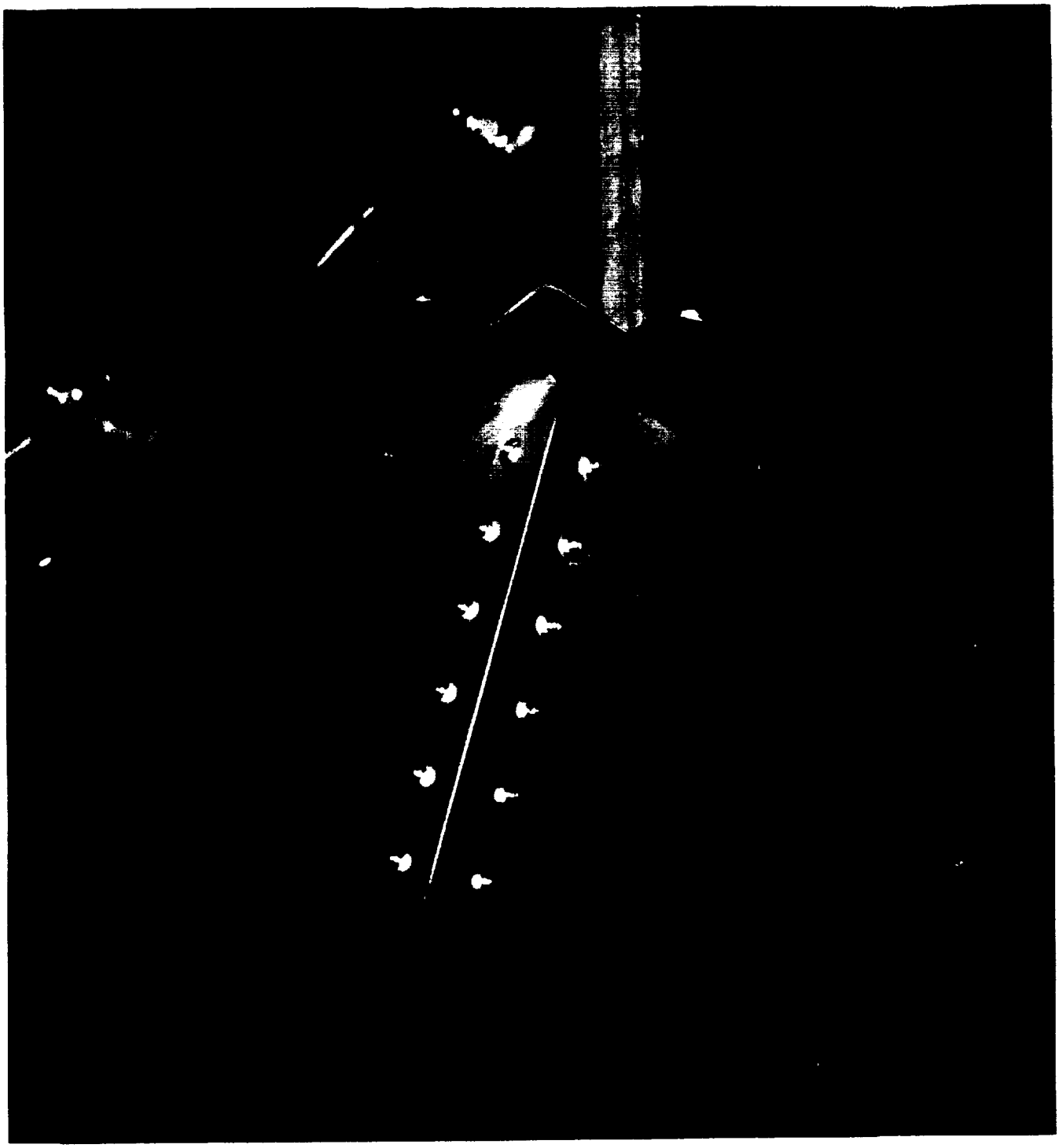

Figure C-20. NASA post-flight photo of exterior of corner of tray F9.

Figure C-21. NASA post-flight photo of exterior of corner of tray C11.

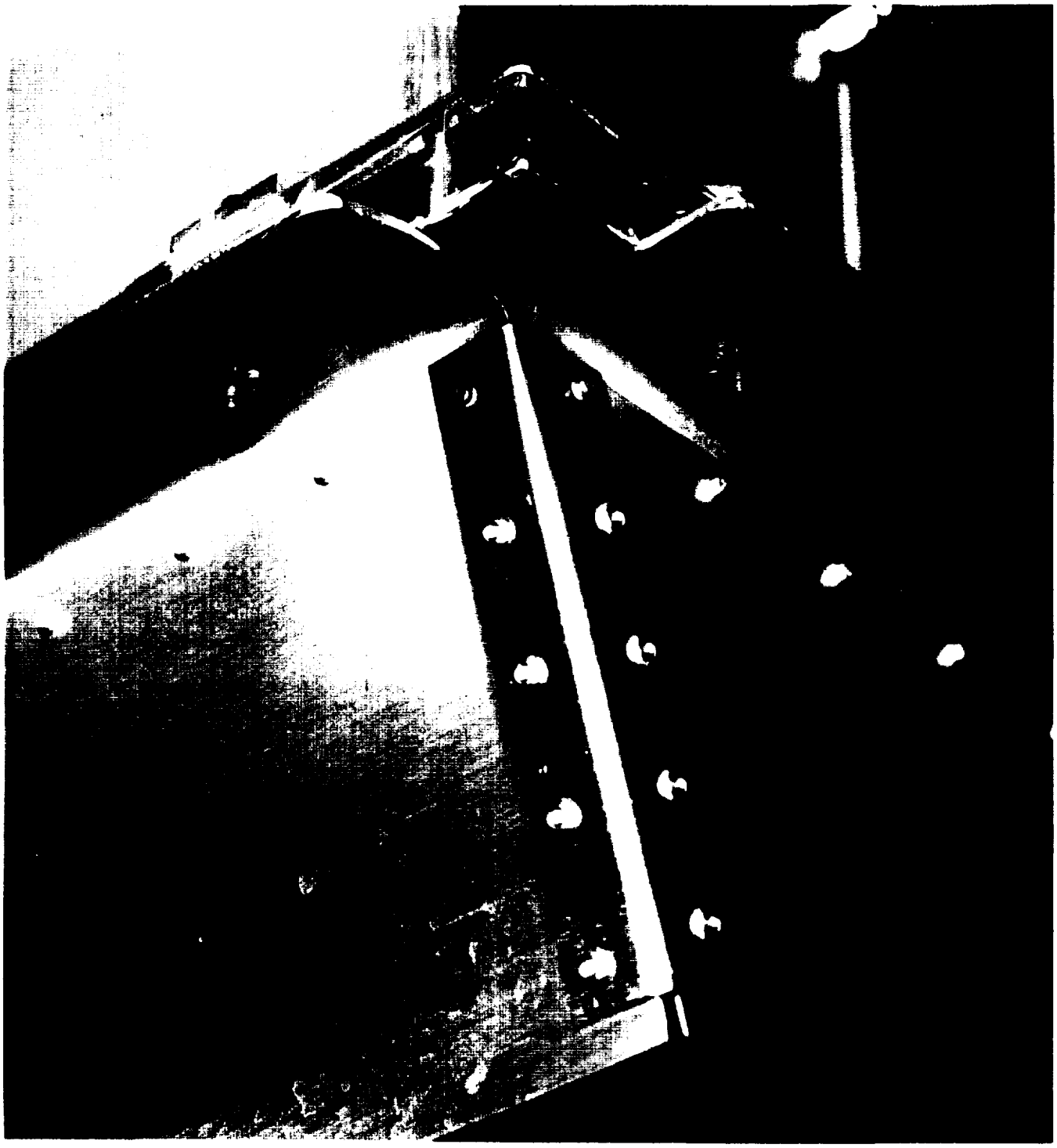

Figure C-22. NASA post-flight photo of exterior of corner of tray C11.

Figure C-23. NASA post-flight photo of exterior of corner of tray F11.

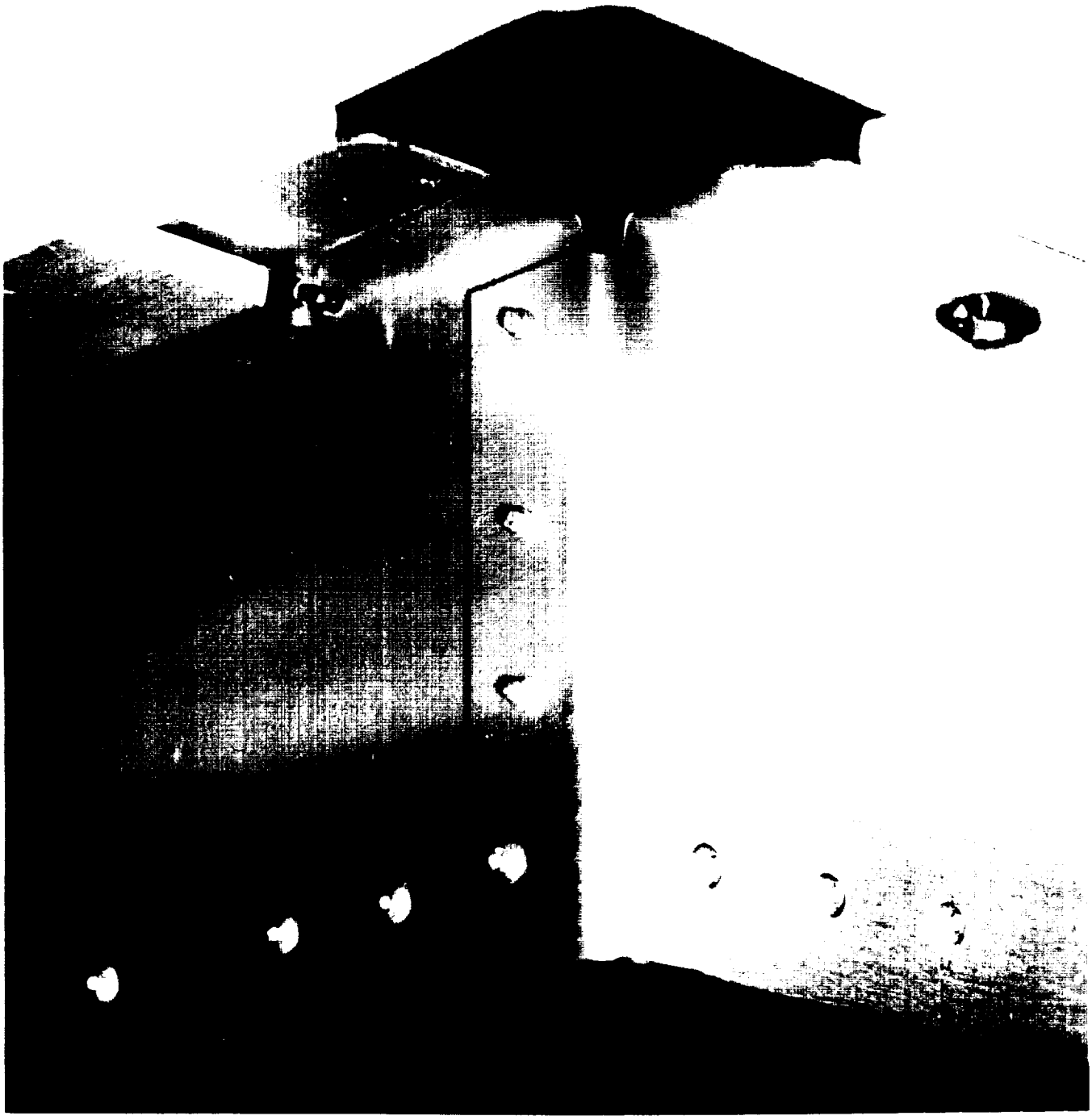

Figure C-24. NASA post-flight photo of exterior of corner of tray F11.

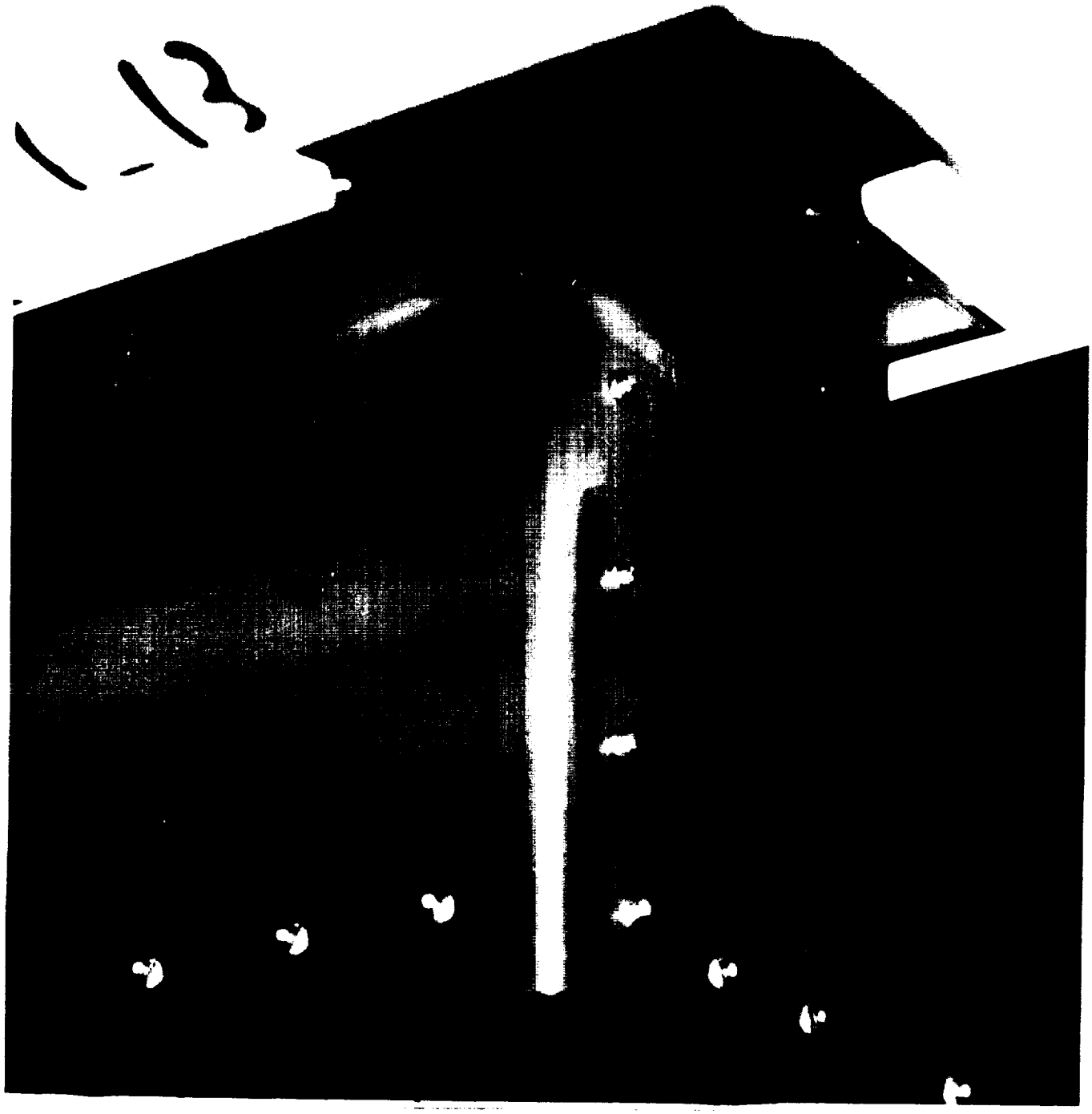

Figure C-25. NASA post-flight photo of exterior of corner of tray F11.

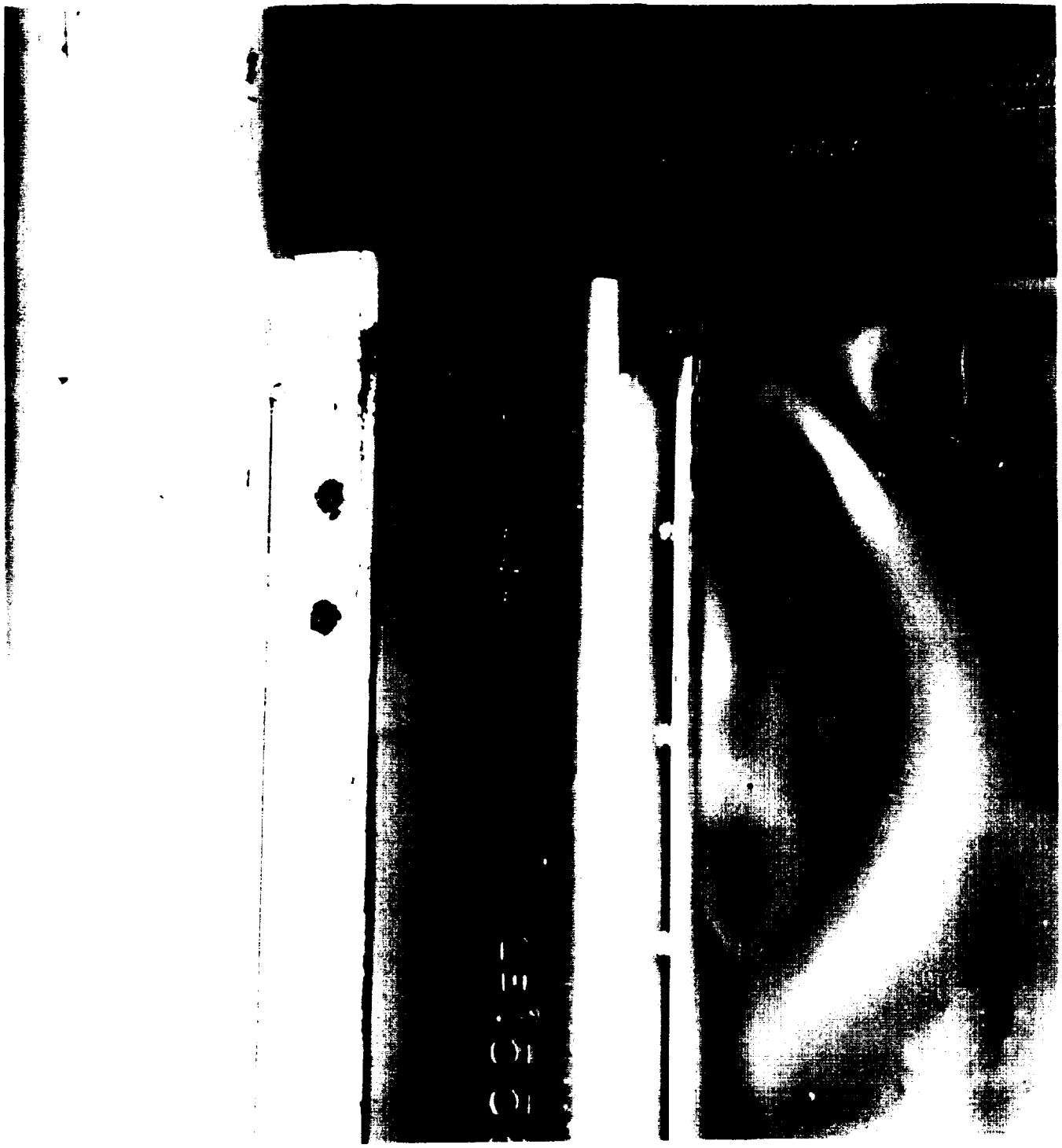

Figure C-26. NASA post-flight photo of outgassing deposits at interior of corner of tray D11.

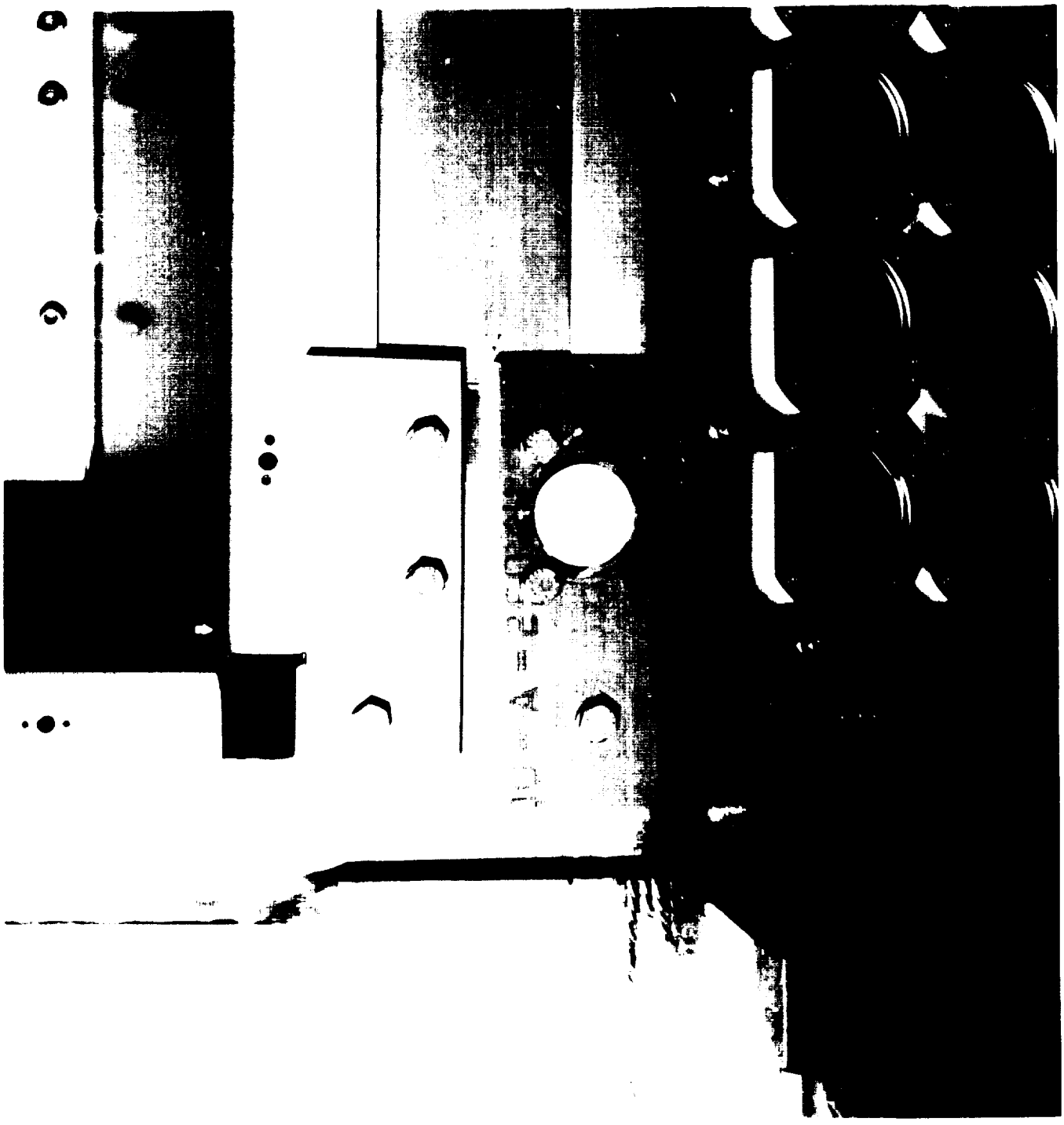

Figure C-27. NASA post-flight photo of leading edge unanodized aluminum tray clamp at space end of C9.

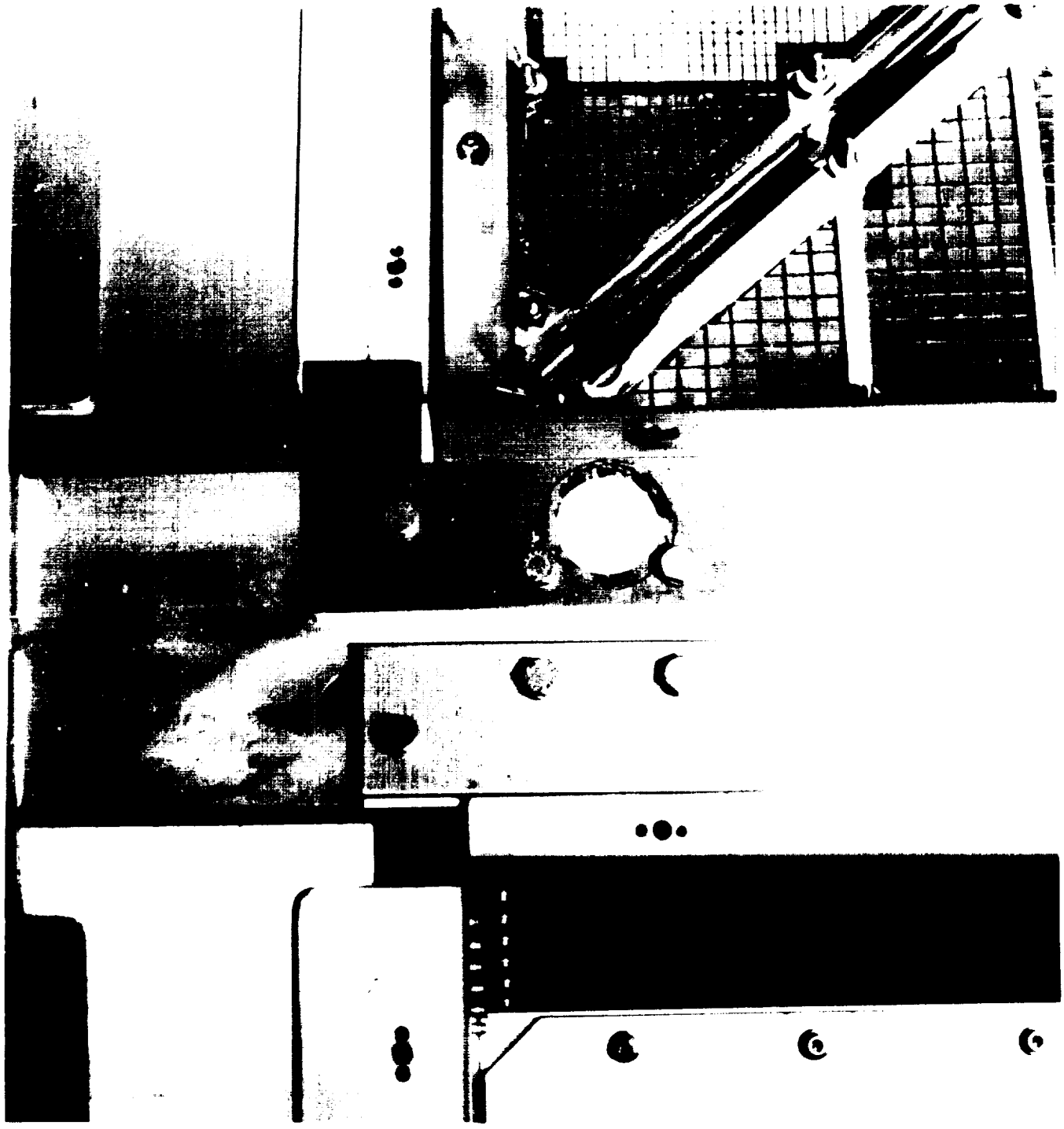

Figure C-28. NASA post-flight photo of leading edge unanodized aluminum tray clamp at Earth end of C9.

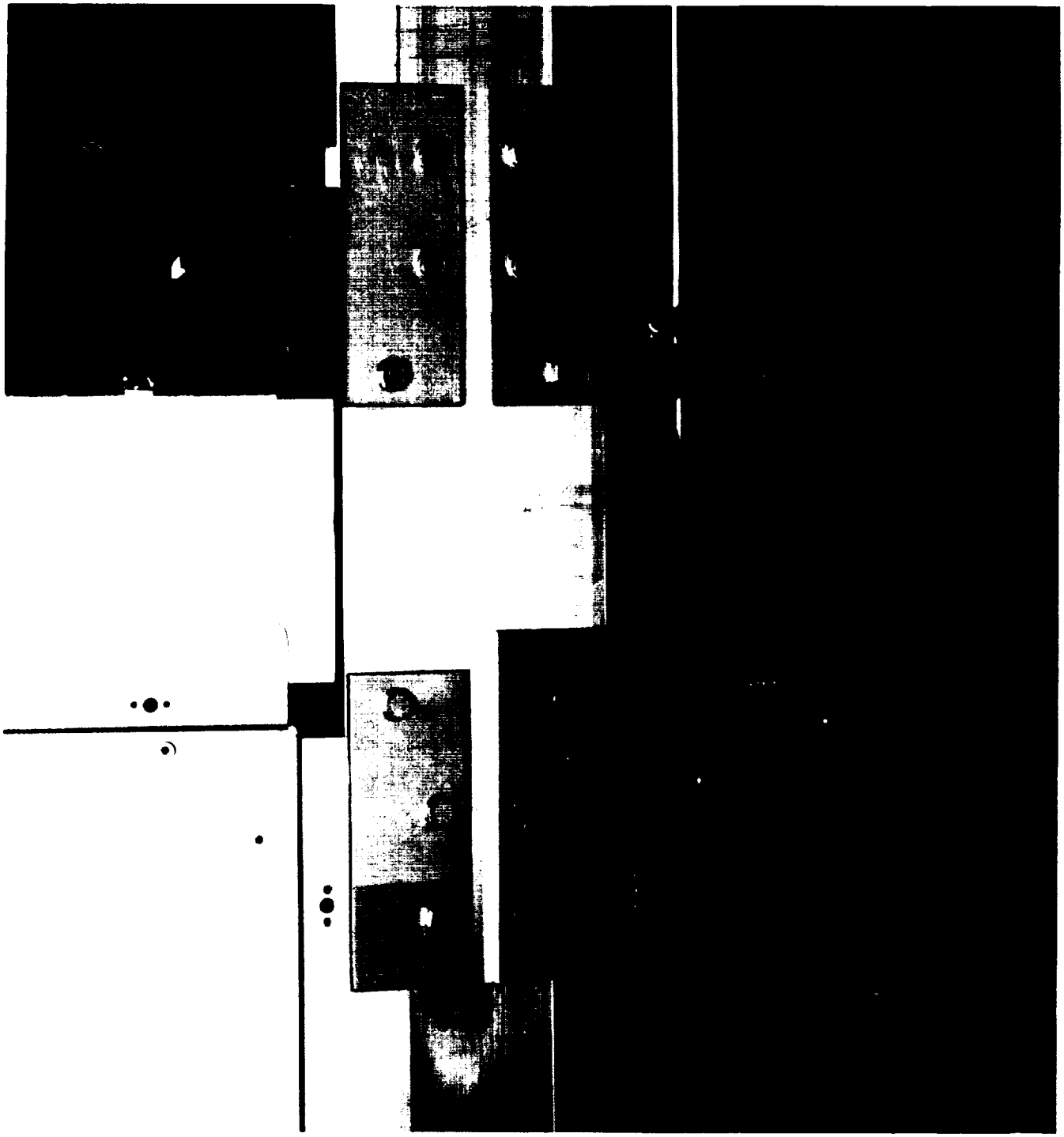

Figure C-29. NASA post-flight photo of trailing edge unanodized aluminum tray clamp on tray C3.

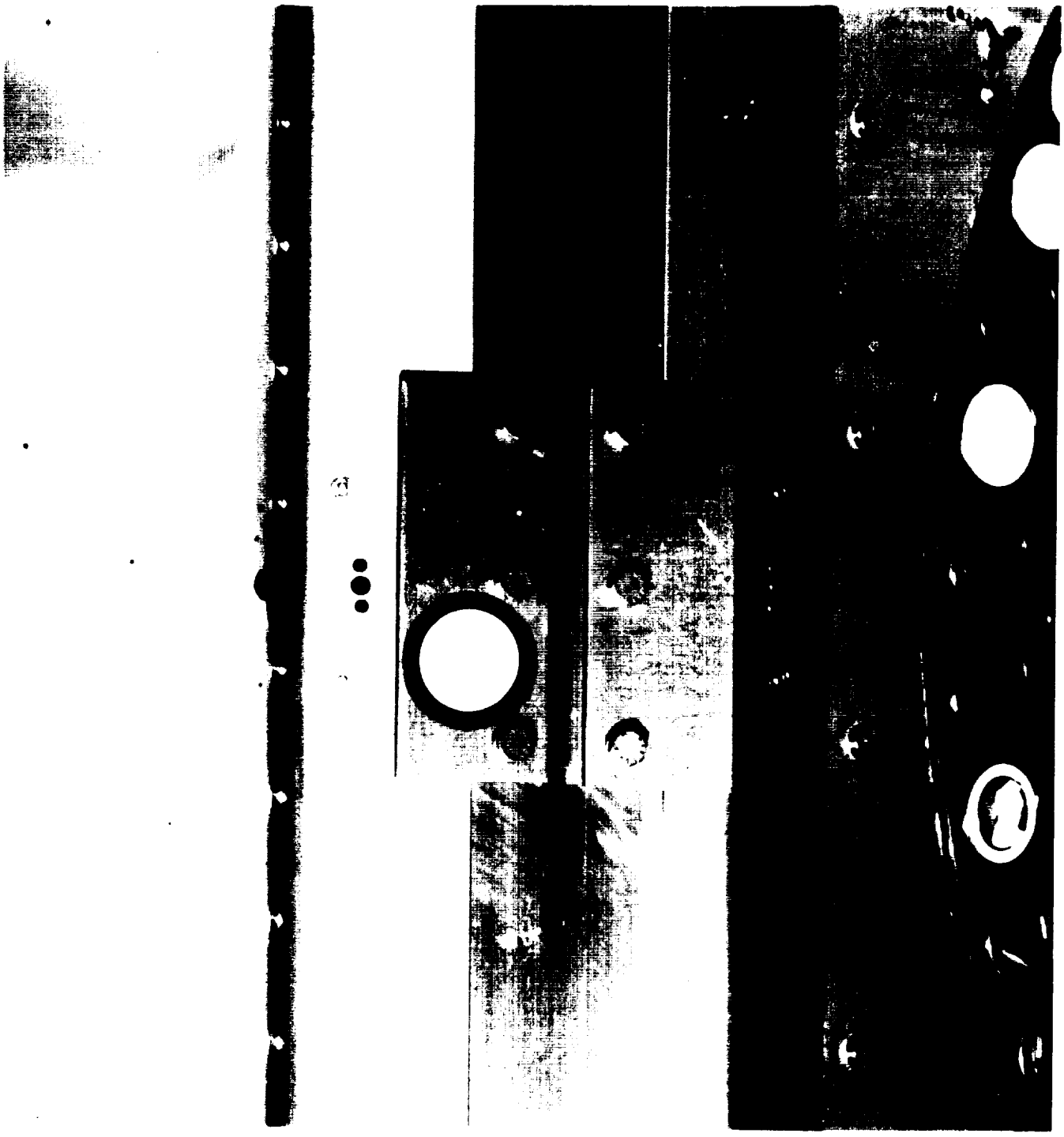

Figure C-30. Close-up of areas of trays A9 and A10 showing environmental effects on a variety of materials.

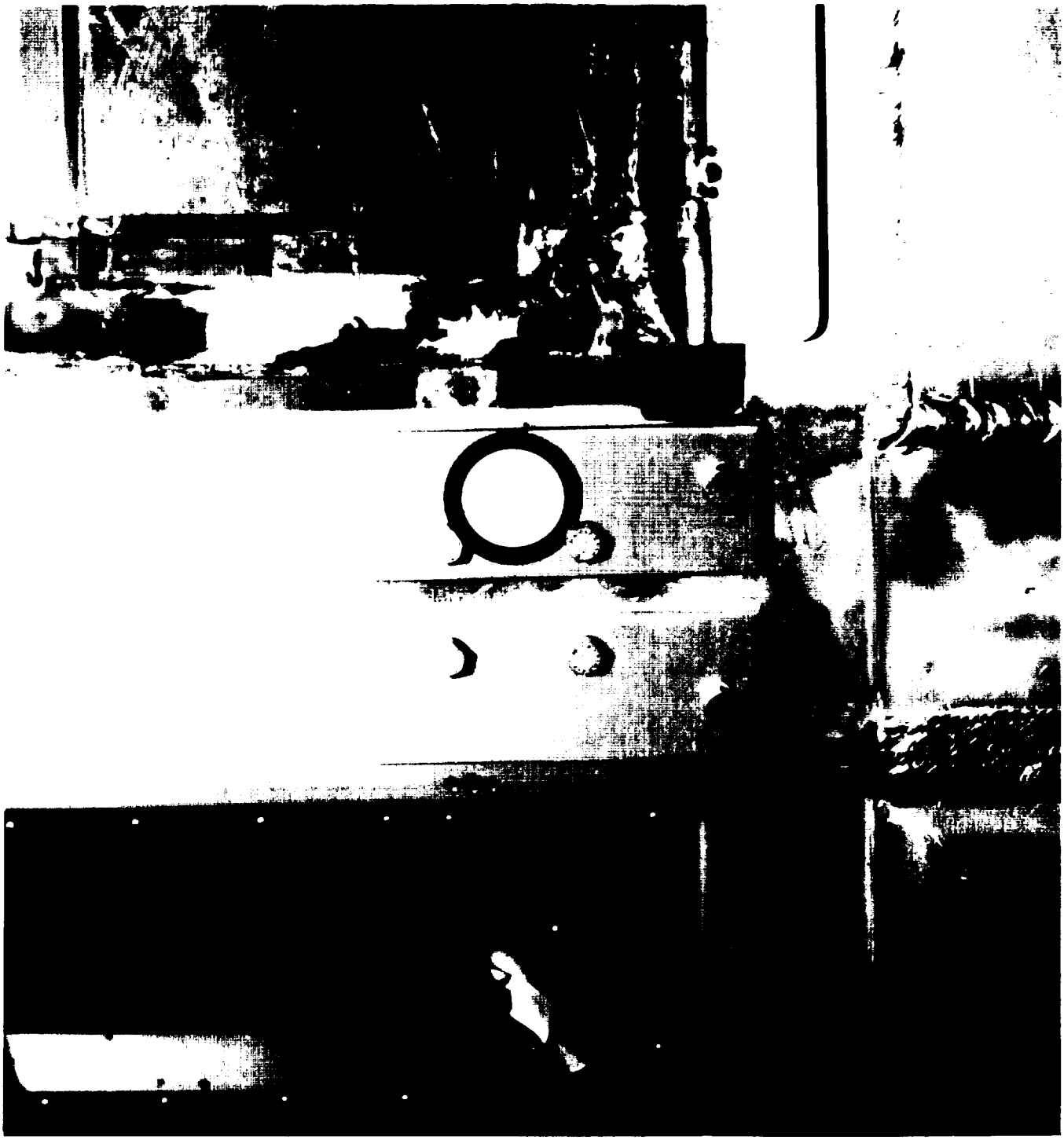

Figure C-31. NASA photo showing close-up of areas on trays D9 and D10.

Figure C-32. NASA post-flight photo of leading edge tray clamp with paint button mounted between trays D10 and D11.

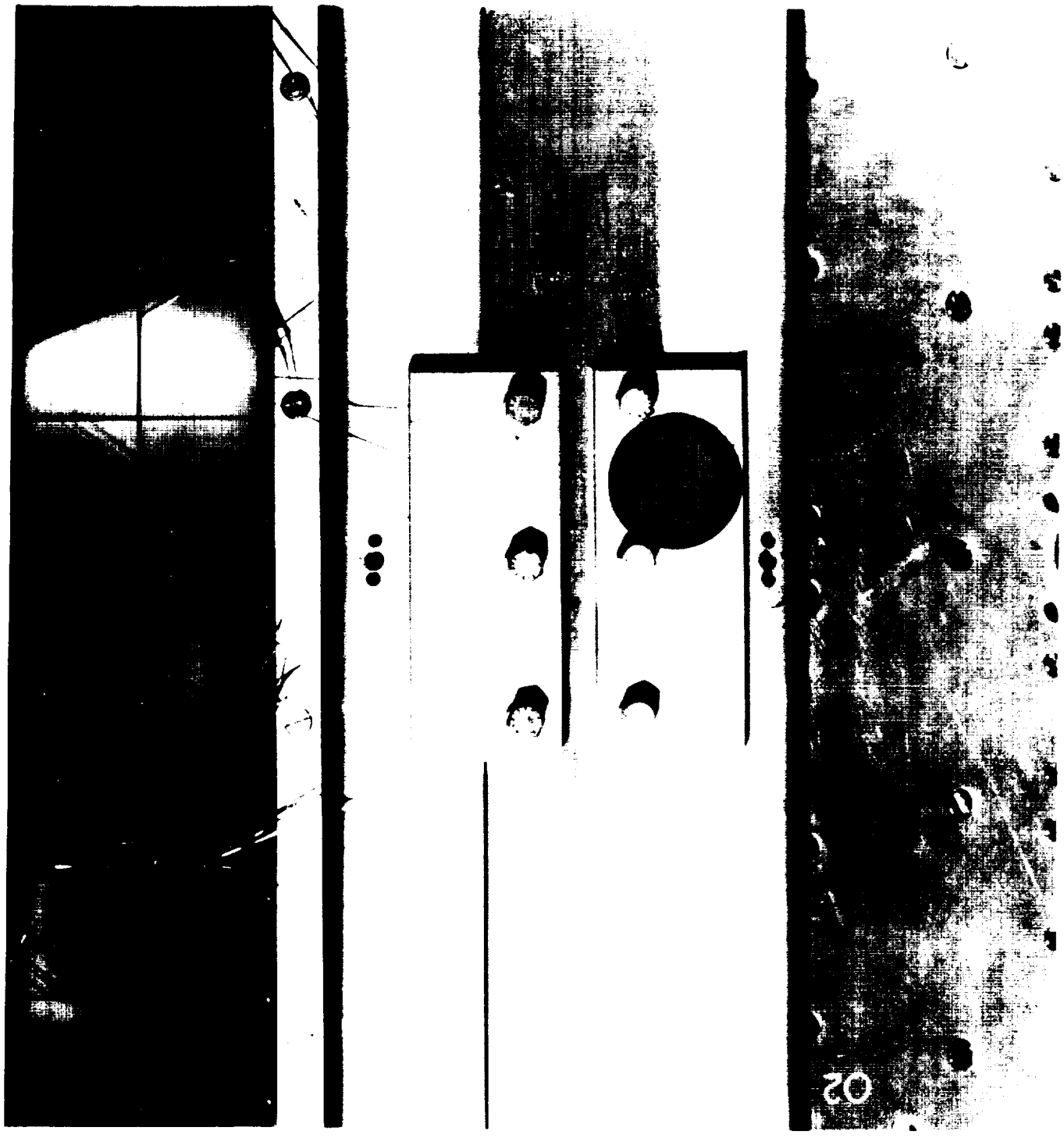

Figure C-33. NASA post-flight photo of trailing edge tray clamp with paint button mounted between trays C2 and C3.

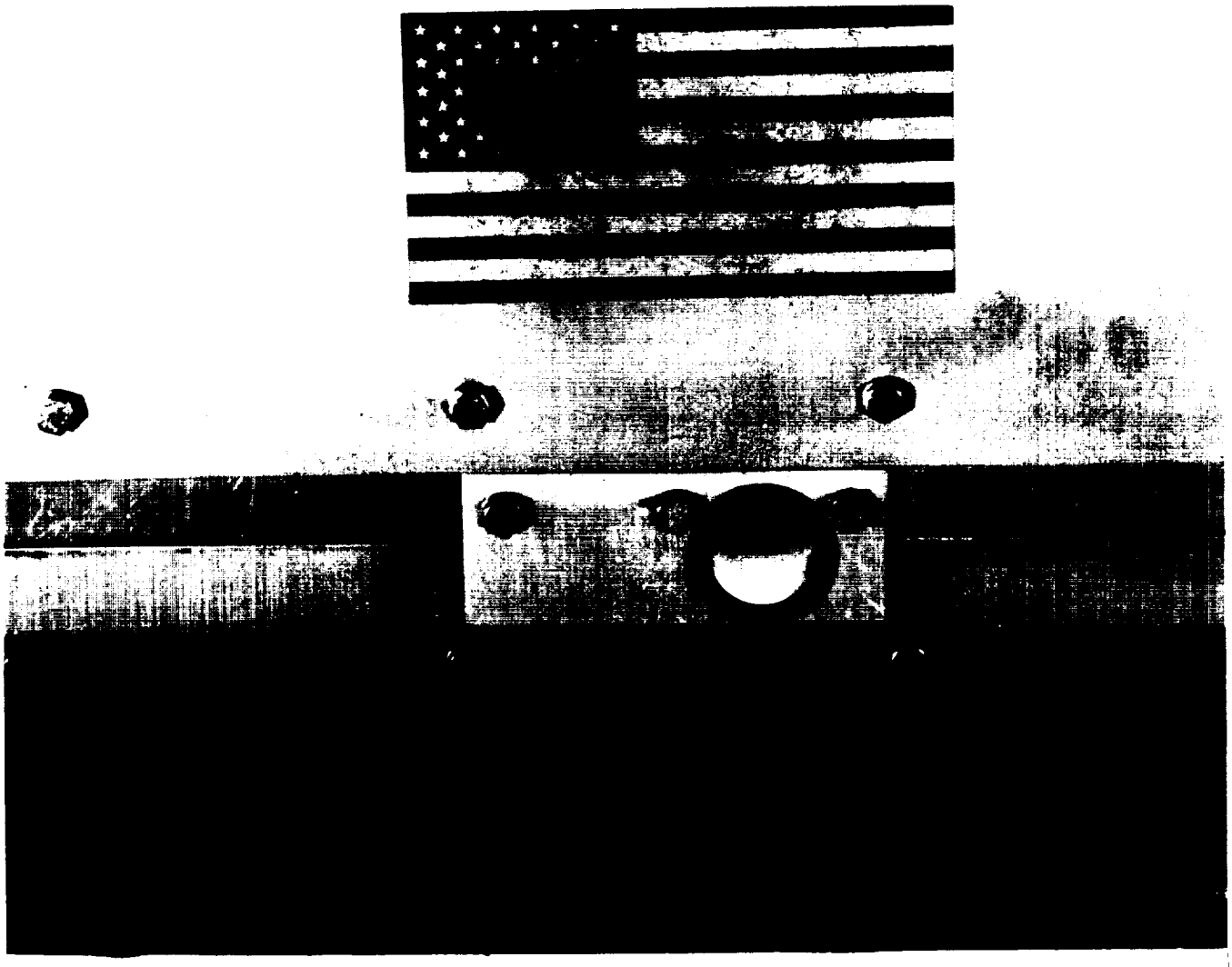

Figure C-34. NASA post-flight photo showing detail of space end of LDEF showing blocking of ram atomic oxygen impingement on a paint button by a tray clamp bolt .

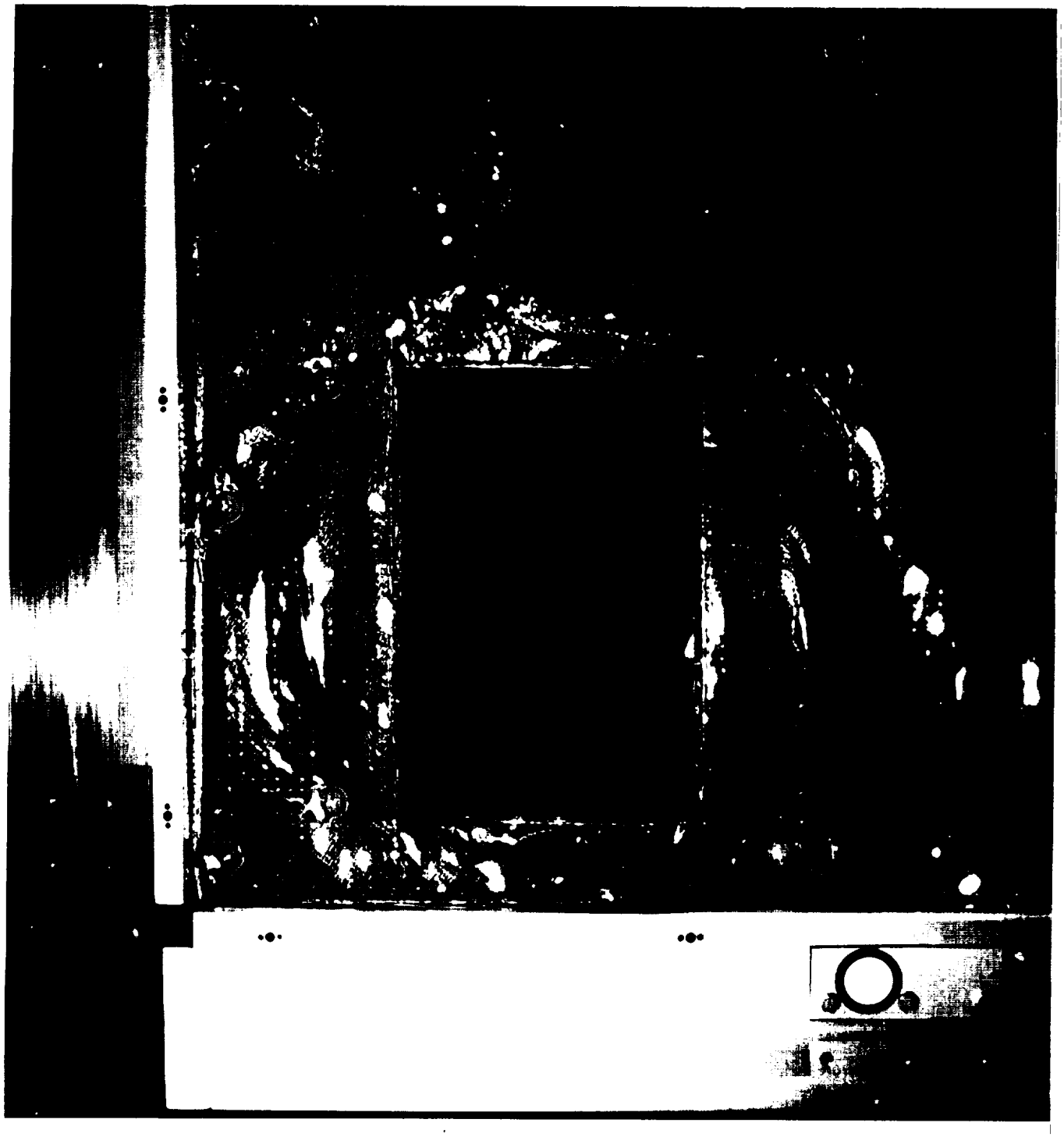

Figure C-35. NASA post-flight photo of radiator panel from tray F9.

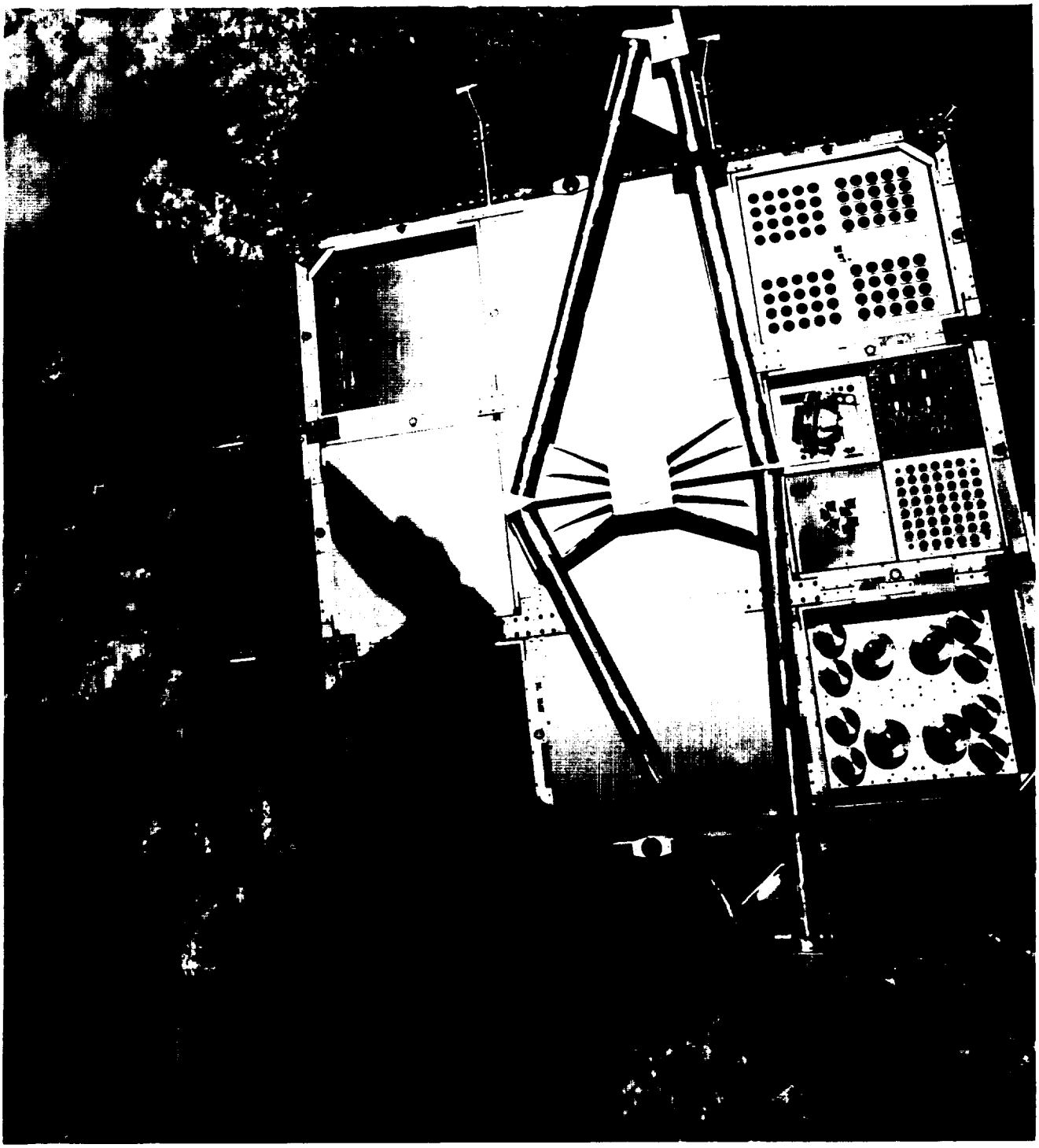

Figure C-36. NASA on-orbit photo of Earth end of LDEF.

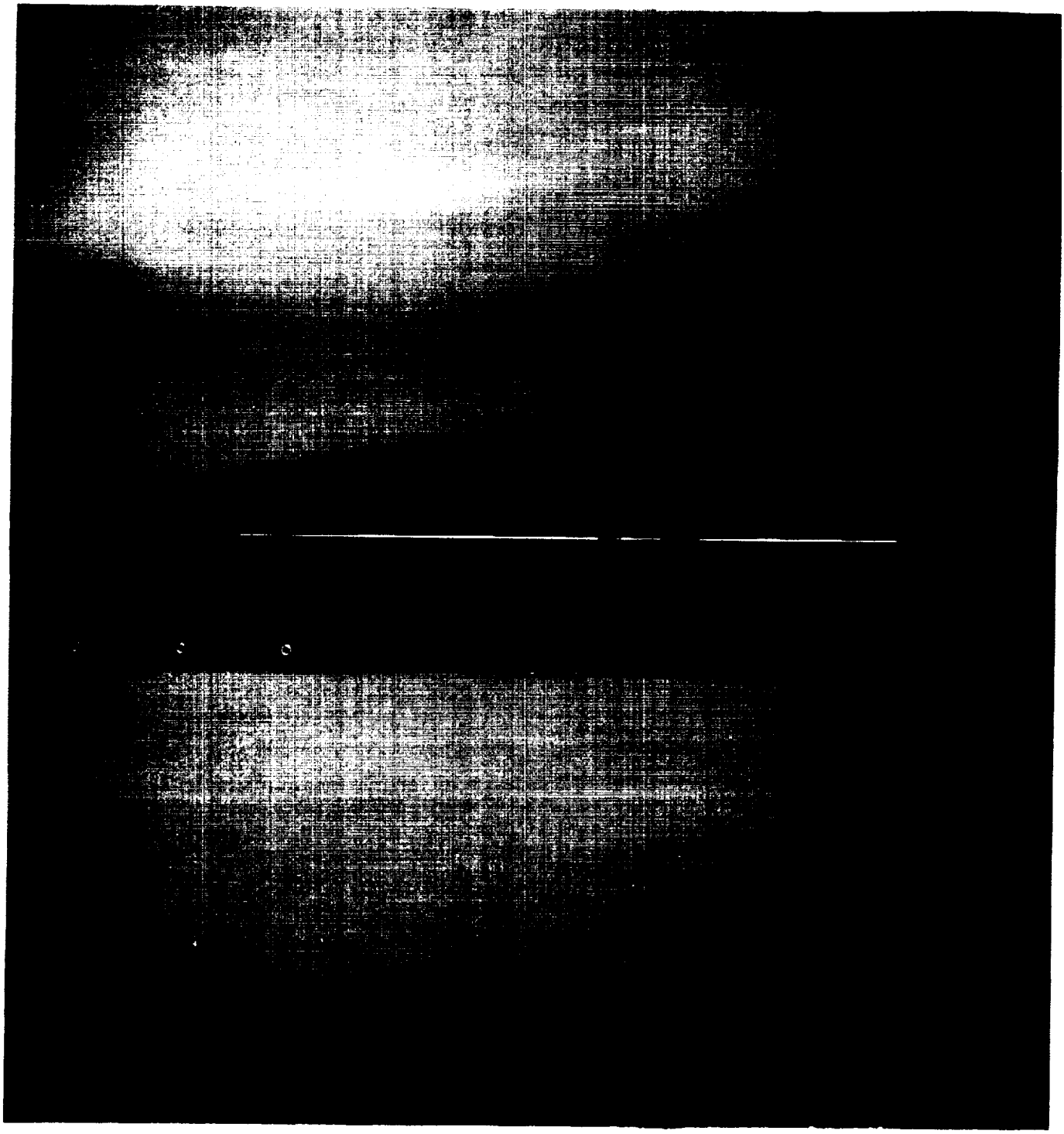

Figure C-37. NASA post-flight photo of panel 916-10A from LDEF Earth end.

REPORT DOCUMENTATION PAGE

Form Approved
OMB No. 0704-0188

1. AGENCY USE ONLY (Leave blank)	2. REPORT DATE	3. REPORT TYPE AND DATES COVERED
	July 1995	Contractor Report (Oct. 1989-March 1995)

4. TITLE AND SUBTITLE
Analysis of Materials Flown on the Long Duration Exposure Facility: Summary of Results of the Materials Special Investigation Group

5. FUNDING NUMBERS
C NAS1-18224
C NAS1-19247

WU 506-43-61-02
WU 233-03-02-02

6. AUTHOR(S)
H. Gary Pippin

7. PERFORMING ORGANIZATION NAME(S) AND ADDRESS(ES)
Boeing Defense & Space Group
P. O. Box 3999
Seattle, WA 98124-2499

8. PERFORMING ORGANIZATION REPORT NUMBER

9. SPONSORING / MONITORING AGENCY NAME(S) AND ADDRESS(ES)
National Aeronautics and Space Administration
Langley Research Center
Hampton, VA 23681-0001

10. SPONSORING / MONITORING AGENCY REPORT NUMBER
NASA CR-4664

11. SUPPLEMENTARY NOTES
Langley Technical Monitor: Joan G. Funk

12a. DISTRIBUTION / AVAILABILITY STATEMENT
Unclassified - Unlimited
Subject Category 23

12b. DISTRIBUTION CODE

13. ABSTRACT *(Maximum 200 words)*

This report documents data from materials flown on or as part of the Long Duration Exposure Facility (LDEF). The LDEF was a fixed flight orientation satellite that carried 57 science and technology experiments in low Earth orbit for 69 months. The report is a combination summary, detailed technical report, and guide to further materials information from LDEF. Data not previously published and/or made widely available are also included.

14. SUBJECT TERMS
LDEF, Low Earth Orbit, Materials, space environmental effects

15. NUMBER OF PAGES
254

16. PRICE CODE
A12

17. SECURITY CLASSIFICATION OF REPORT	18. SECURITY CLASSIFICATION OF THIS PAGE	19. SECURITY CLASSIFICATION OF ABSTRACT	20. LIMITATION OF ABSTRACT
Unclassified	Unclassified	Unclassified	UL